January 2009

Developing New Methodologies for Crosslinked Polymeric Nanostructure Syntheses, Chemoselective Modifications, and Applications as Imaging and Delivery Agents

Guorong Sun
Washington University in St. Louis

WASHINGTON UNIVERSITY IN ST. LOUIS

Department of Chemistry

Dissertation Examination Committee:
Prof. Karen L. Wooley, Chairperson
Prof. Michael J. Welch
Prof. John-Stephen A. Taylor
Prof. William E. Buhro
Prof. Jay R. Turner
Prof. Suzanne Lapi

Developing New Methodologies for Crosslinked Polymeric Nanostructure Syntheses, Chemoselective Modifications, and Applications as Imaging and Delivery Agents

by

Guorong Sun

A dissertation presented to the
Graduate School of Arts and Sciences
of Washington University in
partial fulfillment of the
requirements for the degree
of Doctor of Philosophy

August 2009

Saint Louis, Missouri

ABSTRACT OF THE DISSERTATION

Developing New Methodologies for Crosslinked Polymeric Nanostructure Syntheses, Chemoselective Modifications, and Applications as Imaging and Delivery Agents

By

Guorong Sun

Doctor of Philosophy in Chemistry

Washington University in Saint Louis, 2009

Professor Karen L. Wooley, Chairperson

The overall emphasis of this dissertation research includes the syntheses of amphiphilic block copolymers bearing functional groups through controlled radical polymerization techniques, followed by the aqueous assembly of these block copolymer precursors to construct polymeric nanostructures with different sizes and morphologies. Further chemical modification of the nanostructures afforded functional crosslinked nano-objects with reporting probes for imaging and biocompatible "stealth" materials for tuning the *in vivo* fate of nanostructures.

Amphiphilic block copolymers poly(acrylic acid)-*block*-polystyrene (PAA-*b*-PS) with well-defined structures were prepared through nitroxide-mediated radical polymerization (NMP). Using novel pre-functionalization strategies, these block copolymer precursors were functionalized with DOTA for chelating ^{64}Cu and were then assembled into micelles and crosslinked throughout the micelle shell domain to afford the shell crosslinked nanoparticles (SCKs), containing large numbers of effective DOTAs per

particle for ^{64}Cu radiolabeling These ^{64}Cu–complexed nanoparticles showed impressive specific activities (*ca.* 400 μCi μg^{-1}), which suggest that they will serve as highly sensitive *in vivo* positron emission tomography (PET) tracers at low administering doses.

The "pre-grafting" strategy was further extended to accomplish SCKs with variable biodistributions. PAA-*b*-PS amphiphilic block copolymers were modified with varying numbers of poly(ethylene oxide) (PEO) chains, together with DOTA, before assembling into block copolymer micelles and crosslinking throughout the micellar shell regions. After chelation of ^{64}Cu tracers, the *in vivo* fate of PEGylated SCKs was evaluated by means of biodistribution experiments and PET imaging. The blood retention of PEGylated-SCKs exhibited tunabilities, depending on the mPEG grafting density and the nanoparticle surface properties.

Various bi-functional pyrazine-based chromophores were used as crosslinkers to probe directly their incorporation efficiencies into the shells of block copolymer micelles, which further determined the actual crosslinking extents ─ a critical factor for developing SCKs as PET imaging agents. The micelles were made to carry poly(*N*-acryloxysuccinimide) (PNAS) as pre-installed amine-reactive functionalities along amphiphilic triblock copolymer precursors (PEO-*b*-PNAS-*b*-PS) prepared through reversible addition-fragmentation chain transfer (RAFT) radical polymerizations. The incorporation/crosslinking efficiencies were dependent upon the type of crosslinker and the applied stoichiometries.

The intrinsic reactivity of aldehyde motivated the developments of well-defined polymers having reactive carbonyl side chain substituents. Amphiphilic block copolymers bearing poly(4-vinyl benzaldehyde) (PVBA) block segments with controlled

molecular weights and low polydispersities were obtained through RAFT polymerizations and assembled into polymeric vesicles and micelles. The vesicles were crosslinked and functionalized with fluorescent molecules through chemoselectively-reductive amination and were shown to display interesting *in vitro* cell association behaviors. The micelles were modified with near-infrared fluorescent dyes and crosslinked with diamino crosslinkers, each *via* reductive amination, to prepare robust nanoparticles with optimized luminescent characteristics for *in vivo* optical imaging.

To my wife, Rui

ACKNOWLEDGEMENTS

I would like to acknowledge my advisor and mentor, Professor Karen L. Wooley for her invaluable guidance and never ending support during my Ph.D. study. I always consider myself very fortunate to have been her student. Her broad knowledge and everlasting passion to science encouraged me to overcome and accomplish. Her concerns over me, willingness to listen and offerings of encouragement have made me feel at home. I am really grateful for all the advices and opportunities that she provided for my career development. It is no doubt that the past five years in her laboratory is the most vital experience in my life.

I appreciate the time and efforts spent by Professor Michael J. Welch and Professor John-Stephen Taylor serving as my research committee members and guiding me through the past five years. I thank them for their helpful direction, suggestions, and offering collaborations for this research. I also appreciate the time and efforts spent by Professor William E. Buhro, Professor Jay R. Turner, and Professor Suzanne Lapi reading and providing critical suggestions about my dissertation while serving on my defense committee.

I want to extend my deepest gratitude to Dr. Chong Cheng for spending time working together with me and helping me smoothly “merging” into polymer chemistry and nanotechnology. His insight in developing the systems and solving the problems are very enlightening; his earnest attitude towards science and his preciseness in doing research are worthy of great efforts to emulate.

Most of my Ph.D. researches involved close collaborations, across disciplines. I highly appreciate our PEN team members, especially Dr. Aviv Hagooly, Dr. Raffaella Rossin, Dr. Huafeng Fang, and Dr. Mikhail Y. Berezin, for their significant contributions to the results, for their invaluable discussions and suggestions, and for their hard work on proofreading and revising the manuscripts. Their help made my graduate research journey enjoyable and productive. I also would like to acknowledge the collaborations from Dr. Jinda Fan and Mr. Peng Lu.

I would like to thank all of the past and present Wooley group members for creating family-like laboratory environment to work and for offering friendship. I wish to express my deepest gratitude to Dr. Jinqi Xu, Dr. Yali Li, Dr. Zicheng Li, Dr. Andreas M. Nyström, Dr. Wenjun Du, Mr. Ke Zhang, Mr. Jun Ma, and Mr. Nam S. Lee for their collaborations and friendship.

I want to thank our Covidien collaborators Dr. Dennis A. Moore, Dr. William L. Neumann, Dr. John N. Freskos, Dr. Jeng J. Shieh and Dr. Richard B. Dorshow for offering collaborative opportunities and for providing generous supports.

Finally, I wish to express numerous thanks to my wife, Rui Wang, for her companionship across the country, for her understanding and sacrifice, and for her love and support. I owe her too much. I would like to say thanks to my parents for raising me up and giving their continuous love, to my sister for their unconditional love and support. Without their love, encouragement, and support, nothing here was possible.

TABLE OF CONTENTS

LIST OF FIGURES

Chapter 2

Chapter 3

Chapter 4

Chapter 7

LIST OF SCHEMES

LIST OF TABLES

GLOSSARY OF TERMS AND ABBREVIATIONS

AA	Acrylic acid
AIBN	2,2'-Azobisisobutyronitrile
AFM	Atomic force microscopy
ATRP	Atom transfer radical polymerization
CTA	Chain transfer agent
CHO	Chinese hamster ovary
DDMAT	*S*-1-Dodecyl-*S*′-(α,α′-dimethyl-α′′-acetic acid)trithiocarbonate
$\boldsymbol{D_{av}}$	Number-average particle diameter
$\boldsymbol{D_{\mathrm{h}}}$	Hydrodynamic diameter
DLS	Dynamic light scattering
DMF	*N*,*N*′-dimethylformamide
DOTA	1,4,7,10-Tetraazacyclodecane-N,N′,N′′,N′′′-tetraacetic acid
DP	Number-average degree of polymerization
DTPA	Diethylenetriaminepentaacetic acid
DTPS	4-(Dimethylamino)pyridinium 4-toluenesulfonate
EDCI	1-[3′-(Dimethylamino)propyl]-3-ethylcarbodiimide methiodide
EO	Ethylene oxide
FGT	Functional group transformation

FPLC Fast protein liquid chromatography

FRET Förster resonance energy transfer

GPC Gel permeation chromatography

HeLa Human cervix carcinoma

HOBT 1-Hydroxybenzotriazole

IR Infrared

KBr Potassium bromide

M_n Number-average molecular weight

mPEG Methoxy-terminated poly(ethylene glycol)

MWCO Molecular weight cut-off

N_{agg} Aggregation number

NAS *N*-acryloxysuccinimide

NIR Near-infrared

NMP Nitroxide-mediated polymerization

NP Nanoparticle

PAA Poly(acrylic acid)

PBS Phosphate buffer saline

PDI Polydispersity index

PEG Poly(ethylene glycol)

PEO Poly(ethylene oxide)

PET	Positron emission tomography
PNAS	Poly(*N*-acryloxysuccinimide)
PS/PSt	Polystyrene
PTA	Phosphotungstic acid
P*t*BA	Poly(*tert*-butyl acrylate)
PVBA	Poly(4-vinylbenzaldehyde)
QY	Quantum yield
RAFT	Reversible addition-fragmentation chain transfer
SCK	Shell crosslinked (knedel-like) nanoparticle
SEM	Scanning electron microscopy
St	Styrene
SUV	Standardized uptake value
TEM	Transmission electron microscopy
TFA	Trifluoacetic acid
T_g	Glass transition temperature
UV-vis	Ultraviolet-visible
VBA	4-Vinylbenzaldehyde
ζ	Zeta potential

Chapter 1

Introduction

The groundbreaking lecture by Richard Feynman in 1959,[1] "There's Plenty of Room at the Bottom", triggered the campaign to study and manipulate matters over atomic and/or molecular scale and opened the "Nano-window" to natural scientists. Different from conventional science and technology, in which the size of objects usually are below 0.1 nm, the targets of nanoscience and technology are focused onto the "things" from molecular-based assemblies and/or objects with size scales between 0.1 nm to 100 nm, as well as single atoms and molecules. During the past 50 years, through the efforts and devotions from several generations of scientific researchers, nanoscience and technology have achieved significant innovations in academic and industrial laboratories, across disciplines, and become a robust and well-accepted scientific field.[2, 3] Meanwhile, profound impacts of nanoscience and technology have been growing explosively worldwide in the manufacturing and R&D areas such as miniaturization of electronic and memory devices, design and synthesis of more robust and efficient catalysts, development of more accurate and effective diagnostic procedures, and exploration of more potent drugs with "smart" abilities to recognize and attack only the diseased sites.

In modern nanotechnology, there are two basic approaches to realize the syntheses of nanostructures, the *Top-down* and *Bottom-up* approaches. The *Top-down* approach is based on physics and lithography techniques,[4-10] while the *Bottom-up* is mainly influenced by chemical principles.[11-18] Both approaches provide specific

capacities that can be implemented by the other.[19-23] However, the relatively broader substrate scope and more precise tuning of chemical binding strength and orientations offer extra driving forces for the *Bottom-up* approach to evolve and advance nanotechnology.

The self assembly of amphiphilic polypeptides into proteins with intricate supramolecular structures and variety of functionalities represents one of the elegant manners in constructing complex assembles by Nature. This phenomenon inspired scientists to exploit nano-scale material mimics having unique optical, electric, catalytic, and biological properties.[24, 25] Utilizing synthetic amphiphiles as assembly components, many nanostructures ranging from atomic to supramolecular dimensions have been assembled through weak non-covalent interactions, which included van der Waals, electrostatic, hydrophobic interactions, hydrogen and coordination bonds,[26-30] *via* a balanced reversible process.[31-33] These nano-assembles exhibited diverse non-spherical morphologies, such as belt,[34] cylinder,[35] fiber,[36-39] helix[40-42], lamella[43], and vesicle,[44-46] depending upon the intrinsic compositions and physical properties of the amphiphiles and the assembly conditions.

Among the synthetic amphiphiles, amphiphilic block copolymers have gained significant attentions recently by both academic and industry investigators.[47-49] In contrast to small surfactants, the amphiphilic block copolymer systems exhibit the following advantages: the facile tuning of dimensions, compositions, and components; the easier introduction of functionalities; the much larger phase segregation tendency;[50, 51] the significantly slower assembly kinetics;[52] and the enhanced robustness and morphological variation of resulting structures. Amphiphilic block copolymers can

construct a wide range of supramacromolecular assemblies including conventional morphologies like spheres (the most common morphology), cylinders/worms[53-59] and vesicles,[60-70] and many other novel morphologies such as bamboos,[71] bowls,[72] discs,[73] helices,[74] and toroids.[75] Moreover, the spherical micelles can undergo higher-order segregation in inter- and/or intra-micellar fashion to create Janus,[76-78] multicompartment,[79-81] and onion[82, 83] micelles. The versatility in composition and assembly behaviors offer a rich selection of building blocks for the construction of nanostructured materials as well as their use in biomedical and catalytic applications.

Advances in living polymerization techniques, especially in the development of controlled radical polymerizations (CRP)[84] have dramatically improved the availability of well-defined block polymers, thereby facilitating the numbers and types of nanoassemblies that can be prepared and studied. Using different CRP techniques, atom transfer radical polymerization (ATRP),[85, 86] nitroxide-mediated radical polymerization (NMP),[87, 88] and reversible addition-fragmentation chain transfer (RAFT) polymerization,[89-91] various kinds of polymers having narrow molecular weight distributions, controlled architectures, and low polydispersities can be produced. Moreover, CRP realizes better tolerance of functionalities during the polymerization process, which enables the facile preparation of functional polymers allowing for post-modifications.[92]

The heightened impact of nanotechnology in healthcare generates a specific filed ─ Nanomedicine,[93-100] the medical applications of nanotechnology to improve the properties of existing therapeutic and diagnostic modalities and to establish novel modalities for diagnostics, treatment, and therapy of diseases. Block copolymer

micelles[101-105] and vesicles[104, 106-109] have already been widely applied in nanomedicine and found promising applications in both therapeutic agent delivery and diagnostics. However, both self-assembled entities are equilibrium products formed in solution and under diluted conditions (concentrations below the critical micelle/vesicle concentrations, which usually at the order of 10^{-7} M), their ordered structures will collapse and re-organization of the unimer (amphiphilic block copolymer precursor) will occur. Covalent[110-115] and non-covalent[116] crosslinkings have been introduced to micellar assemblies to enforce the structural stability of and obviate the self correction. Several new classes of materials termed shell crosslinked (SCK) nanoparticles and core crosslinked (CCK) nanoparticles have been constructed, depending upon the location inside the micellar structure where the crosslinking reaction is conducted. The same strategy has also been applied to vesicular structures where the crosslinking was confined into the wall domains.[70, 117-119]

The advantage of crosslinking is not limited only for providing robust nanostructures. Recent reports highlighted that core crosslinking could enhance the cargo "holding" ability of nanostructures[120] and the increasing of shell crosslinking extents prolonged the blood retention time of nanoparticles.[121] Moreover, functionalized nanostructures can be directly derived by using crosslinkers bearing diverse functionalities,[122, 123] in addition to their structural roles. This dissertation is focused on the design, synthesis, and characterization of functionalizable crosslinked nanostructures (micelles and vesicles) bearing characteristics allowed for chemoselective modification and their utilizations as nanoplatforms for molecular imagings.

Previous studies on shell crosslinked knedel-like nanoparticle (SCKs) suggest that these materials can serve as good templates for biomedical applications.[124] To render the SCKs functional, post-modification of pre-established SCKs with functionalities stands a versatile and straightforward method that allows for multiple numbers and types of ligands to be attached onto a well-defined scaffold.[125-127] However, the reaction efficiency usually suffers a variety of factors, especially the steric and electrostatic factors, due to the fact that most of the SCK modification reactions are conducted in aqueous media. As found during the study of post-functionalization of SCKs with DOTA (1,4,7,10-tetraazocyclododecane-*N,N′,N″,N‴*-tetraacetic acid) derivatives having different features, even a "tiny" structural difference (one carboxylate and 4 atoms) caused *ca.* 7- to 10-fold of reaction efficiency variations.[128] **Chapter 2** of this dissertation is focus on the development of new synthetic strategy for preparation of SCK nanoparticles having "high-dense" functionalities as potential positron emission tomography (PET) imaging[129-132] contrast agents through *Bottom-up* pathway. The DOTA-functionalized SCKs in **chapter 2** were constructed through a "pre-grafting" approach, which involved coupling the functionalities to amphiphilic block copolymer precursor before assembly into nanostructures, in order to reduce the complexity of nanostructure functionalization. This strategy provided easier quantification of functionalities per nanostructure, but also was demonstrated as a facile and effective methodology for incorporation of highly sensitive *in vivo* PET tracers into nanoscale frameworks to allow for administration of low doses *in vivo*.

The determination of the *in vivo* distribution of nanoparticulate carriers following systemic administration and the development of imaging modalities for visualizing the

biodistribution over time take top priority in nanomedicine.[133] In **chapter 3**, monomethoxy-terminated poly(ethylene glycol) (mPEG) and radionuclide ^{64}Cu chelator were sequentially installed onto the block copolymer precursor prior to assembly and crosslinking to afford SCK nanoparticles with different surface characteristics. The *in vivo* fates of these SCKs were then evaluated through the combination of biodistribution and PET imaging techniques. This study represented extension of applying the "pre-grafting" strategy for construction of multifarious nanostructures having quantifiable functionalities, but also demonstrated the biodistributions of nanovectors can be manipulated in tunable fashion. A semi-quantitative model of the density of mPEG surface coverage as a function of *in vivo* behavior was applied to enhance the understanding of this system. The distance between exposed mPEG molecules on nanoparticle surface was found to determine the blood retention time of the corresponding SCK nanoparticles through opposing blood protein absorption mechanism and the calculated results were consistent with the theoretical predictions proposed by de Gennes and co-workers.[134, 135]

Because the general methodology for the preparation of SCKs involves crosslinking reactions between polymer chain segments that constitute the corona of block copolymer micelles, the nature of the crosslinking agent and the degree to which crosslinking is conducted allows for tuning of the SCK surface characteristics and the shell permeability. In fact, the phenomena that higher crosslinking extent caused a reduction of the radiolabeling efficiency (**chapter 2**), but benefited the *in vivo* fate (**chapter 3**) have already been noticed. Therefore, a precise balance between the above issues needs to be managed for developing SCK nanoparticles as potential imaging

agents. Research presented in c**hapter 4** describes the fundamental investigations for exploring the incorporation efficiencies of crosslinkers into the shells of block copolymer micelles, which further determines the actual crosslinking extents, by utilizing pyrazine-based crosslinkers as reporting probes. In order to minimize other factors related with the carbodiimide-mediated amidation, the block copolymer micelles were made to carry pre-installed reactive functionalities (*N*-acryloxysuccinimide, NAS) along the central block of amphiphilic triblock copolymer as amidation sites. It was revealed that the incorporation/crosslinking efficiencies were dependent upon the intrinsic properties of crosslinker, the conditions used for crosslinking, and the applied stoichiometries. In the meantime, unique photo-physical properties of the optical-active SCKs at lower crosslinking extents (13% to 20%) were observed. Compared with the crosslinkers as small molecules, the maximum absorption peaks of SCKs exhibited blue-shifts of *ca.* 35 to 40 nm. More interestingly, SCKs showed dual emissions of the fluorescence (498 nm and 555 nm, respectively) while the fluorogenic probes only afforded single emissions at 555 nm without the internal nanostructure environment.

Chapter 5 depicts the development of well-defined homopolymer and block copolymer systems bearing pendant benzaldehyde functionalities through RAFT polymerizations. The motivation of this work comes from the intrinsic reactivity of benzaldehyde, one of the most reactive and diverse electrophiles that undergoes reaction under mild conditions. By taking advantage of the higher functional group tolerance in RAFT polymerization, poly(4-vinyl benzaldehyde)s (PVBA) with controlled number-average molecular weight (M_n) and low polydispersity ($PDI < 1.17$) were obtained. The controlled characteristic of the RAFT polymerization process was confirmed by the

linearity between the M_n values of PVBA and monomer conversions. Well-defined PVBA was further used as a macromolecular chain transfer agent (macro-CTA) in RAFT polymerization of styrene (St), and a block copolymer PVBA-*b*-PSt with relatively low polydispersity (*PDI* = 1.20) was successfully synthesized.

Work towards biological applications of nanoscale objects with PVBA as reactive hydrophobic block segments continues in **chapter 6** and **chapter 7**. **Chapter 6** illustrates the aqueous describe assembly of block copolymer poly(ethylene oxide)-*block*-poly(4-vinyl benzaldehyde) precursors into polymeric vesicles with tunable sizes and the following chemoselctive post-modifications through the reductive amination chemistry. Different from most literature reported[60-70] *AB* diblock copolymer precursors (*A* represents for the hydrophilic block segment while *B* for the hydrophobic segment) for preparing vesicular nanostructures, in which a longer hydrophobic *B* block segment was required, the unimer used in this study, PEO_{45}-*b*-$PVBA_{26}$, had a relative shorter *B* block. The morphology transformation during vesiculation process was investigated and variations from traditional trend (sphere-rod-vesicle), including the forming of vesicles at lower water contents and the "absence" of rods, were noticed from the transmission electron microscopy (TEM) measurements. It was also found that small vesicles could be obtained from the same block copolymer precursor through a "kinetic trapping" protocol, as characterized through a combination of TEM and dynamic light scattering (DLS). The reactivity of the benzaldehyde functionalities was verified by crosslinking the vesicles, and also by a one-pot sequential functionalization and crosslinking approach to further render the vesicles fluorescent, each *via* reductive amination. *In vitro* studies found these labelled vesicles underwent cell membrane associations, as indicated by the confocal

microscopy, which might be related with the interactions between the membrane proteins and the leftover aldehydes.

The last research part of this dissertation (**chapter 7**) introduces the model-predictable optimizations of luminescence efficiency (quantum yield, QY) of fluorescent nanomaterials for the core crosslinked micelles, prepared from PEO-*b*-PVBA through the established one-pot sequential functionalization and crosslinking protocol. Both the experimental and model-predicted data revealed that the nanoparticle QY was related with the dye "loading" stoichiometry and the size of core domain. These two factors determined the distance between adjacent fluorophores, which further decided the extent of non-radiatively transferred energy.

This introduction has encompassed the successes and complications in attempting to develop functionalized crosslinked nanostructures which exhibit selective biological activities, interesting optical properties and other physicochemical properties that are being exploited for tissue selective imaging applications *in vivo*. Moreover, the fundamental strategy behind this dissertation, *i.e.*, synthesizing well-defined amphiphilic block copolymers bearing diverse functionalities; following by assembly the resulting precursors into polymeric nanoscopic objects with various morphologies; and subsequently exerting internal and/or external functionalization/crosslinking through varying methodologies to achieve discrete functional nanomaterials with improved robustness and stability, will remain on the forefront of nanotechnology field.

References

1. Feynman, R. P. "There's Plenty of Room at the Bottom", *Eng. Sci.* **1960**, *23(5)*, 22-36.

2. *Handbook of nanoscience, engineering, and technology,* 2nd ed.; Goddard III, W. A., Brenner, D. W., Lyshevski, S. E., Iafrate, G. J., Eds.; CRC Press: Boca Raton, 2007.

3. *Handbook of Nanotechnology,* 2nd ed.; Bhushan, B., Ed.; Springer: Berlin, 2007.

4. Menard, E.; Meitl, M. A.; Sun, Y.; Park, J.-U.; Shir, D. J.-L.; Nam, Y.-S.; Jeon, S.; Rogers, J. A. "Micro- and Nanopatterning Techniques for Organic Electronic and Optoelectronic Systems", *Chem. Rev.* **2007**, *107(4)*, 1117-1160.

5. Randall, C. L.; Leong, T. G.; Bassik, N.; Gracias, D. H. "3D lithographically fabricated nanoliter containers for drug delivery", *Adv. Drug Delivery Rev.* **2007**, *59(15)*, 1547-1561.

6. Salaita, K.; Wang, Y.; Mirkin, C. A. "Applications of dip-pen nanolithography", *Nat. Nanotechnol.* **2007**, *2(3)*, 145-155.

7. Gratton, S. E. A.; Williams, S. S.; Napier, M. E.; Pohlhaus, P. D.; Zhou, Z.; Wiles, K. B.; Maynor, B. W.; Shen, C.; Olafsen, T.; Samulski, E. T.; DeSimone, J. M. "The Pursuit of a Scalable Nanofabrication Platform for Use in Material and Life Science Applications", *Acc. Chem. Res.* **2008**, *41(12)*, 1685-1695.

8. Nie, Z.; Kumacheva, E. "Patterning surfaces with functional polymers", *Nat. Mater.* **2008**, *7(4)*, 277-290.

9. Xu, Q.; Rioux Robert, M.; Dickey Michael, D.; Whitesides George, M. "Nanoskiving: a new method to produce arrays of nanostructures", *Acc. Chem. Res.* **2008**, *41(12)*, 1566-77.

10. Cavallini, M.; Albonetti, C.; Biscarini, F. "Nanopatterning soluble multifunctional materials by unconventional wet lithography", *Adv. Mater.* **2009**, *21(10-11)*, 1043-1053.

11. Chaterji, S.; Kwon, I. K.; Park, K. "Smart polymeric gels: Redefining the limits of biomedical devices", *Prog. Polym. Sci.* **2007**, *32(8-9)*, 1083-1122.

12. Lu, W.; Lieber, C. M. "Nanoelectronics from the bottom up", *Nat. Mater.* **2007**, *6(11)*, 841-50.

13. Perepichka, D. F.; Rosei, F. "Metal nanoparticles: from "artificial atoms" to "artificial molecules"", *Angew. Chem., Int. Ed.* **2007**, *46(32)*, 6006-6008.

14. Sada, K.; Takeuchi, M.; Fujita, N.; Numata, M.; Shinkai, S. "Post-polymerization of preorganized assemblies for creating shape-controlled functional materials", *Chem. Soc. Rev.* **2007**, *36(2)*, 415-435.

15. Xu, H.; Srivastava, S.; Rotello, V. M. "Nanocomposites based on hydrogen bonds", *Adv. Polym. Sci.* **2007**, *207*, 179-198.

16. Bonderer, L. J.; Studart, A. R.; Gauckler, L. J. "Bioinspired Design and Assembly of Platelet Reinforced Polymer Films", *Science* **2008**, *319(5866)*, 1069-1073.

17. Tait, S. L. "Function Follows Form: Exploring Two-Dimensional Supramolecular Assembly at Surfaces", *ACS Nano* **2008**, *2(4)*, 617-621.

18. Zabet-Khosousi, A.; Dhirani, A.-A. "Charge Transport in Nanoparticle Assemblies", *Chem. Rev.* **2008**, *108(10)*, 4072-4124.

19. Cheng, J. Y.; Ross, C. A.; Smith, H. I.; Thomas, E. L. "Templated self-assembly of block copolymers: top-down helps bottom-up", *Adv. Mater.* **2006**, *18(19)*, 2505-2521.

20. Black, C. T. "Polymer Self-Assembly as a Novel Extension to Optical Lithography", *ACS Nano* **2007**, *1(3)*, 147-150.

21. Darling, S. B. "Directing the self-assembly of block copolymers", *Prog. Polym. Sci.* **2007**, *32(10)*, 1152-1204.

22. Huck, W. T. S. "Self-assembly meets nanofabrication: recent developments in microcontact printing and dip-pen nanolithography", *Angew. Chem., Int. Ed.* **2007**, *46(16)*, 2754-2757.

23. Segalman, R. A. "Directing Self-Assembly Toward Perfection", *Science* **2008**, *321(5891)*, 919-920.

24. Pelesko, J. A., *Self Assembly: The science of things that put themselves together*. Chapman & Hall/CRC: Boca Raton, 2007.

25. Lee, Y. S., *Self-assembly and Nanotechnology: A force balance approach*. John Wiley & Sons: Hoboken, 2007.

26. Raymo, F. M.; Bartberger, M. D.; Houk, K. N.; Stoddart, J. F. "The magnitude of [C−H···O] hydrogen bonding in molecular and supramolecular assemblies", *J. Am. Chem. Soc.* **2001**, *123(38)*, 9264-9267.

27. Tsonchev, S.; Schatz, G. C.; Ratner, M. A. "Hydrophobically-driven self-assembly: A geometric packing analysis", *Nano Lett.* **2003**, *3(5)*, 623-626.

28. Stendahl, J. C.; Rao, M. S.; Guler, M. O.; Stupp, S. I. "Intermolecular forces in the self-assembly of peptide amphiphile nanofibers", *Adv. Funct. Mater.* **2006**, *16(4)*, 499-508.

29. Schatz, G. C. "Using theory and computation to model nanoscale properties", *Proc. Natl. Acad. Sci. USA* **2007**, *104(17)*, 6885-6892.

30. Chen, C. L.; Zhang, P. J.; Rosi, N. L. "A new peptide-based method for the design and synthesis of nanoparticle superstructures: Construction of highly ordered gold nanoparticle double helices", *J. Am. Chem. Soc.* **2008**, *130(41)*, 13555-13557.

31. Lehn, J.-M. "Toward Self-Organization and Complex Matter", *Science* **2002**, *295(5564)*, 2400-2403.

32. Whitesides, G. M.; Grzybowski, B. "Self-Assembly at All Scales", *Science* **2002**, *295(5564)*, 2418-2421.

33. Hamley, I. W. "Nanotechnology with Soft Materials", *Angew. Chem., Int. Ed.* **2003**, *42(15)*, 1692-1712.

34. Cui, H.; Muraoka, T.; Cheetham, A. G.; Stupp, S. I. "Self-Assembly of Giant Peptide Nanobelts", *Nano Lett.* **2009**, *9(3)*, 945-951.

35. Prehm, M.; Liu, F.; Baumeister, U.; Zeng, X. B.; Ungar, G.; Tschierske, C. "The Giant-Hexagon cylinder network - A liquid-crystalline organization formed by a T-shaped quaternary amphiphile", *Angew. Chem., Int. Ed.* **2007**, *46(42)*,7972-7975.

36. Hartgerink, J. D.; Beniash, E.; Stupp, S. I. "Self-assembly and mineralization of peptide-amphiphile nanofibers", *Science* **2001**, *294(5547)*, 1684-1688.

37. Velonia, K.; Rowan, A. E.; Nolte, R. J. M. "Lipase Polystyrene Giant Amphiphiles", *J. Am. Chem. Soc.* **2002**, *124(16)*, 4224-4225.

38. Guler, M. O.; Stupp, S. I. "A self-assembled nanofiber catalyst for ester hydrolysis", *J. Am. Chem. Soc.* **2007**, *129(40)*, 12082-12083.

39. Shao, H.; Parquette, J. R. "Controllable Peptide-Dendron Self-Assembly: Interconversion of Nanotubes and Fibrillar Nanostructures", *Angew. Chem., Int. Ed.* **2009**, *48(14)*, 2525-2528.

40. Berl, V.; Huc, I.; Khoury, R. G.; Krische, M. J.; Lehn, J. M. "Interconversion of single and double helices formed from synthetic molecular strands", *Nature* **2000**, *407(6805)*, 720-723.

41. Percec, V.; Dulcey, A. E.; Balagurusamy, V. S. K.; Miura, Y.; Smidrkal, J.; Peterca, M.; Nummelin, S.; Edlund, U.; Hudson, S. D.; Heiney, P. A.; Hu, D. A.; Magonov, S. N.; Vinogradov, S. A. "Self-assembly of amphiphilic dendritic dipeptides into helical pores", *Nature* **2004**, *430(7001)*, 764-768.

42. Iwaura, R.; Hoeben, F. J. M.; Masuda, M.; Schenning, A.; Meijer, E. W.; Shimizu, T. "Molecular-level helical stack of a nucleotide-appended oligo(p-phenylenevinylene) directed by supramolecular self-assembly with a complementary oligonucleotide as a template", *J. Am. Chem. Soc.* **2006**, *128(40)*, 13298-13304.

43. Lamm, M. S.; Rajagopal, K.; Schneider, J. P.; Pochan, D. J. "Laminated morphology of nontwisting beta-sheet fibrils constructed via peptide self-assembly", *J. Am. Chem. Soc.* **2005**, *127(47)*, 16692-16700.

44. Holowka, E. P.; Pochan, D. J.; Deming, T. J. "Charged polypeptide vesicles with controllable diameter", *J. Am. Chem. Soc.* **2005**, *127(35)*, 12423-12428.

45. Yan, X. H.; He, Q.; Wang, K. W.; Duan, L.; Cui, Y.; Li, J. B. "Transition of cationic dipeptide nanotubes into vesicles and oligonucleotide delivery", *Angew. Chem., Int. Ed.* **2007**, *46(14)*, 2431-2434.

46. Schatz, C.; Louguet, S.; Le Meins, J. F.; Lecommandoux, S. "Polysaccharide-block-polypeptide Copolymer Vesicles: Towards Synthetic Viral Capsids", *Angew. Chem., Int. Ed.* **2009**, *48(14)*, 2572-2575.

47. *Block Copolymers*; Calleja, F. J. B., Roslaniec, Z., Eds.; Marcel Dekker: New York, 2000.

48. *Block copolymers: Synthetic strategies, physical properties and applications*; Hadjichristidis, N., Pispas., Floudas, G., Eds.; Wiley-Interscience: New York, 2003.

49. *Block Copolymers in Nanoscience*; Lazzari, M., Liu, G., Lecommandoux, S., Eds.; Wiley-VCH: Weinheim, 2006.

50. De Gennes, P. G., *Scaling concerpts in polymer physics*. Cornell University Press: Ithaca, 1979.

51. Hamley, I. W., *Block Copolymers in Solution: Fundamentals and Applications*. John Wiley & Sons: West Sussex, 2005.

52. Hashimoto, T. ""Mechanics" of molecular assembly: Real-time and in-situ analysis of nano-to-mesoscopic scale hierarchical structures and nonequilibrium phenomena", *Bull. Chem. Soc. Jpn.* **2005**, *78(1)*, 1-39.

53. Won, Y.-Y.; Davis, H. T.; Bates, F. S. "Giant Wormlike Rubber Micelles", *Science* **1999**, *283(5404)*, 960-963.

54. Geng, Y.; Discher, D. E. "Hydrolytic Degradation of Poly(ethylene oxide)-*block*-Polycaprolactone Worm Micelles", *J. Am. Chem. Soc.* **2005**, *127(37)*, 12780-12781.

55. Cui, H.; Chen, Z.; Zhong, S.; Wooley, K. L.; Pochan, D. J. "Block Copolymer Assembly via Kinetic Control", *Science* **2007**, *317(5838)*, 647-650.

56. Wang, X.; Guerin, G.; Wang, H.; Wang, Y.; Manners, I.; Winnik, M. A. "Cylindrical Block Copolymer Micelles and Co-Micelles of Controlled Length and Architecture", *Science* **2007**, *317(5838)*, 644-647.

57. Njikang, G.; Han, D.; Wang, J.; Liu, G. "ABC Triblock Copolymer Micelle-Like Aggregates in Selective Solvents for A and C", *Macromolecules* **2008**, *41(24)*, 9727-9735.

58. Saito, N.; Liu, C.; Lodge, T. P.; Hillmyer, M. A. "Multicompartment Micelles from Polyester-Containing ABC Miktoarm Star Terpolymers", *Macromolecules* **2008**, *41(22)*, 8815-8822.

59. Zhu, J.; Hayward, R. C. "Wormlike Micelles with Microphase-Separated Cores from Blends of Amphiphilic AB and Hydrophobic BC Diblock Copolymers", *Macromolecules* **2008**, *41(21)*, 7794-7797.

60. Zhang, L.; Eisenberg, A. "Multiple Morphologies and Characteristics of "Crew-Cut" Micelle-like Aggregates of Polystyrene-*b*-poly(acrylic acid) Diblock Copolymers in Aqueous Solutions", *J. Am. Chem. Soc.* **1996**, *118(13)*, 3168-3181.

61. Ding, J.; Liu, G. "Water-Soluble Hollow Nanospheres as Potential Drug Carriers", *J. Phys. Chem. B* **1998**, *102(31)*, 6107-6113.

62. Discher, B. M.; Won, Y.-Y.; Ege, D. S.; Lee, J. C. M.; Bates, F. S.; Discher, D. E.; Hammer, D. A. "Polymersomes: Tough vesicles made from diblock copolymers", *Science* **1999**, *284(5417)*, 1143-1146.

63. Napoli, A.; Valentini, M.; Tirelli, N.; Muller, M.; Hubbell, J. A. "Oxidation-responsive polymeric vesicles", *Nat. Mater.* **2004**, *3(3)*, 183-189.

64. Power-Billard, K. N.; Spontak, R. J.; Manners, I. "Redox-Active Organometallic Vesicles: Aqueous Self-Assembly of a Diblock Copolymer with a Hydrophilic Polyferrocenylsilane Polyelectrolyte Block", *Angew. Chem., Int. Ed.* **2004**, *43(10)*, 1260-1264.

65. Koide, A.; Kishimura, A.; Osada, K.; Jang, W. D.; Yamasaki, Y.; Kataoka, K. "Semipermeable Polymer Vesicle (PICsome) Self-Assembled in Aqueous Medium from a Pair of Oppositely Charged Block Copolymers: Physiologically Stable Micro-/Nanocontainers of Water-Soluble Macromolecules", *J. Am. Chem. Soc.* **2006**, *128(18)*, 5988-5989.

66. Li, Y.; Lokitz, B. S.; McCormick, C. L. "Thermally responsive vesicles and their structural "locking" through polyelectrolyte complex formation", *Angew. Chem., Int. Ed.* **2006**, *45(35)*, 5792-5795.

67. Qin, S.; Geng, Y.; Discher, D. E.; Yang, S. "Temperature-controlled assembly and release from polymer vesicles of poly(ethylene oxide)-*block*-poly(N-isopropylacrylamide)", *Adv. Mater.* **2006**, *18(21)*, 2905-2909.

68. Zheng, R.; Liu, G. "Water-Dispersible Oil-Filled ABC Triblock Copolymer Vesicles and Nanocapsules", *Macromolecules* **2007**, *40(14)*, 5116-5121.

69. Pasparakis, G.; Alexander, C. "Sweet talking double hydrophilic block copolymer vesicles", *Angew. Chem., Int. Ed.* **2008**, *47(26)*, 4847-4850.

70. Walther, A.; Goldmann, A. S.; Yelamanchili, R. S.; Drechsler, M.; Schmalz, H.; Eisenberg, A.; Muller, A. H. E. "Multiple Morphologies, Phase Transitions, and Cross-Linking of Crew-Cut Aggregates of Polybutadiene-block-poly(2-vinylpyridine) Diblock Copolymers", *Macromolecules* **2008**, *41(9)*, 3254-3260.

71. Chen, T.; Wang, L.; Jiang, G.; Wang, J.; Wang, X. j.; Zhou, J.; Wang, W.; Gao, H. "Large-size bamboo-shape nanotube from self-assembly of poly(ferrocenyldimethylsilane-*b*-dimethylsiloxane) block copolymer", *Polymer* **2005**, *46(18)*, 7585-7589.

72. Liu, X.; Kim, J.-S.; Wu, J.; Eisenberg, A. "Bowl-Shaped Aggregates from the Self-assembly of an Amphiphilic Random Copolymer of Poly(styrene-*co*-methacrylic acid)", *Macromolecules* **2005**, *38(16)*, 6749-6751.

73. Li, Z.; Chen, Z.; Cui, H.; Hales, K.; Qi, K.; Wooley, K. L.; Pochan, D. J. "Disk Morphology and Disk-to-Cylinder Tunability of Poly(Acrylic Acid)-*b*-Poly(Methyl Acrylate)-*b*-Polystyrene Triblock Copolymer Solution-State Assemblies", *Langmuir* **2005**, *21(16)*, 7533-7539.

74. Zhong, S.; Cui, H.; Chen, Z.; Wooley, K. L.; Pochan, D. J. "Helix self-assembly through the coiling of cylindrical micelles", *Soft Matter* **2008**, *4(1)*, 90-93.

75. Pochan, D. J.; Chen, Z. Y.; Cui, H. G.; Hales, K.; Qi, K.; Wooley, K. L. "Toroidal triblock copolymer assemblies", *Science* **2004**, *306(5693)*, 94-97.

76. Erhardt, R.; Boker, A.; Zettl, H.; Kaya, H.; Pyckhout-Hintzen, W.; Krausch, G.; Abetz, V.; Muller, A. H. E. "Janus Micelles", *Macromolecules* **2001**, *34(4)*, 1069-1075.

77. Erhardt, R.; Zhang, M.; Boker, A.; Zettl, H.; Abetz, C.; Frederik, P.; Krausch, G.; Abetz, V.; Muller, A. H. E. "Amphiphilic Janus Micelles with Polystyrene and Poly(methacrylic acid) Hemispheres", *J. Am. Chem. Soc.* **2003**, *125(11)*, 3260-3267.

78. Voets, I. K.; Fokkink, R.; Hellweg, T.; King, S. M.; Waard, P. d.; Keizer, A. d.; Stuart, M. A. C. "Spontaneous symmetry breaking: formation of Janus micelles", *Soft Matter* **2009**, *5(5)*, 999-1005.

79. Li, Z.; Kesselman, E.; Talmon, Y.; Hillmyer, M. A.; Lodge, T. P. "Multicompartment Micelles from ABC Miktoarm Stars in Water", *Science* **2004**, *306(5693)*, 98-101.

80. Kubowicz, S.; Baussard, J. F.; Lutz, J. F.; Thünemann, A. F.; von Berlepsch, H.; Laschewsky, A. "Multicompartment Micelles Formed by Self-Assembly of Linear ABC Triblock Copolymers in Aqueous Medium", *Angew. Chem., Int. Ed.* **2005**, *44(33)*, 5262-5265.

81. Lodge, T. P.; Rasdal, A.; Li, Z.; Hillmyer, M. A. "Simultaneous, Segregated Storage of Two Agents in a Multicompartment Micelle", *J. Am. Chem. Soc.* **2005**, *127(50)*, 17608-17609.

82. Prochazka, K.; Martin, T. J.; Webber, S. E.; Munk, P. "Onion-Type Micelles in Aqueous Media", *Macromolecules* **1996**, *29(20)*, 6526-6530.

83. Talingting, M. R.; Munk, P.; Webber, S. E.; Tuzar, Z. "Onion-Type Micelles from Polystyrene-*block*-poly(2-vinylpyridine) and Poly(2-vinylpyridine)-*block*-poly(ethylene oxide)", *Macromolecules* **1999**, *32(5)*, 1593-1601.

84. Braunecker, W. A.; Matyjaszewski, K. "Controlled/living radical polymerization: Features, developments, and perspectives", *Prog. Polym. Sci.* **2007**, *32(1)*, 93-146.

85. Tsarevsky, N. V.; Matyjaszewski, K. ""Green" atom transfer radical polymerization: From process design to preparation of well-defined environmentally friendly polymeric materials", *Chem. Rev.* **2007**, *107(6)*, 2270-2299.

86. Matyjaszewski, K.; Xia, J. H. "Atom transfer radical polymerization", *Chem. Rev.* **2001**, *101(9)*, 2921-2990.

87. Hawker, C. J.; Bosman, A. W.; Harth, E. "New polymer synthesis by nitroxide mediated living radical polymerizations", *Chem. Rev.* **2001**, *101(12)*, 3661-3688.

88. Sciannamea, V.; Jerome, R.; Detrembleur, C. "In-situ nitroxide-mediated radical polymerization (NMP) processes: Their understanding and optimization", *Chem. Rev.* **2008**, *108(3)*, 1104-1126.

89. Perrier, S.; Takolpuckdee, P. "Macromolecular design via reversible addition-fragmentation chain transfer (RAFT)/Xanthates (MADIX) polymerization", *J. Polym. Sci. Part A: Polym. Chem.* **2005**, *43(22)*, 5347-5393.

90. Lowe, A. B.; McCormick, C. L. "Reversible addition-fragmentation chain transfer (RAFT) radical polymerization and the synthesis of water-soluble (co)polymers under homogeneous conditions in organic and aqueous media", *Prog. Polym. Sci.* **2007**, *32(3)*, 283-351.

91. Moad, G.; Rizzardo, E.; Thang, S. H. "Radical addition-fragmentation chemistry in polymer synthesis", *Polymer* **2008**, *49(5)*, 1079-1131.

92. Klok, H.-A.; Gibson, M. I.; Gauthier, M. A. "Post-Polymerization Modification", *Angew. Chem., Int. Ed.* **2009**, *48(1)*, 48-58.

93. Moghimi, S. M.; Hunter, A. C.; Murray, J. C. "Nanomedicine: current status and future prospects", *FASEB J.* **2005**, *19(3)*, 311-330.

94. Farokhzad, O. C.; Langer, R. "Nanomedicine: Developing smarter therapeutic and diagnostic modalities", *Adv. Drug Delivery Rev.* **2006**, *58(14)*, 1456-1459.

95. Liu, Y. Y.; Miyoshi, H.; Nakamura, M. "Nanomedicine for drug delivery and imaging: A promising avenue for cancer therapy and diagnosis using targeted functional nanoparticles", *Int. J. Cancer* **2007**, *120(12)*, 2527-2537.

96. Jain, K. K. "Nanomedicine: Application of nanobiotechnology in medical practice", *Med. Princ. Pract.* **2008**, *17(2)*, 89-101.

97. Venugopal, J.; Prabhakaran, M. P.; Low, S.; Choon, A. T.; Zhang, Y. Z.; Deepika, G.; Ramakrishna, S. "Nanotechnology for nanomedicine and delivery of drugs", *Curr. Pharm. Des.* **2008**, *14(22)*, 2184-2200.

98. Farokhzad, O. C.; Langer, R. "Impact of Nanotechnology on Drug Delivery", *ACS Nano* **2009**, *3(1)*, 16-20.

99. Riehemann, K.; Schneider, S. W.; Luger, T. A.; Godin, B.; Ferrari, M.; Fuchs, H. "Nanomedicine-Challenge and Perspectives", *Angew. Chem., Int. Ed.* **2009**, *48(5)*, 872-897.

100. Sandhiya, S.; Dkhar, S. A.; Surendiran, A. "Emerging trends of nanomedicine - an overview", *Fundam. Clin. Pharmacol.* **2009**, *23(3)*, 263-269.

101. Rosler, A.; Vandermeulen, G. W. M.; Klok, H. A. "Advanced drug delivery devices via self-assembly of amphiphilic block copolymers", *Adv. Drug Delivery Rev.* **2001**, *53(1)*, 95-108.

102. Lavasanifar, A.; Samuel, J.; Kwon, G. S. "Poly(ethylene oxide)-*block*-poly(L-amino acid) micelles for drug delivery", *Adv. Drug Delivery Rev.* **2002**, *54(2)*, 169-190.

103. Harada, A.; Kataoka, K. "Supramolecular assemblies of block copolymers in aqueous media as nanocontainers relevant to biological applications", *Prog. Polym. Sci.* **2006**, *31(11)*, 949-982.

104. Letchford, K.; Burt, H. "A review of the formation and classification of amphiphilic block copolymer nanoparticulate structures: micelles, nanospheres, nanocapsules and polymersomes", *Eur. J. Pharm. Biopharm.* **2007**, *65(3)*, 259-269.

105. Torchilin, V. P. "Micellar nanocarriers: Pharmaceutical perspectives", *Pharm. Res.* **2007**, *24(1)*, 1-16.

106. Blanazs, A.; Armes, S. P.; Ryan, A. J. "Self-Assembled Block Copolymer Aggregates: From Micelles to Vesicles and their Biological Applications", *Macromol. Rapid Commun.* **2009**, *30(4-5)*, 267-277.

107. Soussan, E.; Cassel, S.; Blanzat, M.; Rico-Lattes, I. "Drug Delivery by Soft Matter: Matrix and Vesicular Carriers", *Angew. Chem., Int. Ed.* **2009**, *48(2)*, 274-288.

108. Discher, D. E.; Ahmed, F. "Polymersomes", *Annu. Rev. Biomed. Eng.* **2006**, *8(1)*, 323-341.

109. Discher, D. E.; Ortiz, V.; Srinivas, G.; Klein, M. L.; Kim, Y.; Christian, D.; Cai, S.; Photos, P.; Ahmed, F. "Emerging applications of polymersomes in delivery: From molecular dynamics to shrinkage of tumors", *Prog. Polym. Sci.* **2007**, *32(8-9)*, 838-857.

110. Thurmond, K. B., II; Kowalewski, T.; Wooley, K. L. "Water-Soluble Knedel-like Structures: The Preparation of Shell-Cross-Linked Small Particles", *J. Am. Chem. Soc.* **1996**, *118(30)*, 7239-7240.

111. Huang, H.; Kowalewski, T.; Remsen, E. E.; Gertzmann, R.; Wooley, K. L. "Hydrogel-Coated Glassy Nanospheres: A Novel Method for the Synthesis of Shell Crosslinked Knedels", *J. Am. Chem. Soc.* **1997**, *119(48)*, 11653-11659.

112. Bütün, V.; Billingham, N. C.; Armes, S. P. "Synthesis of Shell Cross-Linked Micelles with Tunable Hydrophilic/Hydrophobic Cores", *J. Am. Chem. Soc.* **1998**, *120(46)*, 12135-12136.

113. Ding, J.; Liu, G. "Polystyrene-*block*-poly(2-cinnamoylethyl methacrylate) Nanospheres with Cross-Linked Shells", *Macromolecules* **1998**, *31(19)*, 6554-6558.

114. Sanji, T.; Nakatsuka, Y.; Ohnishi, S.; Sakurai, H. "Preparation of Nanometer-Sized Hollow Particles by Photochemical Degradation of Polysilane Shell Cross-Linked Micelles and Reversible Encapsulation of Guest Molecules", *Macromolecules* **2000**, *33(23)*, 8524-8526.

115. Zhang, Z.; Liu, G.; Bell, S. "Synthesis of Poly(solketal methacrylate)-*block*-poly(2-(dimethylamino)ethyl methacrylate) and Preparation of Nanospheres with Cross-Linked Shells", *Macromolecules* **2000**, *33(21)*, 7877-7883.

116. Chen, D.; Jiang, M. "Strategies for Constructing Polymeric Micelles and Hollow Spheres in Solution via Specific Intermolecular Interactions", *Acc. Chem. Res.* **2005**, *38(6)*, 494-502.

117. Discher, B. M.; Bermudez, H.; Hammer, D. A.; Discher, D. E.; Won, Y.-Y.; Bates, F. S. "Cross-linked Polymersome Membranes: Vesicles with Broadly Adjustable Properties", *J. Phys. Chem. B* **2002**, *106(11)*, 2848-2854.

118. Hales, M.; Barner-Kowollik, C.; Davis, T. P.; Stenzel, M. H. "Shell-Cross-Linked Vesicles Synthesized from Block Copolymers of Poly(D,L-lactide) and Poly(N-isopropyl acrylamide) as Thermoresponsive Nanocontainers", *Langmuir* **200**4, *20(25)*, 10809-10817.

119. Du, J.; Armes, S. P. "pH-Responsive Vesicles Based on a Hydrolytically Self-Cross-Linkable Copolymer", *J. Am. Chem. Soc.* **2005**, *127(37)*, 12800-12801.

120. Gao, H.; Jones, M.-C.; Chen, J.; Prud'homme, R. E.; Leroux, J.-C. "Core Cross-Linked Reverse Micelles from Star-Shaped Polymers", *Chem. Mater.* **2008**, *20(9)*, 3063-3067.

121. Sun, G.; Hagooly, A.; Xu, J.; Nystrom, A. M.; Li, Z.; Rossin, R.; Moore, D. A.; Wooley, K. L.; Welch, M. J. "Facile, Efficient Approach to Accomplish Tunable Chemistries and Variable Biodistributions for Shell Cross-Linked Nanoparticles", *Biomacromolecules* **2008**, *9(7)*, 1997-2006.

122. Joralemon, M. J.; O'Reilly, R. K.; Matson, J. B.; Nugent, A. K.; Hawker, C. J.; Wooley, K. L. "Dendrimers clicked together divergently", *Macromolecules* **2005**, *38(13)*, 5436-5443.

123. Lee, N. S.; Sun, G.; Neumann, W. L.; Freskos, J. N.; Shieh, J. J.; Dorshow, R. B.; Wooley, K. L. "Photonic Shell-Crosslinked Nanoparticle Probes for Optical Imaging and Monitoring", *Adv. Mater.* **2009**, *21(13)*, 1344-1348.

124. Li, Y.; Sun, G.; Xu, J.; Wooley, K. L., Shell crosslinked nanoparticles: A progress report of their design for drug delivery. In *Nanotechnology in Therapeutics: Current technology and applications*, Peppas, N. A.; Hilt, Z. J.; Thomas, B. J., Eds.; Horizon Bioscience: Wymondham, 2007; pp 381-407.

125. Becker, M. L.; Remsen, E. E.; Pan, D.; Wooley, K. L. "Peptide-Derivatized Shell-Cross-Linked Nanoparticles. 1. Synthesis and Characterization", *Bioconjugate Chem.* **2004**, *15(4)*, 699-709.

126. Pan, D.; Turner, J. L.; Wooley, K. L. "Shell Cross-Linked Nanoparticles Designed To Target Angiogenic Blood Vessels via $\alpha_v\beta_3$ Receptor-Ligand Interactions", *Macromolecules* **2004**, *37(19)*, 7109-7115.

127. Sun, X.; Rossin, R.; Turner, J. L.; Becker, M. L.; Joralemon, M. J.; Welch, M. J.; Wooley, K. L. "An Assessment of the Effects of Shell Cross-Linked Nanoparticle Size,

Core Composition, and Surface PEGylation on in Vivo Biodistribution", *Biomacromolecules* **2005**, *6(5)*, 2541-2554.

128. Xu, J.; Sun, G.; Rossin, R.; Hagooly, A.; Li, Z.; Fukukawa, K.-i.; Messmore, B. W.; Moore, D. A.; Welch, M. J.; Hawker, C. J.; Wooley, K. L. "Labeling of Polymer Nanostructures for Medical Imaging: Importance of Cross-Linking Extent, Spacer Length, and Charge Density", *Macromolecules* **2007**, *40(9)*, 2971-2973.

129. Phelps, M. E. "Positron emission tomography provides molecular imaging of biological processes", *Proc. Natl. Acad. Sci. USA* **2000**, *97(16)*, 9226-9233.

130. Weissleder, R.; Mahmood, U. "Molecular Imaging", *Radiology* **2001**, *219(2)*, 316-333.

131. Gambhir, S. S. "Molecular imaging of cancer with positron emission tomography", *Nat. Rev., Cancer* **2002**, *2(9)*, 683-693.

132. Lappin, G.; Garner, R. C. "Big Physics, small doses: The use of AMS and PET in human microdosing of development drugs", *Nat. Rev., Drug Discov.* **2003**, *2(3)*, 233-240.

133. Sanhai, W. R.; Sakamoto, J. H.; Canady, R.; Ferrari, M. "Seven challenges for nanomedicine", *Nat. Nanotech.* **2008**, *3(5)*, 242-244.

134. Jeon, S. I.; Lee, J. H.; Andrade, J. D.; De Gennes, P. G. "Protein-surface interactions in the presence of polyethylene oxide. I. Simplified theory", *J. Colloid Interface Sci.* **1991**, *142(1)*, 149-158.

135. Joen, S. I.; Andrade, J. D. "Prorein-surface interactions in the presence of polyethylene oxide. II. Effect of protein size", *J. Colloid Interface Sci.* **1991**, *142(1)*, 159-166.

Chapter 2

Strategies for Optimized Radiolabelling of Nanoparticles for *in vivo* PET Imaging

[Portions of this work have been published previously as Guorong Sun, Jinqi Xu, Aviv Hagooly, Raffaella Rossin, Zicheng Li, Dennis A. Moore, Craig J. Hawker, Michael J. Welch and Karen L. Wooley *Adv. Mater.* **2007**, *19(20)*, 3157-3162.]

Abstract

Driven by the motivation for optimizing ^{64}Cu radiolabelling efficiency of nanoparticles for *in vivo* PET imaging, a new strategy has been developed. This strategy involved a complete redesign of the nanoparticle system, utilizing macromolecular precursors that were pre-loaded with labelling sites and programmed for supramolecular assembly into discrete, functional nanoscale objects. A series of shell crosslinked nanoparticles (SCKs) have been constructed by grafting a copper chelating agent (DOTAlysine) onto amphiphilic block copolymers (PAA-*b*-PS), self assembling the functionalized block copolymer precursors into micelles, and crosslinking the micellar corona to afford the expected nanoobjects. These pre-DOTAlysine-SCKs showed impressive results on ^{64}Cu radiolabelling (~ 400 copper atoms per spherical nanoparticle).

Introduction

Among the molecular imaging modalities, positron emission tomography (PET) is widely used as a powerful diagnostic tool by clinicians and scientists.[1-3] Compared with other imaging methods, it bears the advantages of high sensitivity (the level of detection approaches 10^{-11} M of tracer) and isotropism (*i.e.*, ability to detect expression accurately, regardless of tissue depth), which provide reliability for quantitative imaging analyses of *in vivo* abnormalities. As the pharmaceutical industry began applying PET imaging for assisting drug discovery,[4-10] small animal PET scanners with spatial resolution up to 1 mm were developed and have been considered to be one of the major achievements for PET technology during the past two decades.[11] ^{64}Cu is an attractive radionuclide for PET imaging because of its suitable half-life ($t_{1/2}$ = 12.7 h) and positron emission energy (0.65 MeV), as well as the relatively convenient radiolabelling *via* coordination with specially designed ligands (chelators).[12-15] The formation of thermodynamically-stable metal complexes reduces the copper binding with plasma proteins which minimizes its non-specific background activity and its accumulation and resultant toxicity in the liver and kidney.[16] Under the present instrumental conditions, optimizations and improvements of the specific activity of radiopharmaceuticals are of special interest to ^{64}Cu-based PET systems for achieving high quality images even at low doses, especially when the targets can be readily saturated *in vivo*. One practical resolution is to encapsulate or conjugate the chelating agents with nanocarriers, which have already been utilized by many

research groups[17-21] including ourselves[22, 23] and have been found to exhibit exciting potential in both high loading capacities and re-direction of the bio-distributions of small molecule ligands (*e.g.* for tissue targeting) or guests (*e.g.* for pharmaceutical effect).[24]

Our research has focused upon shell crosslinked knedel-like nanoparticles (SCKs)[25] as the nanoscale framework for the attachment of macrocyclic chelators and labelling by ^{64}Cu radionuclides. SCKs have been established from the self assembly of amphiphilic block copolymers to afford micelles with core-shell morphology that are then covalently crosslinked throughout the shell domain. Recently, it was confirmed that by tuning the nanoparticle properties, especially the size and rigidity, increased *in vivo* circulation times and improved bio-distributions could be reached for ^{64}Cu-TETA SCK conjugates.[23] Although these preliminary results are promising, several challenges require further investigations. Among them, efficient radiolabelling takes the highest priority. Previously, the direct conjugation of macrocyclic chelators onto pre-established SCKs afforded limited coupling and radiolabelling yields, due to steric and electrostatic factors.[23, 26] As part of our ongoing efforts, we now report an alternative strategy to construct chelator-SCK conjugates with high radiolabelling efficiencies, which is expected to lead to nanoscale objects that can be administered in small quantities for ultra-sensitive PET imaging.

Results and Discussion

SCKs used in this study were comprised of polystyrene (PS) and poly(acrylic acid) (PAA), a particle composition previously demonstrated to have long blood circulation times[23] and characteristic low cytotoxicity and low immunogenicity when crosslinked with 2,2'-(ethylenedioxy)-bis(ethylamine).[27] The particle sizes were controlled by the relative balance of hydrophobic PS block length *vs.* the hydrophilic PAA segment.[28, 29] The amphiphilic block copolymer precursors (PAA-*b*-PS) were acquired *via* sequential living radical polymerization of *tert*-butyl acrylate and styrene, followed by acidolysis of the *tert*-butyl ester protecting groups. In all cases, the block copolymers had well-defined structures and narrow polydispersities (PDI < 1.20).

As shown in Scheme 2.1, a lysine derivative of 1,4,7,10-tetraazocyclododecane-*N,N',N'',N'''*-tetraacetic acid (DOTA), DOTAlysine, was grafted onto the amphiphilic PAA-*b*-PS block polymer precursors, with a fixed hydrophilic PAA segment length (DP_n = 60) and varied hydrophobic PS segment lengths (DP_n = 30, 60, 140). Conventional amidation chemistry was employed in organic solvent to afford *ca.* 65 to 75% isolated yield, for which the coupling yields were > 85%. After purification by dialysis against water and lyophilization, the numbers of DOTAlysines per polymer chain were determined by ^{1}H NMR spectroscopy analyses. For PAA_{60}-*b*-PS_{30} and PAA_{60}-*b*-PS_{60} block copolymers, the grafting numbers were 2, 4, and 7, for three different samples. Grafting more DOTAlysines (> 10 DOTAlysines/chain) was also attempted, but the

resulting DOTAlysine-*g*-copolymers suffered from poor solubility in organic solvents and generated nanoparticles with broad size distributions. The same problem was encountered for the PAA_{60}-*b*-PS_{140} after coupling 7 DOTAlysines, so only 2 and 4 DOTAlysines/chain were studied.

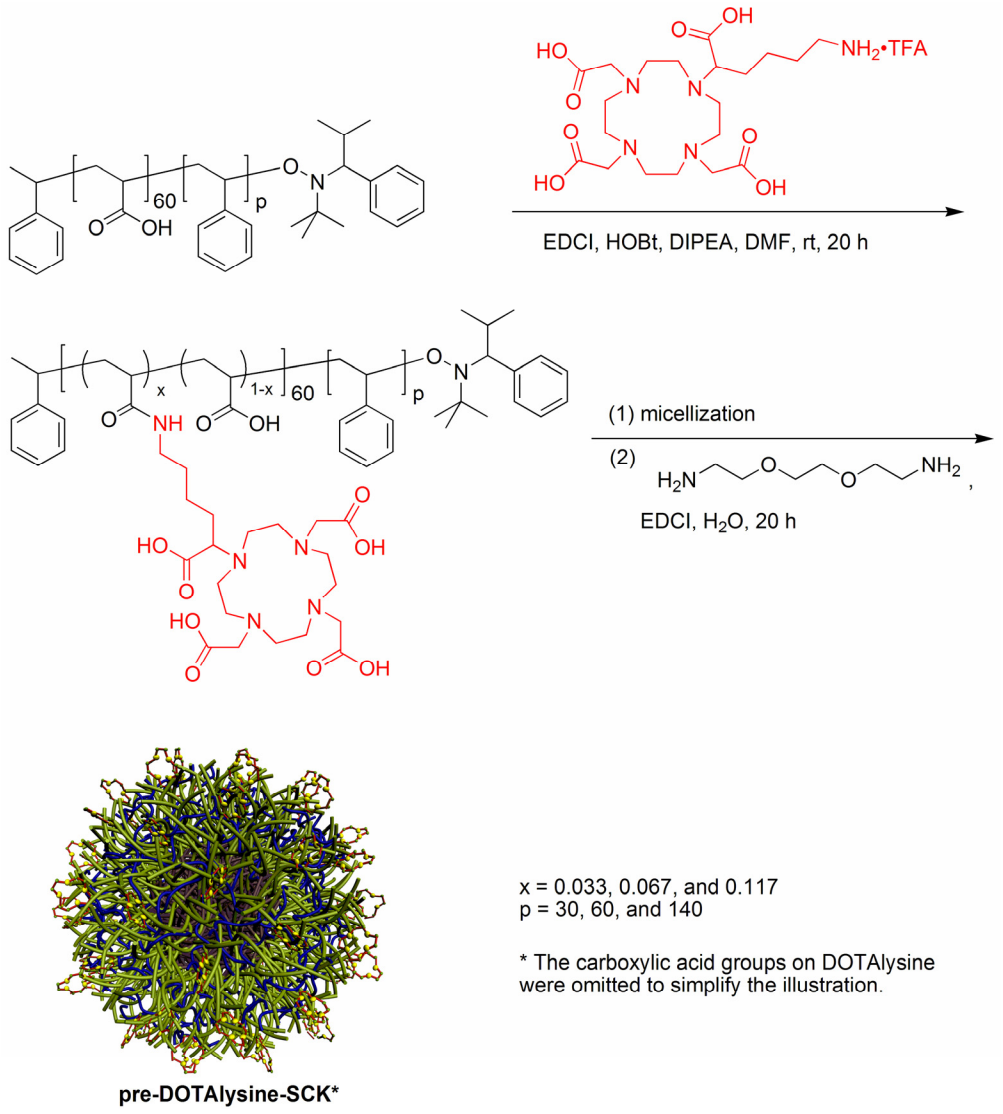

Scheme 2.1. A two-step synthetic route was developed for the preparation of pre-DOTAlysine-SCKs: (1) labelling of three different amphiphilic block copolymers, PAA_{60}-*b*-PS_p, with three different levels of DOTAlysine; (2) their self assembly into micelles in water and shell crosslinking to two different extents. Overall, eight micelles and sixteen SCKs resulted from this scheme (see also Table 2.1).

Each amphiphilic block copolymer was assembled into micelles in aqueous solution by a standard micellization protocol[30, 31] and crosslinked throughout the shell layer to differing degrees (20% and 50%, according to the chemical stoichiometry). A series of micelles and SCKs having different dimensions and shell properties (electrostatic character, permeability, and residual carboxylic acid concentrations) was obtained and characterized by dynamic light scattering (DLS) and transmission electron microscopy (TEM) (Table 2.1 and Figure 2.1).

Table 2.1. Characterization data for pre-DOTAlysine-SCKs and control SCK samples (lacking DOTA functionalities).

Sample[a] (Extents of Crosslinking)	$(D_h)_n$[b] (nm)	D_{av}[c] (nm)	(DOTAlysine$_m$-*g*-PAA$_n$)-*b*-PS$_p$			N_{agg}[e]
			m	n	p	
SCK1 (20%)	21 ± 3	11 ± 1	2	58	30	125
SCK2 (20%)	21 ± 3	16 ± 2	2	58	60	240
SCK3 (20%)	21 ± 6	11 ± 2	2	58	140	40
SCK4 (20%)	21 ± 3	12 ± 2[d]	4	56	30	160[d]
SCK5 (20%)	47 ± 7	19 ± 2[d]	4	56	60	340[d]
SCK6 (20%)	17 ± 2	11 ± 2	4	56	140	40
SCK7 (20%)	26 ± 6	11 ± 2	7	53	30	125
SCK8 (20%)	25 ± 6	19 ± 2	7	53	60	400
SCK9 (50%)	21 ± 3	11 ± 1	2	58	30	125
SCK10 (50%)	24 ± 3	16 ± 2	2	58	60	240
SCK11 (50%)	13 ± 4	12 ± 2	2	58	140	40
SCK12 (50%)	22 ± 4	15 ± 2[d]	4	56	30	160[d]
SCK13 (50%)	43 ± 5	18 ± 3[d]	4	56	60	340[d]
SCK14 (50%)	17 ± 4	13 ± 2	4	56	140	40
SCK15 (50%)	24 ± 5	11 ± 2	7	53	30	125
SCK16 (50%)	28 ± 4	19 ± 2	7	53	60	400
Control1 (50%)	18 ± 2	11 ± 1	0	60	30	125
Control2 (50%)	22 ± 1	17 ± 1	0	60	60	240
Control3 (50%)	34 ± 4	25 ± 1	0	60	140	330

[a] All samples were dispersed in 5.0 mM pH 7.3 PBS (with 5.0 mM NaCl) buffer solutions. [b] The number-averaged hydrodynamic diameters ($(D_h)_n$) were determined by DLS. Samples were passed through PVDF filters with 220 nm average pore size before conducting DLS measurements. [c] The TEM average diameter (D_{av}) values were measured for the nanoparticle cores. [d] Only spherical nanoparticles were counted. [e] The aggregation numbers (N_{agg}) were calculated based upon TEM micrographs.

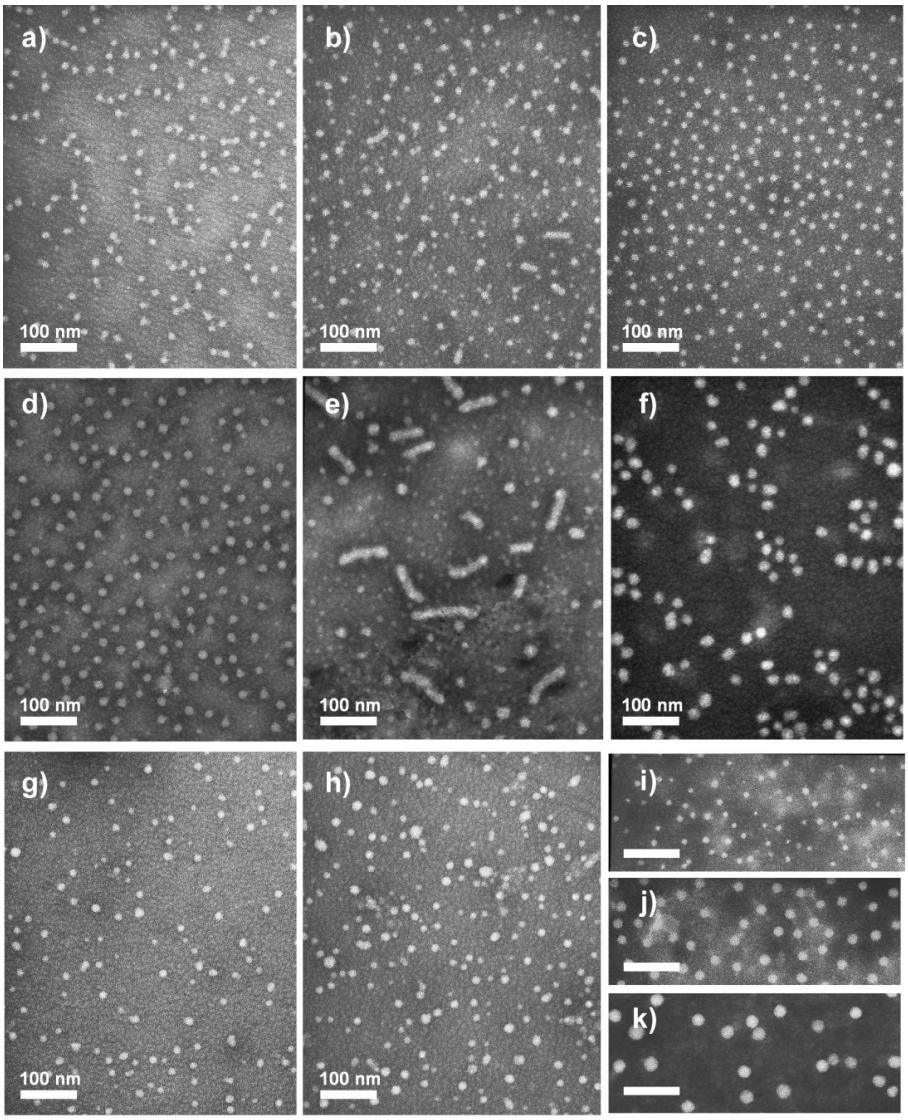

Figure 2.1. TEM micrographs of 50% crosslinked SCKs prepared from DOTAlysine$_m$-*g*-PAA$_n$-*b*-PS$_p$ block copolymer precursors: (a), (b), (c), and (i) are images of **SCK9**, **SCK12**, **SCK15**, and **Control1**, prepared from PAA$_{60}$-*b*-PS$_{30}$ with 2, 4, 7, and 0 DOTAlysine grafts, respectively; (d), (e), (f), and (j) are images of **SCK10**, **SCK13**, **SCK16**, and **Control2**, prepared from PAA$_{60}$-*b*-PA$_{60}$ with 2, 4, 7, and 0 DOTAlysine grafts, respectively; (g), (h), and (k) are images of **SCK11**, **SCK14**, and **Control3**, prepared from PAA$_{60}$-*b*-PA$_{140}$ with 2, 4, and 0 DOTAlysine grafts, respectively. Scale bars in (i), (j), and (k): 100 nm.

Based upon the TEM image analysis, the number of grafting DOTAlysines greatly influenced the morphologies of the nanoparticles. All pre-DOTAlysine-SCKs

constructed from the three different amphiphilic block copolymers, each having 2 DOTAlysines/polymer chain (**SCK1**-**3** having undergone 20% crosslinking, and **SCK9**-**11**, with 50% crosslinking) exhibited spherical morphologies with relatively narrow particle size distributions. This similarity could be attributed to the fact that the small percentage of modification (< 4%) across the PAA backbone did not generate significant variation over the entire block copolymer properties, *i.e.* the balance between the hydrophilic and hydrophobic blocks remained little affected. When p = 30 or 60, the pre-DOTAlysine$_2$-*g*-PAA$_{58}$-*b*-PS$_p$ polymers gave uniform assembly (**SCK1**, **SCK2**, **SCK9**, and **SCK10**) to afford SCK dimensions that were in agreement with control SCKs (Figure 2.1i and 2.1j), prepared from PAA$_{60}$-*b*-PS$_{30}$ and PAA$_{60}$-*b*-PS$_{60}$, respectively. In these cases, the loss of hydrophilicity (*i.e.*, transformation of carboxylic acid to amide linkage) and the increased steric repulsion caused by the rigid macrocyclic moiety of DOTAlysine could be partially compensated by the *ca*. 10% increase of carboxylic acid residues (from DOTAlysine) over the length of the PAA$_{60}$ segments. In contrast, the DOTAlysine-functionalized amphiphilic block copolymers with the longest PS chain segment, DOTAlysine$_2$-*g*-PAA$_{58}$-*b*-PS$_{140}$ underwent assembly into unusually small micelles to afford **SCK3** and **SCK11** that were significantly smaller in size and aggregation number than was the control assembly from PAA$_{60}$-*b*-PS$_{140}$ (Figure 2.1k) We are still investigating the reasons for the atypical assembly for these block copolymers.

For pre-DOTAlysine-SCKs with *ca*. 4 DOTAlysines/chain (20% crosslinking for **SCK4-6** and 50% crosslinking for **SCK12-14**), their morphologies became much more complex. As the DOTAlysine$_4$-*g*-PAA$_{56}$-*b*-PS$_{30}$ was assembled, in addition to the major spherical morphology (> 80%), small rod-like structures appeared with *ca.* 60 nm length (Figure 2.1b). Such unusual observation became extreme for SCKs prepared from DOTAlysine$_4$-*g*-PAA$_{56}$-*b*-PS$_{60}$, in which half of the nanoobjects were rods with average lengths of *ca.* 100 nm (Figure 2.1e). It is unclear whether the sphere-to-rod morphological transition results from interruptions on the local Coulombic interactions within the nanostructures, a hydrophilicity change in the shell domain, or a combination of these factors. Detailed studies to better understand the "driving force" of this uncommon morphological transition are currently underway. In the case of SCKs from DOTAlysine$_4$-*g*-PAA$_{56}$-*b*-PS$_{140}$ (**SCK6** and **SCK14**), spheres still remained dominant, but their particle size distributions were broad (Figure 2.1h).

Interestingly, as the grafting DOTAlysine number continued to increase, the four SCKs (**SCK7**, **SCK8**, **SCK16**, and **SCK17**) from DOTAlysine$_7$-*g*-PAA$_{53}$-*b*-PS$_{30(60)}$ returned to the more thermodynamically favourable spherical morphology. It is surprising that, even at this high proportion of modification (*i.e.*, the introduction of *ca*. 21 additional carboxylic acid groups per hydrophilic chain segment and the concomitant increased hydrophilic ratio and increased steric effects) along the polymer backbones, their assembly sizes and shapes remained similar to the control SCKs. Again, the block

copolymer having the longest PS block length and coupling of *ca*. 7 DOTAlysines per polymer was unusual, in that it experienced poor solubility and could not be assembled into uniform micelles.

Radiolabelling of these micelles and their corresponding SCKs with ^{64}Cu were investigated thoroughly. All the pre-DOTAlysine-SCKs/micelles exhibited high specific activity (Figure 2.2) compared with the SCKs prepared by coupling the DOTA onto pre-established nanoparticles (post-DOTA-SCKs, **Control4** in Figure 2.2).[26] The specific activities of the pre-DOTAlysine-SCKs increased by 10 to 40 fold. This high radiolabelling on a per particle basis creates an opportunity for reliable use with administration of a minimum amount of polymeric nanoparticles for *in vivo* PET imaging.

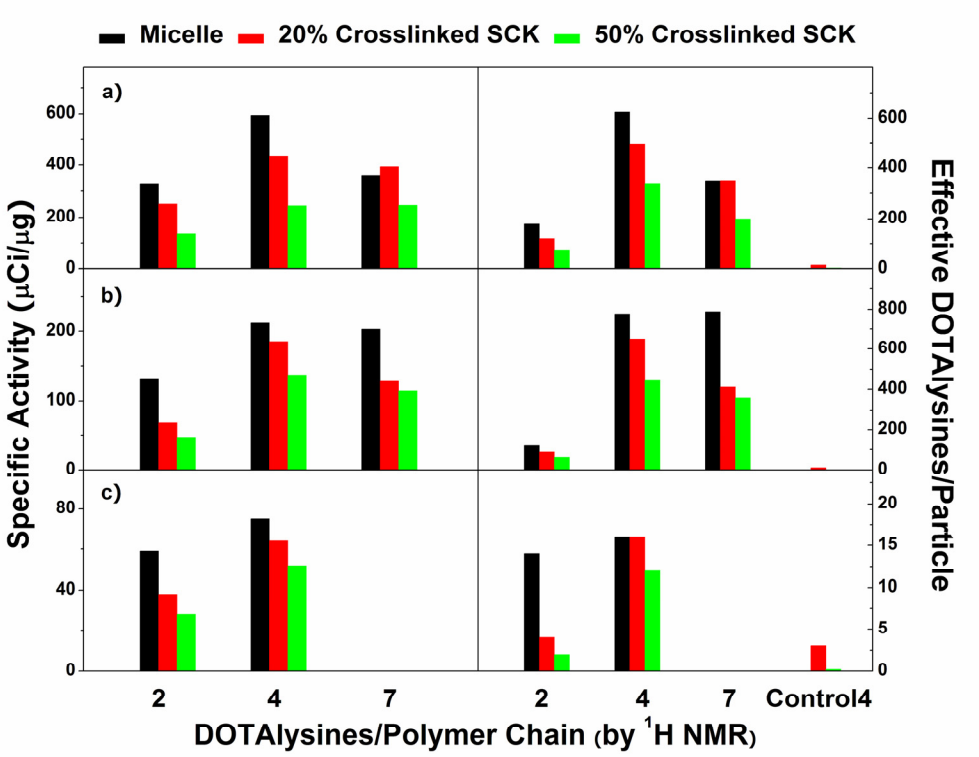

Figure 2.2. Radiolabelling results for pre-DOTAlysine-SCKs: (a) SCKs from functionalized PAA_{60}-*b*-PS_{30}; (b) SCKs from functionalized PAA_{60}-*b*-PS_{60}; (c) SCKs from functionalized PAA_{60}-*b*-PS_{140}. The numbers of effective DOTAlysines/particle (with ± 5% standard deviation) were obtained from the numbers of effective DOTAlysines/polymer chain (determined from isotopic dilution experiments, see Experimental Section) and the calculated particle aggregation number (Table 2.1). **Control4** were post-DOTA-SCKs.[26]

The specific activity and the number of effective DOTAlysines per SCK did not follow the expected tendency, which would be an increase in labelling with an increase in DOTAlysine grafting density. Rather, it appeared that the proportion of DOTAs available for ^{64}Cu chelation reached a "saturation point" after 4 DOTAlysine grafts per polymer chain. Since not all grafting DOTAlysines were located on the particle surface, the membrane-like structures within the shell regions of SCKs[29] might hinder the formation of ^{64}Cu-DOTAlysine complexes due to steric crowding and prevention of the

DOTAlysine macrocyclic from assuming a configuration amenable to stable ^{64}Cu coordination.[32] It is uncertain whether morphological differences (sphere *vs*. rod) also play a role.

Moreover, for SCKs prepared from a fixed DOTAlysine graft number per polymer chain (Figure 2.2), it was found that: (i) as the extents of crosslinking increased (from 0% to 50%), less DOTAlysines were available for coordinating with copper; (ii) as the proportion of the hydrophilic PAA comprising the entire nanostructure decreased, so did the number of effective DOTAlysines and the overall specific activity. The lower permeability within the shell domains of the SCKs having higher extents of crosslinking[29] could hinder the diffusion of ^{64}Cu to approach the DOTAlysine chelators located throughout the sub-surface and deep-shell areas. For instance, the number of effective DOTAlysines per DOTAlysine$_7$-*g*-PAA$_{53}$-*b*-PS$_{30}$ chain determined by isotopic dilution experiments (see Experimental Section) was *ca*. 2.8, much lower than 7.0, which was determined by ^1H NMR analysis. The second trend observed further suggests the complexities on the self-assembly behaviour of DOTAlysine-*g*-PAA-*b*-PS block copolymers. The lower radiolabelling efficiency on micelles and SCKs established from the longer hydrophobic PS block (while the DOTAlysine-*g*-PAA segment was invariable) could be related with their atypical morphological characteristics (*vide supra*). Nevertheless, all micelles and SCKs prepared from DOTAlysine-*g*-PAA-*b*-PS exhibited high radiolabelling results, providing a library of nanoparticles with varying

characteristic parameters to be employed for PET imaging when a minimum amount of imaging agent is needed.

It is noteworthy that this grafting strategy affords nanoobjects with remarkably improved radiolabelling efficiencies, relative to the post-functionalization of pre-established SCKs,[26] but also introduces complications with the assembling process, presenting unusual morphologies in some cases. More efforts are being devoted to investigate these morphological variations. Although micelles give the highest radiolabelling, their stability concerns, *i.e.,* stable architectures exist only above their critical micelle concentrations, remain challenging for *in vivo* applications.[23] Considering both the radiolabelling results and the SCK morphological properties, we conclude, tentatively, that the current optimum sample for *in vivo* PET imaging are SCKs having 20% shell crosslinking and prepared from PAA_n-*b*-PS_p containing *ca*. 2 DOTAlysine per polymer chain.

Conclusions

In summary, we have developed a new strategy to construct shell crosslinked nanoparticles, containing large numbers of DOTAlysines per particle (> 400) that were accessible for ^{64}Cu radiolabeling. These nanoparticles originated from conveniently prepared DOTAlysine-*g*-PAA-*b*-PS block copolymer precursors. The morphology of these pre-DOTAlysine-SCKs was, however, complicated by the number of DOTAlysine

grafts per polymer chain. Nonetheless, the ^{64}Cu–complexed pre-DOTAlysine-SCK nanoparticles showed impressive specific activities (*ca.* 400 μCi μg^{-1}), which suggest that these nanoparticles might be used to develop highly sensitive *in vivo* PET tracers at low administering doses. This "pre-grafting" strategy may also be employed to couple other molecules for targeting interested epitopes and/or for improving the *in vivo* bio-distribution of nanoobjects.

Experimental Section

PAA-*b*-PS Block Copolymer Synthesis. All block copolymers were synthesized by acidolysis of P*t*BA-*b*-PS precursors, which were prepared by sequential polymerization of *tert*-butyl acrylate and styrene *via* nitroxide mediated radical polymerization (NMP), with trifluoroacetic acid (TFA) as reported in the literature.[33]

General Procedure for DOTAlysine-*g*-PAA-*b*-PS Synthesis. Grafting DOTAlysines onto PAA-*b*-PS by amidation involved the following: To a round-bottom flask equipped with a magnetic stir bar, was added a sample of PAA-*b*-PS block copolymer and anhydrous *N*,*N*-dimethylformamide (DMF). The mixture was stirred for 1 h at room temperature to ensure that a clear and homogeneous solution was obtained. To this solution, was added 1-[3'-(dimethylamino)propyl]-3-ethylcarbodiimide methiodide (EDCI) and 1-hydroxybenzotriazole (HOBt) and the reaction mixture was allowed to stir for 1 h at rt. Finally, a pre-mixed solution of DOTAlysine·TFA and *N*,*N*-

diisopropylethylamine (DIPEA) in anhydrous DMF was added and the reaction mixture was further stirred for 20 h at rt. The reaction mixture was then transferred to pre-soaked dialysis tubing (MWCO *ca.* 6,000 to 8,000 Da) and dialyzed against nano-pure H_2O (18.0 MΩ cm, pre-treated with Chelex100®) for 4 d to remove the organic solvent and small molecule by-products. The aqueous solution was then lyophilized to afford the product as white solid.

General Procedure for the Micellization of DOTAlysine-g-PAA-b-PS. To a round-bottom flask equipped with a magnetic stir bar, was added DOTAlysine-*g*-PAA-*b*-PS, followed by anhydrous DMF. The mixture was sonicated for 10 min and stirred for 2 h at rt to ensure that a clear and homogeneous solution (final concentration, *ca.* 1.0 mg/mL) had formed. To this solution, was added dropwise *via* a syringe pump at a rate of 15.0 mL/h, an equal volume of nano-pure H_2O (18.0 MΩ cm) and the mixture was further stirred for 16 h at rt. Finally, the solution was transferred to pre-soaked dialysis tubing (MWCO *ca.* 6,000 to 8,000 Da) and dialyzed against nano-pure H_2O (18.0 MΩ cm, pre-treated with Chelex100®) for 4 d to afford a clear solution of micelles.

General Procedure for the Preparation of Pre-DOTAlysine-SCKs. To a 250 mL round-bottom flask equipped with a magnetic stir bar, was added a solution of DOTAlysine-*g*-PAA-*b*-PS micelles in nano-pure H_2O (18.0 MΩ cm) (50.0 mL, 0.054 mmol of carboxylic acid residues). To this solution was added dropwise over 10 min, a solution of 2,2'-(ethylenedioxy)-bis(ethylamine) (0.9 mg, 0.006 mmol for 20%

crosslinking extent; or 2.2 mg, 0.015 mmol for 50% crosslinking extent) in nano-pure H_2O (18.0 MΩ cm) (2.0 mL). The reaction mixture was allowed to stir for 2 h at rt. To this solution was added, dropwise *via* a syringe pump over 1 h, a solution of EDCI (4.0 mg, 0.014 mmol for 20% crosslinking extent; or 10.0 mg, 0.034 mmol for 50% crosslinking extent) in nano-pure H_2O (18.0 MΩ cm) (2.0 mL) and the reaction mixture was further stirred for 16 h at rt. Finally, the reaction mixture was transferred to pre-soaked dialysis tubing (MWCO *ca.* 6,000 to 8,000 Da) and dialyzed against 5.0 mM PBS (pH 7.3, with 5.0 mM NaCl, pre-treated with Chelex100®) for 5 d to remove the small molecule by-products and afford aqueous solutions of pre-DOTAlysine-SCKs.

^{64}Cu labelling and isotopic dilution experiments of the pre-DOTAlysine-SCKs. A 100 μL pre-DOTAlysine-SCK solution in 5.0 mM PBS (pH 7.3, with 5.0 mM NaCl, 0.2-0.3 mg/mL) was diluted with 100 μL of 0.1 M ammonium acetate buffer (pH 5.5) and to this solution, $^{64}Cu(OAc)_2$ was added (*ca*. 1.0 mCi). The resulting solution was incubated at 43 °C for 2 h, and then subjected to DTPA challenge. The labelling yield was determined by radio-TLC on ITLC-SG plates using methanol/$CH_3CO_2NH_4$ (aq) as eluent. The number of effective DOTAlysines/polymer chain was determined by isotopic dilution experiments. A series of known amounts of "hot plus cold" copper (Cu^{2+} solution spiked with ^{64}Cu) were added to several 100 μL SCK solutions respectively. After a 2 h incubation at 43 °C and DTPA challenge, each solution aliquot was analyzed

by radio-ITLC to determine the number of effective DOTAlysine per polymer chain, as previously reported.[23]

Acknowledgement This material is based upon work supported by the National Heart Lung and Blood Institute of the National Institutes of Health as a Program of Excellence in Nanotechnology (HL080729). The production of ^{64}Cu is supported by the National Cancer Institute (CA86307). The authors thank Ms. N. Kohrt and Prof. S. Sakiyama-Elbert for their assistance with DLS measurements, and Mr. G. M. Veith for TEM imaging.

References

1. Phelps, M. E. "Positron emission tomography provides molecular imaging of biological processes." *Proc. Natl. Acad. Sci. USA* **2000**, *97*, 9226-9233.

2. Weissleder, R.; Mahmood, U. "Molecular Imaging." *Radiology* **2001**, *219*, 316-333.

3. Gambhir, S. S. "Molecular imaging of cancer with positron emission tomography." *Nat. Rev., Cancer* **2002**, *2*, 683-693.

4. West, C. M. L.; Jones, T.; Price, P. "The potential of positron-emission tomography to study anticancer-drug resistance." *Nat. Rev., Cancer* **2004**, *4*, 457-469.

5. Lappin, G.; Garner, R. C. "Big Physics, Small Doses: The use of AMS and PET in human microdosing of development drugs." *Nat. Rev., Drug Discov.* **2003**, *2*, 233-240.

6. Weber, W. A. "Chaperoning drug development with PET." *J. Nucl. Med.* **2006**, *47*, 735-737.

7. Kornblum, H. I.; Cherry, S. R. "The use of microPET for the development of neural repair therapeutics: studies in epilepsy and lesion models." *J. Clin. Pharm.* **2001**, *41*, 55S-63S.

8. Sossi, V.; Ruth, T. J. "Micropet imaging: in vivo biochemistry in small animals." *J Neural. Transm.* **2005**, *112*, 319-30.

9. Wang, J.; Maurer, L. "Positron Emission Tomography: Applications in drug discovery and drug development." *Curr. Top. Med. Chem.* **2005**, *5*, 1053-1075.

10. Li, G. C.; He, F.; Ling, C. C. "Hyperthermia and gene therapy: potential use of microPET imaging." *Int. J. Hyperthermia* **2006**, *22*, 215-221.

11. Cherry, S. R. "The 2006 Henry N. Wagner lecture of mice and men (and positrons)-advances in PET imaging technology." *J. Nucl. Med.* **2006**, *47*, 1735-1745.

12. Smith, S. V. "Molecular imaging with copper-64." *J. Inorg. Biochem.* **2004**, *98*, 1874-1901.

13. Anderson, C. J.; Welch, M. J. "Radiometal-Labeled Agents (Non-Technetium) for Diagnostic Imaging." *Chem. Rev.* **1999**, *99*, 2219-2234.

14. Laforest, R.; Rowland, D. J.; Welch, M. J. "MicroPET imaging with nonconventional isotopes." *IEEE Trans.Nucl. Sci.* **2002**, *49*, 2119-2126.

15. Wadas, T. J.; Wong, E. H.; Weisman, G. R.; Anderson, C. J. "Copper chelation chemistry and its role in copper radiopharmaceuticals." *Curr. Pharm. Des.* **2007**, *13*, 3-16.

16. Boswell, C. A.; Sun, X.; Niu, W.; Weisman, G. R.; Wong, E. H.; Rheingold, A. L.; Anderson, C. J. "Comparative *in vivo* Stability of Copper-64-Labeled Cross-Bridged and Conventional Tetraazamacrocyclic Complexes." *J. Med. Chem.* **2004**, *47*, 1465-1474.

17. Trubetskoy, V. S. "Polymeric micelles as carriers of diagnostic agents." *Adv. Drug Delivery Rev.* **1999**, *37*, 81-88.

18. Brigger, I.; Dubernet, C.; Couvreur, P. "Nanoparticles in cancer therapy and diagnosis." *Adv. Drug Delivery Rev.* **2002**, *54*, 631-651.

19. Torchilin, V. P. "PEG-based micelles as carriers of contrast agents for different imaging modalities." *Adv. Drug Delivery Rev.* **2002**, *54*, 235-252.

20. Brannon-Peppas, L.; Blanchette, J. O. "Nanoparticle and targeted systems for cancer therapy." *Adv. Drug Delivery Rev.* **2004**, *56*, 1649-1659.

21. Lukyanov, A. N.; Torchilin, V. P. "Micelles from lipid derivatives of water-soluble polymers as delivery systems for poorly soluble drugs." *Adv. Drug Delivery Rev.* **2004**, *56*, 1273-1289.

22. Rossin, R.; Pan, D.; Turner, J. L.; Sun, X.; Wooley, K. L.; Welch, M. J., "^{64}Cu-Labeled Folate-Conjugated Shell Cross-Linked Nanoparticles for Tumor Imaging and Radiotherapy: Synthesis, Radiolabeling, and Biologic Evaluation." *J. Nucl. Med.* **2005**, *46*, 1210-1218.

23. Sun, X.; Rossin, R.; Turner, J. L.; Becker, M. L.; Joralemon, M. J.; Welch, M. J.; Wooley, K. L. "An assessment of the effects of shell cross-linked nanoparticle size, core composition, and surface pegylation on in vivo biodistribution." *Biomacromolecules* **2005**, *6*, 2541-2554.

24. Mitra, A.; Nan, A.; Line, B. R.; Ghandehari, H. "Nanocarriers for nuclear imaging and radiotherapy of cancer." *Curr. Pharm. Des.* **2006**, *12*, 4729-4749.

25. Wooley, K. L. "Shell crosslinked polymer assemblies: Nanoscale constructs inspired from biological systems." *J. Polymer Sci., Part A: Polymer Chem.* **2000**, *38*, 1397-1407.

26. Xu, J.; Sun, G.; Rossin, R.; Hagooly, A.; Li, Z.; Fukukawa, K.; Messmore, B. M.; Moore, D. A.; Welch, M. J.; Hawker, C. J.; Wooley, K. L. "Labeling of polymeric nanostructures for medical imaging: importance of cross-linking extent, spacer length, and charge density." *Macromolecules.* **2007**, *40*, 2971-2973.

27. Becker, M. L.; Liu, J.; Wooley, K. L. "Functionalized Micellar Assemblies Prepared via Block Copolymers Synthesized by Living Free Radical Polymerization upon Peptide-Loaded Resins." *Biomacromolecules* **2005**, *6*, 220-228.

28. Huang, H.; Kowalewski, T.; Remsen, E. E.; Gertzmann, R.; Wooley, K. L. "Hydrogel-Coated Glassy Nanospheres: A Novel Method for the Synthesis of Shell Cross-Linked Knedels." *J. Am. Chem. Soc.* **1997**, *119*, 11653-11659.

29. Thurmond, K. B.; Kowalewski, T.; Wooley, K. L. "Shell Cross-Linked Knedels: A Synthetic Study of the Factors Affecting the Dimensions and Properties of Amphiphilic Core-Shell Nanospheres." *J. Am. Chem. Soc.* **1997**, *119*, 6656-6665.

30. Zhang, L.; Eisenberg, A. "Multiple Morphologies of "Crew-Cut" Aggregates of Polystyrene-*b*-poly(acrylic acid) Block Copolymers." *Science* **1995**, *268*, 1728-1731.

31. Zhang, L.; Eisenberg, A. "Multiple Morphologies and Characteristics of "Crew-Cut" Micelle-like Aggregates of Polystyrene-*b*-poly(acrylic acid) Diblock Copolymers in Aqueous Solutions." *J. Am. Chem. Soc.* **1996**, *118*, 3168-3181.

32. Riesen, A.; Zehnder, M.; Kaden, T. A. "Cu-DOTA crystal structure." *Helv. Chim. Acta* **1986**, *69*, 2067-2073.

33. O'Reilly, R. K.; Joralemon, M. J.; Wooley, K. L.; Hawker, C. J. "Functionalization of Micelles and Shell Cross-linked Nanoparticles Using Click Chemistry." *Chem. Mater.* **2005**, *17*, 5976-5988.

Chapter 3

Facile, Efficient Approach to Accomplish Tunable Chemistries and Variable Biodistributions for Shell Crosslinked Nanoparticles (SCKs)

[Portions of this work have been published previously as Guorong Sun, Aviv Hagooly, Jinqi Xu, Andreas M. Nyström, Zicheng Li, Raffaella Rossin, Dennis A. Moore, Karen L. Wooley and Michael J. Welch *Biomacromolecules* **2008**, *9(7),* 1997-2006.]

Abstract

The *in vivo* behavior of shell crosslinked knedel-like (SCK) nanoparticles is shown to be tunable, *via* a straightforward and versatile process that advances SCKs as attractive nanoscale carriers in the field of nanomedicine. Tuning of the pharmacokinetics was accomplished by grafting varied numbers of methoxy-terminated poly(ethylene glycol) (mPEG) chains to the amphiphilic block copolymer precursors, together with chelators for the radioactive tracer and/or therapeutic agent ^{64}Cu, followed by self assembly into block copolymer micelles and chemical crosslinking throughout the shell regions. ^{64}Cu-radiolabeling was then performed in order to evaluate the SCKs *in vivo* by means of biodistribution experiments and positron emission tomography (PET). It was found that the blood retention of PEGylated SCKs could be tuned, depending on the mPEG grafting density and the nanoparticle surface properties. A semi-quantitative model of the density of mPEG surface coverage as a function of *in vivo* behavior was applied to enhance the understanding of this system.

Introduction

There are many types of nanoparticle platforms that are undergoing investigation as multi-functional agents for packaging, transport and delivery of imaging and therapeutic agents in the broad field of nanomedicine.[1-6] Many such nanostructures derive from the supramolecular assembly of small molecule or polymer components. For any new agent, it is critical that the composition, structure and properties be well-defined and controlled. The multimolecular association of amphiphilic block copolymers into core-shell micellar nanoassemblies has received particular attention.[7-10] Covalent crosslinking throughout the shell domains of spherical micelles, which are established from the self assembly of amphiphilic block copolymers, can afford shell crosslinked knedel-like (SCK) nanoparticles as discrete nanoscale objects.[11, 12] With the benefits of robust character, offered *via* the crosslinking, and the amphiphilic core-shell morphology, imposed by the self assembly process, SCKs, and also internally-crosslinked block copolymer micelles, have received significant attention as sophisticated hosts for purposes of diagnosis and therapy toward acute vascular injury, acute lung injury and cancer.[13, 14] In each case, it is important that the nanostructures be able to circulate for a sufficient period in the bloodstream to increase their probability to target specific tissues.

It is well known that systemically-administered nanoparticles tend to be sequestrated by the mononuclear phagocyte system (MPS), and accumulate mainly in the liver and spleen. Clearance from the bloodstream begins with the adsorption of plasma proteins onto the nanoparticle surface (opsonization), which triggers complement activation and macrophage recognition, and depends on particle size, surface chemistry and other factors.[15, 16] Surface modification with polyethylene glycol (PEG) based units

is one of the most successful techniques to avoid nanoparticle opsonization and, therefore, to slow down macrophage recognition.[15-17] PEG is water-soluble, non-toxic, and gives low immunogenic response.[18, 19] It can be adsorbed onto or chemically conjugated with bioactive agents, leading to improvement of their *in vivo* stability and enhancement of their pharmacokinetic profiles.[20, 21] Also, surface PEGylation of polymeric nanoparticles was shown to decrease aggregation and to prolong blood circulation times.[1, 7, 8, 10, 15-17] Although the mechanism is still controversial, many studies have suggested that the presence of PEG on the surface of a nanoparticle can exert entropic and steric repulsions to resist and minimize the adsorption of plasma proteins and the subsequent macrophage recognition.[7, 8, 15-17] For each new nanostructured material under development, the chemical composition, together with size,[22] shape,[23, 24] and flexibility,[25] are believed to require tuning in order to determine their interactions with biomacromolecules and, therefore, their fate *in vivo*. In general, entire "coverage" of the nanoparticle surface with PEG is considered to be vital to achieve "stealth" characteristics.[26-36] Therefore, it is critical that chemical methodologies are available to control and confirm the number of PEG chains and density of PEGylation. It is also important that the chemistry allows for the incorporation of probes that can track the nanoparticles and be used for imaging purposes. In this work, we employ ^{64}Cu-radiolabeling for biodistribution evaluation and positron emission tomography (PET), as a highly sensitive and non-invasive imaging technique,[37, 38] to assess the effect of PEGylation on blood retention and MPS uptake.[39-41]

Experimental Section

Materials. All reagents and solvents were obtained from commercial sources (Sigma-Aldrich, Acrose, and Fluka) and used without further purification unless otherwise noted. ^{64}Cu was prepared on the Washington University Medical School CS-15 Cyclotron by the ^{64}Ni(p,n)^{64}Cu nuclear reaction at a specific activity of 50–200 mCi/μg at the end of bombardment. The buffers used for dialysis after SCK preparation and during ^{64}Cu-labeling were treated overnight with Chelex-100® resin (Bio-Rad Laboratories, Hercules, CA) before use.

Measurements. ^{1}H NMR spectra were recorded in solutions on a Varian Mogli 500 spectrometer with the residual solvent signal as an internal standard. Gel permeation chromatography (GPC) was conducted on a Waters 1515 HPLC (Waters Chromatography, Inc.) equipped with a Waters 2414 differential refractometer, a PD2020 dual-angle (15° and 90°) light scattering detector (Precision Detectors, Inc.), and a three-column series PL gel 5μm Mixed C, 500 Å, and 10^4 Å, 300 × 7.5 mm columns (Polymer Laboratories Inc.). The system was equilibrated at 35 °C in anhydrous tetrahydrofuran (THF), which served as the polymer solvent and eluent with a flow rate of 1.0 mL/min. Polymer solutions were prepared at a known concentration (*ca.* 3 mg/mL) and an injection volume of 200 μL was used. Data collection and analysis were performed, respectively, with Precision Acquire software and Discovery 32 software (Precision Detectors, Inc.). Interdetector delay volume and the light scattering detector calibration constant were determined by calibration using a nearly monodispersed polystyrene standard (Pressure Chemical Co., M_p = 90 kDa, M_w/M_n < 1.04). The differential refractometer was calibrated with standard polystyrene reference material

(SRM 706 NIST), of known specific refractive index increment dn/dc (0.184 mL/g). The dn/dc values of the analyzed polymers were then determined from the differential refractometer response.

Samples for transmission electron microscopy (TEM) measurements were diluted with 1 wt% of phosphotungstic acid (PTA) stain solution (v/v, 1:1). Carbon grids were exposed to oxygen plasma treatment to increase the surface hydrophilicity. Micrographs were collected at 100,000× magnification and calibrated using a 41 nm polyacrylamide bead from NIST. The number average particle diameters (D_{av}) and standard deviations were generated from the analysis of a minimum of 150 particles from at least three different micrographs.

Hydrodynamic diameters (D_h) and size distributions for the SCKs in aqueous solutions were determined by dynamic light scattering (DLS). The DLS instrumentation consisted of a Brookhaven Instruments Limited (Worcestershire, U.K.) system, including a model BI-200SM goniometer, a model BI-9000AT digital correlator, a model EMI-9865 photomultiplier, and a model 95-2 Ar ion laser (Lexel, Corp.; Farmindale, NY) operated at 514.5 nm. Measurements were made at 20 ± 1 °C. Prior to analysis, solutions were filtered through a 0.22 μm Millex®-GV PVDF membrane filter (Millipore Corp., Medford, MA) and then centrifuged in a model 5414 microfuge (Brinkman Instruments, Inc.; Westbury, NY) for 10 minutes to remove dust particles. Scattered light was collected at a fixed angle of 90°. The digital correlator was operated with 522 ratio spaced channels, and initial delay of 5 μs, a final delay of 100 ms, and a duration of 10 minutes. A photomulitplier aperture of 400 μm was used, and the incident laser intensity was adjusted to obtain a photon counting of between 200 and 300 kcps. Only

measurements in which the measured and calculated baselines of the intensity autocorrelation function agreed to within 0.1 % were used to calculate particle size. The calculations of the particle size distributions and distribution averages were performed with the ISDA software package (Brookhaven Instruments Company), which employed single-exponential fitting, cumulants analysis, non-negatively constrained least-squares (NNLS) and CONTIN particle size distribution analysis routines. All determinations were made in triplicate and the data were presented as mean values ± standard deviations between runs.

Zeta potential (ζ) values for the nanoparticle solution samples in 5 mM phosphate buffered saline (PBS) were determined with a Brookhaven Instrument Co. (Holtsville, NY) model Zeta Plus zeta potential analyzer. Data were acquired in the phase analysis light scattering (PALS) mode following solution equilibration at 25 °C. Calculation of ζ from the measured nanoparticle electrophoretic mobility (μ) employed the Smoluchowski equation: $\mu = \varepsilon\zeta/\eta$, where ε and η are the dielectric constant and the absolute viscosity of the medium, respectively. Measurements of ζ were reproducible to within ± 2 mV of the mean value given by 16 determinations of 10 data accumulations.

The aggregation number was calculated based upon the diameter measured from TEM by using the following equation:

$$N_{aggr} = \frac{\frac{4}{3}\pi r^3 \rho}{\overline{M_n}} \times N_A$$

where r is the radius of the SCK, ρ is the density of polystyrene, M_n is the number-average molecular weight of polystyrene block segment, and N_A is the Avogadro constant.

A Bioscan 200 scanner (Bioscan, Washington, DC) was used to read the instant thin layer chromatography (ITLC) plates (Pall ITLC-SG plates, VWR International, Batavia, IL). Fast protein liquid chromatography (FPLC) and radio-FPLC were performed using an ÄKTA FPLC system (GE Healthcare Biosciences) equipped with a Beckman 170 Radioisotope Detector (Beckman Instruments, Fullerton, CA). The radioactivity was measured in a Beckman gamma-counter 8000 (Beckman instrument, Irvine, CA)

The imaging studies were carried out using the MicroPET® Focus (Siemens Medical Solutions Inc., Knoxville, TN) and the MicroCAT II (CTI-Imtek, Knoxville, TN) scanners.

Preparation of mPEG2000-*g*-PAA-*b*-PS Block Copolymers. The poly(acrylic acid)-*b*-polystyrene (PAA-*b*-PS, PAA_{60}-*b*-PS_{60} for this work) block copolymer was prepared as previously published (for the PAA_{60}-*b*-PS_{60} block copolymer precursor, poly(*tert*-butyl acrylate)-*b*-polysteyrene, P*t*BA_{60}-*b*-PS_{60}, $M_{n,GPC}$ = 13,500 Da, M_w/M_n = 1.2).[42] Grafting mPEG2000 onto PAA-*b*-PS involved the following: to a solution of PAA_{60}-*b*-PS_{60} block copolymer in anhydrous *N*,*N*-dimethylformamide (DMF), 1-[3'-(dimethylamino)propyl]-3-ethylcarbodiimide methiodide (EDCI) and 1-hydroxybenzotriazole (HOBt) were added and the reaction mixture was allowed to stir for 1 h at room temperature (rt). Then, a solution of mono-amine terminated mPEG2000 in anhydrous DMF was added and the reaction mixture was further stirred for 30 h at rt. The relative ratios of PAA_{60}-*b*-PS_{60} block copolymer:EDCI:HOBt:mPEG-NH_2 were varied to alter the grafting densities, whereby to achieve grafting densities of 1, 2.5 and 5.5 mPEGs per macromolecule, the stoichiometries were 1.0:1.3:1.3:1.3, 1.0:3.5:3.5:3.5, and 1.0:7.0:7.0:7.0, respectively. The final grafted block copolymers were isolated by

transferring the reaction mixtures to pre-soaked dialysis tubing (MWCO 6,000 to 8,000 Da) and dialyzing against nano-pure H_2O (18.0 MΩ cm) for 4 d to remove the organic solvent and the small molecule by-products. The aqueous solutions were then lyophilized to afford the products as a white solid. ^{1}H-NMR (500 MHz, CD_2Cl_2, ppm): δ 1.20-2.40 (br, -C*H*$_2$- and -C*H*- of the polymer backbone), 3.34 (s, mPEG terminal C*H*$_3$O-Hs), 3.42-3.80 (br, mPEG backbone -OC*H*$_2$C*H*$_2$O- Hs), 6.16-7.11 (br, aromatic Hs).

mPEG2000$_1$-*g*-PAA$_{59}$-*b*-PS$_{60}$ PAA$_{60}$-*b*-PS$_{60}$ (110.0 mg, 10.4 μmol), EDCI (4.0 mg, 13.5 μmol), HOBt (1.8 mg, 13.5 μmol), and mono-amine terminated mPEG2000 (27.0 mg, 13.5 μmol) in anhydrous DMF (15.0 mL). Yield: 72%.

mPEG2000$_{2.5}$-*g*-PAA$_{57.5}$-*b*-PS$_{60}$ PAA$_{60}$-*b*-PS$_{60}$ (120.0 mg, 11.3 μmol), EDCI (11.8 mg, 39.6 μmol), HOBt (5.4 mg, 40.0 μmol), and mono-amine terminated mPEG2000 (79.2 mg, 39.6 μmol) in anhydrous DMF (15.0 mL). Yield: 75%.

mPEG2000$_{5.5}$-*g*-PAA$_{54.5}$-*b*-PS$_{60}$ PAA$_{60}$-*b*-PS$_{60}$ (110.0 mg, 10.4 μmol), EDCI (21.6 mg, 72.8 μmol), HOBt (9.9 mg, 73.3 μmol), and mono-amine terminated mPEG2000 (145.6 mg, 72.8 μmol) in anhydrous DMF (15.0 mL). Yield: 75%.

Preparation of mPEG2000-*g*-DOTAlysine-*g*-PAA-*b*-PS Block Copolymers. The DOTAlysine (a lysine derivative for 1,4,7,10-tetraazocyclododecane-*N,N′,N″,N‴*-tetraacetic acid, DOTA) was grafted onto mPEG2000-*g*-PAA-*b*-PS by following a procedure similar to that used to graft mPEG2000 (described above). To a solution of mPEG2000-*g*-PAA-*b*-PS block copolymer (10.3 μmol) in anhydrous DMF (10.0 mL), EDCI (11.6 mg, 39.1 μmol) and HOBt (5.3 mg, 39.3 μmol) were added and the reaction mixture was allowed to stir for 1 h at rt. Then, a solution of DOTAlysine (trifluoroacetic acid (TFA) salt, 23.1 mg, 39.2 μmol) and *N,N*-diisopropylethylamine (DIPEA, 25.4 mg,

19.6 mmol) in anhydrous DMF (2.0 mL) was added and the reaction mixture was further stirred for 30 h at rt. The final grafted block copolymers were isolated by transferring the reaction mixtures to pre-soaked dialysis tubing (MWCO 6,000 to 8,000 Da) and dialyzing against nano-pure H_2O (18.0 MΩ cm) for 5 d to remove the organic solvent and the small molecule by-products. The aqueous solutions were then lyophilized to afford the products as a white solid. Yield: 65%. ^{1}H-NMR (500 MHz, CD_2Cl_2 with 2 drops of CF_3CO_2D, ppm): δ 1.20-2.40 (br, -C*H*$_2$- and -C*H*- of the polymer backbone, overlap with DOTAlysine Hs), 2.40-2.70 (br, DOTAlysine macrocyclic Hs), 3.34 (s, mPEG terminal C*H*$_3$O- Hs), 3.42-3.80 (br, mPEG backbone -OC*H*$_2$C*H*$_2$O- Hs), 6.16-7.11 (br, aromatic Hs).

Micellization of mPEG2000-*g*-DOTAlysine-*g*-PAA-*b*-PS. To a solution of mPEG2000-*g*-DOTAlysine-*g*-PAA-*b*-PS in anhydrous DMF (*ca.* 1.0 mg/mL), was added dropwise an equal volume of nano-pure H_2O *via* a syringe pump at a rate of 15.0 mL/h, and the mixture was further stirred for 16 h at rt. The solution was then transferred to pre-soaked dialysis tubing (MWCO *ca.* 6,000 to 8,000 Da) and dialyzed against nano-pure H_2O for 4 d to afford a clear solution of micelles.

Construction of mPEGylated DOTA-SCKs. To a solution of mPEG2000-*g*-DOTAlysine-*g*-PAA-*b*-PS micelles in nano-pure H_2O was added a solution of 2,2'-(ethylenedioxy)-bis(ethylamine) in nano-pure H_2O dropwise over 10 min. The reaction mixture was allowed to stir for 2 h at rt. EDCI in nano-pure H_2O was then added to the resulting solution, dropwise *via* a syringe pump over 1 h. The general stoichiometry employed to achieve 20% nominal crosslinking was 9:2.2:1 for carboxylic acid units:EDCI:crosslinker, and to achieve 50% nominal crosslinking, the stoichiometry was

3.6:2.2:1. The reaction mixture was further stirred for 16 h at rt. Finally, the mixture was transferred to pre-soaked dialysis tubing (MWCO *ca.* 6,000 to 8,000 Da) and dialyzed against 5.0 mM PBS (pH 7.3, with 5.0 mM NaCl) for 5 d to remove the small molecule by-products and afford aqueous solutions of mPEGylated DOTA-SCKs.

Preparation of SCK6.

Synthesis of mPEG5000$_3$-*g*-PAA$_{57}$-*b*-PS$_{60}$ Block Copolymer A similar procedure as grafting mPEG2000 described above was followed with a relative ratio of PAA$_{60}$-*b*-PS$_{60}$ block copolymer:EDCI:HOBt:mPEG5000-NH$_2$ = 1.0:4.0:4.0:4.0.

Synthesis of mPEG5000$_3$-*g*-DOTAlysine$_2$-*g*-PAA$_{55}$-*b*-PS$_{60}$ Block Copolymer A similar protocol as the preparation of **mPEG2000-*g*-DOTAlysine-*g*-PAA-*b*-PS** block copolymers described above was followed.

Micellization and crosslinking throughout the shell domain of the micelle to afford **SCK6** were carried out following the same protocol as described above.

Preparation of SCK7. Monomethoxy poly(ethylene glycol) hydroxyl terminated (mPEG5000-OH), nominal molecular weight 5000 Da, was purified by flash column chromatography on silica gel eluted with methanol/DCM 5:95 (v/v). Styrene and *tert*-butyl acrylate (*t*-BA) were distilled over calcium hydride prior to use.

Synthesis of Poly(ethylene glycol) Macroinitiator (mPEG5000Ini) A dry 250 mL round bottom flask equipped with a stir bar was charged with mPEG5000-OH (16.5 g, 3.30 mmol), triethylamine (TEA, 0.70 g, 6.93 mmol), 4-dimethylaminopyridine (DMAP, 0.20 g, 1.64 mmol), and 200 mL of dichloromethane (DCM). The solution was stirred at 0 °C for 30 min after which 2-bromoisobutyryl bromide (1.52 g, 6.60 mmol) was added drop-wise to the reaction mixture with the aid of a dropping funnel. The reaction was left

to proceed for 24 h after which the solution was filtered and the filtrate concentrated under vacuum. The crude reaction mixture was redissolved in 300 mL of DCM and washed with a 10 w/w % sodium hydrogen sulfate solution (3 x 150 mL), followed by a 10 w/w % sodium bisulfate solution (3 x 150 mL). The organic phase was dried over magnesium sulfate ($MgSO_4$), filtered, and concentrated in vacuum. The crude product was purified by repeated precipitation in diethyl ether from DCM. The product was collected by filtration and dried under vacuum to give **mPEG5000Ini** as a white solid (12.1 g, 71%). ^{1}H NMR ($CDCl_3$, ppm): δ 1.93 (s, 6H, -CO(CH_3)$_2$-Br), 3.38 (s, 3H, mPEG terminal CH_3O- Hs), 3.42-3.80 (br, mPEG backbone-OCH_2CH_2O- Hs).

Synthesis of mPEG5000-*b*-P*t*BA$_{100}$ Block Copolymer A dry 25 mL Schlenk flask equipped with a stir bar was charged with *t*-BA (8.36 g, 65.2 mmol), **mPEG5000Ini** (1.0 g, 0.22 mmol), Cu(I)Br (62.0 mg, 0.43 mmol), anisole (5.0 g, 46.2 mmol), and THF (1.0 g, 13.9 mmol). After the reaction mixture was frozen in liquid nitrogen *N,N,N′,N″,N″*-pentamethyldiethylenetriamine (PMDETA, 7.0 mg, 0.43 mmol) was added *via* a gas-tight syringe. Three freeze-pump-thaw cycles were performed, and the mixture was back-filled with nitrogen and brought to rt. The flask was heated to 50 °C, and the reaction was let to proceed for 28 h (28 % conversion), and after which it was quenched by immersion of the reaction flask in liquid nitrogen. The reaction mixture was then dissolved in THF, passed through a neutral aluminium oxide column, and concentrated under vacuum. The reaction mixture was then dissolved in THF and transferred to pre-soaked dialysis tubing (MWCO 6,000–8,000 Da) and dialyzed against a methanol/H_2O mixture (30:70 by volume) for 4 d to remove the residual monomer. The aqueous solution was then lyophilized to afford the product **mPEG5000-*b*-P*t*BA$_{100}$** as white solid

(2.0 g, 60 %). M_n = 20.0 kDa, M_w/M_n = 1.20. ^{1}H-NMR ($CDCl_3$, ppm): δ 1.20-1.70 (br, meso and racemo -CH_2- of the polymer backbone), 1.30-1.60 (br, (CH_3)$_3$C- of the *tert*-butyl ester), 2.11-2.40 (br, -C*H*- of the polymer backbone), 3.38 (s, 3H, mPEG terminal CH_3O- Hs), 3.42-3.80 (br, mPEG backbone -OCH_2CH_2O- Hs).

Synthesis of mPEG5000-*b*-P*t*BA$_{100}$-*b*-PS$_{50}$ Block Copolymer A dry 25 mL Schlenk flask equipped with a stir bar was charged with styrene (1.52 g, 14.6 mmol), **mPEG5000-*b*-P*t*BA$_{100}$** (1.0 g, 0.049 mmol), Cu(I)Br (20.9 mg, 0.15 mmol), and anisole (1.8 g, 16.7 mmol). After the reaction mixture was frozen in liquid nitrogen PMDETA (25.0 mg, 0.15 mmol) was added *via* a gas-tight syringe. Three freeze-pump-thaw cycles were performed, and the mixture was back-filled with nitrogen and brought to rt. The flask was heated to 60 °C, and the reaction was allowed to proceed for 31 h (16.5 % conversion), and after which it was quenched by immersion of the reaction flask in liquid nitrogen. The reaction mixture was then dissolved in THF, passed through a neutral aluminium oxide column, and concentrated under vacuum. The reaction mixture was then dissolved in THF and transferred to pre-soaked dialysis tubing (MWCO 6,000–8,000 Da) and dialyzed against a methanol/H_2O mixture (30:70 by volume) for 4 d to remove the residual monomers. The aqueous solution was then lyophilized to afford the product **mPEG5000-*b*-P*t*BA$_{100}$-*b*-PS$_{50}$** as white solid (0.88 g, 71 %). M_n = 24.0 kDa, M_w/M_n = 1.20. ^{1}H-NMR ($CDCl_3$, ppm): δ 1.15-1.65 (br, meso and racemo -CH_2- of the polymer backbone), 1.30-1.60 (br, (CH_3)$_3$C- of the *tert*-butyl ester), 2.11-2.40 (br, -C*H*- of the polymer backbone), 3.39 (s, 3H, mPEG terminal CH_3O- Hs), 3.40-3.80 (br, mPEG backbone -OCH_2CH_2O- Hs), 6.15-6.83 (br, *o-Ar)*, 6.85-7.11 (br, *m,p-Ar*).

Synthesis of mPEG5000-*b*-PAA$_{100}$-*b*-PS$_{50}$ Block Copolymer A 25 mL round bottom flask equipped with a stir bar was charged with **mPEG5000-*b*-P*t*BA$_{100}$-*b*-PS$_{50}$** (250 mg, 0.010 mmol), 5 mL of DCM and 5 mL of TFA. The reaction was left to proceed at rt for 24 h after which it was concentrated under vacuum. The crude product was then dissolved in THF and transferred to pre-soaked dialysis tubing (MWCO 6,000–8,000 Da) and dialyzed against nano-pure H_2O (18.0 MΩ cm) for 4 d to remove small molecule impurities. The aqueous solution was then lyophilized to afford the product **mPEG5000-*b*-PAA$_{100}$-*b*-PS$_{50}$** as white solid (0.18 g, 95 %). ^{1}H-NMR (DMSO-d_6, ppm): δ 1.10-2.05 (br, meso and racemo -CH_2- of the polymer backbone), 2.11-2.21 (br, -C*H*- of the polymer backbone), 3.30 (s, 3H, mPEG terminal CH_3O- Hs), 3.42-3.90 (br, mPEG backbone -OCH_2CH_2O- Hs), 6.12-6.80 (br, *o-Ar)*, 6.90-7.20 (br, *m,p-Ar*), 11.0-14.0 (br, -COOH).

Synthesis of mPEG-*b*-(DOTAlysine$_7$-*g*-PAA$_{93}$)-*b*-PS$_{50}$ Block Copolymer Grafting of the DOTAlysines onto **mPEG5000-*b*-PAA$_{100}$-*b*-PS$_{50}$** by amidation was achieved by the same procedure as described above.

Micellization and crosslinking throughout the shell domain of the micelle to afford **SCK7** were carried out following the same protocol as described above.

General Method for ^{64}Cu Labeling. A solution of mPEGylated DOTA-SCK (*ca.* 0.2–0.3 mg/mL) in 5.0 mM PBS (pH 7.3, with 5.0 mM NaCl) was diluted with an equal volume of 0.1 M ammonium acetate buffer (pH 5.5) and ^{64}Cu-acetate (*ca*.30–500 μCi) was added. A Tween-20 solution in PBS was added to prevent non specific adsorption of the labeled nanoparticles on the labeling vials and other laboratory glassware (0.1% Tween-20, v/v, in the final solution). The labeling mixtures were incubated at 43 °C for

1 h, and then 5 μL of a 10 mM aqueous diethylenetriaminepentaacetic acid (DTPA) solution was added. The sample was allowed to incubate for 10 min at rt. The purity of the labeled samples was monitored by radio-ITLC using a 1:1 mixture (v/v) of 10 wt% ammonium acetate and methanol as developing solvent. The samples were filtered through 0.45 μm PVDF filters (Millipore Corp., Medford, MA). Samples with < 95 % radiochemical purity (RCP) were purified by using size exclusion cartridges (Zeba spin desalting column 2 mL, Pierce). Using 10 mM PBS (pH 7.4) as elute (up to 500 μL total volume of sample and PBS). The Zeba column has > 95% retention of salts and other small molecules (*MW* < 1000 Da) and tends to retain excess of DTPA. Tween-20 with *MW* around 1,200 Da may also retain under this conditions. Since the eluted sample was diluted for at least five times the reaction volume no more than 0.02% of Tween-20 was injected. FPLC analysis was used to determinate the purity of the injected samples. The purified samples were diluted with 10 mM PBS (pH 7.4) to prepare appropriate doses for bidistribution and imaging studies.

General Method for FPLC Analysis. A 50–100 μL of the labeled SCK was injected into a Superose 12 gel filtration column (GE Healthcare Biosciences) and eluted with 20 mM 4-(2-hydroxyethyl)piperazine-1-ethanesulfonic acid (HEPES) with 150 mM NaCl (pH 7.3) at 0.8 mL/min. The UV wavelength was preset to 280 nm and the radioactivity was monitored by an in-line radio-detector. Under these conditions, the retention times of the native and radiolabeled SCKs were 10 min while the retention times of free ^{64}Cu and ^{64}Cu-DTPA were 20–22 min. Samples with RCP > 95% were used for animal studies.

General Method for Specific Activity Measurement. A 100 μL of mPEGylated DOTA-SCK solution (*ca.* 0.2–0.3 mg/mL) in 5.0 mM PBS (pH 7.3, with 5.0 mM NaCl) was diluted with 100 μL of 0.1 M ammonium acetate buffer (pH 5.5) and to this solution, ^{64}Cu-acetate was added (*ca*. 1 mCi). The resulting solution was incubated at 43 °C for 2 h, and then subjected to DTPA challenge. The labeling yield was determined by radio-TLC on ITLC-SG plates using methanol/$CH_3CO_2NH_4$ (aq) as eluent. The number of effective DOTAlysines/polymer chain was determined by isotopic dilution experiments. A series of known amounts of "hot plus cold" copper (Cu^{2+} solution spiked with ^{64}Cu) were added to 100 μL SCK solution aliquots. After 2 h incubation at 43 °C and DTPA challenge, each solution was analyzed by radio-ITLC to determine the number of effective DOTAlysine per polymer chain, as previously reported.[39]

Biodistribution and small animal PET imaging studies of PEGylated SCKs. All animal studies were performed in compliance with guidelines set by the Washington University Animal Studies Committee. Normal female Sprague-Dawley rats (180–200 g, n = 4 per time point) were anesthetized with 1–2% vaporized isoflurane and injected with *ca.* 30 μCi of activity in 200 μL *via* the tail vein (*ca*. 20–25 μg/kg rat body weight). At specific time points post injection, organs and tissues of interest were harvested, blotted dry, and the radioactivity was measured in a Beckman gamma-counter 8000 (Beckman instrument, Irvine, CA). For blood and muscle, total activity was calculated assuming that these tissues constitute 6 and 41% of the total body weight, respectively. Diluted standard doses (1:100) were prepared and counted along with the samples. All the data were corrected for ^{64}Cu decay. The percent injected dose per gram tissue (%ID/g) values were calculated using the following equation:

$$\%ID/g = \frac{(cpm\ in\ sample - background) \times 10^2}{(decay\ correction\ \ factor) \times (sample\ weight) \times (cpm\ in\ standard)}$$

One-way analysis of variance (ANOVA) and post-hoc multiple comparison (Bonferroni's t-test) on the biodistribution data were performed by using Prism v. 4.00 (Graphpad, San Diego, CA). Groups with $P < 0.05$ were considered significantly different.

Normal female Balb/c mice (n = 2) weighing 20–30 g were injected with *ca*. 100–200 μCi of ^{64}Cu-labeled SCK (0.15–0.3 mg/kg mouse body weight) in 150 μL *via* tail vein and anesthetized with 1–2% vaporized isoflurane for data collection at specific time points. MicroPET and microCT image co-registration was accomplished using a landmark registration technique (by using fiducial markers directly attached to the animal bed) and AMIRA image display software (TGS Inc., Richmond, TX). Data analysis of microPET images was performed using the manufacturer software (ASIPRO, Siemens Medical Solutions). Data were calculated in terms of standardized uptake values (SUVs) in 3D regions of interests (ROIs) using the following equation:

$$SUV = \frac{Radioactivity\ Concentration\ in\ ROI\ [\mu Ci/cc]}{Injected\ Dose\ [\mu Ci]/Animal\ Weight\ [g]}$$

Results and Discussion

Previous *in vivo* evaluation of SCKs led to the hypothesis that both size and core composition played a synergistic role in influencing the blood circulation times, while surface chemistry (*i.e.*, PEGylation) was shown to have little effect on particle biodistribution.[39] However, the synthetic route for the introduction of PEG onto pre-established particles allowed for neither reliable reproducibility, because of the

complexity of aqueous amidation chemistry,[43] nor accurate quantification of the degree of PEGylation, unless chromophore-functionalized PEG was used.[44] In more recent studies, we have developed a new "pre-grafting" strategy, which couples the desired functionalities (metal chelators) onto block copolymer precursors from which SCKs are assembled.[42] This methodology was shown to provide functionalized SCKs with enhanced labeling for potential application in molecular imaging. Herein, the "pre-grafting" strategy is applied to attach an accurate number of PEG chains onto the SCKs. The stealth properties of these nanoparticles were evaluated *in vivo* by means of biodistribution experiments and small animal PET imaging, focusing our attention on blood retention and accumulation in the main MPS organs (liver and spleen). The results indicate that "pre-grafting" is a facile and practical method to obtain various degrees of PEGylated SCKs, making it feasible to retain the SCKs in blood up to 48 h after intravenous administration. At the same time, pre-conjugation of chelators for ^{64}Cu ($t_{1/2}$ = 12.7 h; β^+ = 17.8%, E_{max} = 0.653 MeV), such as DOTA, followed by radiolabeling affords SCKs with high specific activity (greater than 100 μCi/μg polymer), which can be useful for PET imaging when signal intensity is of concern (*i.e.*, when targeting low abundance molecular targets).

Construction of mPEGylated DOTA-SCKs with High ^{64}Cu Specific Activity. Mono-amine terminated methoxyPEG (mPEG-NH_2, M_n = 2,000 Da, *PDI* = 1.06) and DOTAlysine (a lysine derivative of DOTA for ^{64}Cu chelation),[42, 43, 45] were grafted sequentially onto PAA_{60}-*b*-PS_{60} block copolymer through conventional amidation chemistry in organic solvent (Figure 3.1, and see Experimental Section) with *ca.* 75% and 65% isolated yield, respectively. The numbers of mPEG grafts per block copolymer

chain were varied by the stoichiometry of mPEG-NH_2 *vs.* PAA_{60}-*b*-PS_{60}, and were determined by ^{1}H NMR spectroscopy for three samples as 1.0 (16 wt %), 2.5 (32 wt %), and 5.5 (51 wt %), respectively, using the proton resonances at 3.6-3.8 ppm (mPEG ethylene oxide backbone Hs) and 3.34 ppm (terminal methoxy Hs). The number of DOTAlysines (*ca.* 2 per polymer chain, determined by comparison of the integration area of the aliphatic proton resonances at δ 1.20 – 2.70 ppm *vs*. the polystyrene aromatic protons resonating at 6.16-7.11 ppm, before and after DOTAlysine grafting) was held constant for all samples, as confirmed by ^{1}H NMR spectroscopy. Such extents of DOTAlysine grafting was shown to be sufficiently high for effective ^{64}Cu complexation, while also being sufficiently low to allow polymer assembly into a globular morphology during the block copolymer micellization process.[42]

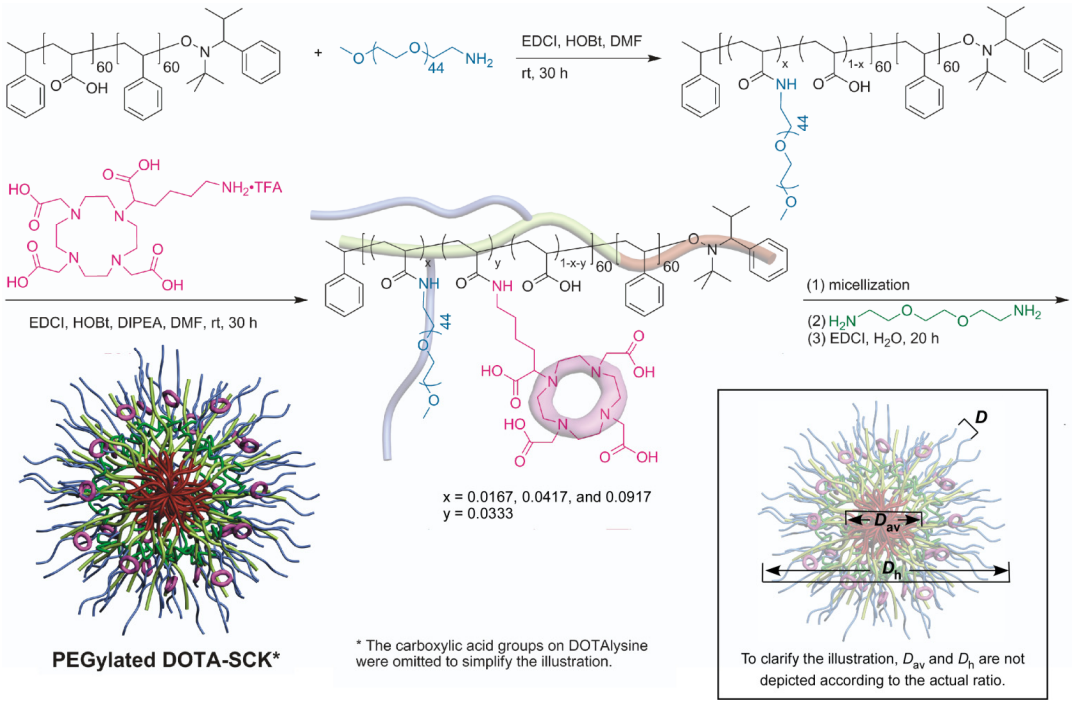

Figure 3.1. Schematic drawing of the synthetic route for the construction of mPEGylated SCKs.

The preparation of mPEGylated SCKs from these mPEG2000-*g*-DOTAlysine-*g*-PAA-*b*-PS block copolymers was conducted by following an established standard protocol (Figure 1, and see Experimental Section).[42, 43] These SCKs were characterized by DLS, TEM, and zeta potential measurements (Figure 3.2 and Table 3.1). Compared with the non-mPEGylated **SCK1**, mPEGylated **SCK2-5** showed similar particle sizes and nearly spherical morphology with relatively narrow polydispersity, which allowed for estimation of nanoparticle surface PEG density (*vide infra*). ^{64}Cu-labeled **SCK1-5** were obtained with high specific activities (> 100 μCi/μg polymer), which enabled the administration of low doses to normal rodents (*ca*. 5 μg per animal) for the *in vivo* studies.

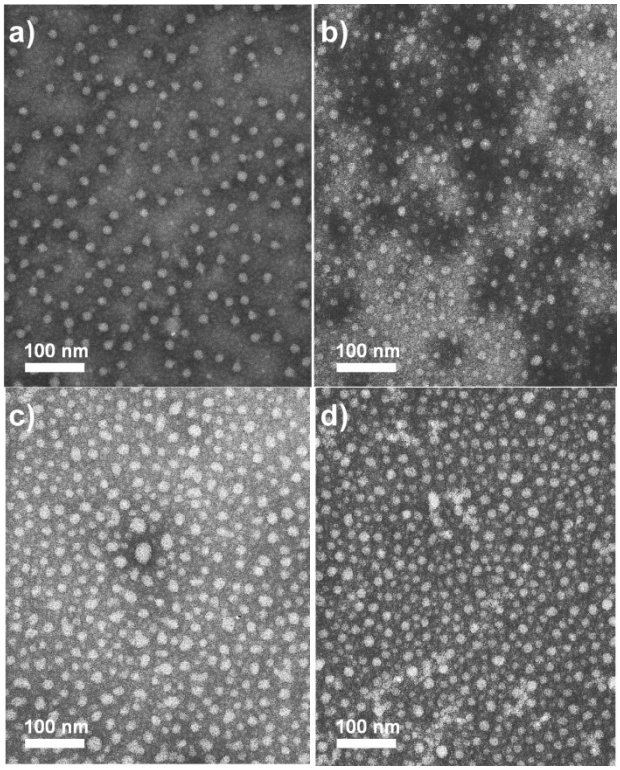

Figure 3.2. TEM characterization of PEGylated SCKs. a) TEM micrograph of **SCK1** (after negative stain with PTA). b) TEM micrograph of **SCK2** (after negative stain with PTA). c) TEM micrograph of **SCK3** (after negative stain with PTA). d) TEM micrograph of **SCK4** (after negative stain with PTA).

Table 3.1. Physical properties of mPEGylated DOTA-SCKs. **SCK1-6** originated from $mPEG_x$-*g*-$DOTAlysine_2$-*g*-PAA_{58-x}-*b*-PS_{60} block copolymer precursors, according to Scheme 1. **SCK7** originated from a triblock copolymer of mPEG-*b*-($DOTAlysine_7$-*g*-PAA_{93})-*b*-PS_{50}.

Sample[a]	mPEG2000 /Chain, x	DOTA /Chain	Crosslinking Extents[b]	$(D_h)_n$[c] (DLS, nm)	D_{av}[d] (TEM, nm)	Zeta Potential (mV)	Polydispersity
SCK1	0	2.0	20%	21 ± 3	16 ± 2	-38.5 ± 0.8	0.14
SCK2	1.0	2.0	20%	20 ± 4	16 ± 2	-40.9 ± 0.6	0.20
SCK3	2.5	2.0	20%	19 ± 4	14 ± 3	-31.9 ± 1.3	0.21
SCK4	5.5	2.0	20%	20 ± 4	14 ± 2	-30.2 ± 0.5	0.20
SCK5	5.5	2.0	50%	20 ± 4	15 ± 2	-20.8 ± 0.5	0.20
SCK6	3.0[f]	2.0	20%	21 ± 4	16 ± 2	-14.6 ± 0.6	0.19
SCK7	1.0	7.0	20%	22 ± 2	18 ± 2	-14.1 ± 1.3	0.09

[a] Sample concentrations were 0.20-0.30 mg/mL in 5 mM PBS buffer (pH 7.2 with 5 mM NaCl). [b] These values are based on the stoichiometry used during the crosslinking reaction. [c] Number-average hydrodynamic diameters. [e] D_{av} were measured for the SCK core domains, for at least 150 particles. [f] mPEG5000 was used instead of mPEG2000.

Semi-Quantitative Model for Estimation of mPEGylated SCK Surface Coverage. Although quantitative values can be obtained for self-assembled monolayers from grafted polymers on flat substrates,[46-56] the actual density of coverage for a nanostructure with a high degree of surface curvature is an unknown parameter. Given the radius of gyration (R_g) of mPEG2000 (about 1.8 nm[57]), and the shell thickness of the nanoparticles (*ca.* 2.0 to 3.0 nm, based upon the DLS and TEM measurements), a hypothesis could be made that almost all of the terminal portions of the mPEG chains were exposed around the periphery of the mPEGylated SCKs, due to the fact that the thickness of the shell domain is less than $2\times R_g$. The glassy PS block, which forms the hydrophobic core domain during the micellization process, was selected based upon the results from previous investigations[39, 43, 58] that found the nanostructures to exist as rigid spheres that underwent little structural deformation, even upon adsorption onto a solid

substrate.[58] Therefore, the PS-core SCKs should experience low degrees of structural deformation in rapidly flowing capillaries *in vivo*, so that they can be modeled as spheres. The surface coverage could be expressed *via* the average distance (D, see Figure 3.1 insertion for illustration) between the exposed mPEG molecules,[47] which was calculated through the following equation:

$$D = \sqrt{\frac{\pi (D_h)^2}{N}} \text{ nm}$$

where N denotes the number of mPEGs per SCK nanoparticle (obtained from the number of mPEGs per polymer chain and the aggregation number of polymer chains estimated to be within each SCK nanoparticle), and D_h is the hydrodynamic diameter of the corresponding SCK.

The results calculated based upon this hypothesis, summarized in Table 3.2, were consistent with zeta potential measurement data (Table 3.1). As expected, a decrease in ζ value (**SCK3** *vs.* **SCK2**) was observed as the mPEG surface coverage increased (decreased D values), indicating that both the surface negative charges and the mobility decreased.[59] The similar ζ values for **SCK4** and **SCK3**, in spite of a two-fold increase in mPEG grafts for **SCK4** with respect to **SCK3**, might be associated with near complete surface coverage and/or reduced mPEG conformational degrees of freedom after a certain number of mPEG2000 grafts per polymer chain. As expected, the consumption of a higher number of carboxylic acid groups during the crosslinking process resulted in a dramatic decrease of surface charge for **SCK5** compared to **SCK4**.

Table 3.2. Calculation of mPEG2000 surface coverage of mPEGylated **SCK1-4**, which originated from $mPEG2000_x$-*g*-$DOTAlysine_2$-*g*-PAA_{58-x}-*b*-PS_{60} block copolymer precursors, according to Figure 3.1.

Sample	mPEG[a] /Chain	D_{av} (nm)	N_{agg}	mPEG[a] /SCK	D_h (nm)	S_t[b] (nm^2)	(S_t/mPEG)[c] (nm^2)	D[d] (nm)
SCK1	0	16 ± 2	240	0	21 ± 3	1390 ± 130	0	0
SCK2	1.0	16 ± 2	240	240	20 ± 4	1260 ± 160	5.3 ± 0.7	2.3 ± 0.2
SCK3	2.5	14 ± 3	200	500	19 ± 4	1140 ± 140	2.3 ± 0.3	1.5 ± 0.1
SCK4	5.5	14 ± 2	200	1100	20 ± 4	1260 ± 160	1.2 ± 0.2	1.1 ± 0.1

[a] mPEG2000. [b] Surface area of mPEGylated SCKs. [c] Surface area per mPEG chain at the periphery of the SCK. [d] Average distance between mPEG chains at the periphery of the SCK.

Stealth Property of mPEGylated SCKs. Although the influence of mPEGylation on SCK biodistribution cannot be predicted by simply evaluating the SCK surface PEG coverage, these calculations provided the rationale to explain the dramatic differences observed *in vivo*. From the calculations performed by de Gennes and co-workers,[47, 48] the value of D should be *ca.* 1 nm to oppose the adsorption of small proteins (diameter *ca.* 2 nm) and *ca.* 1.5 nm for larger proteins (diameter *ca.* 6-8 nm). Therefore, no or low PEG surface coverage would result in no resistance to opsonization, which can explain the rapid disappearance of **SCK1** (no PEG) and **SCK2** (D = 2.3 ± 0.2 nm) from the blood circulation (< 0.5 percent injected dose per gram (%ID/gram) at 10 min post injection) and their rapid uptake in the liver and spleen (Figure 3.3A). The mPEG surface coverage of **SCK3** (D = 1.5 ± 0.1 nm) is, theoretically, effective in limiting the adsorption of large proteins but not that of small ones. In fact, **SCK3** exhibited a slightly longer blood retention (1.2 ± 0.2 %ID/gram at 10 min post injection) compared to **SCK1** and **SCK2** but was eliminated within one hour from the administration, and accumulated in the liver and spleen. To maintain the SCKs in circulation, an exceptionally high amount of PEG is required, as confirmed by the *in vivo* behavior of **SCK4** (D = 1.1 ± 0.1 nm).

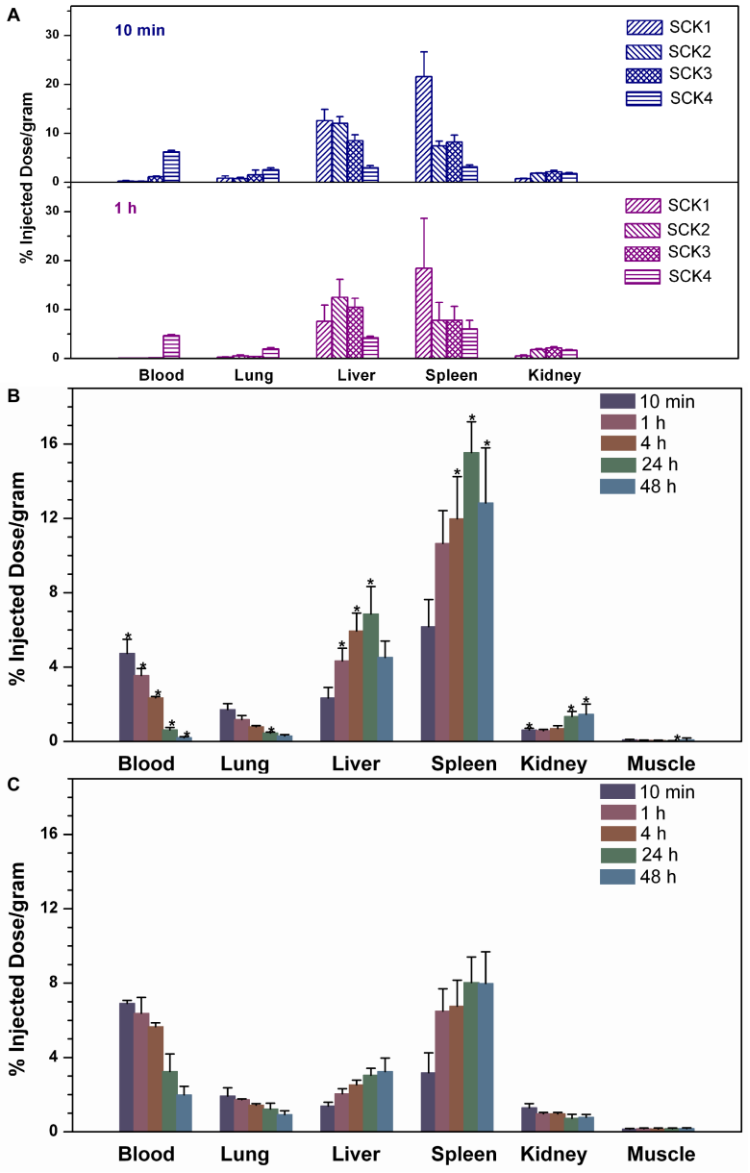

Figure 3.3. Biodistribution data for ^{64}Cu-labeled mPEGylated SCKs (which originated from mPEG2000$_x$-*g*-DOTAlysine$_2$-*g*-PAA$_{58-x}$-*b*-PS$_{60}$ block copolymer precursors, according to Scheme 1) in Sprague-Dawley rats (*ca*. 25 μg/kg rat body weight). Data are expressed as percent injected dose per gram (%ID/gram) ± one standard deviation (n = 4; ANOVA, $p < 0.0001$; *: $p < 0.05$, compared to **SCK5**). (A) Biodistribution of **SCK1-4** at 10 min and 1 h post injection. (B) Biodistribution of **SCK4** up to 48 h post injection. (C) Biodistribution of **SCK5** up to 48 h post injection.

In fact, the presence of approximately 1100 mPEG2000 grafts per nanoparticle led to a nearly full surface coverage for **SCK4**, and gave a high retention in blood over the first few hours after administration (2.3 ± 0.1 %ID/gram at 4 h) and an effective

clearance thereafter (0.2 ± 0.1 %ID/gram at 48 h post injection, Figure 3.3B). The prolonged circulation is the result of a low MPS uptake, reasonably due to slow opsonization and recognition by the macrophages of liver and spleen (up to 75% less dose in liver and spleen with respect to **SCK1** at 48 h post injection). As a note, the nonspecific binding of nanoscale objects with large vascular carrier proteins and red blood cells[60] might also play important roles for the *in vivo* fate of the SCKs. However, the latter issue could also be reduced because of the sufficient surface PEG coverage, which also directly related with their charge characteristics. No significant uptake in lung, muscle and kidney was detected.

mPEG Length Effect on Biodistribution. Besides surface graft density, the length of the mPEG grafts has been reported to be of paramount importance in order to maintain nanoparticles in the blood stream.[28, 30, 35, 41, 47, 61] Therefore, to assess whether PEG length effects also apply to SCKs, mPEGylated SCKs (**SCK6**) from $mPEG5000_3$-*g*-$DOTAlysine_2$-*g*-PAA_{55}-*b*-PS_{60} block copolymer precursors were prepared, ^{64}Cu-labeled and tested in normal rodents (Figure 3.4). The use of mPEG5000 grafts produced a longer nanoparticle blood circulation time and a lower liver uptake compared to the mPEG2000-containing analog with similar grafting density (**SCK3**). However, relative to **SCK3**, higher splenic accumulation was observed for **SCK6** at both considered time points. Noticeably, at 1 h, a nearly two-fold increase in spleen uptake was observed. Furthermore, clearance of **SCK6** from the bloodstream was faster than that observed for the SCKs with higher surface density of mPEG2000 grafts (**SCK4** and **SCK5**). The observation that PEG grafting density is more important than PEG length is supported by a recently report from Li and coworkers[62] on long circulating core crosslinked

nanoparticles ($t_{1/2,\beta}$ = 46.2 h) with hydrophilic shell domains constructed from very short PEG chains (nine ethylene oxide repeating units)

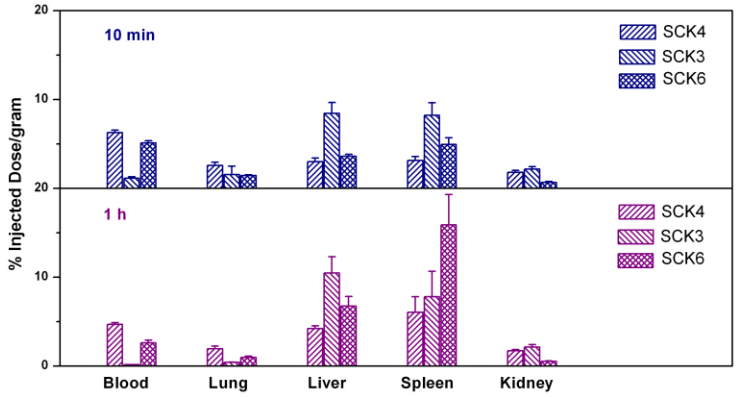

Figure 3.4. Biodistribution data of ^{64}Cu-labeled **SCK3**, **4**, (from mPEG2000-*g*-DOTAlysine-*g*-PAA-*b*-PS block copolymer precursors) and **6** (from mPEG5000-*g*-DOTAlysine-*g*-PAA-*b*-PS block copolymer precursors) in Sprague-Dawley rats (*ca*. 25 μg/kg rat body weight) at 10 min and 1 h post injection. Data are expressed as percent injected dose per gram (%ID/gram) ± one standard deviation (n = 4).

mPEG Location: Block Copolymer Structural Backbone *vs.* Pendent Grafts. A different approach for constructing PEGylated nanoparticles from triblock copolymers containing one PEG chain as the terminal unit (**SCK7**, Figure 3.5) could not achieve the prolonged blood circulation time obtained for **SCK4-6** (Figure 3.5C). From the intrinsic properties of PEG and the SCK PS core domain, as reported by Caldwell *et al.*,[63] a portion of the PEG chains may adsorb onto the PS core and not extend to the nanoparticle surface. The multiple PEG grafts in **SCK4-6** provides an excess for PEG coverage of the surface. Moreover, a combination of short and long PEG segments can be expected to extend from the surface of **SCK4-6**, based upon the chemical methodology used for the preparation of these particles which involved the introduction of mPEG along the block copolymer hydrophilic chain segment prior to nanoparticle assembly. In fact, a mixture of mPEG lengths have been found to provide a more effective steric barrier against

protein adsorption compared to a homogeneous population of longer chains.[64, 65] Further studies are needed in order to correlate the improved biodistribution for the SCKs, with the combination of effects such as the variation in mPEG chain length, decreased negative charge, increased nanoparticle rigidity, decreased mobility, and conformational degrees of freedom[66] for the mPEG grafts.

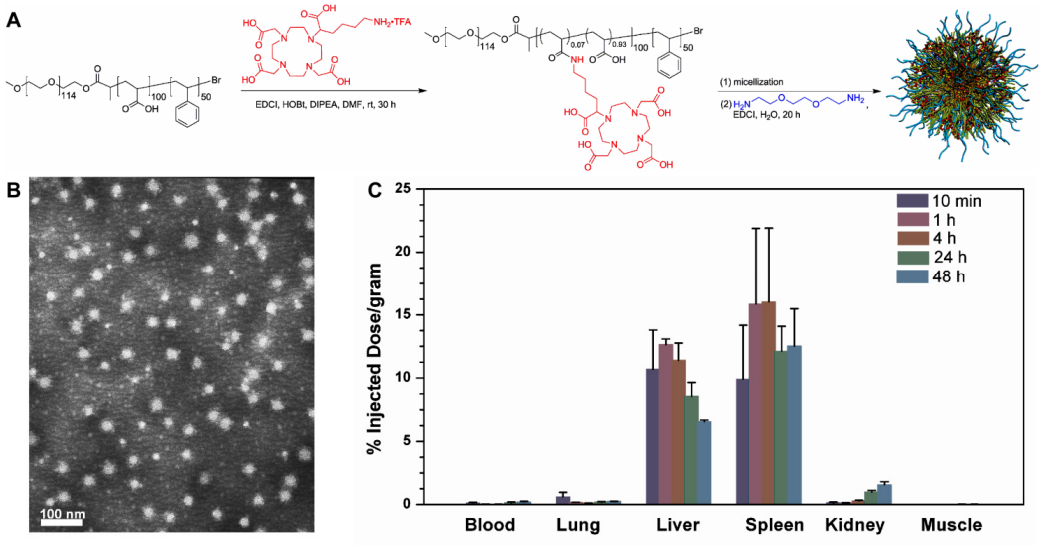

Figure 3.5. Preparation, TEM characterization, and *in vivo* evaluation of **SCK7**. (A) Schematic drawing of the preparation of **SCK7** from $DOTA_7$-*g*-PEG5000-*b*-PAA_{93}-*b*-PS_{50}. (B) TEM micrograph of **SCK7** (after negative stain with PTA). (C) Biodistribution of ^{64}Cu-labeled **SCK7** in Sprague-Dawley rats (*ca*. 25 μg/kg rat body weight; data are expressed as percent injected dose per gram (%ID/gram) ± one standard deviation, n = 4).

Crosslinking Extents (Surface Property) Effects. The influence of shell crosslinking extents on SCK bioavailability was also investigated. In general, increasing the crosslinking extent provides a more robust nanostructure with fewer negative charges (carboxylates) remaining on the surface. A slightly anionic surface was found to exert beneficial effects on nanoparticle blood circulation and MPS sequestration due to a reduction of non-specific binding of plasma opsonins.[67] However, high surface charge was found to have negative impact on the biodistribution, and several studies have

concluded that neutral particles exhibit lower rates of opsonization.[15, 16, 68] **SCK5** having *ca*. 50% surface charge reduction relative to **SCK4**, exhibited significantly higher retention in blood and lower accumulation in liver and spleen compared to **SCK4** at each time point evaluated (Figure 3.3C).

Small Animal PET Imaging Evaluation. Except for the spleen uptake, the results of small animal PET imaging (Figure 3.6A-3.6F and Table 3.3) showed a general concordance with the biodistribution findings. Little activity was detected in the heart of normal mice injected with ^{64}Cu-labeled **SCK1** at 4 and 24 h post injection (Figure 3.6A-3.6B), suggesting that no significant amounts of particles were circulating in blood at these time points. On the contrary, when imaging mice injected with ^{64}Cu-labeled **SCK4** (Figure 3.6C-3.6D) and **SCK5** (Figure 3.6E-3.6F), the heart of the mice was clearly visible up to 4 and 24 h post injection, respectively, as a consequence of the long blood retention. No significant activity was detected in kidneys and bladder of all the mice used for the imaging study, due to the lack of urinary excretion, while the presence of diffuse signal in the abdominal area suggested slow elimination through the intestine. Interestingly, **SCK5** exhibited the highest splene standardized uptake value (SUV) among the evaluated particles, suggesting high splenic uptake. This contradictory result between biodistribution and PET data is possibly due to a different interaction between nanoparticles and macrophage receptor populations in different animal species (rat *vs.* mouse).[16]

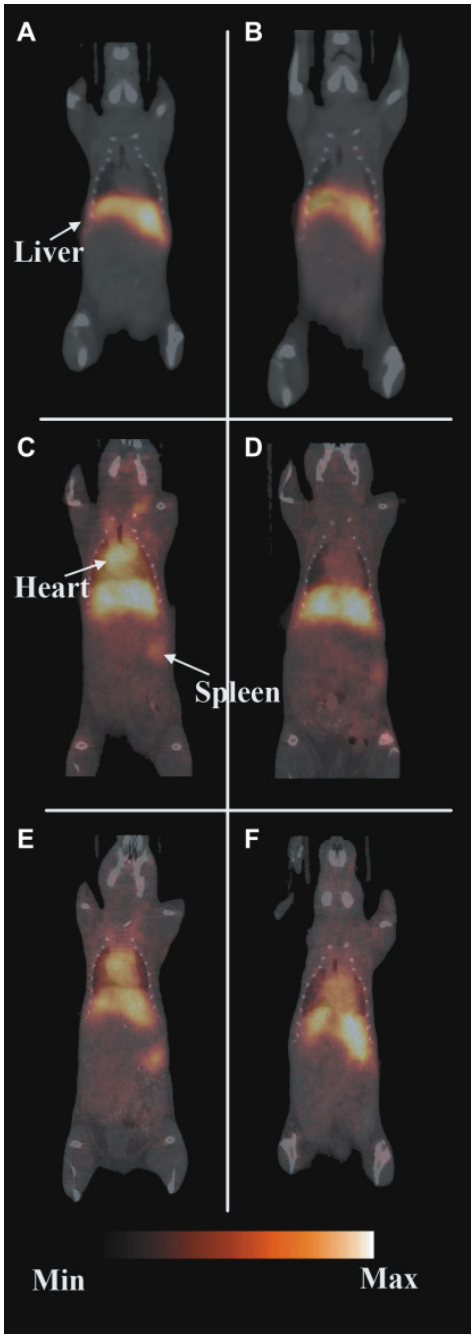

Figure 3.6. Co-registered small animal PET/CT images (coronal slices) of Balb/C mice (n = 2) injected with ^{64}Cu-labeled, mPEGylated SCKs (*ca*. 100 – 200 μCi of ^{64}Cu-labeled SCKs (0.15 – 0.3 mg/kg mouse body weight in 150 μL *via* tail vein). (A-B) **SCK1** at 4 and 24 h post injection, respectively. (C-D) **SCK4** at 4 and 24 h post injection, respectively. (E-F) **SCK5** at 4 and 24 h post injection, respectively. The image intensity is decay corrected and scaled by max/min frame. White arrows indicate heart, liver and spleen.

Table 3.3. Comparative organ-by-organ standardized uptake values (SUVs) for the ^{64}Cu-radiolabeled SCKs from the quantitation of small animal PET images in normal Balb/c mice.

Sample	SUV[a]					
	Heart		Liver		Spleen	
	4 h p.i[b]	24 h p.i	4 h p.i	24 h p.i	4 h p.i	24 h p.i
SCK1	0.3 ± 0.1	0.5 ± 0.1	8.3 ± 1.5	5.4 ± 0.8	1.9 ± 0.4	1.8 ± 0.4
SCK4	4.2 ± 0.9	1.7 ± 0.3	4.9 ± 0.3	5.1 ± 0.1	2.6 ± 0.1	2.3 ± 0.2
SCK5	4.6 ± 0.1	2.5 ± 0.5	5.3 ± 0.2	4.7 ± 0.1	4.0± 0.4	4.5 ± 0.5

[a] Data were obtained from 3D regions of interest in the selected organs, and are presented as mean SUV ± standard deviation. [b] Post injection.

Conclusions

In summary, we have employed a facile "pre-grafting" strategy to attach mPEG chains and DOTA chelators onto SCKs and their *in vivo* behaviors have been studied after ^{64}Cu radiolabeling. It is clear that mPEGylated SCKs exhibited longer blood circulation, in comparison to non-mPEGylated analogs. More importantly, the blood retention of these nanoparticles correlated well with the densities of mPEG grafts on the particle surfaces, which were controlled by the stoichiometry during the chemical modifications of the diblock copolymer precursors used for the construction of these nanoparticles. The study of *in vitro* interaction of plasma protein with mPEGylated SCKs and the development of mPEGylated SCKs bearing radionuclides and further labeled with high affinity targeting ligands and filled with therapeutic agents, as multi-functional devices for PET imaging-based diagnosis and monitoring of various disease states and their regression, are in progress.

Acknowledgement. This material is based upon work supported by the National Heart Lung and Blood Institute of the National Institutes of Health as a Program of Excellence in Nanotechnology (HL080729). The production of ^{64}Cu is supported by the National Cancer Institute (CA86307). The authors thank N. Kohrt and Prof. S. Sakiyama-Elbert for their assistance with DLS and Zeta Potential measurements, M. G. Veith for TEM imaging, N. Fettig, A. Roth, D. Werner, M. Morris, L. Strong, A. Stroncek, and J. Rutlin for the technical assistance with animal studies and Dr. J. S. Lewis and T. Voller for ^{64}Cu production. Postdoctoral and assistant professor fellowship provided by the Knut and Alice Wallenberg Foundation is gratefully acknowledged (A.M.N).

References

1. Brigger, I.; Dubernet, C.; Couvreur, P. "Nanoparticles in cancer therapy and diagnosis." *Adv. Drug Delivery Rev.* **2002,** *54*, 631-651.

2. Bianco, A.; Kostarelos, K.; Partidos, C. D.; Prato, M. "Biomedical applications of functionalised carbon nanotubes." *Chem. Commun.* **2005**, 571-577.

3. Ferrari, M. "Cancer nanotechnology: opportunities and challenges." *Nat. Rev. Cancer* **2005,** *5*, 161-171.

4. Farokhzad, O. C.; Langer, R. "Nanomedicine: Developing smarter therapeutic and diagnostic modalities." *Adv. Drug Delivery Rev.* **2006,** *58*, 1456-1459.

5. Kabanov, A. V. "Polymer genomics: An insight into pharmacology and toxicology of nanomedicines." *Adv. Drug Delivery Rev.* **2006,** *58*, 1597-1621.

6. Gajbhiye, V.; Kumar, P. V.; Tekade, R. K.; Jain, N. K. "Pharmaceutical and biomedical potential of PEGylated dendrimers." *Curr. Pharm. Des.* **2007,** *13*, 415-429.

7. Torchilin, V. P. "PEG-based micelles as carriers of contrast agents for different imaging modalities." *Adv. Drug Delivery Rev.* **2002,** *54*, 235-252.

8. Admas, M. L.; Lavasanifar, A.; Kwon, G. S. "Amphiphilic block copolymers for drug delivery." *J. Pharm. Sci.* **2003,** *92*, 1343-1355.

9. Gaucher, G.; Dufresne, M. H.; Sant, V. P.; Kang, N.; Maysinger, D.; Leroux, J. C. "Block copolymer micelles: preparation, characterization and application in drug delivery." *J. Controlled Release* **2005,** *109*, 169-188.

10. Nishiyama, N.; Kataoka, K. "Current state, achievements, and future prospects of polymeric micelles as nanocarriers for drug and gene delivery." *Pharmacol. Ther.* **2006,** *112*, 630-648.

11. Thurmond, K. B.; Kowalewski, T.; Wooley, K. L. "Shell Cross-Linked Knedels: A Synthetic Study of the Factors Affecting the Dimensions and Properties of Amphiphilic Core-Shell Nanospheres." *J. Am. Chem. Soc.* **1997,** *119*, 6656-6665.

12. Joralemon, M. J.; O'Reilly, R. K.; Hawker, C. J.; Wooley, K. L. "Shell Click-Crosslinked (SCC) Nanoparticles: A New Methodology for Synthesis and Orthogonal Functionalization." *J. Am. Chem. Soc.* **2005,** *127*, 16892-16899.

13. Li, Y.; Sun, G.; Xu, J.; Wooley, K. L. Shell crosslinked nanoparticles: A progress report of their design for drug delivery. In *Nanotechnology in Therapeutics: Current technology and applications*, Peppas, N. A., Hilt, Z. J., Thomas, B. J., Eds.; Horizon Bioscience: Wymondham, 2007; pp 381-407.

14. Read, E. S.; Armes, S. P. "Recent advances in shell cross-linked micelles." *Chem. Commun.* **2007**, 3021-3035.

15. Owens III, D. E.; Peppas, N. A. "Opsonization, biodistribution, and pharmacokinetics of polymeric nanoparticles." *Int. J. Pharm.* **2006,** *307*, 93-102.

16. Vonarbourg, A.; Passirani, C.; Saulnier, P.; Benoit, J. P. "Parameters influencing the stealthiness of colloidal drug delivery systems." *Biomaterials* **2006,** *27*, 4356-4373.

17. Moghimi, S. M.; Szebeni, J.; Hunter, A. C.; Murray, J. C. "Long-circulating and target-specific nanoparticles: theory to pratice." *Pharmacol. Rev.* **2001,** *53*, 283-318.

18. Harris, J. M., *Poly(ethylene Glycol) Chemistry: Biotechnical and Biomedical Applications*. Plenum Press: New York, 1992.

19. Yamaoka, T.; Tabata, Y.; Ikada, Y. "Distribution and tissue uptake of polyethylene glycol with different molecular weights after intravenous administration to mice." *J. Pharm. Sci.* **1994,** *83*, 601-606.

20. Harris, J. M.; Chess, R. B. "Effects of PEGylation on pharmaceuticals." *Nat. Rev. Drug Discov.* **2003,** *2*, 214-221.

21. Pasut, G.; Veronese, F. M. "PEGylation of proteins as tailored chemistry for optimized bioconjuates." *Adv. Polym. Sci.* **2006,** *192*, 95-134.

22. LaVan, T. M.; McGuire, T.; Langer, R. "Small-scale systems for in vivo drug delivery." *Nat. Biotechnol.* **2003,** *21*, 1184-1191.

23. Champion, J. A.; Katare, Y. K.; Mitragotri, S. "Particle shape: a new design parameter for micro- and nanoscale drug delivery carriers." *J. Controlled Release* **2007,** *121*, 3-9.

24. Geng, Y.; Dalhaimer, P.; Cai, S.; Tsai, R.; Tewari, M.; Minko, T.; Discher, D. E. "Shape effects of filaments versus spherical particles in flow and drug delivery." *Nat. Nanotech.* **2007,** *2*, 249-255.

25. Srinivas, G.; Discher, D. E.; Klein, M. L. "Key roles for chain flexibility in block copolymer membranes that contain pores or make tubes." *Nano Lett.* **2005,** *5*, 2343-2349.

26. Vittaz, M.; Bazile, D.; Spenlehauer, G.; Verrecchia, T.; Veillard, M.; Puisieux, F.; Labarre, D. "Effect of PEO surface density on long-circulating PLA-PEO nanoparticles which are very low complement activators." *Biomaterials* **1996,** *17*, 1575-1581.

27. Luck, M.; Parlke B.R.; Schroder, W.; Blunt, T.; Muller, R. H. "Analysis of plasma protein adsorption on polymeric nanoparticles with different surface characteristics." *J. Biomed. Mater. Res., Part A* **1998,** *39*, 478-485.

28. Gref, R.; Luck, M.; Quellec, P.; Marchand, M.; Dellacherie, E.; Harnisch, S.; Blunk, T.; Muller, R. H. ""Stealth" corona-core nanoparticles surface modified by polyethylene glycol (PEG): influences of the corona (PEG chain length and surface density) and of the core composition on phagocytic uptake and plasma protein adsorption." *Colloid. Surf., B* **2000,** *18*, 301-313.

29. Mosqueira, V. C. F.; Legrand, P.; Gulik, A.; Bourdon, O.; Gref, R.; Labarre, D.; Barratt, G. "Relationship between complement activation, cellular uptake and surface physicochemical aspects of novel PEG-modified nanocapsules." *Biomaterials* **2001,** *22*, 2967-2979.

30. Riley, T.; Stolnik, S.; Heald, C. R.; Xiong, C. D.; Garnett, M. C.; Illum, L.; Davis, S. S. "Physicochemical evaluation of nanoparticles assembled from poly(lactic acid)-poly(ethylene glycol) (PLA-PEG) block copolymers as drug delivery vehicles." *Langmuir* **2001,** *17*, 3168-3174.

31. Riley, T.; Heald, C. R.; Stolnik, S.; Garnett, M. C.; Illum, L.; Davis, S. S.; King, S. M.; Heenan, R. K.; Purkiss, S. C.; Barlow, R. J.; Gellert, P. R.; Washington, C. "Core-

Shell Structure of PLA-PEG Nanoparticles Used for Drug Delivery." *Langmuir* **2003,** *19*, 8428-8435.

32. Avgoustakis, K. "PEGylated poly(lactide) and poly(lactide-co-glycolide) nanoparticles: preparation, properties and possible application in drug delivery." *Curr. Drug Deliv.* **2004,** *1*, 321-333.

33. Lazos, D.; Franzka, S.; Ulbricht, M. "Size-Selective Protein Adsorption to Polystyrene Surfaces by Self-Assembled Grafted Poly(ethylene Glycols) with Varied Chain Lengths." *Langmuir* **2005,** *21*, 8774-8784.

34. Craparo, E. F.; Cavallaro, G.; Bondi, M. L.; Mandracchia, D.; Giammona, G. "PEGylated Nanoparticles Based on a Polyaspartamide. Preparation, Physico-Chemical Characterization, and Intracellular Uptake." *Biomacromolecules* **2006,** *7*, 3083-3092.

35. Vonarbourg, A.; Passirani, C.; Saulnier, P.; Simard, P.; Leroux, J. C.; Benoit, J. P. "Evaluation of pegylated lipid nanocapsules versus complement system activation and macrophage uptake." *J. Biomed. Mater. Res. A* **2006,** *78A*, 620-628.

36. Zahr, A. S.; Davis, C. A.; Pishko, M. V. "Macrophage uptake of core-shell nanoparticles surface modified with poly(ethylene glycol)." *Langmuir* **2006,** *22*, 8178-8185.

37. Phelps, M. E. "Positron emission tomography provides molecular imaging of biological processes." *Proc. Natl. Acad. Sci. U.S.A.* **2000,** *97*, 9226-9233.

38. Bartlett, D. B., Su, H., Hildebrandt, I. J., Weber, W. A., Davis, M. E. "Impact of tumor-specific targeting on the biodistribution and efficiency of siRNA nanoparticles measured by multimodality in vivo imaging." *Proc. Natl. Acad. Sci. U.S.A.* **2007,** *104*, 15549-15554.

39. Sun, X.; Rossin, R.; Turner, J. L.; Becker, M. L.; Joralemon, M. J.; Welch, M. J.; Wooley, K. L. "An assessment of the effects of shell cross-linked nanoparticle size, core composition, and surface PEGylation on in vivo biodistribution." *Biomacromolecules* **2005,** *6*, 2541-2554.

40. Liu, Z.; Cai, W.; He, L.; Nakayama, N.; Chen, K.; Sun, X.; Chen, X.; Dai, H. "*In vivo* biodistribution and highly efficient tumour targeting of carbon nanotubes in mice." *Nat. Nanotech.* **2007,** *2*, 47-52.

41. Pressly, E. D.; Rossin, R.; Hagooly, A.; Fukukawa, K.; Messmore, B. W.; Welch, M. J.; Wooley, K. L.; Lamm, M. S.; Hule, R. A.; Pochan, D. J.; Hawker, C. J. "Structural effects on the biodistribution and positron emission tomography (PET) imaging of well-defined 64Cu-labeled nanoparticles comprised of amphiphilic block graft copolymers." *Biomacromolecules* **2007,** *8*, 3126-3134.

42. Sun, G.; Xu, J.; Hagooly, A.; Rossin, R.; Li, Z.; Moore, D. A.; Hawker, C. J.; Welch, M. J.; Wooley, K. L. "Strategies for optimized radiolabelling of nanoparticles for in vivo PET imaging." *Adv. Mater.* **2007,** *19*, 3157-3162.

43. Xu, J.; Sun, G.; Rossin, R.; Hagooly, A.; Li, Z.; Fukukawa, K.; Messmore, B. W.; Moore, D. A.; Welch, M. J.; Hawker, C. J.; Wooley, K. L. "Labeling of Polymer Nanostructures for Medical Imaging: Importance of Cross-Linking Extent, Spacer Length, and Charge Density." *Macromolecules* **2007,** *40*, 2971-2973.

44. Pan, D.; Turner, J. L.; Wooley, K. L. "Folic acid-conjugated nanostructured materials designed for cancer cell targeting." *Chem. Commun.* **2003**, 2400-2401.

45. Moore, D. A., Metal complexes of tetraazamacrocycle derivatives. *PCT Int. Appl.* WO 2007106546 2007.

46. Gombotz, W. R., Wang, G. H.; Horbett, T. A., Hoffman, A. S. "Protein adsorption to poly(ethylene oxide) surfaces." *J. Biomed. Mater. Res.* **1991,** *25*, 1547-1562.

47. Jeon, S. I.; Lee, J. H.; Andrade, J. D.; DeGennes, P. G. "Protein-surface interactions in the presence of polyethylene oxide. I. Simplified theory." *J. Colloid Interface Sci.* **1991,** *142*, 149-158.

48. Joen, S. I.; Andrade, J. D. "Prorein-surface interactions in the presence of polyethylene oxide. II. Effect of protein size." *J. Colloid Interface Sci.* **1991,** *142*, 159-166.

49. Szleifer, I. "Protein adsorption on surfaces with grafted polymers: a theroretical approach." *Biophys. J.* **1997,** *72*, 595-612.

50. Herrwerth, S.; Eck, W.; Reinhardt, S.; Grunze, M. "Factors that determine the protein resistance of oligoether self-assembled monolayers - internal hydrophilicity, terminal Hydrophilicity, and lateral packing density." *J. Am. Chem. Soc.* **2003,** *125*, 9359-9366.

51. VandeVondele, S.; Voros, J.; Hubbell, J. A. "RGD-grafted poly-L-lysine-*graft*-(polyethylene glycol) copolymers block non-specific protein adsorption while promoting cell adhesion." *Biotechnol. Bioeng.* **2003,** *82*, 784-790.

52. Groll, J.; Amirgoulova, E. V.; Ameringer, T.; Heyes, C. D.; Rocker, C.; Nienhaus, G. U.; Moller, M. "Biofunctionalized, ultrathin coating of cross-linked star-shaped poly(ethylene oxide) allow reversible folding of immoblized proteins." *J. Am. Chem. Soc.* **2004,** *126*, 4234-4239.

53. Feller, L. M.; Cerritelli, S.; Textor, M.; Hubbell, J. A.; Tosatti, S. G. P. "Influence of Poly(propylene sulfide-*block*-ethylene glycol) Di- and Triblock Copolymer

Architecture on the Formation of Molecular Adlayers on Gold Surfaces and Their Effect on Protein Resistance: A Candidate for Surface Modification in Biosensor Research." *Macromolecules* **2005,** *38*, 10503-10510.

54. Love, J. C.; Estroff, L. A.; Kriebel, J. K.; Nuzzo, R. G.; Whitesides, G. M. "Self-assembled monolayers of thiolates on metals as a form of nanotechnology." *Chem. Rev.* **2005,** *105*, 1103-1170.

55. Dedinaite, A.; Iruthayaraj, J.; Gorochovceva, N.; Makuska, R.; Claesson, P. M. "Interfacial properties of chitosan-PEO graft oligomers: surface competition with unmodified chitosan oligomers." *Prog. Colloid Polym. Sci.* **2006,** *132*, 124-130.

56. Morgenthaler, S.; Zink, C.; Stadler, B.; Voros, J.; Lee, S.; Spencer, N. D.; Tosatti, S. G. P. "Poly(l-lysine)-*grafted*-poly(ethylene glycol)-based surface-chemical gradients. Preparation, characterization, and first applications." *Biointerphases* **2006,** *1*, 156-165.

57. Devanand, K.; Selser, J. "Asymptotic behavior and long-range interactions in aqueous solutions of poly(ethylene oxide)." *Macromolecules* **1991,** *24*, 5943-5947.

58. Huang, H.; Kowalewski, T.; Remsen, E. E.; Gertzmann, R.; Wooley, K. L. "Hydrogel-Coated Glassy Nanospheres: A Novel Method for the Synthesis of Shell Cross-Linked Knedels." *J. Am. Chem. Soc.* **1997,** *119*, 11653-11659.

59. Remsen, E. E.; Thurmond, K. B.; Wooley, K. L. "Solution and Surface Charge Properties of Shell Cross-Linked Knedel Nanoparticles." *Macromolecules* **1999,** *32*, 3685-3689.

60. Chambers, E.; Mitragotri, S. "Long circulating nanaparticles via adhesion on red blood cells: mechamism and extended circulation." *Exp. Biol. Med.* **2007,** *232*, 958-966.

61. Mao, S.; Neu, M.; Germershaus, O.; Merkel, O.; Sitterberg, J.; Bakowsky, U.; Kissel, T. "Influence of Polyethylene Glycol Chain Length on the Physicochemical and Biological Properties of Poly(ethylene imine)-*graft*-Poly(ethylene glycol) Block Copolymer/SiRNA Polyplexes." *Bioconjugate Chem.* **2006,** *17*, 1209-1218.

62. Yang, Z.; Zheng, S.; Harrison, W. J.; Harder, J.; Wen, X.; Gelovani, J. G.; Qiao, A.; Li, C. "Long-Circulating Near-Infrared Fluorescence Core-Cross-Linked Polymeric Micelles: Synthesis, Characterization, and Dual Nuclear/Optical Imaging." *Biomacromolecules* **2007,** *8*, 3422-3428.

63. ter Veen, R.; Fromell, K.; Caldwell, K. D. "Shifts in polystyrene particle surface charge upon adsorption of the Pluronic F108 surfactant." *J. Colloid Interface Sci.* **2005,** *288*, 124-128.

64. Stenkamp, V. S.; Berg, J. C. "The role of long tails in steric stabilization and hydrodynamic layer thickness." *Langmuir* **1997,** *13*, 3827-3832.

65. Pavey, K. D.; Olliff, C. J. "SPR analysis of the total reduction of protein adsorption to surfaces coated with mixutres of long- and short-chain polyethylene oxide block copolymers " *Biomaterials* **1999,** *20*, 885-890.

66. Peracchia, M. T.; Vauthier, C.; Passirani, C.; Couvreur, P.; Labarre, D. "Complement consumption by poly(ethylene glycol) in different conformations chemically coupled to poly(iso-butyl 2-cyanoacrylate) nanoparticles." *Life Sci.* **1997,** *61*, 749-761.

67. Yamamoto, Y.; Nagasaki, Y.; Kato, Y.; Sugiyama, Y.; Kataoka, K. "Long-circulating poly(ethylene glycol)-poly(D,L-lactide) block copolymer micelles with modulated surface charge." *J. Controlled Release* **2001,** *77*, 27-38.

68. Roser, M.; Fischer, D.; Kissel, T., "Surface-modified biodegradable albumin nano- and microspheres. II. Effect of surface charges on in vitro phagocytosis and biodistribution in rats." *Eur. J. Pharm. Biopharm.* **1998,** *46*, 255-263.

Chapter 4

A Fundamental Investigation of Cross-linking Ffficiencies within Discrete Nanostructures: Using the Cross-linker as a Reporting Molecule

[Portions of this work have been previously published as Guorong Sun, Nam S. Lee, William L. Neumann, John N. Freskos, Jeng J. Shieh, Richard B. Dorshow and Karen L. Wooley *Soft Matter* **2009**, accepted.]

Abstract

Various bi-functional pyrazine-based chromophores were used as cross-linkers to probe directly the efficiencies of their incorporation into the shell of block copolymer micelles. In addition, the block copolymer micelles were made to carry pre-installed reactive functionalities along the central block of an amphiphilic triblock copolymer. Unique photo-physical characteristics were observed, depending upon the type of pyrazine cross-linker, the conditions used for cross-linking and the stoichiometries applied.

Introduction

During the past decade, nano-scale micelles assembled from amphiphilic block copolymer precursors have attracted much attention due to their promising applications in the field of nanomedicine,[1-12] ranging from controlled delivery of diagnostic and therapeutic agents, to targeting of specific diseases and reporting of biological mechanisms *via* introduction of various functionalities.[6, 13] However, the thermodynamic stability of such nano-assemblies is only achieved above the critical micelle concentration and their stability *in vivo* is, therefore, of concern. To overcome this potential limitation, covalent cross-linking throughout the shell/core domain of micelles[14, 15] has been developed and demonstrated as an effective methodology for creating robust nanoscale objects that are capable of sustaining dilution.

The advantage of cross-linking is highlighted also through recent reports that core cross-linking could enhance the cargo "holding" ability of nanostructures[16] and the observation that increasing shell cross-linking extents prolonged the blood retention time of nanoparticles.[17] Moreover, the cross-linker can bring diverse functionality to the nanostructure, in addition to its structural role.[18, 19] While utilization of cross-linking technology grows rapidly in nano science,[20-26] the factors associated with their incorporation require detailed studies to provide fundamental insights for quantification and optimization. Herein, we report our investigations of the reaction efficiency during the shell cross-linking process by varying the cross-linker structures and properties.

Results and Discussion

In this current work, we were interested in building on previous studies, which have revealed that the surface chemistry, cross-linking extent and internal composition of nanoparticles are important parameters for their ultimate properties and potential biological utility. We also intended to advance the chemical methodologies and improve the efficiencies involved in the self assembly and cross-linking of amphiphilic block copolymers that lead to the preparation of well-defined nanoscale objects. Among the cross-linked nanostructures, shell cross-linked knedel-like (SCK) nanoparticles constructed from shell cross-linking with diamino cross-linkers throughout the poly(acrylic acid)-*block*-polystyrene (PAA-*b*-PS) micellar PAA shell domain (corona), *via* carbodiimide-mediated amidation, is one of the earliest and most highly-studied examples.[17, 27-31] While this strategy has been highly successful under controlled conditions, we felt that the activation efficiency of AA residues with the carbodiimide reagents under aqueous conditions could be a point for refinement. Therefore, the acrylic acid residues were replaced with pre-activated *N*-acryloxysuccinimide (NAS) groups. Because the NAS units are of lower hydrophilicity than are AA groups, the addition of a terminal hydrophilic block segment was required to create an amphiphilic block copolymer structure and allow for facile aqueous-phase assembly. This design led to a triblock copolymer structure, poly(ethylene oxide)-*block*-poly(*N*-acryloxysuccinimide)-*block*-polystyrene (PEO-*b*-PNAS-*b*-PS), containing terminal PEO and PS blocks as

hydrophilic and hydrophobic segments, respectively, to drive the assembly, and a central block segment having building blocks from AA active ester monomers (NAS) as pre-installed and pre-activated amidation sites. This triblock copolymer was established and exploited for the construction of functionalizable cross-linked nanoparticles (Figure 4.1). Three pyrazine-based cross-linkers with pendant functionalized amines (Figure 4.1 insertion) were designed as unique UV-vis active probes to report the extent of their incorporation during the cross-linking reactions.

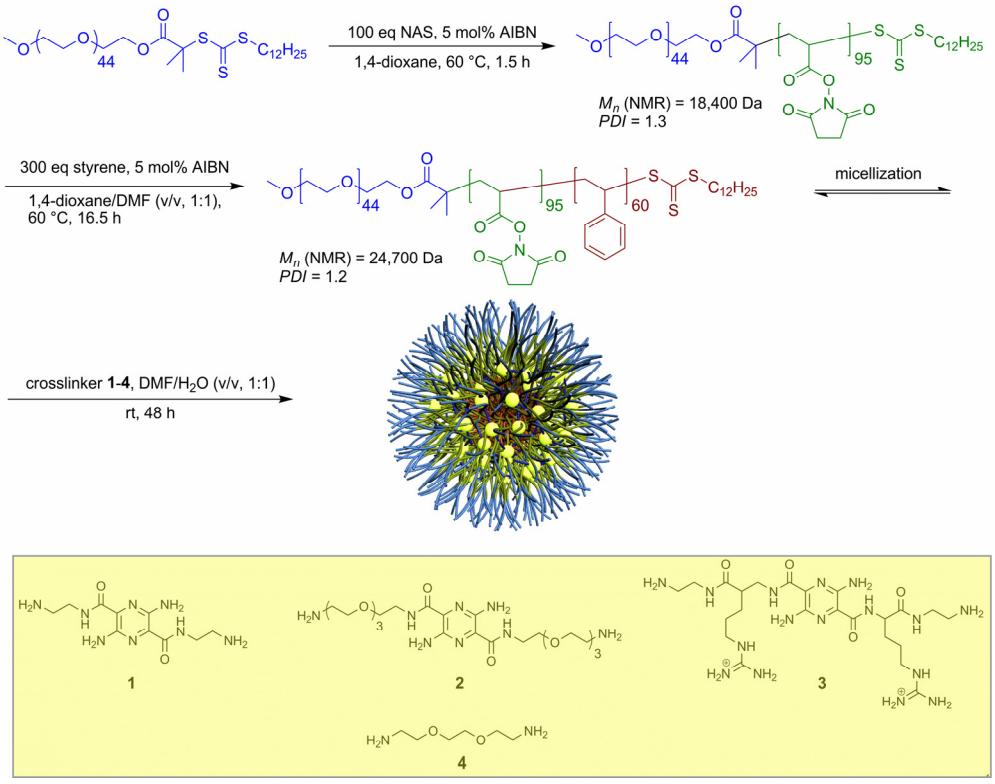

Figure 4.1. Schematic drawing of the synthetic route for the construction of SCK nanoparticles, having a PEO corona, an internal shell cross-linked *via* the UV-active pyrazine cross-linkers, and a hydrophobic PS core.

The triblock copolymer was synthesized by two sequential reversible addition-fragmentation chain transfer (RAFT) polymerizations[6, 7, 32] from a PEO-based macromolecular chain transfer agent (macro-CTA). Beginning from a mono-methoxy-terminated PEO_{45}-macro-CTA, chain extension with the NAS monomer was conducted using azobisisobutyronitrile (AIBN) as initiator in 1,4-dioxane ($[NAS]_0$ = 1 M, $[\text{macro-CTA}]_0:[AIBN]_0:[NAS]_0$ = 1:0.05:100) at 60 ˚C. This procedure was a slightly modified protocol from the reported RAFT polymerization of NAS.[33-35] The rate of NAS polymerization was still found to be rapid (*ca.* 90% conversion after 1.5 h). Gel permeation chromatography (GPC) analysis (Figure 4.2a, upper chromatogram) of the isolated diblock copolymer (after precipitation in diethyl ether) exhibited a mono-modal molecular weight distribution with a polydispersity index (*PDI*) of 1.3. Successful chain extension of the PNAS block (resonances at 1.78 to 2.20, 2.78, and 3.17 ppm) and maintenance of the RAFT agent chain-end group (resonances at 0.80, 1.10, 1.20, and 1.30 ppm) were confirmed by ^{1}H NMR spectroscopy (Figure 4.2b). The controlled polymerization was supported further by the experimental molecular weight, as measured by NMR spectroscopy ($M_{n,NMR}$ = 18,400 Da), being consistent with the theoretical molecular weight ($M_{n,theo}$ = 17,600 Da). Chain extension by styrene polymerization to afford the triblock copolymer also proceeded with control, indicating the retention of the chain end activity. The fact that no residual diblock PEO-*b*-PNAS macro-CTA was observed along the GPC profile of the triblock copolymer with PS as the third block

(Figure 4.2a, lower chromatogram, and Figure 4.2c, $M_{n,NMR}$ = 24,700 Da and *PDI* = 1.2) demonstrated its well-defined structure.

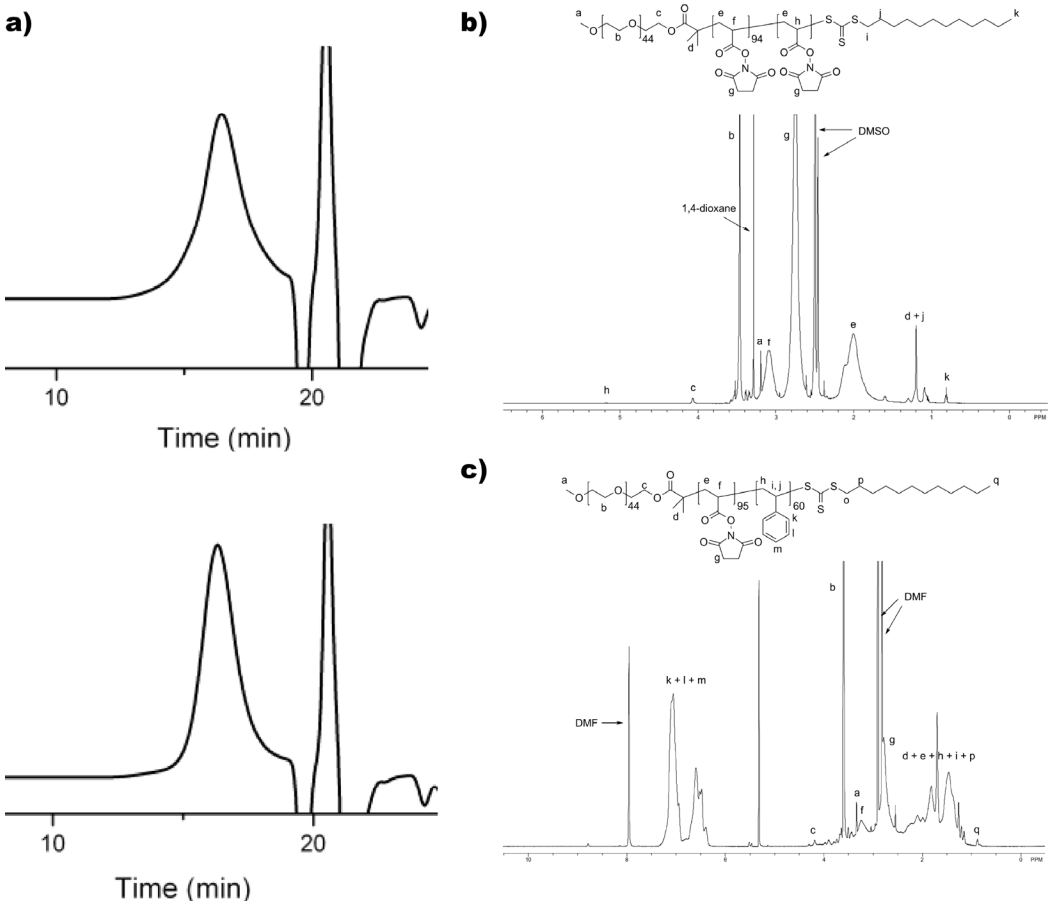

Figure 4.2. Characterizations of PEO_{45}-*b*-$PNAS_{95}$ and PEO_{45}-*b*-$PNAS_{95}$-*b*-PS_{60} block copolymer precursors. a): DMF-GPC profiles of PEO_{45}-*b*-$PNAS_{95}$ (top) and PEO_{45}-*b*-$PNAS_{95}$-*b*-PS_{60} (bottom) block copolymers. b): ^{1}H NMR spectrum of PEO_{45}-*b*-$PNAS_{95}$. c): ^{1}H NMR spectrum of PEO_{45}-*b*-$PNAS_{95}$-*b*-PS_{60}.

Micellization of the PEO_{45}-*b*-$PNAS_{95}$-*b*-PS_{60} triblock copolymer was conducted by adding water (selective solvent for PEO) to the block copolymer precursor solution in *N*,*N*-dimethylformamide (DMF, common solvent for all three blocks, *ca.* 1.0 mg/mL). Water was added to initialize micellization until 50 wt% of water content was achieved

within 2 h. The micelles were then directly characterized through dynamic light scattering (DLS), transmission electron microscopy (TEM), and atomic force microscopy (AFM). The results from DLS measurements showed that these micelles had narrow size distributions (Figure 4.3a-c) with a number-averaged hydrodynamic diameter of 74 ± 12 nm. By TEM (Figure 4.3d), the micelles were observed to have uniform diameters (D_{av} = 25 ± 1 nm), and they also had uniform heights (H_{av} = 20 ± 2 nm), as observed by AFM imaging (Figure 4.3e).

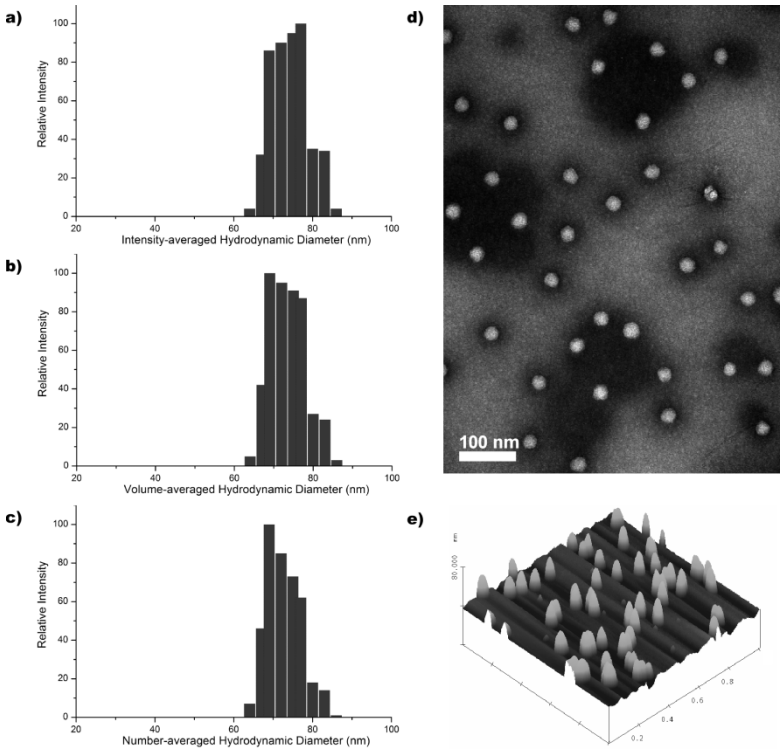

Figure 4.3. DLS, TEM and AFM data for the PEO_{45}-*b*-$PNAS_{95}$-*b*-PS_{60} micelles in DMF/H_2O (v/v = 1:1). DLS (a-c): histograms of micelle intensity-averaged, volume-averaged, and number-averaged hydrodynamic diameter size distributions, respectively. TEM (d): stained negatively with phosphotungstic acid. AFM (e): cast onto mica by spin-coating.

Pseudo *in situ* cross-linking experiments were performed after the micelle formation (see Experimental Section for details), although some amount of hydrolysis of NAS had already been occurring during the micellization process. Three nominal cross-linking extents (20%, 50%, and 100%, based upon the stoichiometric ratios of cross-linker *vs.* initial theoretical NAS residues, *i.e.*, 0.1 eq, 0.25 eq, and 0.5 eq, respectively) were studied. After incubating the micelle with the cross-linker at room temperature for 48 h, the un-reacted cross-linker, DMF, and small molecule by-products were removed through extensive dialysis against pH 7.2 PBS buffer (5 mM with 5 mM NaCl). As a note, a different work-up protocol was applied for the SCK nanoparticles prepared from cross-linker **3**, which involved multiple steps of dialysis due to its cationic character and electrostatic attraction to the nanostructures (see Experimental Section for details and *vide infra*).

Unusual photophysical effects were observed upon coupling of the UV-active cross-linkers into the micellar nanostructure framework. As depicted in Figure 4.4, for all three systems, the UV-vis maximum absorbance peaks of the pyrazine units within the SCKs at nominal 20% cross-linking extents clearly showed blue shifts of ~ 30 nm (from 433 nm to 400 nm) for SCKs derived from **1** and **2** *vs*. the small molecule cross-linkers or the small molecule cross-linkers mixed with PEO-*b*-PAA-*b*-PS micelles. For **3**, the blue shift was increased to ~ 45 nm (from 441 nm to 395 nm). These phenomena were observed also for the SCKs prepared from **1** and **2** with nominally 50% cross-linking, in

which the blue shifts were reduced to ~ 10 nm. For **SCK3** and **SCK7** at nominally 100% cross-linking and **SCK8** (prepared from **3** at nominally 50% cross-linking), no obvious peak shifts were noticed.

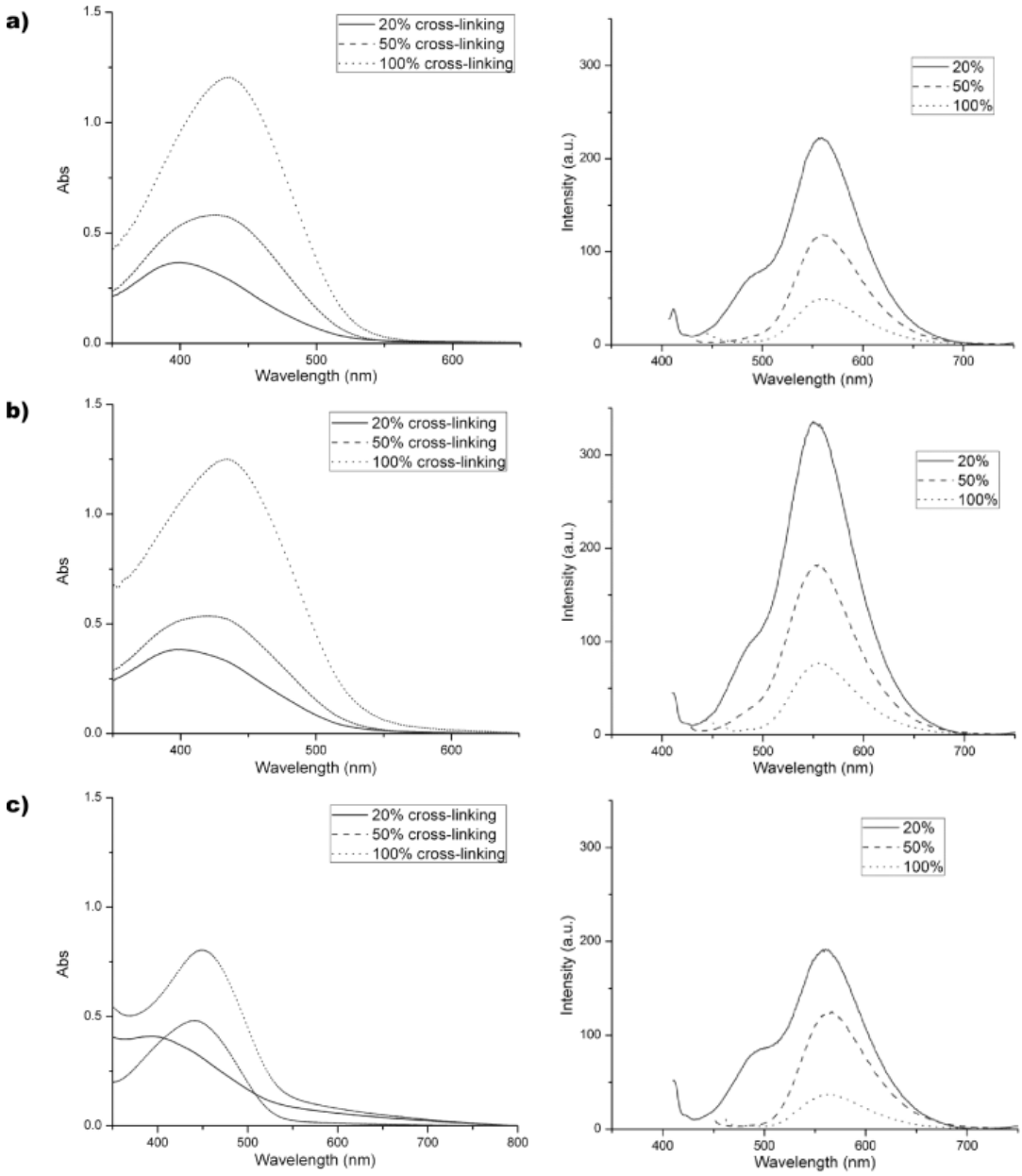

Figure 4.4. UV-vis absorbance and fluorescence emission profiles of SCKs constructed from cross-linking of PEO_{45}-*b*-$PNAS_{95}$-*b*-PS_{60} micelles with cross-linkers **1**-**3** at nominal 20%, 50%, and 100% cross-linking extents. a): UV-vis (left) and fluorescence (right) spectra of SCKs prepared from cross-linking with **1** at nominal 20% (solid), 50% (dashed), and 100% (dotted) cross-linking extents, respectively. b): UV-vis (left) and fluorescence (right) spectra of SCKs prepared from cross-linking with **2** at nominal 20% (solid), 50% (dashed), and 100% (dotted) cross-linking extents, respectively. c): UV-vis (left) and fluorescence (right) spectra of SCKs prepared from cross-linking with **3** at nominal 20% (solid), 50% (dashed), and 100% (dotted) cross-linking extents, respectively.

We hypothesized that the blue shift might be related to functional group transformations of the aromatic amines on the pyrazine moiety, if they were to participate in reactions with the NAS units. While heteroaryl amines are very weakly basic and correspondingly weak nucleophiles, they may participate in coupling reactions due to effects of the nanoenvironment (*e.g.* proximity and potential desolvation of partially coupled linker arms within the shell structure). Once the amides form with the aryl amines, the energy gap between the ground and excited states would be increased due to the excess stabilization effect applied to the ground state, caused by the decrease in electron density on the pyrazine ring with the appearance of electron-withdrawing amides. This hypothesis was partially supported by the cross-linker incorporation efficiency results (*vide infra*) since the blue shift was only observed for SCKs in which less than 30% of the total NAS residues were consumed by the aliphatic amino groups (over 50% of NAS groups remaining) during the cross-linking process. By contrast, the control SCK nanoparticle (**SCK10**), cross-linked at 20% with **3** through our "conventional" synthetic approach,[17, 19, 27-30] did not exhibit the blue shift of the maximum absorbance peak (Figure 4.5a). This result serves as additional evidence for our hypothesis, since the carbodiimide-mediated amidation was carried out under conditions in which the coupling reagent (1-[3'-(dimethylamino)propyl]-3-ethylcarbodiimide methiodide, EDCI) was limited to 20 mol% of the AA residues. Therefore, the formed intermediates would be dominantly consumed by the cross-linker

terminal aliphatic amines while the aromatic amines remained intact. For **SCK9**, a minor red shift of ~ 5 nm was observed; the origin of which was not clear.

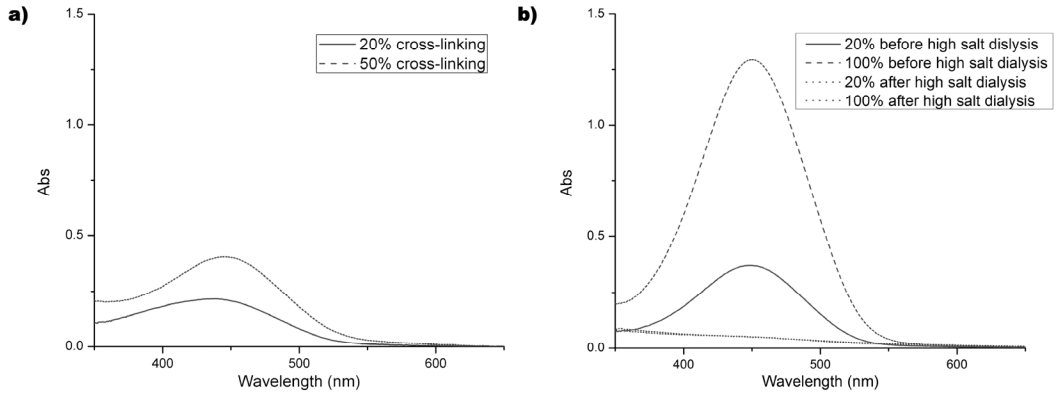

Figure 4.5. UV-vis profiles of control experiment I. a): UV-vis spectra of **SCK10** (solid, nominal 20% of cross-linking) and **SCK11** (dashed, nominal 50% of cross-linking), prepared through conventional carbodiimide-mediated amidation with cross-linker **3**. UV-vis profiles of control experiment II. b): UV-vis spectra of physical mixtures of PEO_{45}-*b*-PAA_{95}-*b*-PS_{60} micelles and **3** before dialysis and at stoichiometries of 0.1 eq. (solid) and 0.5 eq. (dashed) of **3**, relative to the AA residues, respectively. After dialysis against high salt buffers (pH 7.2 5 mM PBS buffer with 150 mM of NaCl) both physical mixture samples gave no signal from **3**, with their UV-vis traces overlapping (dotted).

From a structural viewpoint, cross-linkers **1** and **2** were distinguishable only through the spacer lengths and hydrophilicities, which further was revealed by their similar extinction coefficients (ε = 5,150 $M^{-1}cm^{-1}$ and 5,750 $M^{-1}cm^{-1}$ at pH 7.2, respectively). In contrast to earlier studies with coupling of large negatively-charged macrocycles into the nanoparticle shells,[30] the spacer length was unimportant in this study. No obvious incorporation efficiency differences were observed between **1** and **2** at each of the experimental cross-linking extents (Table 4.1). While the total amount of

cross-linkers increased from 0.1 eq to 0.25 eq (relative to NAS residues), the actual incorporation efficiency decreased from 60% to 40%. A plateau of the incorporation efficiency occurred with further increase of the cross-linker feeding ratio. These results might be associated with the unique core-shell structure of the PEO-*b*-PNAS-*b*-PS micelles. As soon as the micellization was initialized after water addition, the hydrolysis of NAS residues started simultaneously. However, the rate of hydrolysis was much slower compared with the rate of phase segregation-based micellar assembly. Therefore, it is expected that most of the NAS residues were "trapped" into the hydrophobic core domain while a "sub-shell" domain consisted of NAS and AA residues formed at the interface of PEO shell and PNAS/PS core domains. It was speculated that the cross-linking reaction dominantly occurred within this sub-shell region first because of the intrinsic hydrophilicity of the cross-linker, although the hydrophilicity increased from **1** to **3**, and also because of the mode of administration/transport of the cross-linker from the exterior inward As the reaction proceeded and more sub-shell NAS residues were converted into amides and hydrolyzed to AA carboxylates, the sub-shell domain would become increasingly hydrophilic and gradually merge into the "final" shell domain of the nanoparticle.[28] The framework structure would then reduce the permeability of the shell domain[31] and restrict further access of cross-linker to the "refurbished" sub-shell domain. And finally, the "deep onion" PNAS/PAA sub-shell would become un-reachable for the cross-linkers after incorporating over *ca.* 40% of **1** or **2**.

Improvement of incorporation efficiency (Table 4.1) at each nominal extent was achieved while using **3** (ε = 3,470 $M^{-1}cm^{-1}$ at pH 7.2), a cross-linker bearing positive charge. This improvement could be attributed to strong electrostatic interactions between the guanidine moieties of the bifunctional bis-arginyl-pyrazine **3**, and copolymer NAS-derived carboxylates, generated by partial hydrolysis of active esters during the micellization process. The electrostatic interactions could act as "driving force" for "pulling" **3** through the formed shell frameworks. Thus, pre-coordination of **3** with each "onion-like" sub-shell of the micelles *via* guanidine-carboxylate complexes resulted in a vast enhancement of inter-strand amide cross-linking reaction efficiency.

Table 4.1. Incorporation efficiency and maximum cross-linking extents upon varying the cross-linker structures and stoichiometries.

SCKs[a]	Cross-linker	Cross-linking extents[b]	Incorporation efficiency[c]	Maximum cross-linking extents[e]
SCK1	**1**	20 %	62 %	13 %
SCK2	**1**	50 %	45 %	23 %
SCK3	**1**	100 %	44 %[d]	44 %
SCK4	**2**	20 %	60 %	12 %
SCK5	**2**	50 %	40 %	20 %
SCK6	**2**	100 %	40 %[d]	40 %
SCK7	**3**	20 %	98 %	20 %
SCK8	**3**	50 %	69 %	35 %
SCK9	**3**	100 %	56 %	56 %
SCK10[f]	**3**	20 %	58 %	12 %
SCK11[f]	**3**	50 %	57 %	29 %

[a] Sample concentrations were 0.20-0.30 mg/mL in 5 mM PBS buffer (pH 7.2 with 5 mM NaCl). [b] Nominal cross-linking extents, based upon stoichiometry. [c] Calculated by the UV-vis absorption values at 433 nm (for cross-linker **1** and **2**) and 441 nm (for cross-linker **3**). [d] The number was not accurate as the Abs value was over 1.0. [e] See reference 29. [f] Prepared from "conventional" carbodiimide-mediated amidation by using PEO_{45}-*b*-PAA_{95}-*b*-PS_{60} micelles.

To confirm the existence of the electrostatic interactions between **3** and AA carboxylates, the PEO_{45}-*b*-PAA_{95}-*b*-PS_{60} micelles (prepared from micellization of the block copolymer precursor, which was synthesized from hydrolysis of PEO_{45}-*b*-$PNAS_{95}$-*b*-PS_{60}, see Experimental Section for details) were simply mixed physically with **3** under the identical reaction conditions as had been used for the cross-linking reactions (but, without covalent cross-linking being possible). After 5 days of dialysis against pH 7.2 PBS buffer (5 mM with 5 mM of NaCl), the UV-vis spectra of the mixtures (Figure 4.5b, solid and dashed) surprisingly indicated that 78% and 73% of the coordination efficiencies were achieved for 20% and 100% non-covalent cross-linking, respectively. After further dialyzing against 5 mM PBS buffer with much higher salt concentration (150 mM NaCl), which is a common protocol for breaking electrostatic interactions, the UV-vis spectra showed that there was no **3** remaining (Fig 4.5b, overlapping dotted lines). In fact, when **SCK7-9** were exposed to the same work-up process, the difference of **SCK7-9** (especially **SCK9**) UV-vis profiles before and after the high salt dialysis process (Figure 4.6) also supported that **3** could be incorporated into the SCKs through electrostatic interactions. The physical mixing of **3** with the PEO_{45}-*b*-PAA_{95}-*b*-PS_{60} micelles at the special stoichiometry (0.1 eq. of **3**, relative to the NAS/AA residues) did not affect the photo-physical properties of **3**. No maximum absorbance peak shift was found, which serves as additional evidence for our hypothesis that the blue shift was caused by the covalent modifications onto the pyrazine aryl amines.

Another control experiment with **3** was then followed, which involved construction of SCKs from the PEO_{45}-*b*-PAA_{95}-*b*-PS_{60} micelles with **3** through our "conventional" carbodiimide-mediated amidation strategy. Compared with the pre-installed active ester-mediated approach, relatively lower incorporation efficiencies (*ca.* 60%) were achieved at both 20% and 50% nominal cross-linking extents (**SCK10** and **SCK11** in Table 1, respectively). Moreover, attempts at 100% cross-linking failed from this approach, due to the fact that significant visual precipitation was observed. It is uncertain why the traditional methodology experienced this problem, while it did not occur with the new polymer system.

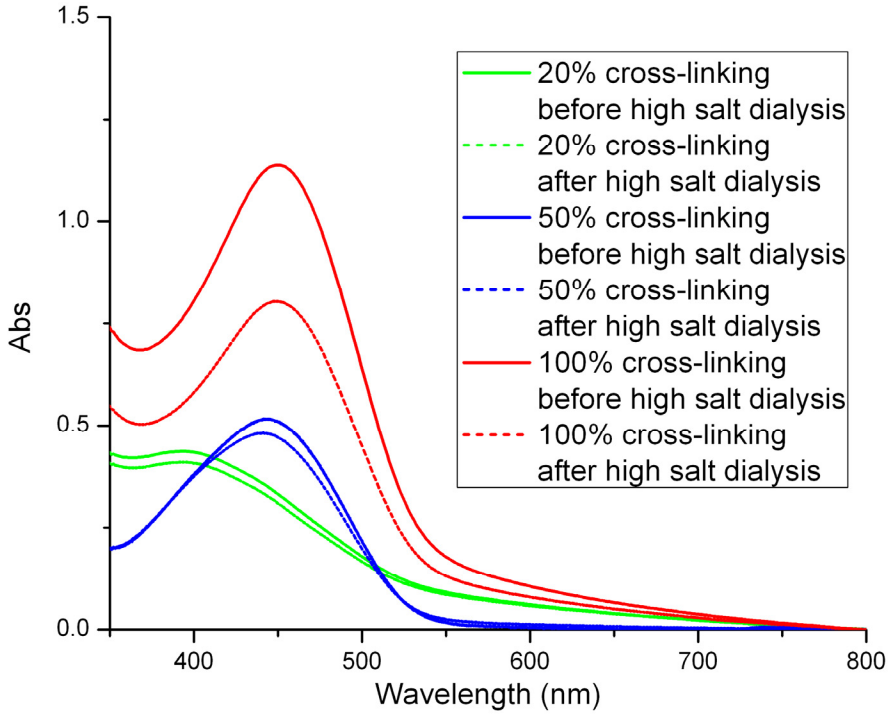

Figure 4.6. UV-vis profiles of **SCK7** (green), **SCK8** (blue), and **SCK9** (red) before (solid line) and after (dashed line) dialysis against pH 7.2 5 mM PBS (with 150 mM of NaCl).

To identify if the nanoparticle morphology changed after the cross-linking, **SCK1-12** were characterized by DLS and TEM; the results are summarized in Table 4.2, Figure 4.7 (the DLS histogram of particle size distribution by number-averaged D_h), and Figure 4.8 (TEM micrographs). From the DLS and TEM characterizations, SCKs prepared from **1** and **2** at lower cross-linking extents (< 30%) showed no morphological variations (Figure 4.8a-b and Fig4.8d-e), compared with the micelle (Figure 4.2d). A clear trend of hydrodynamic diameter decrease was observed with the increase of actual cross-linking extents from 0% to *ca.* 20%, suggesting that the nanostructures underwent "shrinking" after the cross-linking. Further increase of cross-linking extents caused nanostructure morphological changes, as verified by TEM imaging (Figure 4.8c and 4.8f), although the final nanostructures still displayed relatively narrow size distributions (Figure 4.7c and 4.7f, respectively).

Table 4.2. DLS and TEM characterization results for **SCK1-12**.

SCKs[a]	Cross-linker	Cross-linking extents[b]	$D_{h,number}$ (nm)[c]	D_{av} (nm)[d]
SCK1	**1**	13 %	62 ± 7	22 ± 2
SCK2	**1**	23 %	39 ± 2	27 ± 1
SCK3	**1**	44 %	56 ± 5	NAe
SCK4	**2**	12 %	64 ± 4	22 ± 2
SCK5	**2**	20 %	50 ± 2	30 ± 1
SCK6	**2**	40 %	56 ± 8	NA[e]
SCK7	**3**	20 %	104 ± 8	20 ± 1
SCK8	**3**	37 %	69 ± 5	28 ± 2
SCK9	**3**	69 %	91 ± 9	NA[e]
SCK10	**3**	12 %	85 ± 6	20 ± 1
SCK11	**3**	29 %	53 ± 4	28 ± 2
SCK12	**4**	100 %[f]	61 ± 3	28 ± 1

[a] Sample concentrations were 0.20-0.30 mg/mL in 5 mM PBS buffer (pH 7.2 with 5 mM NaCl). [b] Maximum cross-linking extents, based upon incorporation efficiency. [c] Number-averaged hydrodynamic diameter with standard deviation between 5 runs. [d] D_{av} were measured by TEM for the SCK nanoparticle core domains, for at least 150 particles. [e] Not available due to the irregular shape of the nanostructures. [f] Nominal 100% of cross-linking; maximum cross-linking extent could not be determined due to the lack of a chromophore on **4**.

For cross-linker **3**, the situation became more complicated: 1) For **SCK8** and **SCK11** at nominally 50% cross-linking, spherical morphologies were maintained (Figure 4.8h and 4.8k) and their particle sizes were consistent with the hydrodynamic sizes; 2) For **SCK7** and **SCK10** at lower cross-linking extents, the obviously increased D_h (*ca.* 100 nm) and the observed inter-particle association behaviour reflected by the TEM micrograph indicated the existence of strong inter-particle interactions; 3) For **SCK9** with the highest cross-linking extent (*ca.* 70%), "island-like" irregular morphology was noticed. As a note, this kind of morphological alteration caused by high extents of cross-linking was not limited to complicated cross-linkers. For example, **SCK12**, prepared

from a simple molecule 2,2´-(ethylene-dioxy)bis(ethylamine) as cross-linker under similar stoichiometry (0.5 eq, relative to the NAS residues), still displayed atypical morphology (Figure 4.8l).

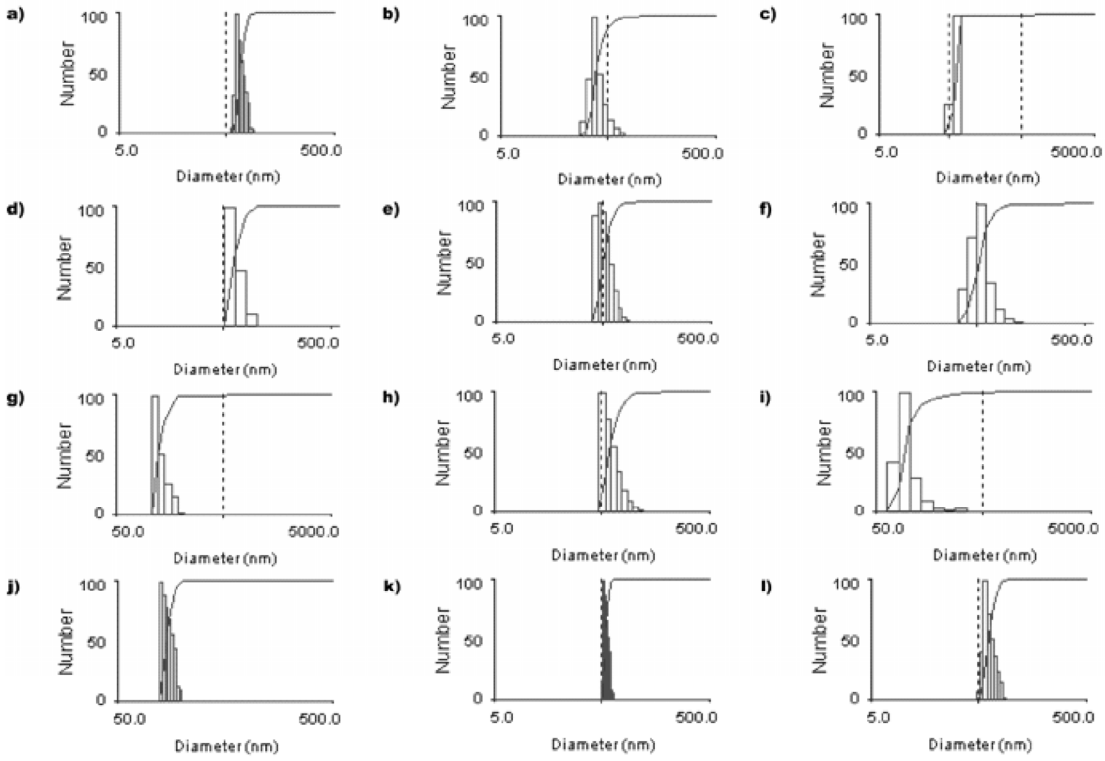

Figure 4.7. Histograms of number-averaged hydrodynamic diameter distributions for **SCK1-12** (a-l, respectively).

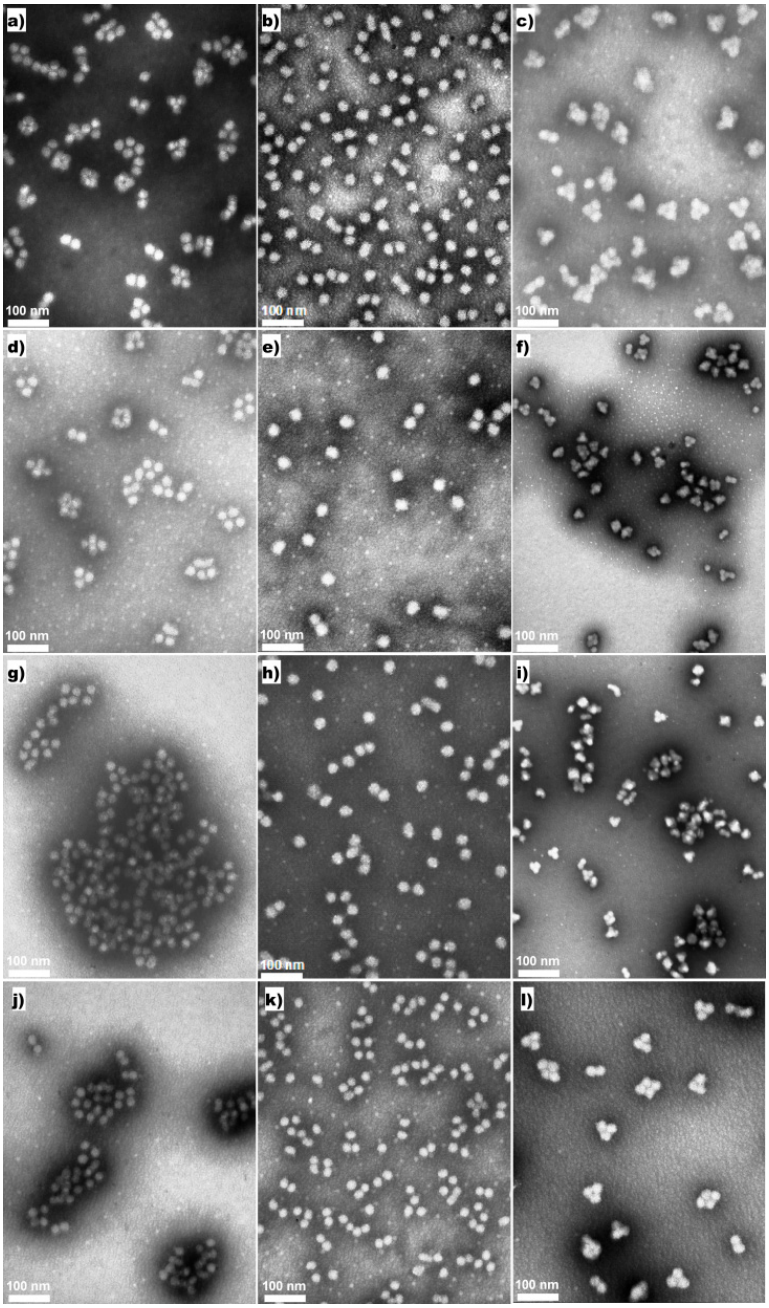

Figure 4.8. TEM micrographs of SCK nanoparticles at nominal 20%, 50%, and 100% cross-linking extents (stained negatively with PTA). a-c): TEM micrographs of **SCK1-3** prepared from cross-linker **1** at nominal 20%, 50%, and 100% cross-linking extents, respectively. d-f): TEM micrographs of **SCK4-6** prepared from cross-linker **2** at nominal 20%, 50%, and 100% cross-linking extents, respectively. g-i): TEM micrographs of **SCK7-9** prepared from cross-linker **3** at nominal 20%, 50%, and 100% cross-linking extents, respectively. j-k): TEM micrographs of **SCK10-11** prepared from cross-linker **3** at nominal 20% and 50% cross-linking extents, respectively. l): TEM micrograph of **SCK12** prepared from cross-linker **4** at nominal 100% cross-linking extent.

Finally, the fluorescence emission properties of **SCK1-9** were studied (Figure 4.4). The fluorescence emission intensities of these SCKs decreased as more pyrazine units were incorporated, which could be attributed to an amplified self-quenching effect between fluorophores. Interestingly, compared with **SCK1**, **SCK4** displayed enhanced fluorescence (*ca.* 50% of intensity increase) although they shared almost identical characteristic parameters (size, concentration, the amount of chromophore per nanoparticle, and the closely intrinsic photophysical-property of the cross-linkers **1** and **2**). This enhancement might be related to the fact that the longer spacer of **2** enabled the pyrazine moiety to adapt suitable conformations within the relatively loose shell domain and avoid self-quenching.

Conclusions

In summary, the amphiphilic and reactive triblock copolymer, PEO-*b*-PNAS-*b*-PS, having a well-defined structure was synthesized through RAFT polymerization and was then utilized for the construction of shell cross-linked nanoparticles using unique photo-active cross-linkers. Three pyrazine-derived bisamino cross-linkers with different spacer lengths and charges were incorporated into the nanostructures to study the factors associated with the reaction efficiency, employing the pyrazine to act as the reporting probe. It was found that the introduction of positive charges onto the cross-linker improved significantly the incorporation efficiency, while the length of the spacer had

little effect. The photo-physical properties of these cross-linked nanostructures were also investigated and a blue shift of over 30 nm was observed for the maximum absorbance peak, for all cross-linkers at lower incorporation levels (< 20%) within the nanoscale frameworks. Further studies on their pH-responsive photo-physical properties and their potential applications for optical imaging and monitoring, are currently underway.

Experimental Section

Materials. The mono-methoxy terminated mono-hydroxy poly(ethylene glycol) (mPEG2k, *MW* = 2,000 Da, PDI = 1.06) was purchased from Intezyne Technologies (Tampa, FL) and was used for the synthesis of macro-CTA[36] without further purification. The cross-linker **1-3** were synthesized according to the previous report.[37] Other chemicals were purchased from Aldrich and Acrose were used without further purification unless otherwise noted. Prior to use, styrene (99%), purchased from Aldrich, were distilled over calcium hydride and stored under N_2. The Supor 25 mm 0.1 μm Spectra/Por Membrane tubes (molecular weight cut-off (MWCO) 6-8 kDa), used for dialysis, were purchased from Spectrum Medical Industries Inc.. Nanopure water (18 mΩ•cm) was acquired by means of a Milli-Q water filtration system (Millipore Corp.; Bedford, MA).

Measurements. ^{1}H and ^{13}C NMR spectra were recorded on a Varian 600 MHz spectrometer interfaced to a UNIX computer using Mercury software. Chemical shifts

are referred to the solvent proton resonance. Infrared spectra were obtained on a Perkin-Elmer Spectrum BX FT-IR system using diffuse reflectance sampling accessories with FT-IR Spectrum v2.00 software.

The molecular weight distribution was determined by Gel Permeation Chromatography (GPC). The *N*,*N*-dimethylformamide (DMF) GPC was conducted on a Waters Chromatography, Inc. (Milford, MA) system equipped with an isocratic pump model 1515, a differential refractometer model 2414, and a two-column set of Styragel HR 4 and HR 4E 5 μm DMF 7.8 × 300 mm columns. The system was equilibrated at 70 °C in pre-filtered DMF containing 0.05 M LiBr, which served as polymer solvent and eluent (flow rate set to 1.00 mL/min). Polymer solutions were prepared at a concentration of *ca.* 3 mg/mL and an injection volume of 200 μL was used. Data collection and analysis was performed with Empower Pro software (Waters, Inc.). The system was calibrated with poly(ethylene glycol) standards (Polymer Laboratories, Amherst, MA) ranging from 615 to 442,800 Da.

The atomic force microscopy (AFM) characterization of micelles was performed by tapping-mode AFM under ambient conditions in air. The AFM instrumentation consisted of a Nanoscope III BioScope system (Digital Instruments, Veeco Metrology Group; Santa Barbara, CA) and standard silicon tips (type, OTESPA-70; L, 160 μm; normal spring constant, 50 N/m; resonance frequency, 246-282 kHz). Samples for AFM imaging analysis were prepared through spin-coating *ca*. 1.0 μL of the micelle solution (0.5

mg/mL) onto freshly cleaved mica plates (Ruby clear mica, New York Mica Co.) and allowed to dry freely in air.

Samples for Transmission Electron Microscopy (TEM) measurements were diluted with a 1 % phosphotungstic acid (PTA) stain (v/v, 1:1). Carbon grids were exposed to oxygen plasma treatment to increase the surface hydrophilicity. Micrographs were collected at 100,000× magnification and calibrated using a 41 nm polyacrylamide bead from NIST. The number average particle diameters (D_{av}) and standard deviations were generated from the analysis of a minimum of 150 particles from at least three different micrographs.

Hydrodynamic diameters (D_h) and size distributions for the vesicles in aqueous solutions were determined by dynamic light scattering (DLS). The DLS instrumentation consisted of a Brookhaven Instruments Limited (Worcestershire, U.K.) system, including a model BI-200SM goniometer, a model BI-9000AT digital correlator, a model EMI-9865 photomultiplier, and a model 95-2 Ar ion laser (Lexel Corp.) operated at 514.5 nm. Measurements were made at 25 ± 1 °C. Scattered light was collected at a fixed angle of 90°. The digital correlator was operated with 522 ratio spaced channels, and initial delay of 5 μs, a final delay of 100 ms, and a duration of 6 minutes. A photomulitplier aperture of 100 μm was used, and the incident laser intensity was adjusted to obtain a photon counting of between, 200 and 300 kcps. Only measurements in which the measured and calculated baselines of the intensity autocorrelation function agreed to within 0.1 % were

used to calculate particle size. The calculations of the particle size distributions and distribution averages were performed with the ISDA software package (Brookhaven Instruments Company), which employed single-exponential fitting, cumulants analysis, and CONTIN particle size distribution analysis routines. All determinations were repeated 5 times.

The UV-vis absorption spectra of SCKs were collected at room temperature using a Varian Cary 100 Bio UV-visible spectrophotometer and plastic cuvettes with 10 mm of light path. For each SCK absorption spectroscopy measurement, the pH 7.2 PBS (5 mM with 5 mM of NaCl) buffer solution outside the dialysis tubing was used as control.

The fluorescence spectra of SCKs were obtained at room temperature using a Varian Cary Eclipse fluorescence spectrophotometer. All fluorescence spectra from SCK solutions were measured at optical densities at the excitation wavelength. If not specially mentioned otherwise, an excitation wavelength of the observed maximum absorption peak was used. Each fluorescence spectrum was normalized with respect to the absorbed light intensity at the excitation wavelength.

Synthesis of PEO_{45}-*b*-$PNAS_{95}$. To a 25 mL Schlenk flask equipped with a magnetic stir bar dried with flame under N_2 atmosphere, was added the mPEG2k macro-CTA (0.24 g, 0.10 mmol) and 1,4-dioxane (10 mL). The reaction mixture was stirred 0.5 h at rt to obtain a homogeneous solution. To this solution was added NAS (1.7 g, 10 mmol) and AIBN (0.8 mg, 5 μmol). The reaction flask was sealed and stirred 10 min at rt. The

reaction mixture was degassed through several cycles of freeze-pump-thaw. After the last cycle, the reaction mixture was stirred for 10 min at rt before being immersed into a pre-heated oil bath at 60 °C to start the polymerization. After 1.5 h, the monomer conversion reached *ca.* 90% by analyzing aliquots collected through ^{1}H-NMR spectroscopy. The polymerization was quenched by cooling the reaction flask with liquid N_2. The solution was diluted with 20 mL of DMSO and precipitated into 600 mL of cold diethyl ether at 0 °C twice. The precipitants were collected, washed with 100 mL of cold ether, and dried under vacuum overnight to afford the PEO_{45}-*b*-$PNAS_{95}$ block copolymer precursor as a yellow solid (1.2 g, 65% yield based upon monomer conversion). ^{1}H NMR (600 MHz, DMSO-d_6, ppm): δ 0.81 (t, J = 6 Hz, 3H, dodecyl *CH₃*), 1.09 (br, 5H, *CH*$_3$ and dodecyl *CH₂*), 1.20 (br, 19H, *CH₃* and dodecyl *CH₂s*), 1.30 (br, 2H, dodecyl *CH₂*), 1.60 (t, J = 6 Hz, 2H, dodecyl *CH₂*), 2.01 (br, PNAS backbone protons), 2.75 (NAS *CH₂CH₂s*), 3.09 (br, PNAS backbone protons), 3.20 (s, mPEG terminal *OCH₃*), 3.47 (m, *OCH₂CH₂O* from the PEG backbone), 4.07 (br, 2H from the PEO backbone terminus connected to the ester linkage); ^{13}C NMR (150 MHz, DMSO-d_6, ppm): δ 172.8, 69.8, 41.2, 25.2; IR (NaCl, cm^{-1}): 2925, 1811, 1780, 1735, 1361, 1206, 1070, 649.

Synthesis of PEO_{45}-*b*-$PNAS_{95}$-*b*-PS_{60}. To a 10 mL Schlenk flask equipped with a magnetic stir bar dried with flame under N_2 atmosphere, was added the PEO_{45}-*b*-$PNAS_{95}$ macro-CTA (0.55 g, 30 μmol), 1,4-dioxane (2.2 mL), and DMF (2.2 mL). The reaction mixture was stirred 0.5 h at rt to obtain a homogeneous solution. To this solution was

added styrene (0.94 g, 9.0 mmol) and AIBN (0.24 mg, 1.5 μmol). The reaction flask was sealed and stirred 10 min at rt. The reaction mixture was degassed through several cycles of freeze-pump-thaw. After the last cycle, the reaction mixture was stirred for 10 min at rt before being immersed into a pre-heated oil bath at 60 °C to start the polymerization. After 16.5 h, the monomer conversion reached *ca.* 19% by analyzing aliquots collected through ^{1}H-NMR spectroscopy. The polymerization was quenched by cooling the reaction flask with liquid N_2. The polymer was purified by precipitation into 250 mL of cold diethyl ether at 0 °C twice. The precipitants were collected and dried under vacuum overnight to afford the block copolymer precursor as a yellow solid (0.58 g, 77% yield based upon monomer conversion). ^{1}H NMR (600 MHz, CD_2Cl_2, ppm): δ 0.81 (br, dodecyl *CH*$_3$), 1.10-2.40 (br, dodecyl Hs, PNAS, and PS backbone protons), 2.75 (NAS *CH*$_2$*CH*$_2$*S*), 3.15 (br, PNAS backbone protons), 3.28 (s, mPEG terminal *OCH*$_3$), 3.60 (m, *OCH*$_2$*CH*$_2$*O* from the PEG backbone), 6.20-7.30 (br, Ar Hs); ^{13}C NMR (150 MHz, DMSO-d_6, ppm): δ 172.8, 145.2, 128.0, 125.7, 69.8, 41.6, 25.2; IR (NaCl, cm^{-1}): 2925, 1810, 1779, 1732, 1452, 1362, 1208, 1070, 813, 699, 648.

General Procedure for Micellization of PEO$_{45}$-*b*-PNAS$_{95}$-*b*-PS$_{60}$. To a solution of PEO$_{45}$-*b*-PNAS$_{95}$-*b*-PS$_{60}$ block copolymer in DMF (*ca.* 1.0 mg/mL), was added dropwise an equal volume of nano-pure H_2O *via* a syringe pump at a rate of 15.0 mL/h, and the mixture was further stirred for 1 h at rt before using for characterizations and cross-linking reactions.

General Procedure for Cross-linking of PEO_{45}-*b*-$PNAS_{95}$-*b*-PS_{60} Micelles. To a solution of PEO_{45}-*b*-$PNAS_{95}$-*b*-PS_{60} micelles (15.0 mg of block copolymer precursor, 57.7 μmol of NAS residues) in 30.0 mL of DMF/H_2O (v:v = 1:1) at rt, was added dropwise over 10 min, a solution of cross-linker (5.8 μmol for nominal 20% of cross-linking, 14.5 μmol for nominal 50% of cross-linking, and 29.0 μmol for nominal 100% of cross-linking, respectively) in nano-pure H_2O. The reaction mixture was allowed to stir for 48 h at rt. For reactions involving cross-linker **1**, **2**, and **4**, the mixture was transferred to pre-soaked dialysis tubing (MWCO 6,000-8,000 Da) and dialyzed against 5.0 mM PBS (pH 7.2, with 5.0 mM NaCl) for 7 days to remove DMF, un-reacted cross-linker, and the small molecule by-products and afford an aqueous solution of cross-linked nanoparticles. For reactions involving cross-linker **3**, the mixture was transferred to pre-soaked dialysis tubing (MWCO 6,000-8,000 Da) and sequentially dialyzed against 5.0 mM PBS (pH 7.2, with 5.0 mM NaCl) for 3 days, 5.0 mM PBS (pH 7.2, with 150 mM NaCl) for 2 days, and 5.0 mM PBS (pH 7.2, with 5.0 mM NaCl) for 2 days to remove DMF, un-reacted cross-linker, and the small molecule by-products and afford an aqueous solution of cross-linked nanoparticles.

Synthesis of PEO_{45}-*b*-PAA_{95}-*b*-PS_{60}. A 25 mL round bottom flask equipped with a stir bar was charged with PEO_{45}-*b*-$PNAS_{95}$-*b*-PS_{60} (100 mg, 4.05 μmol), 10 mL of CH_2Cl_2 and 1 mL of trifluoroacetic acid (TFA). After adding 0.1 mL of water, the reaction mixture was stirred vigorously for 24 h at rt and then, was concentrated under

vacuum. The crude product was dissolved into 10 mL of DMF, transferred into pre-soaked dialysis tubing (MWCO 6,000–8,000 Da) and dialyzed against nano-pure H_2O (18.0 MΩ cm) for 4 days to remove small molecule impurities. The aqueous solution was lyophilized to afford the product as slightly yellow solid (60 mg, 95 % yield). ^{1}H-NMR (600 MHz, DMSO-d_6, ppm): δ 0.81-2.40 (br, docecyl Hs and polymer backbone Hs), 3.37 (s, 3H, mPEG terminal OCH_3), 3.42-3.82 (br, mPEG backbone -OCH_2CH_2O-Hs), 6.22-7.30 (br, Ar Hs), 12.25 (br, -COO*H*); ^{13}C NMR (150 MHz, DMSO-d_6, ppm): δ 175.8, 145.2, 128.0, 125.7, 69.8, 41.6; IR (NaCl, cm^{-1}): 3450-2900, 2925, 1718, 1458, 1258, 1183, 1103, 954, 794, 699.

Micellization of PEO_{45}-*b*-PAA_{95}-*b*-PS_{60}. To a solution of PEO_{45}-*b*-PAA_{95}-*b*-PS_{60} (30 mg) in 30 mL of DMF, was added dropwise 30 mL of nano-pure H_2O *via* a syringe pump at a rate of 15.0 mL/h, and the mixture was further stirred for 16 h at rt. Finally, the mixture was transferred into pre-soaked dialysis tubing (MWCO 6,000-8,000 Da) and dialyzed against nano-pure water for 5 days to afford the micelle solution.

Cross-linking of PEO_{45}-*b*-PAA_{95}-*b*-PS_{60} Micelle with 3 through "Conventional" Amidation. To a solution of PEO_{45}-*b*-PAA_{95}-*b*-PS_{60} micelle (10 mg of PEO_{45}-*b*-PAA_{95}-*b*-PS_{60} block copolymer precursor, 62 μmol of AA residues) in 40 mL of nano-pure water, was added dropwise over 30 min, a solution of **3** (3.7 mg, 6.2 μmol for **SCK10** and 9.2 mg, 15 μmol for **SCK11**, respectively) in nano-pure water. The mixture was stirred 2 h at rt and a freshly prepared EDCI solution (3.8 mg, 13 μmol for **SCK10** and

9.2 mg, 31 μmol for **SCK11**, respectively) in nano-pure water was then added over 1 h. The reaction mixture was further stirred 48 h at rt before transferring into a pre-soaked dialysis tubing (MWCO 6,000-8,000 Da) and sequentially dialyzing against 5 mM pH 7.2 PBS (with 5 mM NaCl) for 3 days, 5 mM pH 7.2 PBS (with 150 mM NaCl) for 2 days, and 5 mM pH 7.2 PBS (with 5 mM NaCl) for 2 days to afford an aqueous solution of the cross-linked nanoparticles.

Acknowledgements This material is based upon work supported partially by the National Heart, Lung and Blood Institute of the National Institutes of Health as a Program of Excellence in Nanotechnology (HL080729). Financial support from Covidien is gratefully acknowledged. N. S. Lee thanks GlaxoSmithKline for their financial support through the ACS Division of Organic Chemistry Graduate Fellowship. The authors thank Mr. G. M. Veith for the kind assistance with TEM imaging; and Dr. J. Kao for assistance with NMR measurements.

References

1. Trubetskoy, V. S. "Polymeric micelles as carriers of diagnostic agents." *Adv. Drug Delivery Rev.* **1999,** *37*, 81-88.

2. Brigger, I.; Dubernet, C.; Couvreur, P. "Nanoparticles in cancer therapy and diagnosis." *Adv. Drug Delivery Rev.* **2002,** *54*, 631-651.

3. Brannon-Peppas, L.; Blanchette, J. O. "Nanoparticle and targeted systems for cancer therapy." *Adv. Drug Delivery Rev.* **2004,** *56*, 1649-1659.

4. Farokhzad, O. C.; Langer, R. "Nanomedicine: Developing smarter therapeutic and diagnostic modalities." *Adv. Drug Delivery Rev.* **2006,** *58*, 1456-1459.

5. Nishiyama, N.; Kataoka, K. "Current state, achievements, and future prospects of polymeric micelles as nanocarriers for drug and gene delivery." *Pharmacol. Ther.* **2006,** *112*, 630-648.

6. Stenzel, M. H. "RAFT polymerization: an avenue to functional polymeric micelles for drug delivery." *Chem. Commun.* **2008**, 3486-3503.

7. York, A. W.; Kirkland, S. E.; McCormick, C. L. "Advances in the synthesis of amphiphilic block copolymers via RAFT polymerization: Stimuli-responsive drug and gene delivery." *Adv. Drug Delivery Rev.* **2008,** *60*, 1018-1036.

8. Hamidi, M.; Azadi, A.; Rafiei, P. "Hydrogel nanoparticles in drug delivery." *Adv. Drug Delivery Rev.* **2008,** *60*, 1638-1649.

9. Liu, Z.; Jiao, Y.; Wang, Y.; Zhou, C.; Zhang, Z. "Polysaccharides-based nanoparticles as drug delivery systems." *Adv. Drug Delivery Rev.* **2008,** *60*, 1650-1662.

10. Oh, J. K.; Drumright, R.; Siegwart, D. J.; Matyjaszewski, K. "The development of microgels/nanogels for drug delivery applications." *Prog. Polym. Sci.* **2008,** *33*, 448-477.

11. Xu, J.; Liu, S. "Polymeric nanocarriers possessing thermoresponsive coronas." *Soft Matter* **2008,** *4*, 1745-1749.

12. De Geest, B. G.; De Koker, S.; Sukhorukov, G. B.; Kreft, O.; Parak, W. J.; Skirtach, A. G.; Demeester, J.; De Smedt, S. C.; Hennink, W. E. "Polyelectrolyte microcapsules for biomedical applications." *Soft Matter* **2009,** *5*, 282-291.

13. Gauthier, M. A.; Gibson, M. I.; Klok, H.-A. "Synthesis of Functional Polymers by Post-Polymerization Modification." *Angew. Chem., Int. Ed.* **2009,** *48*, 48-58.

14. Guo, A.; Liu, G.; Tao, J. "Star Polymers and Nanospheres from Cross-Linkable Diblock Copolymers." *Macromolecules* **1996,** *29*, 2487-2493.

15. Thurmond, K. B.; Kowalewski, T.; Wooley, K. L. "Shell Cross-Linked Knedels: A Synthetic Study of the Factors Affecting the Dimensions and Properties of Amphiphilic Core-Shell Nanospheres." *J. Am. Chem. Soc.* **1997,** *119*, 6656-6665.

16. Gao, H.; Jones, M.-C.; Chen, J.; Prud'homme, R. E.; Leroux, J.-C. "Core Cross-Linked Reverse Micelles from Star-Shaped Polymers." *Chem. Mater.* **2008,** *20*, 3063-3067.

17. Sun, G.; Hagooly, A.; Xu, J.; Nystrom, A. M.; Li, Z.; Rossin, R.; Moore, D. A.; Wooley, K. L.; Welch, M. J. "Facile, Efficient Approach to Accomplish Tunable Chemistries and Variable Biodistributions for Shell Cross-Linked Nanoparticles." *Biomacromolecules* **2008,** *9*, 1997-2006.

18. Joralemon, M. J.; O'Reilly, R. K.; Matson, J. B.; Nugent, A. K.; Hawker, C. J.; Wooley, K. L. "Dendrimers clicked together divergently." *Macromolecules* **2005,** *38*, 5436-5443.

19. Lee, N. S.; Sun, G.; Neumann, W. L.; Freskos, J. N.; Shieh, J. J.; Dorshow, R. B.; Wooley, K. L. "Photonic Shell-Crosslinked Nanoparticle Probes for Optical Imaging and Monitoring." *Adv. Mater.* **2009**, *21*, 1344-1348.

20. Schärtl, W. "Crosslinked Spherical Nanoparticles with core-shell topology." *Adv. Mater.* **2000,** *12*, 1899-1908.

21. Vriezema, D. M.; Comellas Aragones, M.; Elemans, J. A. A. W.; Cornelissen, J. J. L. M.; Rowan, A. E.; Nolte, R. J. M. "Self-Assembled Nanoreactors." *Chem. Rev.* **2005,** *105*, 1445-1490.

22. O'Reilly, R. K.; Hawker, C. J.; Wooley, K. L. "Cross-linked block copolymer micelles: functional nanostructures of great potential and versatility." *Chem. Soc. Rev.* **2006,** *35*, 1068-1083.

23. Shirai, Y.; Morin, J.-F.; Sasaki, T.; Guerrero, J. M.; Tour, J. M. "Recent progress on nanovehicles." *Chem. Soc. Rev.* **2006,** *35*, 1043-1055.

24. Wakabayashi, R.; Kaneko, K.; Takeuchi, M.; Shinkai, S. "Toward the alignment of conjugated polymers into anisotropically-ordered structure." *New J. Chem.* **2007,** *31*, 790-799.

25. Leventis, N. "Three-Dimensional Core-Shell Superstructures: Mechanically Strong Aerogels." *Acc. Chem. Res.* **2007,** *40*, 874-884.

26. Read, E. S.; Armes, S. P. "Recent advances in shell cross-linked micelles." *Chem. Commun.* **2007**, 3021-3035.

27. Huang, H.; Kowalewski, T.; Remsen, E. E.; Gertzmann, R.; Wooley, K. L. "Hydrogel-Coated Glassy Nanospheres: A Novel Method for the Synthesis of Shell Cross-Linked Knedels." *J. Am. Chem. Soc.* **1997,** *119*, 11653-11659.

28. Murthy, K. S.; Ma, Q.; Clark, C. G., Jr.; Remsen, E. E.; Wooley, K. L. *Chem. Commun.* **2001**, 773-774.

29. Huang, H.; Wooley, K. L.; Schaefer, J. *Macromolecules* **2001,** *34*, 547-551.

30. Xu, J.; Sun, G.; Rossin, R.; Hagooly, A.; Li, Z.; Fukukawa, K.-i.; Messmore, B. W.; Moore, D. A.; Welch, M. J.; Hawker, C. J.; Wooley, K. L. "Labeling of Polymer Nanostructures for Medical Imaging: Importance of Cross-Linking Extent, Spacer Length, and Charge Density." *Macromolecules* **2007,** *40*, 2971-2973.

31. Sun, G.; Xu, J.; Hagooly, A.; Rossin, R.; Li, Z.; Moore, D. A.; Hawker, C. J.; Welch, M. J.; Wooley, K. L. "Strategies for optimized radiolabeling of nanoparticles for in vivo PET imaging." *Adv. Mater.* **2007,** *19*, 3157-3162.

32. Lowe, A. B.; McCormick, C. L. "Reversible addition-fragmentation chain transfer (RAFT) radical polymerization and the synthesis of water-soluble (co)polymers under

homogeneous conditions in organic and aqueous media." *Prog. Polym. Sci.* **2007,** *32*, 283-351.

33. Favier, A.; D'Agosto, F.; Charreyre, M.-T.; Pichot, C. "Synthesis of N-acryloxysuccinimide copolymers by RAFT polymerization, as reactive building blocks with full control of composition and molecular weights." *Polymer* **2004,** *45*, 7821-7830.

34. Li, Y.; Lokitz, B. S.; McCormick, C. L. "RAFT Synthesis of a Thermally Responsive ABC Triblock Copolymer Incorporating N-Acryloxysuccinimide for Facile in Situ Formation of Shell Cross-Linked Micelles in Aqueous Media." *Macromolecules* **2006,** *39*, 81-89.

35. Gujraty, K. V.; Yanjarappa, M. J.; Saraph, A.; Joshi, A.; Mogridge, J.; Kane, R. S. "Synthesis of homopolymers and copolymers containing an active ester of acrylic acid by RAFT: scaffolds for controlling polyvalent ligand display." *J. Polym. Sci., Part A: Polym. Chem.* **2008,** *46*, 7249-7257.

36. Sun, G.; Fang, H.; Cheng, C.; Lu, P.; Zhang, K.; Walker, A. V.; Taylor, J.; Wooley, K. L. "Benzaldehyde-functionalized polymer vesicles." *ACS Nano* **2009**, *3*, 673-681.

37. Neumann, W. L.; Rajagopalan, R.; Dorshow, R. B.; Shieh, J. J.; Freskos, J. N.; Lee, N. S.; Wooley, K. L. US Provisional Patent #60/986,171, filed Nov. 7, **2007**.

Chapter 5

Reversible Addition Fragmentation Chain Transfer (RAFT) Polymerization of 4-Vinylbenzaldehyde

[Portions of this work have been published previously as Guorong Sun, Chong Cheng and Karen L. Wooley *Macromolecules* **2007**, *40(4), 793-795.*]

Abstract

The direct reversible addition-fragmentation chain transfer (RAFT) polymerization of 4-vinylbenzaldehyde (VBA) was established as a new synthetic method for the preparation of well-defined poly(vinylbenzaldehyde) (PVBA), a polymer having reactive aldehyde side chain substiuents. RAFT polymerization of VBA was investigated using *S*-1-dodecyl-*S*′-(α,α′-dimethyl-α′′-acetic acid)trithiocarbonate as chain transfer agent and 2,2'-azobis(isobutyronitrile) as initiator in 1,4-dioxane or 2-butanone at 70-75 °C for 7.5-22.5 h. With 45-76% of monomer conversion, the resulting PVBA had well controlled number-average molecular weight (M_n) and low polydispersity (PDI < 1.17). The living characteristic of the RAFT polymerization process was confirmed by the linearity between the M_n values of PVBA and monomer conversions. Well-defined PVBA was further used as a macromolecular chain transfer agent in RAFT

polymerization of styrene (St), and a block copolymer PVBA-*b*-PSt with relatively low polydispersity (*PDI* = 1.20) was successfully synthesized.

Introduction

Construction of polymers with highly reactive functionalities that allow for further diverse functional group transformation (FGT) is an emerging research area in modern polymer chemistry.[1] Among these polymers, polymers bearing aldehyde functionalities are attractive because aldehydes are among the most reactive substrates for FGT under mild reaction conditions.[2] Conventional radical polymerization of aldehyde-functionalized monomers has been studied since 1950s,[3] however, the resulting polymers lacked well-defined structures, due to the non-living nature of the polymerization technique.[4-7] Anionic polymerization provided an alternative synthetic pathway for the preparation of aldehyde-functionalized polymers,[8-13] but the stringent polymerization conditions and tedious preparation procedures (protection of monomer, polymerization, and deprotection of the resulting polymers were required) significantly restrict the applicability of this synthetic route.

To efficiently prepare well-defined aldehyde-functionalized polymers, we investigated living radical polymerization of aldehyde-functionalized monomers. In the past decade, reversible addition fragmentation chain transfer (RAFT) polymerization has been developed and demonstrated as a powerful tool in living radical polymerization.[14,15] Relative to other living radical polymerization techniques, one important advantage of RAFT is that it provides facile and homogenous living polymerization systems applicable for a wide variety of monomers under relatively mild reaction conditions. In this

communication, we report our recent work of RAFT polymerization of 4-vinylbenzaldahyde (VBA), as a new methodology for the construction of well-defined aldehyde-functionalized polymers

Results and Discussion

Several synthetic pathways for the synthesis of VBA have been reported in the literature, including transition metal-catalyzed cross-coupling of 4-bromobenzaldehyde with ethylene or vinyl reagents, Grignard addition to *N*,*N*-dimethyl formamide (DMF) followed by acid hydrolysis, and Wittig olefination.[5-7] We prepared VBA by Wittig olefination of 4-(diethoxymethyl)benzaldehyde, a commercially available mono-protected benzene-1,4-dicarboxaldehyde, followed by deprotection (Scheme 5.1, a slight modification from Dhal's method[6]), because this reliable synthetic pathway had satisfactory yield (82% over 2-steps) with feasible scale-up and simple work-up protocols. As demonstrated by Dhal *et al*.,[6] radical polymerization of the intermediate monomer (diethyl acetal-protected styrene) followed by deprotection can also yield PVBA. However, we prefer to directly introduce aldehyde functionalities by using VBA as a (co)monomer because of our intention to avoid deprotection of polymers and also the key concern that the post-polymerization deprotection step may result in deconstruction of useful functionalities presented on the polymers, including the terminal RAFT functionalities.

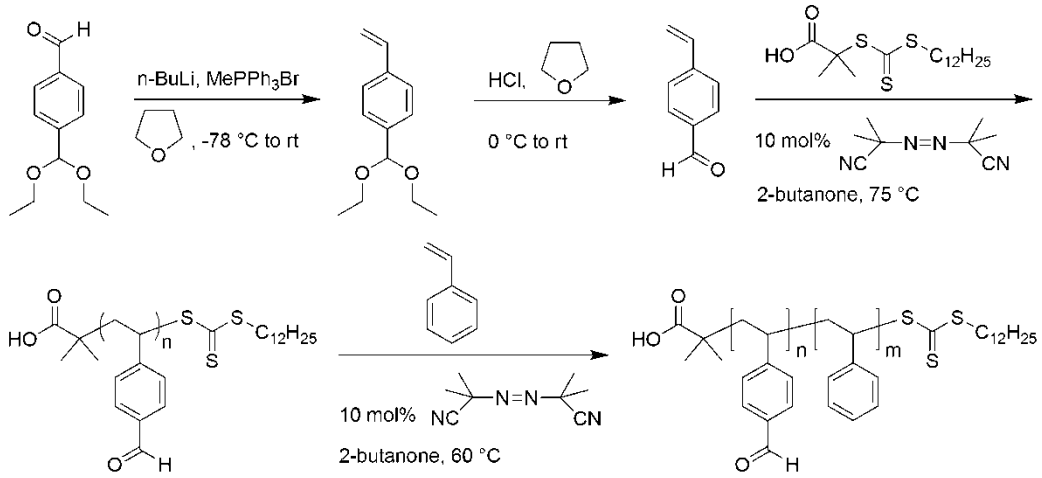

Scheme 5.1. RAFT polymerization of VBA.

RAFT polymerization of VBA was then conducted, and as a result, well-defined PVBA was synthesized (Table 5.1). Relative to other chain transfer agents (CTAs) for RAFT polymerization systems, *S*-1-dodecyl-*S*′-(α,α′-dimethyl-α′′-acetic acid)trithiocarbonate (DDMAT)[16] can be prepared readily and has less unfavorable odor and therefore, it was used as the CTA in our study ($[VBA]_0/[CTA]_0 = 100/1.0$). A typical thermal initiator 2,2'-azobis(isobutyronitrile) (AIBN) was used as initiator ($[CTA]_0/[AIBN]_0 = 1.0/0.1\text{-}0.2$), and the polymerization temperature was chosen at 70-75 °C to maintain a suitable decomposition rate of AIBN to provide initiating radicals. Because of the poor solubility of PVBA in its monomer, either 1,4-dioxane or 2-butanone was used as the polymerization solvent, and 2-butanone was further found as a better solvent than 1,4-dioxane for PVBA.[17] For each trial, the monomer conversion was determined by ^{1}H-NMR analysis of the final polymerization solution based on comparison of the integration area of resonances of aldehyde protons of PVBA at 9.8

ppm and the integration area of resonances of aldehyde protons of VBA at 10.0 ppm corresponding to the aldehyde proton signals from both polymer and monomer, respectively. PVBA was obtained by precipitation of the final polymerization solution twice into cold pentane and drying under vacuum.[18]

Table 5.1. Reversible addition fragmentation chain transfer polymerization of 4-vinylbenzaldehyde (VBA).

Entry	$[VBA]_0$:$[DDMAT]_0$:$[AIBN]_0$	Solvent	T (°C)	t (h)	Conversion[a]	$M_{n,\ calcd}$ (Da)	$M_{n,\ GPC}$ (Da)	PDI[b]
1	100:1.0:0.1	1,4-dioxane (71 vol %)	70	11	56%	7,800	8,800	1.14
2	100:1.0:0.1	1,4-dioxane (71 vol %)	70	22.5	76%	10,400	10,300	1.17
3	100:1.0:0.2	1,4-dioxane (50 vol %)	70	7.5	45%	6,300	7,900	1.09
4	100:1.0:0.1	2-butanone (50 vol %)	75	10	62%	8,500	9,100	1.07
5	100:1.0:0.1	2-butanone (50 vol %)	75	17.5	73%	10,000	10,500	1.06

$M_{n,\ calcd}$: Calculated number-average molecular weight based upon monomer conversion. $M_{n,\ GPC}$: Number-average molecular weight measured by Gel Permeation Chromatography (GPC). *PDI*: Polydispersity index. [a] By ^{1}H-NMR. [b] By GPC.

The well-defined structure of PVBA was verified by ^{1}H NMR and Gel Permeation Chromatography (GPC) analyses (Figure 5.1). As shown in Figure 5.1(a), the integration area ratio of aldehyde protons *vs.* aromatic protons in PVBA was 1.00:2.12:2.03, illustrating the essential absence of side reactions on the aldehyde functionality of VBA during the RAFT process and the quantitative presence of aldehyde functionalities in PVBA. The presence of the ω-trithiocarbonate RAFT functionality in PVBA was indicated by its ^{1}H NMR resonances at 0.88 and 3.22 ppm (for CH_3 and SCH_2, respectively), and the ^{1}H NMR resonances of the benzylic proton of the terminal

VBA unit at 4.84 ppm with an integration area ratio of 1.00:1.93 with the SCH_2 at 3.22 ppm. The number-average degree of polymerization was obtained by ^{1}H NMR spectroscopy (DP_{NMR}), by comparing the intensity of the benzylic proton of the terminal VBA unit at 4.84 ppm with that of the aldehydic proton signal at 9.8 ppm, and was found to agree with the number-average degree of polymerization obtained by GPC (DP_{GPC}) within the error range (for example for sample entry 5 (Table 5.1), the DP_{NMR} and DP_{GPC} values were 78 and 75, respectively). Molecular weight and molecular weight distribution data for the PVBA samples were determined by GPC using THF as eluent (Figure 5.1(b)). All PVBA samples have not only excellent agreements between the GPC and calculated (based on monomer conversion) molecular weights but also monomodal molecular weight distributions with low polydispersties (PDI = 1.06-1.17), indicating well-controlled chain growth and very high chain transfer efficiency of the trithiocarbonate RAFT functionality in the polymerization process.

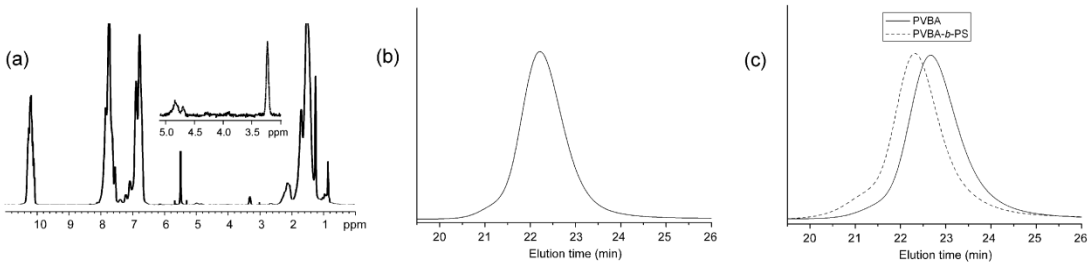

Figure 5.1. RAFT polymerization of 4-vinylbenaldehyde: (a) ^{1}H-NMR spectrum of PVBA (500 MHz, CD_2Cl_2; Table 5.1 entry 5). (b) GPC curve for PVBA (Table 5.1 entry 5). (c) GPC curve for PVBA (Table 5.1 entry 2) and PVBA-*b*-PSt (polymerization conditions: $[Styrene]_0/[macro\text{-}CTA]_0/[Initiator]_0$ = 150/1.0/0.1, 70 vol % of 2-butanone, 60 °C, 12 h).

To confirm the living characteristic of this RAFT polymerization system, the relationships between polymer molecular weights and monomer conversions were studied and the polymerization kinetics was also investigated (Figure 5.2). During polymerization, aliquots were withdrawn from the reaction vessel at predetermined times and analyzed by ^{1}H-NMR spectroscopy for determination of the monomer conversions and by GPC for determination of the polymer molecular weights and polydispersities.

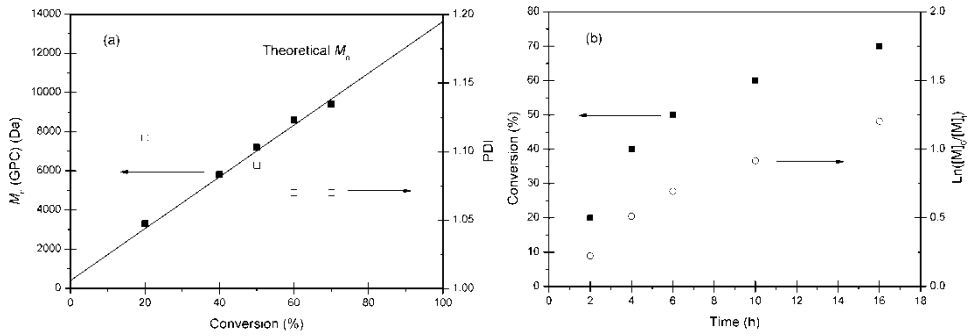

Figure 5.2. Kinetic plots for RAFT polymerization of 4-vinylbenzaldehyde: (a) relationship of number-average molecular weight (M_n, ■) and polydispersity index (*PDI*, □) *versus* monomer conversion; (b) time dependence of monomer conversion [M] and ln([M]$_0$/[M]$_t$). (polymerization conditions: [VBA]$_0$/[Chain Transfer Agent]$_0$/[Initiator]$_0$ = 100/1.0/0.1, 50 vol % of 2-butanone, 75 °C).

As shown in Figure 5.2(a), excellent linear agreement (R^2 = 0.9976) between polymer molecular weight and monomer conversion was obtained, and the resulting polymers also maintained narrow molecular weight distributions (*PDI* = 1.07 to 1.11). Such results verified the living characteristics of the RAFT polymerization process. As shown in Table 5.1, similar to conventional radical polymerization of VBA,[4,5,7a] RAFT polymerization of VBA proceeded relatively slowly. Figure 5.2(b) depicts the kinetic plot of the polymerization. Pseudo first-order kinetics were maintained at the initial

polymerization stage (~4 h), and then the kinetics deviated from linearity. Because AIBN has a short half-life of *ca.* 3 h at 75 °C, such retardation in polymerization might essentially be the result of the decreased radical concentration due to the depletion of AIBN.

The living characteristics of RAFT polymerization has allowed ready preparation of a broad variety of block copolymers.[19] We also investigated the chain extension of the well-defined PVBA having terminal RAFT functionality by RAFT polymerization as a synthetic method for the preparation of aldehyde-functionalized block copolymers. Although copolymerizations of vinylbenzaldehydes with styrene have already been extensively studied,[5,7] so far there is no literature report on the synthesis of block copolymers bearing pendant aldehyde functionalities by radical polymerization. Using PVBA ($M_{n,\,GPC}$ = 10,300 Da, *PDI* = 1.17) as macro-CTA and AIBN as initiator, RAFT polymerization of styrene ($[St]_0/[\text{macro-CTA}]_0/[AIBN]_0$ = 150/1.0/0.1) was conducted at 60 °C in 2-butanone (70 vol%). The polymerization was allowed to proceed for 12 h, and 17% conversion of styrene was obtained, as measured by ^{1}H NMR spectroscopy. As shown in Figure 5.1(c), the formation of diblock copolymer PVBA-*b*-PSt ($M_{n,GPC}$ = 12,500 Da, *PDI* = 1.19) by chain extension from the PVBA-based macro-CTA was verified by GPC analysis. Moreover, the good agreement between the experimental and calculated molecular weights ($M_{n,calcd}$ = 12,900 Da) and the mono-modal molecular

weight distribution of the PVBA-*b*-PSt illustrates the quantitative chain transfer efficiency of the PVBA-based macro-CTA.

Conclusions

In summary, we have established RAFT homopolymerization of 4-vinylbenzaldehyde as a new and facile synthetic method for the preparation of PVBAs with predictable molecular weights and low polydispersities. The chain extension from PVBA for the preparation of block copolymers also has been explored and PVBA-*b*-PSt has been constructed. To our knowledge, this is the first example of block copolymer bearing multiple aldehydes by direct polymerization without protected monomer, which was possible by applying radical polymerization. We believe that these homo- and block (co)polymers can serve as templates for feasible access of polymers with more complex architectures or conjugates with bio-active substrates for biological and medicinal applications *via* well-developed carbonyl chemistry.

Experimental Section

All chemicals were purchased from Aldrich or Acros and were used as received without further purifications unless noted. THF was distilled over sodium and stored under N_2. Styrene was distilled over CaH_2 and stored under N_2. AIBN was recrystallized

from methanol and stored at 0 °C before use. The chain-transfer agent DDMAT was synthesized as reported in the literature[16] and stored at room temperature.

^{1}H NMR and ^{13}C NMR spectra were recorded on solutions in $CDCl_3$ on a Varian Mercury 300 spectrometer with the residual solvent signal as an internal standard. Gel permeation chromatography (GPC) was conducted on a Waters 1515 HPLC (Waters Chromatography, Inc.) equipped with a Waters 2414 differential refractometer, a PD2020 dual-angle (15° and 90°) light scattering detector (Precision Detectors, Inc.), and a three-column series PL gel 5μm Mixed C, 500 Å, and 10^4 Å, 300 × 7.5 mm columns (Polymer Laboratories Inc.). The system was equilibrated at 35 °C in anhydrous THF, which served as the polymer solvent and eluent with a flow rate of 1.0 mL/min. Polymer solutions were prepared at a known concentration (*ca.* 3 mg/mL) and an injection volume of 200 μL was used. Data collection and analysis were performed, respectively, with Precision Acquire software and Discovery 32 software (Precision Detectors, Inc.). Interdetector delay volume and the light scattering detector calibration constant were determined by calibration using a nearly monodispersed polystyrene standard (Pressure Chemical Co., M_p = 90 kDa, M_w/M_n < 1.04). The differential refractometer was calibrated with standard polystyrene reference material (SRM 706 NIST), of known specific refractive index increment dn/dc (0.184 mL/g). The dn/dc values of the analyzed polymers were then determined from the differential refractometer response.

Synthesis of 4-Vinylbenzaldehyde. To a 250 mL RB flask equipped with a magnetic stir bar dried with flame under N_2 atmosphere at room temperature, was added methyltriphenylphosphonium bromide (10.8 g, 30.0 mmol) and 75.0 mL of dried THF. The reaction flask was cooled to -78 °C. To this suspension, was added dropwise a solution of *n*-BuLi (1.6 M in hexane, 18.3 mL, 29.2 mmol) over 20 min. The reaction mixture was stirred 30 min at -78 °C, then slowly was allowed to warm to room temperature and stirred for an additional 10 min at room temperature.

The orange-red solution was cooled to -78 °C. To this solution, a solution of the terephthaldehyde monodiethylacetal (5.0 g, 24 mmol) in 15.0 mL of dry THF was added dropwise over 1 h. The reaction mixture was stirred 30 min at -78 °C, 3 h at 0 °C, and allowed to warm to room temperature over 2 h.

The reaction was quenched by adding 10.0 mL of saturated $NaHCO_3$ solution. Water (100 mL) was added, the organic layer was collected and the aqueous layer was extracted with diethyl ether (20.0 mL × 3). The combined organic layers were washed with brine, dried with anhydrous Na_2SO_4, and concentrated *in vacuo*. The residue was used directly in the next reaction step without purification.

To a solution of the residue in 70.0 mL of THF at 0 °C, was added dropwise, 15.0 mL of 0.1 N HCl solution over 15 min. The reaction mixture was stirred for 1 h at 0 °C, slowly allowed to warm to room temperature, and then stirred for an additional 3 h at room temperature.

The THF was removed *in vacuo*, CH_2Cl_2 (50 mL) was added, and the aqueous layer was extracted three times with 15.0 mL of CH_2Cl_2. The combined organic layers were washed with brine, dried over anhydrous Na_2SO_4, and concentrated. Purification by column chromatography afforded the final product as a colorless oil (1:20 Et_2O/hexane, v/v). Yield 2.7 g, 82%. ^{1}H-NMR (300 MHz, $CDCl_3$, ppm): δ 5.45 (dd, J = 11.0 Hz, 0.6 Hz, 1H), 5.92 (dd, J = 17.4 Hz, 0.6 Hz, 1H), 6.78 (dd, J = 11.0 Hz, 17.4 Hz, 1H), 7.56 (½ABq, J = 6.8 Hz, 1.8 Hz, 2H), 7.85(½ABq, J = 6.8 Hz, 1.8 Hz, 2H), 10.00 (s, 1H); ^{13}C-NMR (75 MHz, $CDCl_3$, ppm): δ 117.6, 126.9, 130.3, 135.8, 136.1, 143.6, 191.9.

Polymerization of 4-Vinylbenzaldehyde. A general procedure of homopolymerization of 4-vinylbenzaldehyde under optimized reaction conditions was performed as follows.

To a 25 mL Schlenk flask equipped with a magnetic stir bar dried with flame under N_2 atmosphere, was added sequentially the DDMAT (45.8 mg, 0.125 mmol), 4-vinylbenzaldehyde (1.7 g, 13 mmol), 2-butanone (2.5 mL), and AIBN (2.1 mg, 0.013 mmol). The reaction flask was sealed and stirred 10 min at room temperature. The reaction mixture was degassed through several cycles of freeze-pump-thaw. After the last cycle, the reaction mixture was recovered back to room temperature and stirred for 10 min before immersing into a pre-heated oil bath at 75 °C to start the polymerization. The polymerization was monitored by analyzing aliquots collected at pre-determined times by ^{1}H-NMR spectroscopy. As the expected monomer conversion was reached, the

polymerization was quenched by quick immersion of the reaction flask into liquid N_2. THF (5.0 mL) was added to the reaction flask and the polymer was purified by precipitation into 150 mL of cold pentane at 0 °C twice. The precipitants were collected, washed with another 50 mL of cold pentane, and dried under vacuum overnight to afford the PVBA as yellow solid. ^{1}H-NMR (300 MHz, $CDCl_3$, ppm): δ 0.88 – 1.24 (br, dodecyl Hs), 1.52 – 2.06 (br, polymer backbone Hs), 3.22 (br, SCH_2 of the chain terminus), 4.84 (br, 1H from the polymer backbone benzylic terminus connected to trithiocarbonate), 6.58 – 6.85 (br ½ABq, aromatic Hs), 7.33 – 7.62 (br ½ABq, aromatic Hs), 9.88 (br, aldehyde Hs); ^{13}C-NMR (75 MHz, $CDCl_3$, ppm): δ 41.1, 128.2, 130.0, 135.1, 151.1, 191.8.

Synthesis of PVBA-*b*-PS. To a 10 mL Schlenk flask equipped with a magnetic stir bar dried with flame under N_2 atmosphere, was added the PVBA as macro-CTA (1.02 g, 0.1 mmol) and 2-butanone (4.0 mL). The reaction mixture was stirred 1 h at room temperature to obtain a homogeneous solution. To this solution was added styrene (1.56 g, 15.0 mmol) and AIBN (1.6 mg, 0.01 mmol). The reaction flask was sealed and stirred 10 min at room temperature. The reaction mixture was degassed through several cycles of freeze-pump-thaw. After the last cycle, the reaction mixture was recovered back to room temperature and stirred for 10 min before immersing into a pre-heated oil bath at 60 °C to start the polymerization. The polymerization was monitored by analyzing aliquots collected at pre-determined times by ^{1}H-NMR spectroscopy. As the expected monomer

conversion was reached, the polymerization was quenched by quick immersion of the reaction flask into liquid N_2. THF (5.0 mL) was added to the reaction flask and the polymer was purified by precipitation into 150 mL of cold pentane at 0 °C twice. The precipitants were collected, washed with another 50 mL of cold pentane, and dried under vacuum overnight to afford the PVBA-*b*-PS as yellow solid.

Acknowledgments Financial support from the National Heart Lung and Blood Institute of the National Institutes of Health as a Program of Excellence in Nanotechnology (U01 HL080729) is gratefully acknowledged. We also acknowledge postdoctoral fellowship support from Unilever Corporation (CC).

References and Notes

1. *Functional Monomers and Polymers;* Takemoto, K., Ottenbrite, R. M., Kamachi, M., Eds.; 2nd ed.; Marcel Dekker: New York, 1997.
2. Larock, R. C. *Comprehensive Organic Transformations — A Guide to Functional Group Transformations,* 2nd ed.; Wiley-VCH: New York, 1999.
3. Wiley, R. H.; Hobson, P. H. *J. Poly. Sci.* **1950**, *5*, 483-486.
4. Mulvaney, J. E.; Chang, D. M. *Macromolecules* **1980**, *13*, 240-243.
5. Pichot, C.; Charleux, B. *Makromol. Chem.* **1992**, *193*, 187-203.

6. (a) Dhal, P. K. *Macromol. Rep.* **1993**, *A30*, 93-99. (b) Dhal, P. K.; Khisti, R. S. *Chem. Mater.* **1993**, *5*, 1618-1623.

7. (a) Heinenberg, M.; Menges, B.; Mittler, S.; Ritter, H. *Macromolecules* **2002**, *35*, 3448-3455. (b) Heinenberg, M.; Ritter, H. *Macromol. Chem. Phys.* **2002**, *203*, 1804-1810.

8. Hirao, A.; Ishino, Y.; Nakahama, S. *Makromol. Chem.* **1986**, *187*, 141-147.

9. Hirao, A.; Nakahama, S. *Macromolecules* **1987**, *20*, 2968-2972.

10. Ishizone, T.; Kato, R.; Ishino, Y.; Hirao, A.; Nakahama, S. *Macromolecules* **1991**, *24*, 1449-1454.

11. Ishizone, T.; Sugiyama, K.; Hirao, A.; Nakahama, S. *Macromolecules* **1993**, *26*, 3009-3018.

12. Ishizone, T.; Sueyasu, N.; Sugiyama, K.; Hirao, A.; Nakahama, S. *Macromolecules* **1993**, *26*, 6976-6984.

13. Ishizone, T.; Utaka, T.; Ishino, Y.; Hirao, A.; Nakahama, S. *Macromolecules* **1997**, *30*, 6458-6466.

14. Rizzardo, E.; Chiefari, J.; Mayadunne, R. T. A.; Moad, G.; Thang, S. H. In *Controlled/Living Radical Polymerization. Progress in ATRP, NMP, and RAFT;* Matyjaszewski, K., Ed.; American Chemical Society: Washing, DC, 2000; Vol. 768, pp 278-296.

15. For comprehensive reviews of RAFT polymerization, see (a) Moad, G.; Rizzardo, E.; Thang, S. H. *Aust. J. Chem.* **2005**, *58*, 379-410. (b) Perrier, S.; Takolpuckdee, P. *J. Polym. Sci. Part A: Polym. Chem.* **2005**, *43*, 5347-5393. (c) Moad, G.; Rizzardo, E.; Thang, S. H. *Aust. J. Chem.* **2005**, *59*, 669-692.

16. Lai, J. T.; Filla, D.; Shea, R. *Macromolecules* **2002**, *35*, 6754-6756.

17. As far the co-solvents have been reported including DMF, 1,4-dioxane, benzene, and 2-butanone. However, we found the PVBA, especially those with relatively high molecular weight (DP > 60), do not dissolve well in either DMF or benzene.

18. Initially we used cold methanol for precipitation. After drying, ^{1}H-NMR spectra of the polymer clearly showed the partial formation of dimethyl acetal (extra signals at δ = 3.3 and 5.3 ppm) because the terminal carboxylic acid functionality catalyzed the "re-protection" reaction of the aldehyde.

19. (a) Lei, P.; Wang, Q.; Hong, J.; Li, Y. *J. Polym. Sci., Part A: Polym. Chem.* **2006**, *44*, 6600-6606. (b) Bussels, R.; Bergman-Gottgens, C.; Klumperman, B.; Meuldijk, J.; Koning, C. *J. Polym. Sci., Part A: Polym. Chem.* **2006**, *44*, 6419-6434. (c) Nguyen, T. L. U.; Eagles, K.; Davis, T. P.; Barner-Kowollik, C.; Stenzel, M. H. *J. Polym. Sci., Part A: Polym. Chem.* **2006**, *44*, 4372-4383. (d) Lai, J. T.; Shea, R. *J. Polym. Sci., Part A: Polym. Chem.* **2006**, *44*, 4298-4316. (e) Bilalis, P.; Pitsikalis, M.; Hadjichristidis, N. *J. Polym. Sci., Part A: Polym. Chem.* **2006**, *44*, 659-665. (f) Monteiro, M. J. *J. Polym. Sci., Part A: Polym.*

Chem. **2005**, *43*, 5643-5651. (g) O'Reilly, R. K.; Joralemon, M. J.; Hawker, C. J.; Wooley, K. L. *J. Polym. Sci., Part A: Polym. Chem.* **2006**, *44*, 5203-5217. (h) Germack, D. S.; Harrisson, S.; Brown, G. O.; Wooley, K. L. *J. Polym. Sci., Part A: Polym. Chem.* **2006**, *44*, 5218-5228.

Chapter 6

Benzaldehyde-functionalized Polymer Vesicles

[Portions of this work have been published previously as Guorong Sun, Huafeng Fang, Chong Cheng, Peng Lu, Ke Zhang, Amy V. Walker, John-Stephen Taylor and Karen L. Wooley *ACS Nano* **2009**, *3(3)*, 673-681.]

Abstract

Polymer vesicles with diameters of *ca.* 100-600 nm and bearing benzaldehyde functionalities within the vesicular walls were constructed through self assembly of an amphiphilic block copolymer PEO_{45}-*b*-$PVBA_{26}$ in water. The reactivity of the benzaldehyde functionalities was verified by crosslinking the polymersomes, and also by a one-pot crosslinking and functionalization approach to further render the vesicles fluorescent, each *via* reductive amination. *In vitro* studies found these labelled nanostructures to undergo cell association.

Introduction

Polymer vesicles, also known as "polymersomes",[1-6] are supramolecular assemblies of amphiphilic block copolymers[7-14] or complementary random copolymers[15] with sizes ranging from tens of nanometers to several hundreds of microns ("giant vesicles"). Similar to liposomes, polymersomes are composed of closed bilayer membranes with hollow cavities and, therefore, have tremendous potential for encapsulation and controlled delivery.[16-20] Moreover, their structures can be manipulated on both polymeric and supramolecular levels to afford tunability of their properties, including size control over nanoscale to microscale dimensions,[21-24] external stimulus responses,[25-32] mechanical properties,[33-35] membrane permeability,[36-39] and *in vivo* fate.[40, 41]

Starting from the middle of the 1990s, a variety of polymer vesicles have been developed and studied as efficient and promising candidates for the delivery of both hydrophilic (encapsulated inside the hollow cavity) and hydrophobic (loaded within the bilayer membrane wall) molecules. However, most of them consisted of amphiphilic block copolymers with limited functionalities for chemical transformations after vesicle construction. While polymersome surface functionalizations have been reported through reactions with the functionalities installed at the chain ends of the hydrophilic segments,[42, 43] there are limited literature reports associated with modifications of wall domains of polymersomes. Up to date, only radical polymerization,[33, 44] photo-induced

[2+2] cyclo-addition,[15, 45-47] base-catalyzed self condensation of siloxanes,[28, 48] and ring-opening of epoxides[49] have been employed to crosslink the walls of polymer vesicles.

With the increasing interests in potential biomedical applications that utilize the membrane of polymersomes as a functional unit,[18, 41, 50-53] introduction of highly reactive functionalities into polymer vesicles is being explored to expand the scope of chemistries that can be incorporated within such nanostructures. Herein, we report our approach for constructing size-tunable polymersomes with benzaldehyde functionalities (a diverse electrophile that undergoes reaction under mild conditions), as well as their crosslinking and fluorophore-functionalization *via* reductive amination (Scheme 6.1).

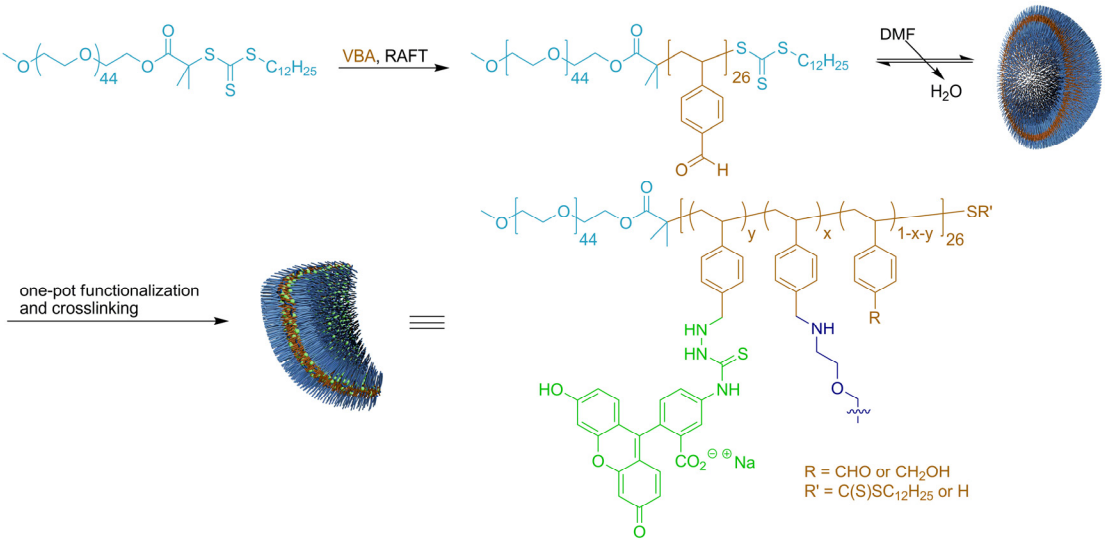

Scheme 6.1. Construction and functionalization of PEO_{45}-*b*-$PVBA_{26}$ vesicles through reductive amination.

Results and Discussion

Synthesis of Amphiphilic Block Copolymer Precursor. Poly(ethylene oxide)-*b*-poly(4-vinyl benzaldehyde) (PEO_{45}-*b*-$PVBA_{26}$), the amphiphilic diblock copolymer precursor for benzaldehyde-functionalized polymersomes, was prepared following our previously established method of reversible addition-fragmentation chain transfer (RAFT) polymerization of VBA.[54] The synthesis was conducted by using a mono-methoxy terminated PEO-based macro-chain transfer agent (macro-CTA, M_n = 2,360 Da, Figure 6.1a) and azobisisobutyronitrile (AIBN) in dry DMF heated at 75 °C for 3 h ($[VBA]_0$:$[CTA]_0$:$[AIBN]_0$ = 55:1:0.25; 55% conversion of VBA). ^{1}H NMR spectroscopic analysis of the isolated block copolymer (Figure 6.1b) confirmed successful chain extension for the formation of the PVBA block (resonances at 1.5 to 2.5, 4.8, 6.5 to 7.5, and 9.8 ppm) and maintenance of the RAFT agent chain-end group (resonances at 0.8 to 1.0, 1.3, and 3.2 ppm). The copolymer had a well-defined block structure of PEO_{45}-*b*-$PVBA_{26}$, which was supported by agreement between the number-average molecular weights by GPC (6,200 Da) and by ^{1}H NMR spectroscopy (5,800 Da, based upon comparison of the intensities of the resonances of the aldehyde proton of the VBA units at 9.8 ppm and methylene protons of EO units at 3.6 ppm with the characteristic resonances of the methine proton of the terminal monomer unit at 4.8 ppm and the SCH_2 protons from the RAFT functionality at 3.2 ppm). GPC analysis further showed that the

block copolymer has a narrow and mono-modal molecular weight distribution (Figure 6.1c) with a polydispersity index (PDI) of 1.2.

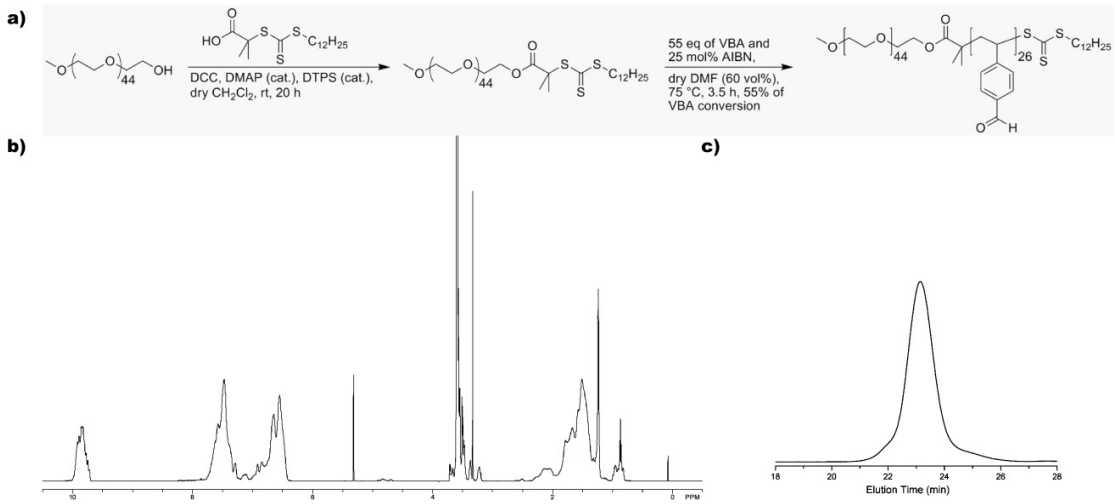

Figure 6.1. Synthesis of and characterizations of PEO_{45}-*b*-$PVBA_{26}$ block copolymer precursor. a) Schematic drawing of the synthesis of PEO_{45}-*b*-$PVBA_{26}$. b) ^1H NMR spectrum of PEO_{45}-*b*-$PVBA_{26}$. c) GPC profile of PEO_{45}-*b*-$PVBA_{26}$.

Construction and Characterization of PEO-*b*-PVBA Vesicles. General conditions under which amphiphilic block copolymers with a glassy hydrophobic segment (T_g = 86 ºC for PVBA) can be assembled in aqueous solutions were then applied.[7, 20, 23, 36, 47] The PEO_{45}-*b*-$PVBA_{26}$ block copolymer precursor was first dissolved into *N*,*N*-dimethylformamide (DMF, a good solvent for both PEO and PVBA blocks, *ca*. 1.0 mg/mL), followed by addition of nanopure water (a selective solvent for the PEO block) until the water content reached 50 wt%. Finally, the DMF was removed by extensive dialysis against water.

The vesicles were characterized by transmission electron microscopy (TEM, Figure 6.2a-b), scanning electron microscopy (SEM, Figure 6.2c-d), and dynamic light scattering (DLS, Figure 6.2e). The vesicular structure was confirmed by TEM and SEM. DLS analyses showed the hydrodynamic diameters of these vesicles were in the range of *ca*. 100 to 600 nm, with an intensity-average hydrodynamic diameter distribution centered at 290 nm and number-average hydrodynamic diameter distribution centered at 250 nm.

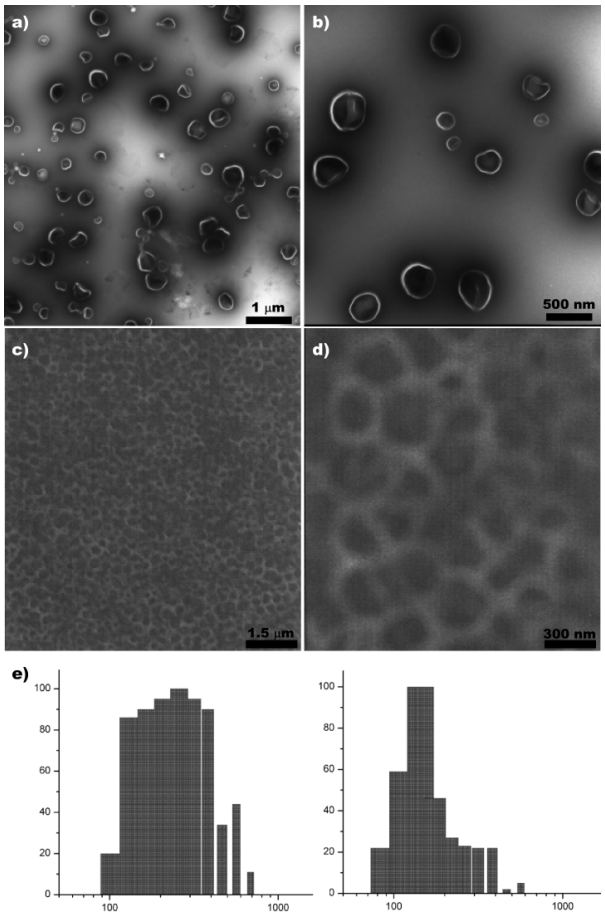

Figure 6.2. Characterization of polymer vesicles prepared from PEO_{45}-*b*-$PVBA_{26}$ block copolymer. a-b) TEM images of vesicles (stained negatively with PTA). c-d) SEM images of vesicles. e) DLS histograms of vesicle size distributions (left: intensity-average hydrodynamic diameter; right: number-average hydrodynamic diameter).

It is well-known that the formation of polymersomes usually passes through a morphological transformation of sphere-rod-vesicle.[4] To test whether this general trend also applied to our system, D_2O was added to a solution of PEO_{45}-*b*-$PVBA_{26}$ in DMF-d_7 (2.0 mg/mL) and aliquots were taken at predetermined water contents (9, 17, 23, and 33 wt%, respectively) for ^1H NMR and TEM measurements, the results are summarized in Figure 6.3.

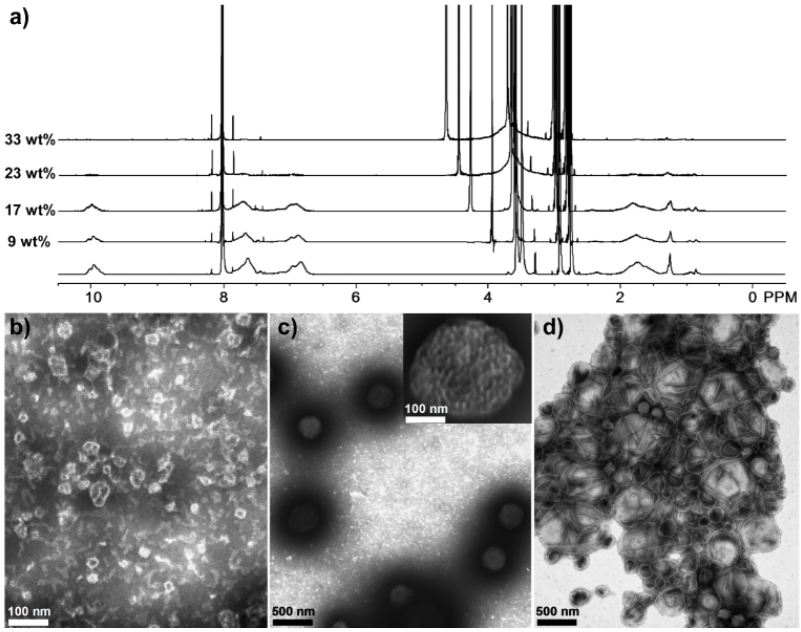

Figure 6.3. Morphological transformation during the self assembly process of PEO_{45}-*b*-$PVBA_{26}$. a) ^1H NMR spectra of aliquots in DMF-d_7 with different D_2O contents. b-d) TEM micrographs of particles and vesicles (stained negative with phosphotungstic acid) at 9, 17, and 23 wt% of water content, respectively.

At a low water content of 9 wt%, the ^1H NMR spectrum (Figure 6.3a) showed no obvious difference with the spectrum of the block copolymer in neat DMF. However, the TEM image (Figure 6.3b) clearly indicated the formation of nano-sized objects with

multiple morphologies including spherical particles, semi-closed membranes, and vesicles, but no rods were observed. As the water content was increased to 17 wt%, the resonance signals corresponding to PEO backbone at 3.5 ppm became broader and the intensities of PVBA resonances (0.8-2.5, 6.7-7.6, and 9.9 ppm) decreased, indicating the reduced flexibility of both structural blocks. TEM imaging (Figure 6.3c) revealed the formation of small nanoparticles whose morphology could not be unambiguously distinguished, and large aggregates (> 200 nm, Figure 6.3c insertion), which displayed large-compound vesicular morphology. Finally, clear vesicular morphology appeared at 23 wt% of water content with varied size ranging from 100 to 600 nm (Figure 6.3d). At this point, essentially no proton resonances from PVBA blocks were observed in the ^{1}H NMR spectrum, presumably because they were "tightly" packed into the vesicle walls without significant mobility. Meanwhile, the resonances of PEO backbone protons were further broadened, likely due to the restricted mobility of the EO units, especially those in close proximity to the PVBA-based vesicle walls.

Interestingly, when the "intermediate" sample with a low water content of 9 wt% was directly dialyzed against water, smaller vesicles with number-average hydrodynamic diameter of *ca.* 90 nm were produced (Figure 6.4). These small vesicles were stable over eight months, with no apparent growth in size. Although such size variation could not be interpreted quantitatively at this stage, these findings indicated kinetic control of self-assembled nanostructures of block copolymers and might provide new insight for

adjusting vesicle size without changing the chemical composition of their polymer precursors.

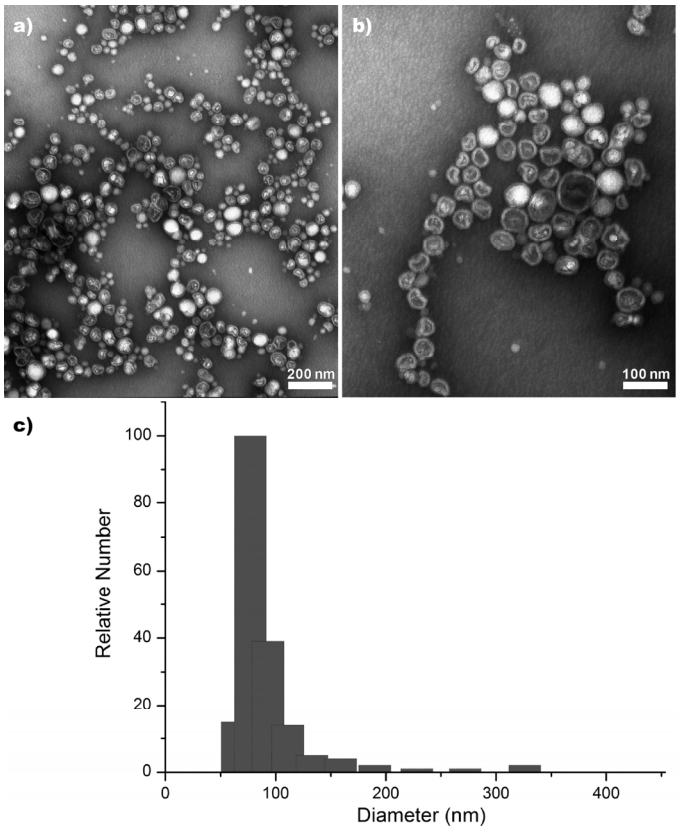

Figure 6.4. Characterization of small PEO_{45}-*b*-$PVBA_{26}$ vesicles. a-b) TEM images of vesicles (stained negatively with PTA). c) DLS histograms of vesicle size distributions (number-average hydrodynamic diameter).

Crosslinking of PEO-*b*-PVBA Vesicles via Reductive Amination. The chemical accessibility of the aldehyde functionality in the vesicular wall was verified by reductive amination-based crosslinking with 2,2′-(ethylene-dioxy)bis(ethylamine) (0.3 eq. relative to the aldehyde residues) and sodium cyanoborohydride (0.6 eq. relative to the aldehyde residues). No significant aggregation of vesicles was observed, based upon the DLS analysis (Figure 6.5a) and TEM imaging (Figure 6.5b), suggesting that only

intra-vesicular crosslinking reactions occurred. It is noteworthy that after crosslinking, the vesicles required buffer (5 mM pH 7.2 PBS with 5 mM of NaCl was used in our experiments) to remain suspended in aqueous solution. The zeta potential (ζ) measurement showed a dramatic decrease of surface negative charge (-65.3 ± 0.7 mV *vs.* -25.7 ± 0.8 mV), which might be associated with protonation of amines that were incorporated into the vesicles as a result of the reductive amination chemistry. The need for buffer and the less negative zeta potential value suggested that the structure of vesicle was chemically changed after crosslinking, which was confirmed by ^{1}H NMR spectroscopy (Figure 6.5e). New resonances corresponding to the diamino crosslinker appeared at 3.3 ppm and the ratio of aldehyde protons *vs.* aromatic protons was decreased from 1.0:4.6 to 1.0:6.2, indicating *ca.* 26% of aldehyde residues were consumed during the reaction (*i.e.*, 43% incorporation efficiency based upon reaction stoichiometry, which was close to the results obtained by utilizing chromophores through the same chemistry, *vide infra*). Typically, crosslinking leads to shorter relaxation times and broadening and losses of solution-state NMR signal intensities. The observation of the new diamino crosslinker resonance may indicate covalent mono-attachment within the vesicles, providing a relatively low degree of crosslinking. However, crosslinking indeed occurred, as was observed by the changes in the robust physical characteristics for the product vesicles. Of the 26% consumption of aldehydes, only a small fraction would be required to effectively crosslink an entire vesicle. Crosslinking significantly increased

the vesicle stability, and no appreciable variations in size or size distribution were found after lyophilization and re-suspension of these vesicles (Figure 6.5d).

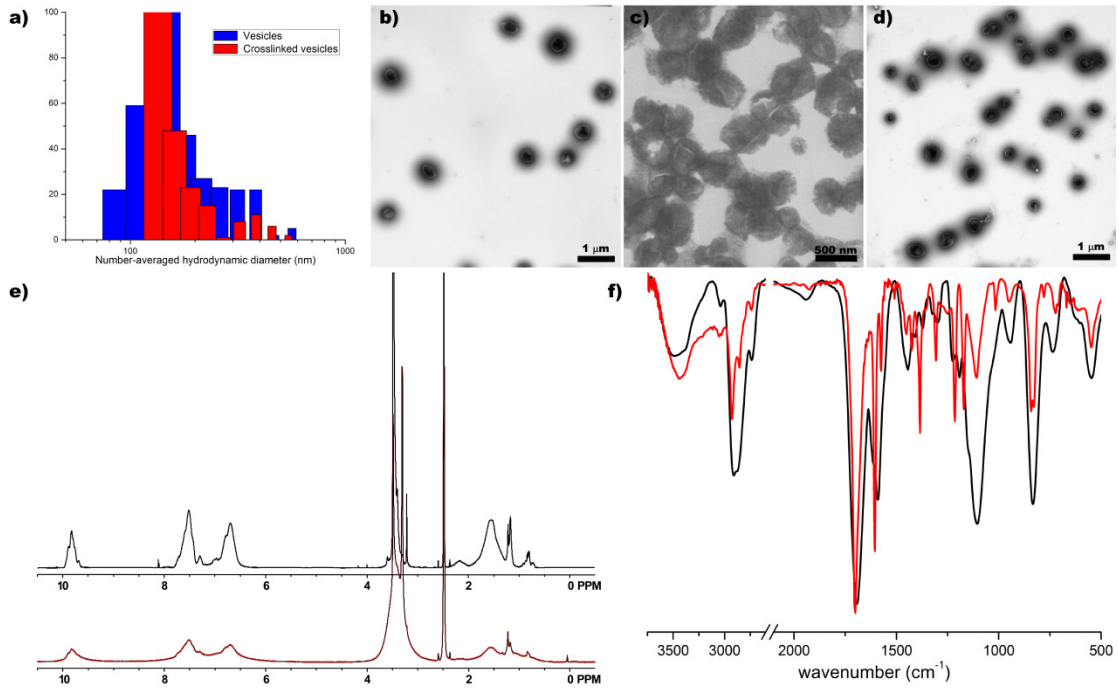

Figure 6.5. Characterization of crosslinked PEO_{45}-*b*-$PVBA_{26}$ vesicles through reductive amination. a) DLS histograms of non-crosslinked (blue) and crosslinked (red) vesicle distributions. b-c) TEM (b) and SEM (c) images of crosslinked vesicles in 5 mM pH 7.2 PBS. d) TEM image of lyophilized crosslinked vesicles after re-suspension in 5 mM pH 7.2 PBS. e) ^{1}H NMR spectra (DMSO-d_6) of lyophilized crosslinked vesicles (red) and polymer precursor (black). f) IR spectra (KBr) of lyophilized crosslinked vesicles (red) and polymer precursor (black).

***In Vitro* Cellular Studies.** Amine-derived dyes were then incorporated into the vesicles either sequentially or coincidentally with the crosslinking reaction *via* the same chemistry, to demonstrate multiple couplings within a single nanostructure and to label the vesicles for biological studies. The vesicles were functionalized with fluorecein and crosslinked (0.02 eq. of dye, 0.5 eq. of crosslinker, 1 eq. of $NaCNBH_3$ relative to the

aldehydes, respectively), each *via* reductive amination in a one-pot approach. UV-vis spectroscopy (Figure 6.6a) showed an absorption at 488 nm corresponding to the fluorescein, with an incorporation efficiency of *ca.* 35 %. And again, no obvious size and morphological variations were observed for the fluorescein-functionalized non-crosslinked and crosslinked vesicles, as confirmed by TEM (Figure 6.6b).

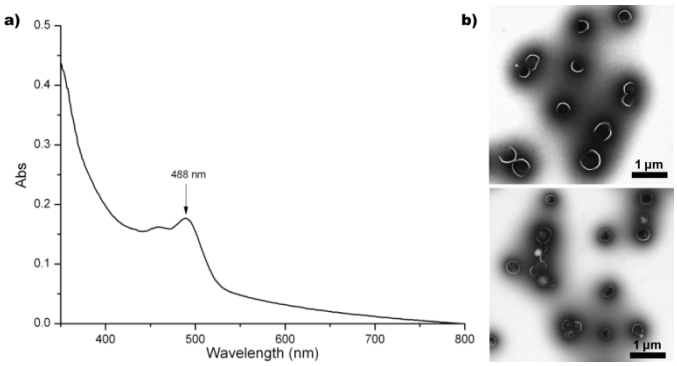

Figure 6.6. a) UV-vis profile of fluorescein dye-functionalized crosslinked vesicles. b) TEM images of non-crosslinked (top) and crosslinked (bottom) fluorescent vesicles.

In vitro CHO and HeLa cell experiments were then conducted for crosslinked and non-crosslinked fluorescein dye-labeled vesicles. By fluorescence confocal microscopy, the vesicles were observed to undergo association with the cells, in a time-dependent manner. No apparent fluorescence signal was detected after 1 and 4 h of incubation at 37 ºC. After 24 h, vesicles were visible under confocal microscopy (Figure 6.7e-h) and quantified by flow cytometry (Figure 6.7i) for both cell lines. Interestingly, an increased fraction of vesicles was observed to be associated with HeLa cells after the vesicles were crosslinked, while the opposite trend was noticed for CHO cells, with a greater fraction of

non-crosslinked vesicles undergoing strong cellular interactions. It is uncertain whether the vesicles are internalized within the cells. Although flow cytometry data confirmed that the vesicles remained associated with the cells under demanding conditions, the confocal microscopy images suggest that the vesicles are localized preferentially near the cell membrane. We hypothesize that such behavior may be the result of physical association or that it could be due to covalent coupling reactions between the aldehyde-loaded vesicles and amino-groups on (membrane bound) proteins. Although equimolar amounts of aldehyde and reducing agent were employed during the preparation of the fluoroescein-labeled, crosslinked vesicles, a portion of aldehydes still remain, as indicated by the ^{1}H NMR (Figure 6.5e) and IR data (Figure 6.5f) collected during the crosslinking experiments (*vide supra*).

The cytotoxicity of the crosslinked vesicles was also tested, using the cationic dendrimer polyfect as a positive control. Compared with polyfect, these vesicles had insignificant cytotoxicity for both cell lines (Figure 6.7j-k), indicating their bio-compatibility and making them promising materials for fundamental studies in biotechnology.

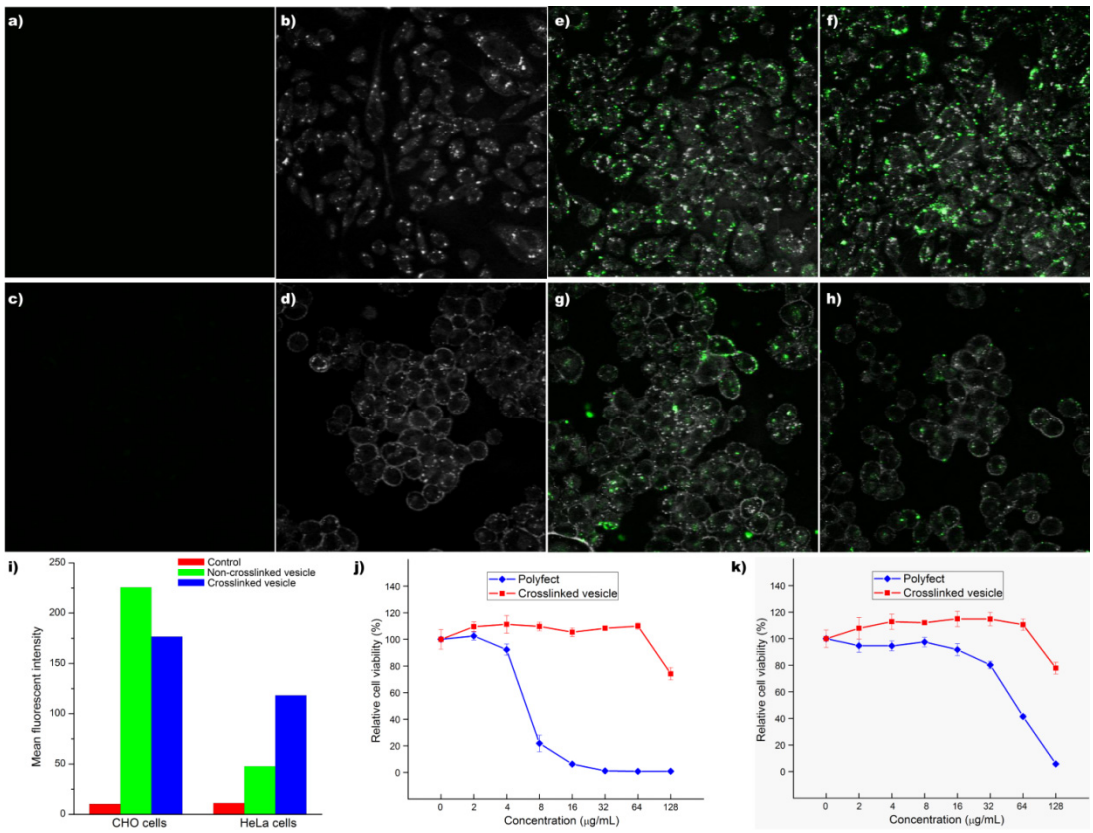

Figure 6.7. *In vitro* evaluations of fluorescein-labeled vesicles. a-b) Fluorescent confocal and bright-field images of CHO cells, respectively, without incubation with fluorescent vesicles. c-d) Fluorescent confocal and bright-field images of HeLa cells, respectively, without incubation with fluorescent vesicles. e-f) Overlay of bright field and fluorescent confocal images of CHO cells incubated with crosslinked and non-crosslinked vesicles, respectively. g-h) Overlay of bright field and fluorescent confocal images of HeLa cells incubated with crosslinked and non-crosslinked vesicles, respectively. i) Flow cytometry results. j-k) Cytotoxicity results for CHO and HeLa cells, respectively.

Conclusions

In summary, we have synthesized polymer vesicles bearing benzaldehyde functionalities in the vesicular walls from self assembly of the block copolymer PEO_{45}-*b*-$PVBA_{26}$. The aldehyde functionalities were shown to allow for modifications through facile and practical chemistry. Further investigations of the chemistry of these synthetic

and reactive vesicles, including optimizing the reaction efficiency, exploring its scope, and incorporating other labels and ligands, are ongoing now. These robust nanostructures, with their ability to associate with the cell membrane, may find application as a nanoscopic device for repair or modification of cellular membrane functions.

Experimental Section

Materials. Mono-methoxy terminated mono-hydroxy poly(ethylene glycol) (mPEG2k, *MW* = 2,000 Da, PDI = 1.06) was purchased from Intezyne Technologies (Tampa, FL) and was used without further purification. *S*-1-dodecyl-*S*′-(α,α′-dimethyl-α′′-acetic acid)trithiocarbonate (DDMAT),[55] 4-(Dimethy1amino)pyridinium 4-Toluenesulfonate (DTPS),[56] and VBA[54] were synthesized according to literature reports. Other reagents and solvents were purchased from commercial sources (Sigma-Aldrich, Acrose, and Fluka) and were used without further purification unless otherwise noted. Methylene chloride (CH_2Cl_2) was distilled from calcium hydride and stored under N_2 before using.

Cell Culture. Chinese Hamster Ovary cells (CHO-K1) and human cervix carcinoma (HeLa) cells were cultivated in DMEM containing 10% FBS, streptomycin (100 μg/mL), and penicillin (100 units/mL) at 37 °C in a humidified atmosphere containing 5% CO_2.

Measurements. ^{1}H NMR spectra were recorded on a Varian 500 MHz spectrometer interfaced to a UNIX computer using Mercury software. Chemical shifts were referred to the solvent proton resonance. Infrared spectra were obtained on a Perkin-Elmer Spectrum BX FT-IR system using diffuse reflectance sampling accessories with FT-IR Spectrum v2.00 software.

Absolute molecular weight and molecular weight distribution were determined by Gel Permeation Chromatography (GPC). GPC was performed on a Waters 1515 HPLC system (Water Chromatography Inc.), equipped with a Waters 2414 differential refractometer, a PD2020 dual-angle (15 and 90) light scattering detector (Precision Detectors Inc.), and a three-column series PL gel 5 μm Mixed columns (Polymer Laboratories Inc.). The eluent was anhydrous tetrahydrofuran (THF) with a flow rate of 1 mL/min. All instrumental calibrations were conducted using a series of nearly monodispersed polystyrene standards. Data were collected upon an injection of a 200 μL of polymer solution in THF (*ca.* 5 mg/mL), and then analyzed using Discovery 32 software (Precision Detectors Inc.).

Samples for Transmission electron microscopy (TEM) measurements were diluted with a 1 % phosphotungstic acid (PTA) stain (v/v, 1:1). Carbon grids were exposed to oxygen plasma treatment to increase the surface hydrophilicity. Micrographs were collected at 10,000, 20,000, 50,000, and 100,000 × magnification and calibrated using a 41 nm polyacrylamide bead from NIST.

Scanning electron microscopy (SEM) measurements were performed on a Field Emission Scanning Electron Microscope (Hitachi s-4500), equipped with a NORAN Instruments energy dispersive x-ray (EDX) microanalysis system, a back scattering detector and a mechanical straining stage. SEM samples were prepared with the following procedure. Silica native oxide wafers (Addison Engineering Inc.) were cleaned with nitric acid and hydrochloride acid (1:3) and then cut into 5 mm × 5 mm square. For each sample, 50 μL of aqueous solution was applied directly on the cleaned Si surface, and the solvent was kept in fume hood to evaporate at ambient temperature (21 ± 2 °C). The samples were immediately transferred to SEM instrument for measurement after completely dried.

Hydrodynamic diameters (D_h) and size distributions for the vesicles in aqueous solutions were determined by dynamic light scattering (DLS). The DLS instrumentation consisted of a Brookhaven Instruments Limited (Worcestershire, U.K.) system, including a model BI-200SM goniometer, a model BI-9000AT digital correlator, a model EMI-9865 photomultiplier, and a model 95-2 Ar ion laser (Lexel Corp.) operated at 514.5 nm. Measurements were made at 25 ± 1 °C. Scattered light was collected at a fixed angle of 90°. The digital correlator was operated with 522 ratio spaced channels, and initial delay of 5 μs, a final delay of 100 ms, and a duration of 6 minutes. A photomulitplier aperture of 100 μm was used, and the incident laser intensity was adjusted to obtain a photon counting of between, 200 and 300 kcps. Only measurements in which the measured and

calculated baselines of the intensity autocorrelation function agreed to within 0.1 % were used to calculate particle size. The calculations of the particle size distributions and distribution averages were performed with the ISDA software package (Brookhaven Instruments Company), which employed single-exponential fitting, cumulants analysis, and CONTIN particle size distribution analysis routines. All determinations were repeated for 5 times.

Zeta potential (ζ) values for the vesicle solution samples in 5 mM phosphate buffered saline (PBS) were determined with a Brookhaven Instrument Co. (Holtsville, NY) model Zeta Plus zeta potential analyzer. Data were acquired in the phase analysis light scattering (PALS) mode following solution equilibration at 25 °C. Calculation of ζ from the measured nanoparticle electrophoretic mobility (μ) employed the Smoluchowski equation: $\mu = \varepsilon\zeta/\eta$, where ε and η are the dielectric constant and the absolute viscosity of the medium, respectively. Measurements of ζ were reproducible to within ± 2 mV of the mean value given by 16 determinations of 10 data accumulations.

The confocal microscopy was collected by using a Leica TCS SP2 confocal microscopy following excitation with an argon laser (488 nm). 5×10^5 cells were incubated on 35 mm MatTek glass bottom microwell dishes (MatTek Co.) for 24 h. Then the medium was replaced with 2 mL of fresh medium containing with non-crosslinked or crosslinked vesicles (10 μg/mL of polymer) and incubated for another 24 h. Cells were washed twice with PBS and the live cells were imaged.

Flow cytometric analysis for the strong association of the vesicles to the cells was performed using a FACS-calibur (Becton Dickinson) equipped with an argon laser exciting at a wavelength of 488 nm. The cells were treated same as above. For each sample, 20,000 events were collected by list-mode data that consisted of side scatter, forward scatter, and fluorescence emission centered at 530 nm. The fluorescence was collected at a logarithmic scale with a 1024 channel resolution. CellQuest software (Becton Dickinson) was applied for the analyses.

The cytotoxicity of crosslinked vesicles was examined by CellTiter-Glo® Luminescent Cell Viability Assay (Promega Co.). The CHO-K1 cells and HeLa cells were seeded respectively in the 96-well plate at a density of 1×10^4 cells/well and cultured for 24 h in 100 μL DMEM containing 10% FBS. Thereafter, the medium was replaced with 100 μL of fresh medium containing with different concentration particles. After 24 h of incubation, 100 μL of the CellTiter-Glo® reagent was added. Mixed contents and allowed the plate to incubate at rt for 10 min to stabilize luminescent signal, recorded the luminescence at Luminoskan Ascent® luminometer (Thermo Scientific) with integration time 1 second per well. The relative cell viability was calculated as: cell viability (%) = (luminescence $_{(sample)}$/luminescence $_{(control)}$) × 100, where luminescence $_{(control)}$ was obtained in the absence of particles and luminescence $_{(sample)}$ was obtained in the presence of particles.

Synthesis of mPEG2k Macro-CTA. To a solution of mPEG2000 (4.0 g, 2.0 mmol) in 40 mL of dry CH_2Cl_2 at room temperature (rt), was added DDMAT (1.2 g, 3.0 mmol) and dicyclohexylcarbodiimide (0.60 g, 2.9 mmol), the reaction mixture was stirred 10 min. After the additions of 4-di(methylamino)pyridine (36.6 mg, 0.3 mmol) and DPTS (375.0 mg, 1.2 mmol), the reaction mixture was further stirred 20 h at rt. Then the reaction mixture was filtered with celite and the filtrate was placed at 4 ºC overnight, filtered with celite, and concentrated to *ca.* 15 mL. After the solution was precipitated into 250 mL of dry ether at 0 ºC twice, the crude product obtained was further purified by flash column chromatography (2-3% MeOH/CH_2Cl_2, v/v) to afford mPEG2k macro-CTA as a yellow solid (3.2 g, 68% yield). ^{1}H NMR (500 MHz, CD_2Cl_2, δ): 0.88 (t, J = 6.5 Hz, 3H), 1.26 (m, 16H), 1.38 (t, J = 6.5 Hz, 2H), 1.66 (t, J = 7.5 Hz, 2H), 1.68 (s, 6H), 3.27 (t, J = 7.2 Hz, 2H), 3.33 (s, 3H), 3.40-3.80 (m, 166H), 4.21 (t, J = 5.0 Hz, 2H).

Synthesis of PEO_{45}-*b*-$PVBA_{26}$. To a 10 mL Schlenk flask equipped with a magnetic stir bar dried with flame under N_2 atmosphere, was added the mPEG2k macro-CTA (0.48 g, 0.20 mmol) and dry DMF (2.5 mL). The reaction mixture was stirred 1 h at rt to obtain a homogeneous solution. To this solution was added VBA (1.46 g, 11.0 mmol) and AIBN (8.1 mg, 50 μmol). The reaction flask was sealed and stirred 10 min at rt. The reaction mixture was degassed through several cycles of freeze-pump-thaw. After the last cycle, the reaction mixture was stirred for 10 min at rt before immersing into a pre-heated oil bath at 75 °C to start the polymerization. After 3.5 h, the monomer conversion

reached *ca.* 55% by analyzing aliquots collected through ^{1}H-NMR spectroscopy. The polymerization was quenched by cooling the reaction flask with liquid N_2. CH_2Cl_2 (5.0 mL) was added to the reaction flask and the polymer was purified by precipitation into 300 mL of cold diethyl ether at 0 °C twice. The precipitants were collected, washed with 100 mL of cold ether, and dried under vacuum overnight to afford the block copolymer precursor as a yellow solid (1.18 g, 90% yield based upon monomer conversion). ^{1}H NMR (500 MHz, CD_2Cl_2, δ): 0.88-1.24 (br, dodecyl Hs), 1.52-2.06 (br, PVBA backbone protons), 3.22 (br, SCH_2 of the chain terminus), 3.33 (s, mPEG terminal OCH_3), 3.34-3.78 (m, OCH_2CH_2O from the PEG backbone), 4.84 (br, 1H from the PVBA backbone benzylic terminus connected to trithiocarbonate), 6.58-6.85 (br, Ar H), 7.33-7.62 (br, Ar H), 9.88 (br, CHO); ^{13}C NMR (150 MHz, DMSO-d_6, δ): 192.3 , 151.3, 134.4, 129.4, 128.0, 69.8, 42.3, 40.4, 29.0; IR (KBr): 3433, 2923, 2856, 2732, 1699, 1604, 1575, 1453, 1425, 1386, 1354, 1306, 1258, 1214, 1171, 1103, 1017, 951, 837, 726, 674, 552.

General Procedure for Construction of PEO_{45}-*b*-$PVBA_{26}$ Vesicles. To a solution of PEO_{45}-*b*-$PVBA_{26}$ block copolymer in DMF (*ca.* 1.0 mg/mL), was added dropwise an equal volume of nano-pure H_2O *via* a syringe pump at a rate of 15.0 mL/h, and the mixture was further stirred for 16 h at rt. The solution was then transferred to pre-soaked dialysis tubing with Molecular Weight Cut Off (MWCO) of *ca.* 3,500 Da and dialyzed against nano-pure H_2O for 4 d to afford a solution of vesicles.

Crosslinking of PEO_{45}-*b*-$PVBA_{26}$ Vesicles. To a solution of PEO_{45}-*b*-$PVBA_{26}$ vesicles (7.4 mg of polymer, 33 μmol of aldehyde residues) in 30.0 mL of nano-pure H_2O, was added a solution of 2,2'-(ethylenedioxy)-bis(ethylamine) (1.5 mg, 10 μmol) in 1.0 mL of nano-pure H_2O dropwise over 10 min. The reaction mixture was allowed to stir for 24 h at rt. $NaBH_3CN$ (1.3 mg, 20 μmol) in 1.3 mL of nano-pure H_2O was then added to the reaction solution and further stirred for 16 h at rt. Finally, the mixture was transferred to pre-soaked dialysis tubing (MWCO: *ca.* 3,500 Da) and dialyzed against 5.0 mM PBS (pH 7.2, with 5.0 mM NaCl) for 5 d to remove the small molecule by-products and afford an aqueous solution of crosslinked vesicles.

One-pot Functionalization and Crosslinking of PEO_{45}-*b*-$PVBA_{26}$ Vesicles. To a solution of PEO_{45}-*b*-$PVBA_{26}$ vesicles (3.2 mg of polymer, 14 μmol of aldehyde residues) in 10.0 mL of nano-pure H_2O, was added a solution of fluorescein-5-thiosemicarbazide (126.3 μg, 0.30 μmol) in 90.0 μL of DMF. The reaction mixture was allowed to stir for 2 h at rt in the absence of light. To this reaction mixture, was added a solution of 2,2'-(ethylenedioxy)-bis(ethylamine) (1.1 mg, 7.2 μmol) in 1.6 mL of nano-pure H_2O dropwise over 10 min. The reaction mixture was further stirred for 24 h at rt in the absence of light. $NaBH_3CN$ (907.2 μg, 14.4 μmol) in 0.4 mL of nano-pure H_2O was then added to the reaction solution and further stirred for 16 h at rt in the absence of light. Finally, the mixture was transferred to pre-soaked dialysis tubing (MWCO *ca.* 3,500 Da) and dialyzed against 5.0 mM PBS (pH 7.2, with 5.0 mM NaCl) for 5 d to remove the

small molecule by-products and afford an aqueous solution of functionalized and crosslinked vesicles.

Acknowledgment. This material is based upon work supported by the National Heart Lung and Blood Institute of the National Institutes of Health as a Program of Excellence in Nanotechnology (U01 HL080729), and also by the National Science Foundation (DMR-0451490). The authors thank Mr. G. M. Veith for the kind assistance with TEM imaging, and Dr. J. Kao and Dr. A. d'Avignon for assistance with NMR measurements.

References

1. Discher, D. E.; Eisenberg, A. "Polymer Vesicles." *Science* **2002,** *297*, 967-973.

2. Antonietti, M.; Förster, S. "Vesicles and Liposomes: A Self-Assembly Principle Beyond Lipids." *Adv. Mater.* **2003,** *15*, 1323-1333.

3. Opsteen, J. A.; Cornelissen, J. J. L. M.; van Hest, J. C. M. "Block copolymer vesicles." *Pure Appl. Chem.* **2004,** *76*, 1309-1319.

4. Soo, P. L.; Eisenberg, A. "Preparation of block copolymer vesicles in solution." *J. Polym. Sci. Part B: Polym. Phys.* **2004,** *42*, 923-938.

5. Kita-Tokarczyk, K.; Grumelard, J.; Haefele, T.; Meier, W. "Block copolymer vesicles--using concepts from polymer chemistry to mimic biomembranes." *Polymer* **2005,** *46*, 3540-3563.

6. Discher, D. E.; Ahmed, F. "Polymersomes." *Annu. Rev. Biomed. Eng.* **2006,** *8*, 323-341.

7. Zhang, L.; Eisenberg, A. "Multiple Morphologies and Characteristics of "Crew-Cut" Micelle-like Aggregates of Polystyrene-b-poly(acrylic acid) Diblock Copolymers in Aqueous Solutions." *J. Am. Chem. Soc.* **1996,** *118*, 3168-3181.

8. Discher, B. M.; Won, Y. Y.; Ege, D. S.; Lee, J. C. M.; Bates, F. S.; Discher, D. E.; Hammer, D. A. "Polymersomes: Tough vesicles made from diblock copolymers." *Science* **1999,** *284*, 1143-1146.

9. Kukula, H.; Schlaad, H.; Antonietti, M.; Förster, S. "The Formation of Polymer Vesicles or "Peptosomes" by Polybutadiene-block-poly(L-glutamate)s in Dilute Aqueous Solution." *J. Am. Chem. Soc.* **2002,** *124*, 1658-1663.

10. Koide, A.; Kishimura, A.; Osada, K.; Jang, W. D.; Yamasaki, Y.; Kataoka, K. "Semipermeable Polymer Vesicle (PICsome) Self-Assembled in Aqueous Medium from a Pair of Oppositely Charged Block Copolymers: Physiologically Stable Micro-/Nanocontainers of Water-Soluble Macromolecules." *J. Am. Chem. Soc.* **2006,** *128*, 5988-5989.

11. Li, Z.; Hillmyer, M. A.; Lodge, T. P. "Laterally Nanostructured Vesicles, Polygonal Bilayer Sheets, and Segmented Wormlike Micelles." *Nano Lett.* **2006,** *6*, 1245-1249.

12. You, L.; Schlaad, H. "An Easy Way to Sugar-Containing Polymer Vesicles or Glycosomes." *J. Am. Chem. Soc.* **2006,** *128*, 13336-13337.

13. Chiu, H.-C.; Lin, Y.-W.; Huang, Y.-F.; Chuang, C.-K.; Chern, C.-S. "Polymer Vesicles Containing Small Vesicles within Interior Aqueous Compartments and pH-Responsive Transmembrane Channels." *Angew. Chem., Int. Ed.* **2008,** *47*, 1875-1878.

14. Pasparakis, G.; Alexander, C. "Sweet talking double hydrophilic block copolymer vesicles." *Angew. Chem., Int. Ed.* **2008,** *47*, 4847-4850.

15. Thibault, R. J.; Uzun, O.; Hong, R.; Rotello, V. M. "Recognition-controlled assembly of nanoparticles using photochemically crosslinked recognition-induced polymersomes." *Adv. Mater.* **2006,** *18*, 2179-2183.

16. Ghoroghchian, P. P.; Frail, P. R.; Susumu, K.; Blessington, D.; Brannan, A. K.; Bates, F. S.; Chance, B.; Hammer, D. A.; Therien, M. J. "Near-infrared-emissive polymersomes: self-assembled soft matter for in vivo optical imaging." *Proc. Natl. Acad. Sci. U. S. A.* **2005,** *102*, 2922-2927.

17. Ahmed, F.; Pakunlu, R. I.; Srinivas, G.; Brannan, A.; Bates, F.; Klein, M. L.; Minko, T.; Discher, D. E. "Shrinkage of a Rapidly Growing Tumor by Drug-Loaded

Polymersomes: pH-Triggered Release through Copolymer Degradation." *Mol. Pharmaceutics* **2006,** *3*, 340-350.

18. Discher, D. E.; Ortiz, V.; Srinivas, G.; Klein, M. L.; Kim, Y.; Christian, D.; Cai, S.; Photos, P.; Ahmed, F. "Emerging applications of polymersomes in delivery: From molecular dynamics to shrinkage of tumors." *Prog. Polym. Sci.* **2007,** *32*, 838-857.

19. Adams, D. J.; Adams, S.; Atkins, D.; Butler, M. F.; Furzeland, S. "Impact of mechanism of formation on encapsulation in block copolymer vesicles." *J. Controlled Release* **2008,** *128*, 165-170.

20. Krack, M.; Hohenberg, H.; Kornowski, A.; Lindner, P.; Weller, H.; Förster, S. "Nanoparticle-Loaded Magnetophoretic Vesicles." *J. Am. Chem. Soc.* **2008,** *130*, 7315-7320.

21. Kabanov, A. V.; Bronich, T. K.; Kabanov, V. A.; Yu, K.; Eisenberg, A. "Spontaneous Formation of Vesicles from Complexes of Block Ionomers and Surfactants." *J. Am. Chem. Soc.* **1998,** *120*, 9941-9942.

22. Bermudez, H.; Brannan, A. K.; Hammer, D. A.; Bates, F. S.; Discher, D. E. "Molecular Weight Dependence of Polymersome Membrane Structure, Elasticity, and Stability." *Macromolecules* **2002,** *35*, 8203-8208.

23. Choucair, A.; Lavigueur, C.; Eisenberg, A. "Polystyrene-b-poly(acrylic acid) Vesicle Size Control Using Solution Properties and Hydrophilic Block Length." *Langmuir* **2004,** *20*, 3894-3900.

24. Wang, X.; Winnik, M. A.; Manners, I. "Synthesis and Self-Assembly of Poly(ferrocenyldimethylsilane-b-dimethylaminoethyl methacrylate): Toward Water-Soluble Cylinders with an Organometallic Core." *Macromolecules* **2005,** *38*, 1928-1935.

25. Chécot, F.; Lecommandoux, S.; Gnanou, Y.; Klok, H.-A. "Water-Soluble Stimuli-Responsive Vesicles from Peptide-Based Diblock Copolymers." *Angew. Chem., Int. Ed.* **2002,** *41*, 1339-1343.

26. Napoli, A.; Valentini, M.; Tirelli, N.; Müller, M.; Hubbell, J. A. "Oxidation-responsive polymeric vesicles." *Nat. Mater.* **2004,** *3*, 183-189.

27. Power-Billard, K. N.; Spontak, R. J.; Manners, I. "Redox-Active Organometallic Vesicles: Aqueous Self-Assembly of a Diblock Copolymer with a Hydrophilic Polyferrocenylsilane Polyelectrolyte Block." *Angew. Chem., Int. Ed.* **2004,** *43*, 1260-1264.

28. Du, J.; Armes, S. P. "pH-Responsive Vesicles Based on a Hydrolytically Self-Cross-Linkable Copolymer." *J. Am. Chem. Soc.* **2005,** *127*, 12800-12801.

29. Rodríguez-Hernández, J.; Lecommandoux, S. "Reversible Inside-Out Micellization of pH-responsive and Water-Soluble Vesicles Based on Polypeptide Diblock Copolymers." *J. Am. Chem. Soc.* **2005,** *127*, 2026-2027.

30. Li, Y.; Lokitz, B. S.; McCormick, C. L. "Thermally responsive vesicles and their structural "locking" through polyelectrolyte complex formation." *Angew. Chem., Int. Ed.* **2006,** *45*, 5792-5795.

31. Qin, S.; Geng, Y.; Discher, D. E.; Yang, S. "Temperature-controlled assembly and release from polymer vesicles of poly(ethylene oxide)-block-poly(N-isopropylacrylamide)." *Adv. Mater.* **2006,** *18*, 2905-2909.

32. Lomas, H.; Canton, I.; MacNeil, S.; Du, J.; Armes, S. P.; Ryan, A. J.; Lewis, A. L.; Battaglia, G. "Biomimetic pH sensitive polymersomes for efficient DNA encapsulation and delivery." *Adv. Mater.* **2007,** *19*, 4238-4243.

33. Discher, B. M.; Bermudez, H.; Hammer, D. A.; Discher, D. E.; Won, Y.-Y.; Bates, F. S. "Cross-linked Polymersome Membranes: Vesicles with Broadly Adjustable Properties." *J. Phys. Chem. B* **2002,** *106*, 2848-2854.

34. Kros, A.; Linhardt, J. G.; Bowman, H. K.; Tirrell, D. A. "From giant vesicles to filaments and wires: Templates for conducting polymers." *Adv. Mater.* **2004,** *16*, 723-727.

35. Reiner, J. E.; Wells, J. M.; Kishore, R. B.; Pfefferkorn, C.; Helmerson, K. "Stable and robust polymer nanotubes stretched from polymersomes." *Proc. Natl. Acad. Sci. U. S. A.* **2006,** *103*, 1173-1177.

36. Wu, J.; Eisenberg, A. "Proton Diffusion across Membranes of Vesicles of Poly(styrene-b-acrylic Acid) Diblock Copolymers." *J. Am. Chem. Soc.* **2006,** *128*, 2880-2884.

37. Kumar, M.; Grzelakowski, M.; Zilles, J.; Clark, M.; Meier, W. Highly permeable polymeric membranes based on the incorporation of the functional water channel protein Aquaporin Z. *Proc. Natl. Acad. Sci. U. S. A.* **2007,** *104*, 20719-20724.

38. Leson, A.; Filiz, V.; Förster, S.; Mayer, C. "Water permeation through block-copolymer vesicle membranes." *Chem. Phys. Lett.* **2007,** *444*, 268-272.

39. Shum, H. C.; Kim, J.-W.; Weitz, D. A. "Microfluidic Fabrication of Monodisperse Biocompatible and Biodegradable Polymersomes with Controlled Permeability." *J. Am. Chem. Soc.* **2008,** *130*, 9543-9549.

40. Photos, P. J.; Bacakova, L.; Discher, B.; Bates, F. S.; Discher, D. E. "Polymer vesicles in vivo: correlations with PEG molecular weight." *J. Controlled Release* **2003,** *90*, 323-334.

41. Broz, P.; Driamov, S.; Ziegler, J.; Ben-Haim, N.; Marsch, S.; Meier, W.; Hunziker, P. "Toward Intelligent Nanosize Bioreactors: A pH-Switchable, Channel-Equipped, Functional Polymer Nanocontainer." *Nano Lett.* **2006,** *6*, 2349-2353.

42. Opsteen, J. A.; Brinkhuis, R. P.; Teeuwen, R. L. M.; Loewik, D. W. P. M.; van Hest, J. C. M. ""Clickable" polymersomes." *Chem. Commun.* **2007**, 3136-3138.

43. Hammer, D. A.; Robbins, G. P.; Haun, J. B.; Lin, J. J.; Qi, W.; Smith, L. A.; Ghoroghchian, P. P.; Therien, M. J.; Bates, F. S. "Leuko-polymersomes." *Faraday Discuss.* **2008,** *139*, 129-141.

44. Hales, M.; Barner-Kowollik, C.; Davis, T. P.; Stenzel, M. H. "Shell-Cross-Linked Vesicles Synthesized from Block Copolymers of Poly(D,L-lactide) and Poly(N-isopropyl acrylamide) as Thermoresponsive Nanocontainers." *Langmuir* **2004,** *20*, 10809-10817.

45. Ding, J.; Liu, G. "Water-Soluble Hollow Nanospheres as Potential Drug Carriers." *J. Phys. Chem. B* **1998,** *102*, 6107-6113.

46. Zheng, R.; Liu, G. "Water-Dispersible Oil-Filled ABC Triblock Copolymer Vesicles and Nanocapsules." *Macromolecules* **2007,** *40*, 5116-5121.

47. Walther, A.; Goldmann, A. S.; Yelamanchili, R. S.; Drechsler, M.; Schmalz, H.; Eisenberg, A.; Müller, A. H. E. "Multiple Morphologies, Phase Transitions, and Cross-Linking of Crew-Cut Aggregates of Polybutadiene-block-poly(2-vinylpyridine) Diblock Copolymers." *Macromolecules* **2008,** *41*, 3254-3260.

48. Du, J.; Chen, Y.; Zhang, Y.; Han, C. C.; Fischer, K.; Schmidt, M. "Organic/Inorganic Hybrid Vesicles Based on A Reactive Block Copolymer." *J. Am. Chem. Soc.* **2003,** *125*, 14710-14711.

49. Zhu, H.; Liu, Q.; Chen, Y. "Reactive Block Copolymer Vesicles with an Epoxy Wall." *Langmuir* **2007,** *23*, 790-794.

50. Choi, H. J.; Montemagno, C. D. "Artificial Organelle: ATP Synthesis from Cellular Mimetic Polymersomes." *Nano Lett.* **2005,** *5*, 2538-2542.

51. Ranquin, A.; Versees, W.; Meier, W.; Steyaert, J.; Van Gelder, P. "Therapeutic Nanoreactors: Combining Chemistry and Biology in a Novel Triblock Copolymer Drug Delivery System." *Nano Lett.* **2005,** *5*, 2220-2224.

52. Holowka, E. P.; Sun, V. Z.; Kamei, D. T.; Deming, T. J. "Polyarginine segments in block copolypeptides drive both vesicular assembly and intracellular delivery." *Nat. Mater.* **2007,** *6*, 52-57.

53. Ben-Haim, N.; Broz, P.; Marsch, S.; Meier, W.; Hunziker, P. "Cell-Specific Integration of Artificial Organelles Based on Functionalized Polymer Vesicles." *Nano Lett.* **2008,** *8*, 1368-1373.

54. Sun, G.; Cheng, C.; Wooley, K. L. "Reversible Addition Fragmentation Chain Transfer Polymerization of 4-Vinylbenzaldehyde." *Macromolecules* **2007,** *40*, 793-795.

55. Lai, J. T.; Filla, D.; Shea, R. "Functional Polymers from Novel Carboxyl-Terminated Trithiocarbonates as Highly Efficient RAFT Agents." *Macromolecules* **2002,** *35*, 6754-6756.

56. Moore, J. S.; Stupp, S. I. "Room temperature polyesterification." *Macromolecules* **1990,** *23*, 65-70.

Chapter 7

Optimizations of Quantum Yield of Fluorescent Nanoparticles for Development of Potential Optical Imaging Contrast Agents

Guorong Sun, Mikhail Y. Berezin, Jinda Fan, Ke Zhang,

Samuel Achilefu, and Karen L. Wooley

Introduction

During the past decades, *in vivo* fluorescence imaging has experienced a renaissance with the "opening" of near-infrared (NIR) window (wavelength between 650 and 900 nm) of electromagnetic spectrum.[1-7] By utilizing fluorescent probes such as quantum dots,[8-10] fluorescent proteins,[11, 12] and organic NIR dyes,[13-20] two main problems (*i.e.* tissue autofluorescense and attenuation) associated with deep tissue imaging have been partially overcome, and now, *in vivo* optical imaging of a few centimeters depth has been achieved.

Among the organic NIR fluorophores (NIRFs), carbocyanine-based dyes are particularly of interest due to their high molar extinction coefficients (usually on the order of 10^5 M^{-1} cm^{-1}) and tunability of photo-physical properties.[19] These fluorophores are also facile to be functionalized with bioactive ligands to enable targeted imaging.[15, 21-

[23] However, the *in vivo* application of cyanine dyes generally suffers from high degradation rate, short blood circulation times, non-specific tissue/organ accumulations.[24-27] One practical and promising approach for prevailing over the above drawbacks is to encapsulate/couple cyanine dyes within/onto nanoscale platforms, which can provide protection and "stealth" properties from the blood clearance systems.[14, 28-45] The nanoscale platform can further be decorated with multiple homo- or heterogeneous targeting agents to improve targeting efficiency by taking advantage of the multivalent interactions with cell-surface receptors. Furthermore, this approach may allow for the "hybridization" of different probes within a single nanoparticle to enable multimodal imaging for increased of the diagnostic accuracy.[42, 46-50]

Spherical nanoparticles (NPs) represent the most widely applied nanostructures in molecular imaging. To date, cyanine NIRF-functionalized dendrimers,[37, 48] silica NPs,[30, 34, 35, 39, 44, 51, 52] and natural/engineered viruses[29, 33] have been reported from academic and industrial research groups. It is well-known that fluorescent tags often suffer from the fluorescence "self quenching" when placed in close proximity. In order to obtain maximized fluorescence, the distance between fluorophores should be greater than the Forster radius to avoid the non-radiative energy transfer of the same fluorophores. In this work, we investigated the stoichiometry dependence of fluorophores (fluorescein and cypate, respectively) per nanoparticle by calculating the distance of two adjacent fluorophores through both steady-state and dynamic emission spectra, in comparison with

the Forster radius. We also proposed and examined a semi-quantitative model (*vide infra*) for estimating the maximum number of fluorophores per spherical nanoparticle while retaining satisfactory QY of the fluorophores.

Experimental Section

Materials. Mono-methoxy terminated mono-hydroxy poly(ethylene glycol) (mPEG2k and mPEG5k, *MW* = 2,000 and 5,000 Da, respectively, PDI = 1.06 and 1.07, respectively) was purchased from Intezyne Technologies (Tampa, FL) and was used without further purification. Cypate,[14] HL-800,[17] *S*-1-dodecyl-*S*′-(α,α′-dimethyl-α′′-acetic acid)trithiocarbonate (DDMAT),[53] 4-(Dimethy1amino)pyridinium 4-Toluenesulfonate (DTPS),[54] VBA,[55] mPEG2k macro-chain transfer agent (macro-CTA),[56] and poly(ethylene oxide)-*block*-poly(*N*-acryloxysuccinimide)-*block*-polystyrene (PEO_{45}-*b*-$PNAS_{95}$-*b*-PS_{60})[57] were synthesized according to literature reports. Other reagents and solvents were purchased from commercial sources (Sigma-Aldrich, Acrose, and Fluka) and were used without further purification unless otherwise noted. Methylene chloride (CH_2Cl_2) was distilled from calcium hydride and stored under N_2 before using.

Measurements. ^{1}H NMR spectra were recorded on a Varian 500 MHz spectrometer interfaced to a UNIX computer using Mercury software. Chemical shifts were referred to the solvent proton resonance. Infrared spectra were obtained on a Perkin-Elmer

Spectrum BX FT-IR system using diffuse reflectance sampling accessories with FT-IR Spectrum v2.00 software.

Absolute molecular weight and molecular weight distribution were determined by Gel Permeation Chromatography (GPC). GPC was performed on a Waters 1515 HPLC system (Water Chromatography Inc.), equipped with a Waters 2414 differential refractometer, a PD2020 dual-angle (15 and 90) light scattering detector (Precision Detectors Inc.), and a three-column series PL gel 5 μm Mixed columns (Polymer Laboratories Inc.). The eluent was anhydrous tetrahydrofuran (THF) with a flow rate of 1 mL/min. All instrumental calibrations were conducted using a series of nearly monodispersed polystyrene standards. Data were collected upon an injection of a 200 μL of polymer solution in THF (*ca.* 5 mg/mL), and then analyzed using Discovery 32 software (Precision Detectors Inc.).

The *N*,*N*-dimethylformamide (DMF) GPC was conducted on a Waters Chromatography, Inc. (Milford, MA) system equipped with an isocratic pump model 1515, a differential refractometer model 2414, and a two-column set of Styragel HR 4 and HR 4E 5 μm DMF 7.8 × 300 mm columns. The system was equilibrated at 70 °C in pre-filtered DMF containing 0.05 M LiBr, which served as polymer solvent and eluent (flow rate set to 1.00 mL/min). Polymer solutions were prepared at a concentration of *ca.* 3 mg/mL and an injection volume of 200 μL was used. Data collection and analysis was performed with Empower Pro software (Waters, Inc.). The system was calibrated with

poly(ethylene glycol) standards (Polymer Laboratories, Amherst, MA) ranging from 615 to 442,800 Da.

Samples for Transmission electron microscopy (TEM) measurements were diluted with a 1 % phosphotungstic acid (PTA) stain (v/v, 1:1). Carbon grids were exposed to oxygen plasma treatment to increase the surface hydrophilicity. Micrographs were collected at 100,000 × magnification and calibrated using a 41 nm polyacrylamide bead from NIST. The number average particle diameters (D_{av}) and standard deviations were generated from the analysis of a minimum of 150 particles from at least three different micrographs. The aggregation number (N_{aggr}) was calculated based upon the diameter measured from TEM by using the following equation:

$$N_{aggr} = \frac{\frac{4}{3}\pi r^3 \rho}{M_n} \times N_A \qquad (1)$$

where r is the radius of the NP core domain, ρ is the density of poly(4-vinyl benzaldehyde) (PVBA), M_n is the number-average molecular weight of PVBA block segment, and N_A is the Avogadro constant.

Hydrodynamic diameters (D_h) and size distributions for the nanoparticles in aqueous solutions were determined by dynamic light scattering (DLS). The DLS instrument consisted of a Brookhaven Instruments Limited (Worcestershire, U.K.) system, including a model BI-200SM goniometer, a model BI-9000AT digital correlator, a model EMI-9865 photomultiplier, and a model 95-2 Ar ion laser (Lexel Corp.) operated at 514.5 nm.

Measurements were made at 25 ± 1 °C. Scattered light was collected at a fixed angle of 90°. The digital correlator was operated with 522 ratio spaced channels, and initial delay of 5 μs, a final delay of 100 ms, and a duration of 8 minutes. A photomulitplier aperture of 400 μm was used, and the incident laser intensity was adjusted to obtain a photon counting of between, 150 and 200 kcps. Only measurements in which the measured and calculated baselines of the intensity autocorrelation function agreed to within 0.1 % were used to calculate particle size. The calculations of the particle size distributions and distribution averages were performed with the ISDA software package (Brookhaven Instruments Company), which employed single-exponential fitting, cumulants analysis, and CONTIN particle size distribution analysis routines. All determinations were repeated for 5 times and the data were represented as mean values ± standard deviations between runs.

For optical measurements, the fluorescein-based NPs were diluted with 0.1 M NaOH solution. Cypate-based nanoparticles were measured in PBS buffer at pH 7.2 (5 mM with 5 mM of NaCl). Both samples were diluted to a concentration where the absorbance value at maximum absorption peak was less than 0.1 to avoid self-quenching between nanoparticles and photon re-absorption.

The UV-vis absorption spectra of NPs were collected at room temperature using Varian Cary 500 Bio UV-visible spectrophotometer and quartz cuvette with 10 mm of light path.

The fluorescence spectra of NPs were obtained at room temperature using a Varian Cary Eclipse and Fluorolog III fluorescence spectrophotometer. Fluorescence lifetime was measured using TCSPS method as described previously. For NPs bearing fluoresceins, the fluorescence decays were measured in aqueous media using excitation source Nanoled® 460 nm, monitored emission at 570 nm with bandpass 20 nm. For NPs bearing cypate, the fluorescence lifetimes were determined in aqueous media using excitation source Nanoled® 773 nm, monitored emission 820 nm with bandpass 20 nm. In both measurements, a two-exponential decay analysis was applied.

The Foster radius of a homoFRET pair (R_0) was calculated using previously developed FRET calculator from steady-state absorption and emission spectra using known equations:

$$R_0 = 0.211\left(k^2 n^{-4} Q_D J(\lambda)\right)^{1/6} \text{ Å} \qquad (2)$$

where n is the refraction index typically assumed to be 1.4 for biomolecules in aqueous solutions; k^2 is the orientation factor typically equal to 2/3 for random distributed fluorophores; Q_D is the quantum yield of the donor; $J(\lambda)$ is the spectral overlap integral, which is calculated by the following equation:

$$J(\lambda) = \int_0^\infty F_D(\lambda)\varepsilon_A(\lambda)\lambda^4 \, d\lambda \text{ M}^{-1}\text{ cm}^{-1}\text{ nm}^4 \qquad (3)$$

where λ represents the wavelength in nm; $F_D(\lambda)$ represents the normalized fluorescence intensity at wavelength λ; $\varepsilon_A(\lambda)$ represents molar absorptivity of the acceptor at given wavelength.

Synthesis of cypate-diamine. To a DMF solution of Cypate (12.5 mg, 17.7 μmol) and 1-hydroxybenzotriazole (HOBt, 9.6 mg, 70.8 μmol) was added *N*,*N*′-diisopropylcarbodiimide (DIC) (11.0 μL, 70.8 μmol), the resulting mixture was stirred for 10 min. Boc-ethylene diamine (6.7 μL, 42.3 μmol) was then added and the mixture was stirred overnight at room temperature (rt). After removing the DMF in vacuo, a solution of trifluoroacetic acid (TFA), H_2O, phenol, and thioanisole (85:5:5:5, v/v) was added and stirred for 1 h at rt. The volatiles were removed under reduced pressure and the crude product was washed with diethyl ether (3 × 5mL) and purified by medium pressure chromatography with a C-18 reverse phase column (acetonitrile/water as eluent). A green solid was obtained as pure product (10.9 mg, 60.6% yield). MS (EI): 709.0 $(M + 1)^+$.

Synthesis of HL-800-amine. To a solution of HL-800 (10.4 mg, 11.2 μmol) and 2-(1H-7-azabenzotriazol-1-yl)-1,1,3,3-tetramethyl uronium hexafluorophosphate methanaminium (HATU, 6.4 mg, 16.8 μmol) in DMF, was added diisopropylethyl amine (DIEA, 2.9 μL, 16.8 μmol), the resulting mixture was stirred at rt for 10 min. Boc-ethylene diamine (2.1 μL, 20.1 μmol) was added and the mixture was stirred overnight at rt. The reaction mixture was then poured into 150 mL of diethyl ether. Collect the solid precipitated out and a solution of TFA, H_2O, phenol, and thioanisole (85:5:5:5, v/v) was added following by stirring for 1 h at rt. The crude product was precipitated out by diethyl ether, washed with diethyl ether (3×5 mL) and purified by medium pressure

chromatography with a C-18 reverse phase column (acetonitrile/water as eluent). The solvents were evaporated to give HL-800-amine (3.18mg, 29.2% yield) as a green solid. MS (EI): 955.2 $(M + 1)^+$.

Synthesis of mPEG5k macro-CTA. To a solution of mPEG5000 (1.80 g, 0.36 mmol) in 20 mL of dry CH_2Cl_2 at rt, was added DDMAT (0.20 g, 0.54 mmol) and dicyclohexylcarbodiimide (0.12 g, 0.54 mmol), the reaction mixture was stirred 10 min. After the additions of 4-di(methylamino)pyridine (13.2 mg, 0.11 mmol) and DPTS (68.6 mg, 0.22 mmol), the reaction mixture was further stirred 20 h at rt. Then the reaction mixture was filtered with celite and the filtrate was placed at 4 ºC overnight, filtered with celite, and concentrated to *ca.* 8 mL. After the solution was precipitated into 150 mL of dry ether at 0 ºC twice, the crude product obtained was further purified by flash column chromatography (2-3% MeOH/CH_2Cl_2, v/v) to afford mPEG5k macro-CTA as a yellow solid (1.2 g, 60% yield). ^{1}H NMR (500 MHz, CD_2Cl_2, δ): 0.88 (t, J = 6.5 Hz, 3H), 1.26 (m, 16H), 1.38 (t, J = 6.5 Hz, 2H), 1.66 (t, J = 7.5 Hz, 2H), 1.68 (s, 6H), 3.27 (t, J = 7.2 Hz, 2H), 3.33 (s, 3H), 3.40-3.80 (m, 440H), 4.21 (t, J = 5.0 Hz, 2H).

Synthesis of PEO_{45}-*b*-$PVBA_{18}$. To a 10 mL Schlenk flask equipped with a magnetic stir bar dried with flame under N_2 atmosphere, was added the mPEG2k macro-CTA (0.24 g, 0.10 mmol) and dry DMF (2.5 mL). The reaction mixture was stirred 1 h at rt to obtain a homogeneous solution. To this solution was added VBA (0.66 g, 5.0 mmol) and AIBN (3.2 mg, 20 μmol). The reaction flask was sealed and stirred 10 min at rt. The

reaction mixture was degassed through several cycles of freeze-pump-thaw. After the last cycle, the reaction mixture was stirred for 10 min at rt before immersing into a pre-heated oil bath at 75 °C to start the polymerization. After 4 h, the monomer conversion reached *ca.* 30% by analyzing aliquots collected through ^{1}H-NMR spectroscopy. The polymerization was quenched by cooling the reaction flask with liquid N_2. CH_2Cl_2 (5.0 mL) was added to the reaction flask and the polymer was purified by precipitation into 300 mL of cold diethyl ether at 0 °C twice. The precipitants were collected, washed with 100 mL of cold ether, and dried under vacuum overnight to afford the block copolymer precursor as a yellow solid (0.35 g, 80% yield based upon monomer conversion). ^{1}H NMR (500 MHz, CD_2Cl_2, δ): 0.88-1.24 (br, dodecyl Hs), 1.52-2.06 (br, PVBA backbone protons), 3.22 (br, SCH_2 of the chain terminus), 3.33 (s, mPEG terminal OCH_3), 3.34-3.78 (m, OCH_2CH_2O from the PEG backbone), 4.84 (br, 1H from the PVBA backbone benzylic terminus connected to trithiocarbonate), 6.58-6.85 (br, Ar H), 7.33-7.62 (br, Ar H), 9.88 (br, CHO); ^{13}C NMR (150 MHz, DMSO-d_6, δ): 192.3 , 151.3, 134.4, 129.4, 128.0, 69.8, 42.3, 40.4, 29.0; IR (KBr): 3433, 2923, 2856, 2732, 1699, 1604, 1575, 1453, 1425, 1386, 1354, 1306, 1258, 1214, 1171, 1103, 1017, 951, 837, 726, 674, 552.

Synthesis of PEO_{113}-*b*-$PVBA_{46}$. To a 25 mL Schlenk flask equipped with a magnetic stir bar dried with flame under N_2 atmosphere, was added the mPEG5k macro-CTA (0.58 g, 0.11 mmol) and dry DMF (7.0 mL). The reaction mixture was stirred 1 h at rt to obtain a homogeneous solution. To this solution was added VBA (1.5 g, 11.0 mmol)

and AIBN (3.4 mg, 21 μmol). The reaction flask was sealed and stirred 10 min at rt. The reaction mixture was degassed through several cycles of freeze-pump-thaw. After the last cycle, the reaction mixture was stirred for 10 min at rt before immersing into a pre-heated oil bath at 75 °C to start the polymerization. After 5.5 h, the monomer conversion reached *ca.* 47% by analyzing aliquots collected through ^{1}H-NMR spectroscopy. The polymerization was quenched by cooling the reaction flask with liquid N_2. CH_2Cl_2 (5.0 mL) was added to the reaction flask and the polymer was purified by precipitation into 300 mL of cold diethyl ether at 0 °C twice. The precipitants were collected, washed with 100 mL of cold ether, and dried under vacuum overnight to afford the block copolymer precursor as a yellow solid (0.92 g, 75% yield based upon monomer conversion). ^{1}H NMR (500 MHz, CD_2Cl_2, δ): 0.88-1.24 (br, dodecyl Hs), 1.52-2.06 (br, PVBA backbone protons), 3.22 (br, SCH_2 of the chain terminus), 3.33 (s, mPEG terminal OCH_3), 3.34-3.78 (m, OCH_2CH_2O from the PEG backbone), 4.84 (br, 1H from the PVBA backbone benzylic terminus connected to trithiocarbonate), 6.58-6.85 (br, Ar H), 7.33-7.62 (br, Ar H), 9.88 (br, CHO); ^{13}C NMR (150 MHz, DMSO-d_6, δ): 192.3 , 151.3, 134.4, 129.4, 128.0, 69.8, 42.3, 40.4, 29.0; IR (KBr): 3433, 2923, 2856, 2732, 1699, 1604, 1575, 1453, 1425, 1386, 1354, 1306, 1258, 1214, 1171, 1103, 1017, 951, 837, 726, 674, 552.

General procedure for construction of PEO-*b*-PVBA micelles. To a solution of PEO-*b*-PVBA block copolymer in DMF (*ca.* 1.0 mg/mL), was added dropwise an equal volume of nano-pure H_2O *via* a syringe pump at a rate of 15.0 mL/h, and the mixture was

further stirred for 16 h at rt. The solution was then transferred to pre-soaked dialysis tubing with Molecular Weight Cut Off (MWCO) of *ca.* 3,500 Da and dialyzed against nano-pure H_2O for 4 d to afford a solution of micelles.

General procedure for one-pot functionalization and crosslinking of PEO-*b*-PVBA micelles with fluorescein-5-thiosemicarbazide. To a solution of PEO-*b*-PVBA micelles in 10.0 mL of nano-pure H_2O, was added a solution of fluorescein-5-thiosemicarbazide (20 mol%, 2 mol%, 1 mol%, and 0.5 mol%, relative to the aldehyde residues, respectively) in DMF. The reaction mixture was allowed to stir for 2 h at rt in the absence of light. To this reaction mixture, was added a solution of 2,2'-(ethylenedioxy)-bis(ethylamine) (150 mol%, relative to the aldehyde residues) in nano-pure H_2O dropwise over 10 min. The reaction mixture was further stirred for 48 h at rt in the absence of light. $NaBH_3CN$ (200 mol%, relative to the aldehyde residues) in nano-pure H_2O was then added to the reaction solution and further stirred for 16 h at rt in the absence of light. Finally, the mixture was transferred to pre-soaked dialysis tubing (MWCO *ca.* 3,500 Da) and dialyzed against 5.0 mM PBS (pH 7.2, with 5.0 mM NaCl) for 7 d to remove the small molecule by-products and afford an aqueous solution of fluorescein-functionalized crosslinked nanoparticles.

General procedure for one-pot functionalization and crosslinking of PEO_{113}-*b*-$PVBA_{46}$ micelles with cypate-diamine. To a solution of PEO_{113}-*b*-$PVBA_{46}$ micelles (2.7 mg of polymer, 10.8 μmol of aldehyde residues) in 10.0 mL of nano-pure H_2O, was

added a solution of cypate-diamine (1 mol%, 0.5 mol%, and 0.2 mol%, relative to the aldehyde residues, respectively) in DMF. The reaction mixture was allowed to stir for 2 h at rt in the absence of light. To this reaction mixture, was added a solution of 2,2'-(ethylenedioxy)-bis(ethylamine) (2.4 mg, 16.2 μmol) in nano-pure H_2O dropwise over 10 min. The reaction mixture was further stirred for 48 h at rt in the absence of light. $NaBH_3CN$ (1.4 mg, 21.6 μmol) in nano-pure H_2O was then added to the reaction solution and further stirred for 16 h at rt in the absence of light. Finally, the mixture was transferred to pre-soaked dialysis tubing (MWCO *ca.* 6,000-8,000 Da) and dialyzed against 5.0 mM PBS (pH 7.2, with 5.0 mM NaCl) for 7 d to remove the small molecule by-products and afford an aqueous solution of functionalized and crosslinked nanoparticles.

Micellization of PEO_{45}-*b*-$PNAS_{95}$-*b*-PS_{60}. To a solution of PEO_{45}-*b*-$PNAS_{95}$-*b*-PS_{60} block copolymer in DMF (*ca.* 1.0 mg/mL), was added dropwise an equal volume of nano-pure H_2O *via* a syringe pump at a rate of 15.0 mL/h, and the mixture was further stirred for 1 h at rt before using for the following reactions.

Functionalization and crosslinking of PEO_{45}-*b*-$PNAS_{95}$-*b*-PS_{60} micelles with cypate-diamine or HL-800 amine. To a solution of PEO_{45}-*b*-$PNAS_{95}$-*b*-PS_{60} micelles (4.8 mg of block copolymer precursor, 27.0 μmol of NAS residues) in 10 mL of DMF/H_2O (v:v = 1:1) at rt, was added the solution of cypate-diamine (38.3 μg, 0.054 μmol) or HL-800 amine (51.6 μg, 0.054 μmol) in 50 μL of DMF. The reaction mixture

was allowed to stir for 2 h at rt in the absence of light. To this reaction mixture, was added a solution of 2,2'-(ethylenedioxy)-bis(ethylamine) (1.0 mg, 6.8 μmol) in nano-pure H_2O dropwise over 10 min. The reaction mixture was further stirred for 24 h at rt in the absence of light and transferred to pre-soaked dialysis tubing (MWCO 6,000-8,000 Da) and dialyzed against 5.0 mM PBS (pH 7.2, with 5.0 mM NaCl) for 7 days to remove DMF, un-reacted crosslinker, and the small molecule by-products and afford an aqueous solution of crosslinked nanoparticles.

One-pot functionalization and crosslinking of PEO_{113}-*b*-$PVBA_{46}$ micelle with HL-800-amine. To a solution of PEO_{113}-*b*-$PVBA_{46}$ micelles (2.7 mg of polymer, 10.8 μmol of aldehyde residues) in 10.0 mL of nano-pure H_2O, was added a solution of HL-800-amine (20.7 μg, 0.022 μmol) in DMF. The reaction mixture was allowed to stir for 2 h at rt in the absence of light. To this reaction mixture, was added a solution of 2,2'-(ethylenedioxy)-bis(ethylamine) (2.4 mg, 16.2 μmol) in nano-pure H_2O dropwise over 10 min. The reaction mixture was further stirred for 48 h at rt in the absence of light. $NaBH_3CN$ (1.4 mg, 21.6 μmol) in nano-pure H_2O was then added to the reaction solution and further stirred for 16 h at rt in the absence of light. Finally, the mixture was transferred to pre-soaked dialysis tubing (MWCO *ca.* 6,000-8,000 Da) and dialyzed against 5.0 mM PBS (pH 7.2, with 5.0 mM NaCl) for 7 d to remove the small molecule by-products and afford an aqueous solution of functionalized and crosslinked nanoparticles.

Results and Discussion

To construct fluorescent NPs, diblock copolymer (poly(ethylene oxide)-*block*-poly(4-vinyl benzaldehyde, PEO-*b*-PVBA) and triblock copolymer (poly(ethylene oxide)-*block*-poly(*N*-acryloxysuccinimide)-*block*-polystyrene, PEO-*b*-PNAS-*b*-PS) micelles were functionalized with fluorescein-5-thiosemicarbazide and amine-terminated carbocyanine dyes through either reductive amination or amidation chemistry. The PEO-*b*-PVBA diblock copolymers **I** (PEO_{45}-*b*-$PVBA_{18}$, $M_{n,\ NMR}$ = 4,700 Da, $M_{n,\ GPC}$ = 3,900 Da, *PDI* = 1.2, Figure 7.1A) and **II** (PEO_{113}-*b*-$PVBA_{46}$, $M_{n,\ NMR}$ = 12,600 Da, $M_{n,\ GPC}$ = 12,400 Da, *PDI* = 1.4, Figure 7.1B)[58] were used for construction of core functionalizable crosslinked nanoparticles while the PEO-*b*-PNAS-*b*-PS triblock copolyper **III** (PEO_{45}-*b*-$PNAS_{95}$-*b*-PS_{60}, $M_{n,\ NMR}$ = 18,400 Da, *PDI* = 1.2, Figure 7.1C) was utilized as precursor for shell crosslinked nanoparticles. All block copolymers were prepared through reversible addition-fragmentation chain transfer (RAFT) polymerization,[59-61] based upon our previous reports.[56, 57] The PEO (*MW* = 2, 000 and 5,000 Da, respectively) was selected as hydrophilic segment because of its good water solubility, well-known biocompatibility, and low immunogenic response.[62] PVBA was used as the hydrophobic and reactive segment due to the broad reaction scope and the mild reaction condition of aldehyde functionality, especially under aqueous conditions. PNAS acted as pre-installed active ester for reaction with amine-functionalized fluorophores.

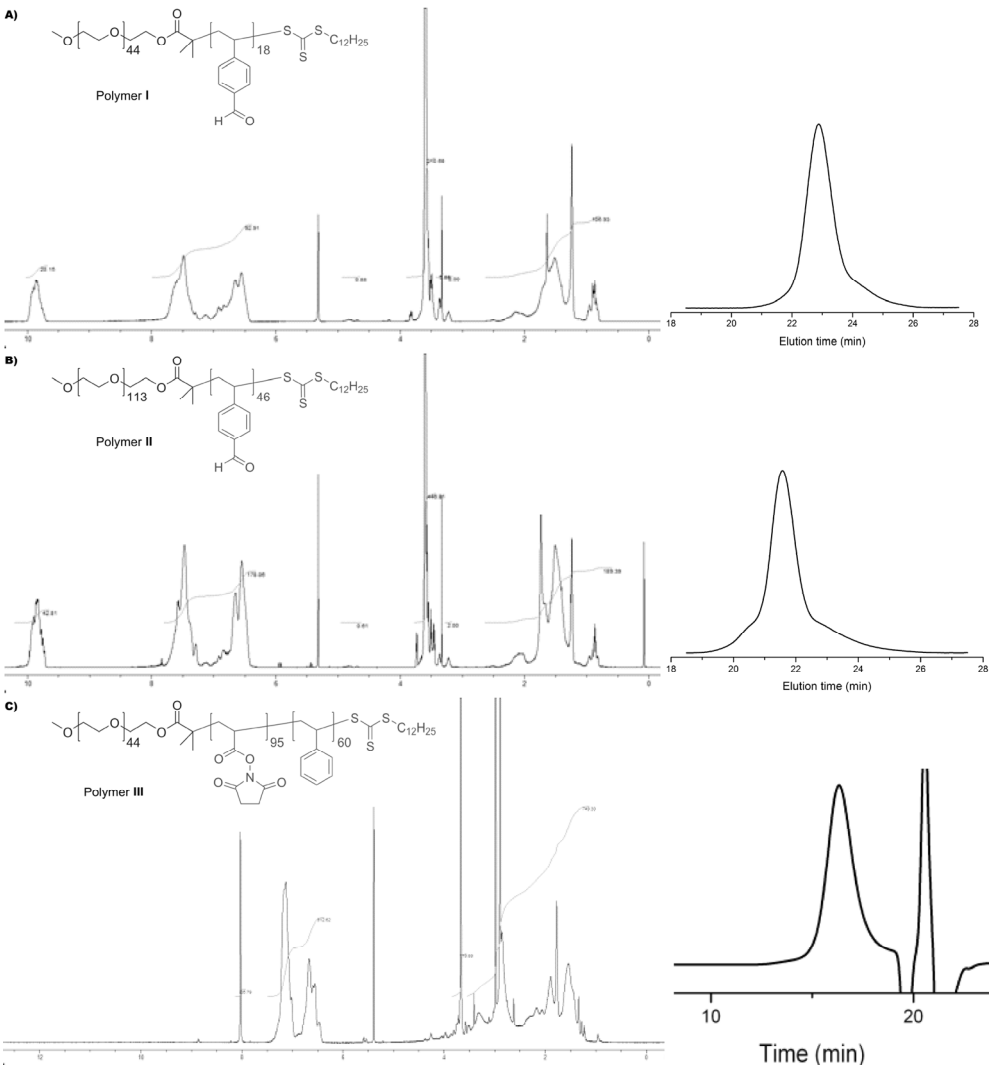

Figure 7.1. Characterizations of PEO_{45}-*b*-$PVBA_{18}$ (**I**), PEO_{113}-*b*-$PVBA_{46}$ (**II**), and PEO_{45}-*b*-$PNAS_{95}$-*b*-PS_{60} (**III**) block copolymer precursors. A): ^{1}H NMR spectrum (left, 500 MHz, CD_2Cl_2) and THF-GPC profile (right) of PEO_{45}-*b*-$PVBA_{18}$ block copolymer. B): ^{1}H NMR spectrum (left, 500 MHz, CD_2Cl_2) and THF-GPC profile (right) of PEO_{45}-*b*-$PVBA_{18}$ block copolymer. C): A): ^{1}H NMR spectrum (left, 600 MHz, CD_2Cl_2) and DMF-GPC profile (right) of PEO_{45}-*b*-$PNAS_{95}$-*b*-PS_{60} block copolymer.

Aqueous assembly of block copolymer **I** and **II** followed conventional methods for micellization of amphiphilic block copolymers with a glassy hydrophobic block segment. PEO selective solvent, *i.e.* water, was slowly (*ca.* 15 mL/h) added to the solution of PEO-*b*-PVBA in organic solvent (DMF, *ca.* 1.0 mg/mL) to induce the

micellization and further stabilize the formed aggregates. Finally, the organic solvent was removed through dialysis against water to afford PEO-*b*-PVBA micelles with PEO shell and PVBA core domains. The uniformity and narrow size distribution of the assembled micelles were demonstrated through the combination of DLS and TEM (Figure 7.2). The DLS measurements showed that these micelles had intensity-averaged hydrodynamic diameter ($D_{h,\ intensity}$) of 23 ± 2 nm (from PEO_{45}-*b*-$PVBA_{18}$) and 26 ± 2 nm (from PEO_{113}-*b*-$PVBA_{46}$), respectively. TEM micrograph revealed their globular shape with an average core domain diameter (D_{av}) of 13 ± 1 nm and 19 ± 1 nm, respectively, depending upon the length of PVBA block segment.

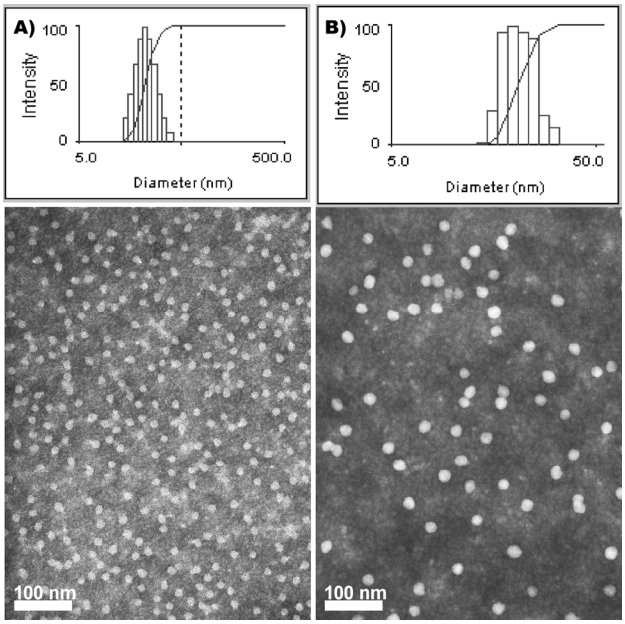

Figure 7.2. Characterization of PEO-*b*-PVBA micelles. A) Intensity-average weighted hydrodynamic diameter distribution histogram by DLS (top) and TEM micrograph (bottom, stained with PTA) of PEO_{45}-*b*-$PVBA_{18}$ micelle. B) Intensity-average weighted hydrodynamic diameter distribution histogram by DLS (top) and TEM micrograph (bottom, stained with PTA) of PEO_{113}-*b*-$PVBA_{46}$ micelle.

One-pot chemical functionalization with fluorescein-5-thiosemicarbazide and crosslinking with diamine crosslinker of the PEO_{45}-*b*-$PVBA_{18}$ micelles were achieved, following our previously established reductive amination protocol (Scheme 7.1A).[56] Similar to our previous reports,[56] buffer solutions with certain ionic strength (pH 7.2 5 mM PBS with 5 mM of NaCl in this study) were found to be required to prevent the precipitation of the crosslinked nanoparticles. For **NP1** (prepared with a feeding ratio of fluoresceins/aldehydes = 0.2:1), the DLS ($D_{h,\ intensity}$ = 21 ± 1 nm) and TEM (D_{av} = 13 ± 1 nm) characterizations of the functionalized crosslinked NPs showed no obvious morphology, size, and size distribution variations (Figure 7.3A), compared with the micelle precursors (Figure 7.2A). UV-Vis measurement of the fluorescein-NP solutions revealed that a slight red-shift of *ca.* 8 nm (Figure 7.3E left) occurred for the maximum absorption peak (λ_{max}, 496 nm for the fluorescein-functionalized NPs *v.s.* 488 nm for the unconjugated fluorescein), which might be related to the change of fluorescein local environment before and after incorporation into the nanostructure. Although the thiosemicarbazide is a strong nucleophile, the coupling efficiency of fluorescein into NP was only *ca.* 12%. This might be associated with the low accessibility of hydrophilic fluoresein to the hydrophobic benzaldehyde functionalities (packed inside the hydrophobic core domain of the micelle).

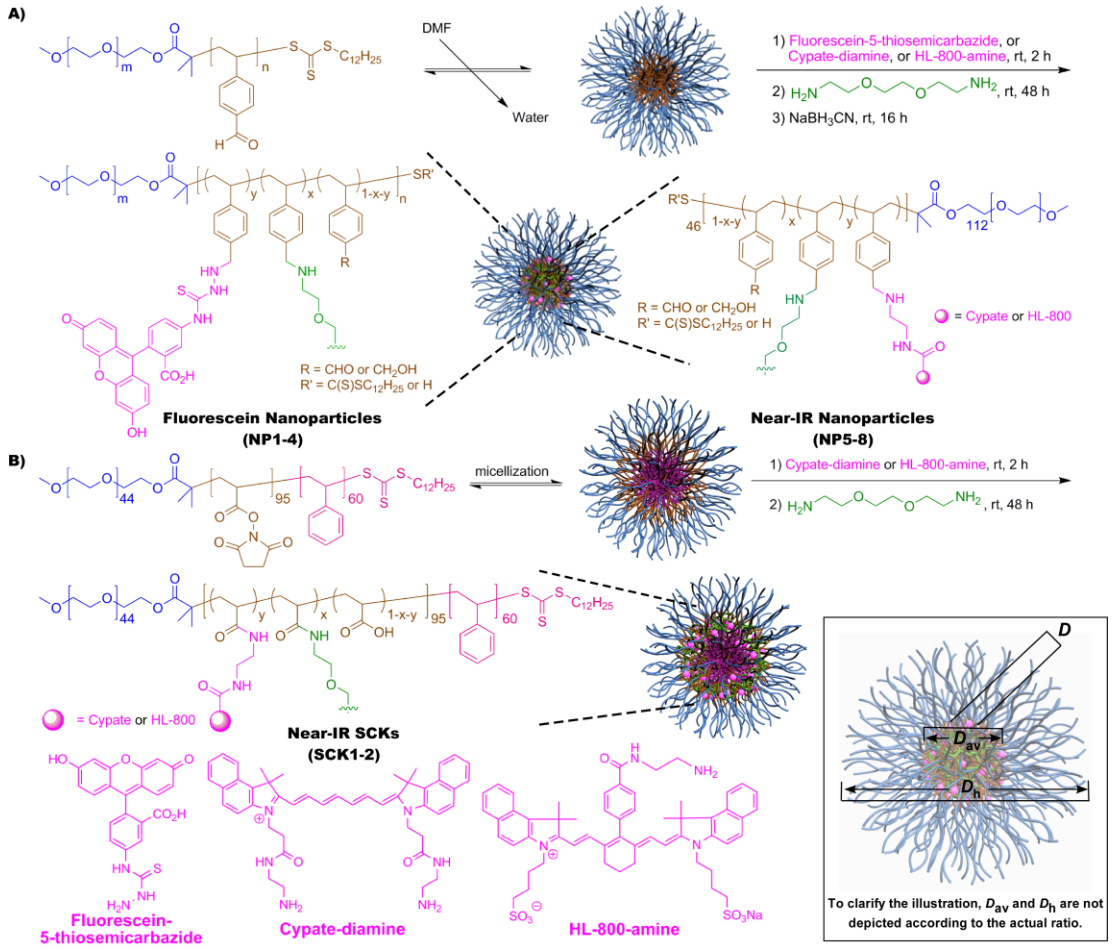

Scheme 7.1. Construction of fluorescent nanoparticles through reductive amination (A) and amidation (B).

Steady state fluorescence spectrum of the diluted NP solution was recorded at the excitation wavelength of 450 nm over the range of 465-650 nm and shown in Figure 7.3E. Compared with small fluorescein molecule, much lower fluorescence emission intensity of the **NP1** sample (200-fold drop at the same concentration magnitude) was observed. We attributed the decrease in fluorescence of attached fluorescein moieties to intra-nanoparticle self-quenching, *i.e.*, the combined effects of homoFRET (non-radiative energy transfer of the same fluorophores located in close proximity to each other) caused

by incorporating *ca.* 150 dyes into a confined space with *ca.* 13 nm of diameter (*vide infra*).

We also conducted the R_0 measurement (see Experimental Section for details) and the result was 4.67 nm, similar to the literature value (4.4 nm). The distance between two fluorescein moieties on the NPs (r) were calculated from both steady-state and dynamic emission spectra by using the following equations:

$$r = R_0 \left(\frac{F_{da}/Abs_{da}}{F_d/Abs_d}\right)^{1/6} \text{ nm for steady-state emission} \qquad (4)$$

where F_{da} is the fluorescence intensity of the donor in the presence of acceptor, and F_d is the fluorescence intensity of the donor in the absence of acceptor, Abs_{da} is absorbance of the donor in the presence of acceptor, Abs_d is absorbance of the donor in the absence of acceptor.

$$\text{and } r = R_0 \left(\frac{\tau_{da}}{\tau_d}\right)^{1/6} \text{ nm for dynamic emission} \qquad (5)$$

where τ_{da} represents the relative fluorescence lifetime of the donor in the presence of acceptor, and τ_d in the absence of acceptor. The calculated results, together with the experimentally optical characteristics of the samples, were summarized in Table 7.1.

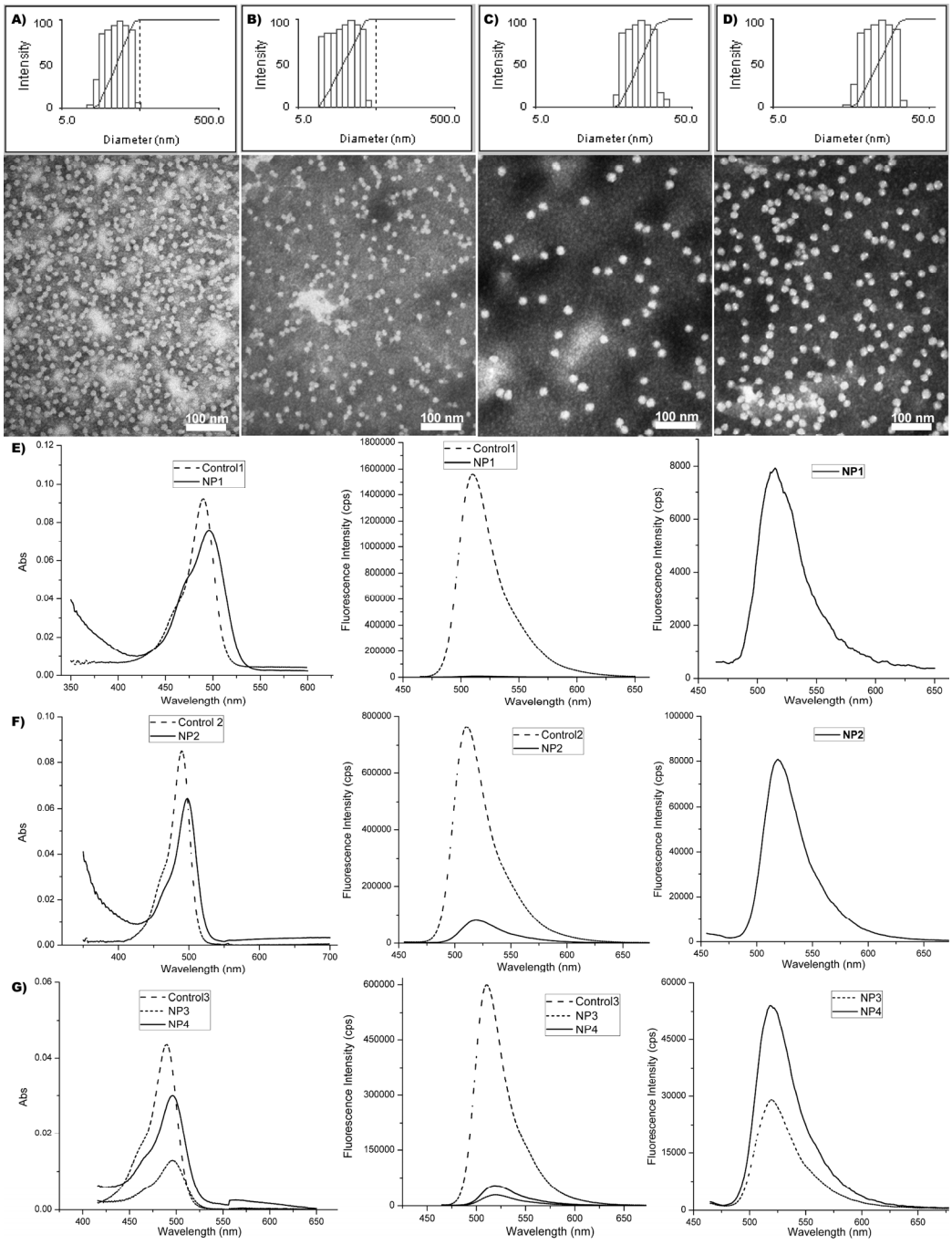

Figure 7.3. Characterizations of **NP1-4**. A-D) Intensity-average weighted hydrodynamic diameter distribution by DLS (top) and TEM micrograph (bottom, stained with PTA) of NP**1-4**, respectively. E) UV-Vis (left) and fluorescence emission (middle and right) spectra of **Control1** (**Fluorescein**, dashed) and **NP1** (solid). F) UV-Vis (left) and fluorescence emission (middle and right) spectra of **Control2** (**Fluorescein**, dashed) and **NP2** (solid). G) UV-Vis (left) and fluorescence emission (middle and right) spectra of **Control3** (**Fluorescein**, dashed), **NP3** (short dashed) and **NP4** (solid).

Table 7.1. Calculated distance between two adjacent fluorescein moieties incorporated into nanoparticles and the optical characteristics of fluorescent nanoparticles.

Sample	$D_{h,\ intensity}$ (nm)	D_{av} (nm)	N_{agg}	Dyes/NP[a]	D (nm)	τ[b] (ns)	$r(\tau)$[c] (nm)	Φ[d]	$r(\Phi)$[e] (nm)
Control1[f]	—	—	—	—	—	3.95	—	0.79	—
NP1	21 ± 1	13 ± 1	350	150	1.88	2.07	4.75	0.005	2.0
Control2[f]	—	—	—	—	—	3.88	—	0.79	—
NP2	22 ± 2	13 ± 1	350	15	5.95	2.97	5.69	0.088	3.3
Control3[f]	—	—	—	—	—	3.92	—	0.79	—
NP3	24 ± 2	19 ± 1	430	15	8.69	3.33	6.23	0.233	4.04
NP4	24 ± 2	19 ± 1	430	30	6.15	3.11	5.84	0.215	3.97

[a] Calculated based upon $\varepsilon = 66{,}000\ M^{-1}\ cm^{-1}$. [b] Fluorescence average lifetime. [c] Distance between two fluorophores based upon lifetime measurement. [d] Fluorescence quantum yield. [e] Distance between two fluorophores based upon quantum yield. [f] Fluorescein as control (**Control1** for **NP1** measurement, **Control 2** for **NP2** measurement, and **Control3** for **NP3** and **NP4** measurements, respectively).

We have previously established a semi-quantitative model for evaluation of the nanoparticle surface coverage density.[63] Because only ~ 2.5% of the VBA units were actually "decorated" with fluorescein, the fluorescein molecules should be attached to the most accessible VBA units, *i.e.* benzaldehydes around the periphery of the core domain. Therefore, the previous model could be easily revised to estimate the distance between adjacent fluorecein molecules (depicted as D in Scheme 7.1 insertion) through the following equation:

$$D = \sqrt{\frac{\pi (D_{av})^2}{N}} \quad \text{nm} \qquad (6)$$

where N denotes the number of fluorophores per NP (obtained from the number of fluorophores per polymer chain and the aggregation number of polymer chains estimated to be within each NP, see Experimental Section for details), and D_{av} is the averaged diameter of the core domain of NP.

Theoretically, no energy would be transferred and therefore no quenching would occur if the distance between two fluororeceins exceeds 9 nm. For **NP1**, the calculated distances between two fluorescein molecules, both from our model prediction using eq. (6) (1.88 nm) and from the experimental calculations (2.00 nm from steady state and 4.75 nm from dynamic state, respectively), were far below 9 nm and substantial self-quenching (over 45% of the emission energy was transferred to acceptors) were expected. The variation of the distance between steady-state and dynamic emission spectra was attributed to the more complex decay of **NP1**. In fact, the average lifetime results in Table 7.1 were the results of deconvolution of decays using two-exponential decay laws and the multiexponentiality of decays suggested the presence of many distance between fluorescein moieties.

To reduce the homoFRET effect, the easiest method was to decrease the number of fluorophores per nanoparticle. Therefore, **NP2** with *ca.* 15 fluoreceins per NP was prepared from the same block copolymer micelle as **NP1**, maintaining similar size ($D_{h,\ intensity}$ = 22 ± 2 nm and D_{av} = 13 ± 1 nm) and size distribution (Figure 7.3B).[64] Significant improvement of QY was observed by a factor of 18 (Table 7.1), due to the increase of the distance between fluorescein moieties, as calculated from experimental data and the proposed model (Table 7.1).

However, the QY for **NP2** was still below 0.1. Also, *ca*. 25% of the energy was non-radiatively transferred to other fluoresceins, based upon the lifetime measurement.

Further decrease of fluorescein density is expected to enhance QY, but the overall fluorescence intensity per NP still would not reach a desired level due to the lack of fluorophores. Theoretical estimation indicated that, for the PEO_{45}-*b*-$PVBA_{18}$ system (13 nm diameter core), there can be no more than 5 fluoresceins per particle that are separated by at least 9 nm. The prediction made this system less attractive for further optimization because at such a small loading capacity, even the QY for each fluorophore can be enhanced, the overall fluorescence cannot be indefinitely improved due to the fewer number of fluorophores per particle.

From equation (6), there exists a linear relationship between D and D_{av} at fixed dye loadings, which indicates that the size increase of nanoparticle core domain would facilitate the enhancement of luminescence efficiency. Therefore, it is desired to use particles with larger cores for fluorophore functionalization. **NP3** and **NP4** with larger core sizes (19 *vs.* 13 nm, Table 7.1 and Figure 7.3C-D) were then prepared from PEO_{113}-*b*-$PVBA_{46}$ block copolymer micelles.[65]

With a core size of 19 nm and 15 fluorescein molecule/NP, the calculated D for **NP3** was 8.69 nm, which was close to the "9 nm requirement". In fact, only 15.7% of the absorbed energy was non-radiatively transferred between fluorescein moieties (based upon lifetime measurement). As a result, QY of **NP3** was increased to 0.233, a 2.5-fold enhancement compared with **NP2**. For **NP4**, which bears 30 fluoreceins per particle, a slight drop of QY (0.215) was observed, likely due to the relative proximity between

fluorophores (D = 6.15 nm). However, the slightly decreased QY was compensated by the much increased number of fluorophores, rendering its overall fluorescence intensity 190% as large as than that of **NP3** (Figure 7.3G right).

The PEO_{113}-*b*-$PVBA_{46}$ micelle system and the optimized stoichiometry of fluorescein loading (less than 1 mol%, relative to the aldehydes) were then extend to construct NIR fluorescent nanoparticles. **NP5-7** with *ca.* 70, 45, and 10 cypates per particle, respectively, were synthesized and subjected to photo-physical studies. Compared with the coupling yields of fluoresceins at ~ 12% to 15%, the cypate exhibited ~ 36% to 47% incorporation efficiencies. This improvement could to be attributed to the fact that cypate was much more hydrophobic than fluorescein and had more preference for the hydrophobic PVBA core.

As shown in Figure 7.4A-C, **NP5-7** displayed well-defined globular shape and narrow size distributions. Interestingly, although the UV-Vis spectra (Figure 7.4D) showed that **NP5-7** had the identical maximum absorption wavelength at 800 nm, the fluorescence emission spectrum of **NP7** bearing the least number of cypates exhibited a clear blue-shift of *ca.* 11 nm (813 nm *vs.* 824 nm for **NP5** and **6**, Figure 7.4E). The origin of this blue-shift was believed to be associated with the increased molecular asymmetry[20] of cypate-diamine after incorporation into the nanostructures at lower stoichiometry, *i.e.*, some of the cypate-diamines had both amine groups reacted while some only had one reacted.

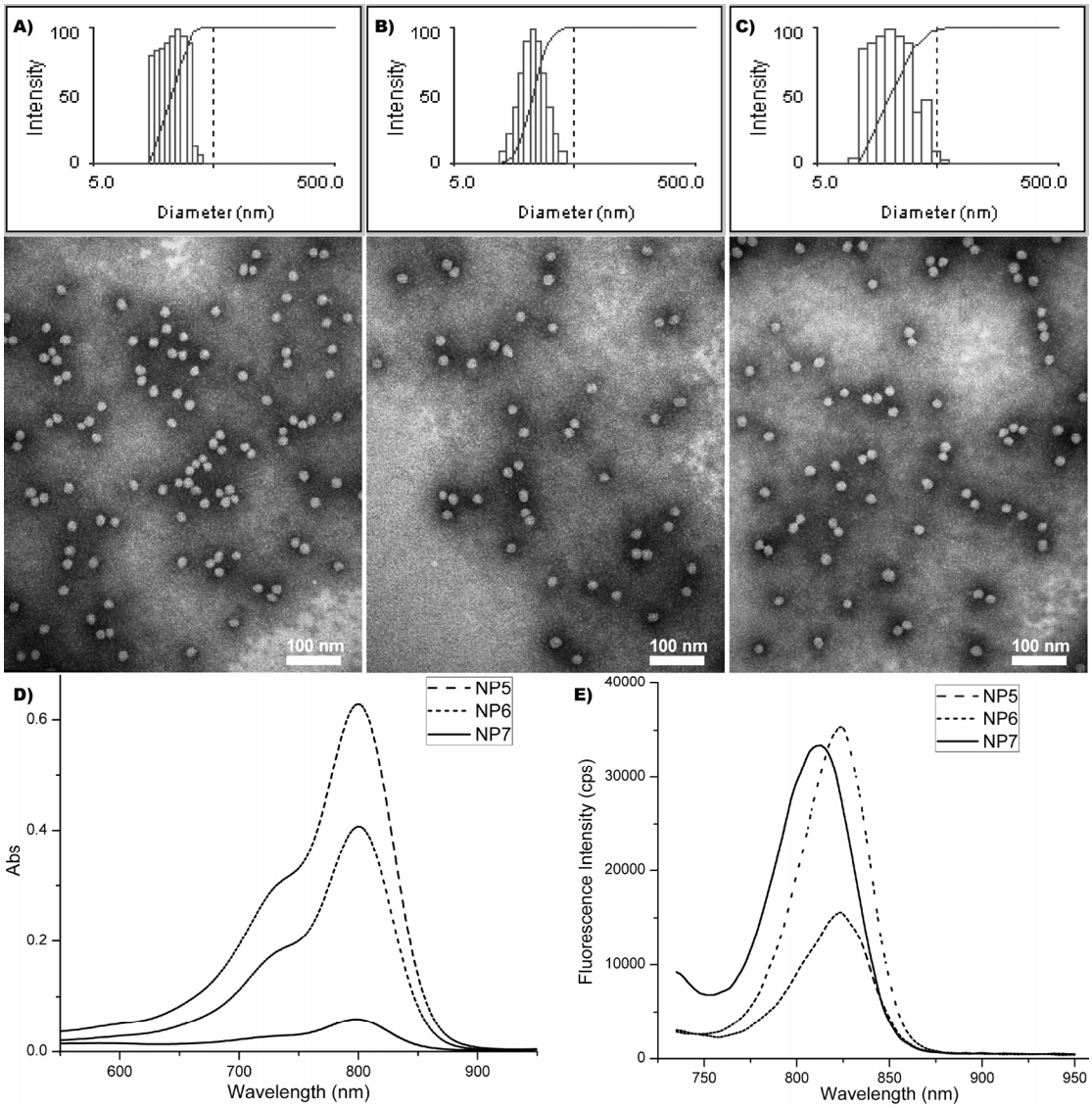

Figure 7.4. A-C) Intensity-average weighted hydrodynamic diameter distribution histogram by DLS (top) and TEM micrograph (bottom, stained with PTA) of **NP5**, **NP6**, and **NP7**, respectively. D-E) UV-Vis and fluorescence profiles of **NP5** (dashed), **NP6** (short dashed), and **NP7** (solid), respectively.

Based upon the model prediction equation (eq. (6)), the distance between neighboring cypate molecules for **NP5-7** was 4.0 nm, 5.0 nm, and 10.7 nm, respectively (Table 7.2). Compared with the general "non-homoFRET criterion" (> 12 nm), it could speculate that **NP5** and **NP6** would exhibit very low QYs, which were further confirmed

through the steady-state (QY = 0.001 and 0.004, respectively) and dynamic (lifetime less than 0.3 ns) measurements. For **NP7**, increased QY value was expected due to the increased D value (over 10 nm). The actual QY value was measured by steady state fluorescence to be 0.019, very close to free cypate in water (0.021).

Table 7.2. Characterizations and optical characteristics of NIR fluorescent nanoparticles from PEO_{113}-*b*-$PVBA_{46}$ system.

Sample	$D_{h,\ intensity}$ (nm)	D_{av} (nm)	N_{agg}	Dyes/NP[a]	D (nm)	Φ[b]	τ[c] (ns)
NP5	23 ± 1	19 ± 1	430	70	4.0	0.001	0.2[d]
NP6	23 ± 1	19 ± 1	430	45	5.0	0.004	0.2[d]
NP7	22 ± 2	19 ± 1	430	10	10.7	0.019	0.6

[a] Calculated based upon ε = 200,000 M^{-1} cm^{-1}. [b] Relative to ICG in methanol (QY=0.09). [c] Fluorescence average lifetime. [d] Due to the limitation of instrument, the lifetime below 0.3 ns was not accurate.

The lifetime and quantum yield of carbocyanine dye were also related with the property of local environment, *i.e.*, the micropolarity of the media.[66] For example, the lifetime of cypate was markedly increased from less than 0.2 ns to 1 ns as the solvent was switched from water to chloroform. QY could also be affected but was less predictable. For the core crosslinked PEO-*b*-PVBA system, since the reactive aldehydes were located inside the core and the core-shell interfacial domains, the covalently conjugated NIR dyes were also confined to core periphery and core-shell interface areas and were theoretically exposed to relatively less polar surroundings, compared with the pure water molecules. To test whether the QY of cypate-functionalized NPs was affected by fluorophore location, shell-crosslinked NIR fluorescent nanoparticles (NIR-SCKs, **SCK1**-**2**) were

prepared, in which the carbocyanine molecules (Cypate for **SCK1** and HL-800 for **SCK2**, respectively) were distributed throughout the shell domain (Scheme 7.1B).

As mentioned earlier, the NIR-SCKs were synthesized through functionalization and crosslinking the PEO_{45}-*b*-$PNAS_{95}$-*b*-PS_{60} micelle with pendent NAS functionalities as pre-installed amidation sites along the polymer backbone for amine-terminated cyanine dyes and diamine crosslinkers. After the work-up process (extensive dialysis against PBS buffer), the unreacted NAS residues were hydrolyzed to acrylic acids and then became components of shell domain of nanoparticles. The cypate incorporation efficiency (*ca.* 15%) was lower compared with the PEO-*b*-PVBA system under similar cypate-diamine feeding ratio (0.2 mol%, relative to the reactive functionalities). The particles showed relatively narrow size distributions and globular shape observed through DLS and TEM (Figure 7.5A-B). The physical characteristics of **SCK1** and **SCK2** were summarized in Table 7.3.

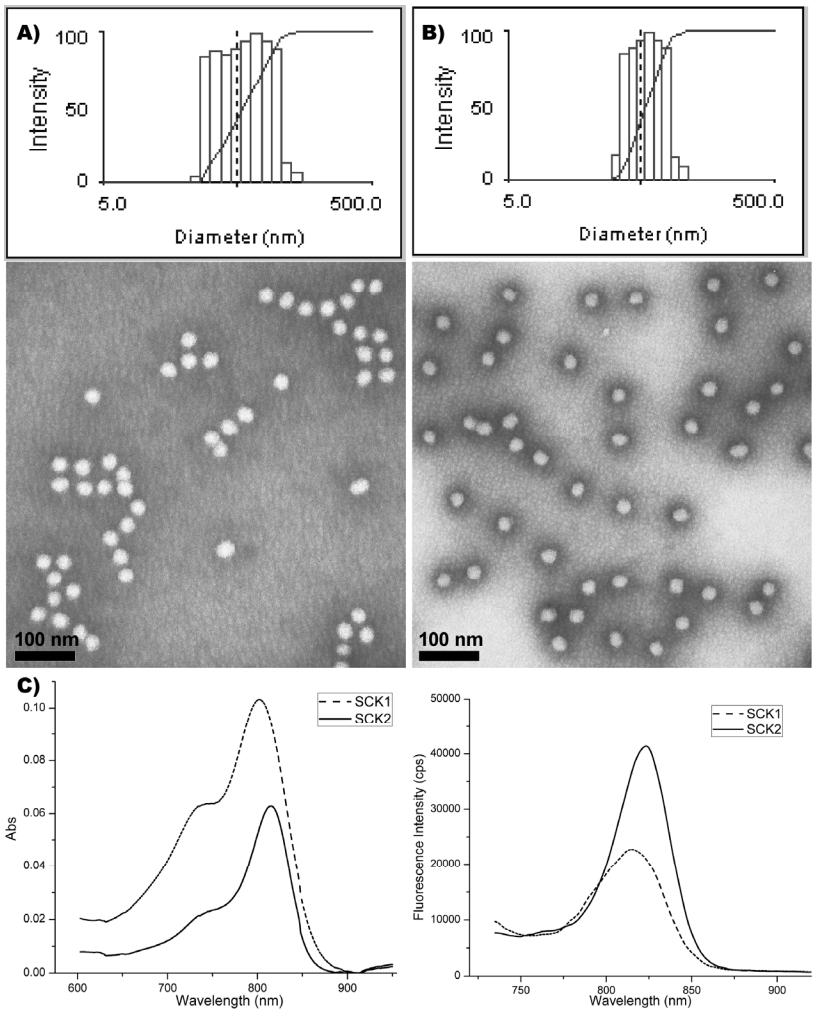

Figure 7.5. Characterizations and photo-physical properties of shell crosslinked NIR fluorescent nanoparticles. A-B) Intensity-average weighted hydrodynamic diameter distribution histogram by DLS (top) and TEM micrograph (bottom, stained with PTA) of **SCK1** and **SCK2**, respectively. C) UV-Vis (left) and fluorescence (right) profiles of **SCK1** (dashed) and **SCK2** (solid), respectively.

Table 7.3. Characterizations and optical characteristics of NIR-SCKs from PEO_{45}-*b*-$PNAS_{95}$-*b*-PS_{60} micelles.

Sample	$D_{h,\ intensity}$ (nm)	D_{av} (nm)	N_{agg}	Dyes/NP[a]	Φ[b]
SCK1	59 ± 3	30 ± 1	1450	40	0.005
SCK2	56 ± 2	30 ± 1	1450	20	0.036

[a] Calculated based upon ε = 200,000 M^{-1} cm^{-1}. [b] Relative to ICG in methanol (QY=0.09).

Similar to **NP7**, the fluorescence emission spectrum of **SCK1** showed a 10 nm blue-shift for the maximum emission peak (dashed curve in Figure 7.5D). The blue-shift could also be attributed to the raise of cypate molecular asymmetry after conjugation. Although the particle size increased in both core and shell domains (59 nm *vs.* 23 nm for hydrodynamic diameter and 30 nm *vs.* 19 nm for core diameter), and NIR dye loading was decreased (40 *vs.* 45), the QY of **SCK1** (0.005, Table 7.3) was still low. Based upon our model prediction, the D value was between the range of 8.41 nm and 15.63 nm, where 8.41 nm represented the extreme that all dyes were located to the periphery of core domain and 15.63 nm represented the other extreme that all dyes were placed on the margin of shell domain. And therefore, it was speculated that the limited enhancement of luminance efficiency might be originated from the increased environmental micropolarity after incorporation into the more hydrophilic shell domain.

NIR-SCKs with improved optical characteristics were achieved while the cypate was replaced by HL-800 at a loading capacity of 20 HL-800s/SCK (**SCK2**, and the D value was between the range of 11.89 nm to 22.19 nm). The QY of **SCK2** (0.036, Table 7.3) was enhanced by a factor of 7 and the overall fluorescence intensity gained a 2-fold increase, relative to **SCK1**. HL-800 was further introduced into the PEO_{113}-*b*-$PVBA_{46}$ system for synthesis of **NP8** bearing 5 dyes/NP while keeping similar size as **NP5-7** (Figure 7.6A, $D_{h,\ intensity}$ = 22 ± 1 nm and D_{av} = 19 ± 1 nm) and comparable D as **SCK2** (D = 15.06 nm). Dramatic decrease of QY was observed (0.002 *vs.* 0.019), even though

the error of **NP8** calculation was high due to the unreliable level of absorption intensity (Figure 7.6B). These results suggested that the HL-800 might exhibit a reversed solvent-polarity response as cypate and the mechanism was not clear now.

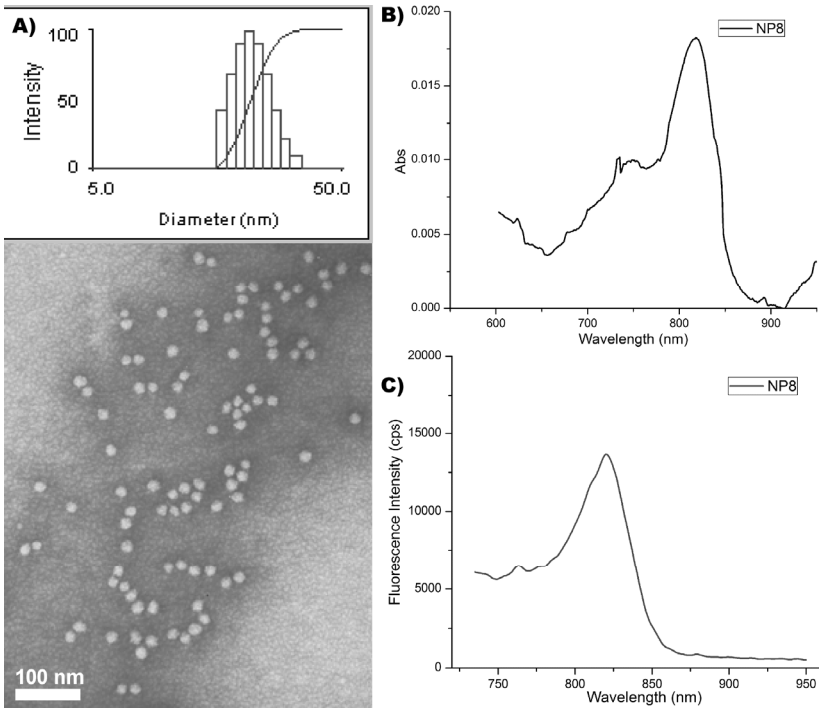

Figure 7.6. A) Intensity-average weighted hydrodynamic diameter distribution by DLS (top) and TEM micrograph (bottom) of **NP8**. B-C) UV-Vis and fluorescence spectrum of **NP8**, respectively.

Conclusions

In summary, we have tested the photo-physical properties of crosslinked nanoparticles functionalized with fluoresceins or NIR carbocyanine (Cypate and HL-800) dyes at different stoichiometric loadings. It is clear that the nanoparticle QY and fluorescence lifetime was determined by the distance between adjacent fluorophores. More importantly, the NP maximum dye loading capacity for retaining sufficient QY

could be predicted through a semi-quantitative model, which correlated well with the experimental results. These fundamental results could be applied to the development of nanoparticle-based NIR optical devices for fluorescence imaging.

References and Notes

1. Frangioni, J. V. "*In vivo* near-infrared fluorescence imaging." *Curr. Opin. Chem. Biol.* **2003,** *7*, 795-805.

2. Ntziachristos, V.; Ripoll, J.; Wang, L. V.; Weissleder, R. "Looking and listening to light: the evolution of whole-body photonic imaging." *Nat. Biotechnol.* **2005,** *23*, 313-320.

3. Licha, K.; Olbrich, C. "Optical imaging in drug discovery and diagnostic applications." *Adv. Drug Delivery Rev.* **2005,** *57*, 1087-1108.

4. Ntziachristos, V. "Fluorescence Molecular Imaging." *Annu. Rev. Biomed. Eng.* **2006,** *8*, 1-33.

5. Rao, J.; Dragulescu-Andrasi, A.; Yao, H. "Fluorescence imaging in vivo: recent advances." *Curr. Opin. Biotech.* **2007,** *18*, 17-25.

6. Ntziachristos, V. "Fluorescence imaging: overview and applications in biomedical research." *Genomic Pers. Med.* **2009,** *1*, 524-531.

7. Tsui, B. M. W.; Kraitchman, D. L. "Recent Advances in Small-Animal Cardiovascular Imaging." *J. Nucl. Med.* **2009,** *50*, 667-670.

8. Gao, X.; Cui, Y.; Levenson, R. M.; Chung, L. W. K.; Nie, S. "In vivo cancer targeting and imaging with semiconductor quantum dots." *Nat. Biotechnol.* **2004,** *22*, 969-976.

9. Michalet, X.; Pinaud, F. F.; Bentolila, L. A.; Tsay, J. M.; Doose, S.; Li, J. J.; Sundaresan, G.; Wu, A. M.; Gambhir, S. S.; Weiss, S. "Quantum dots for live cells, *in vivo* imaging, and diagnostics." *Science* **2005,** *307*, 538-544.

10. So, M. K.; Xu, C.; Leoning, A. M.; Gambhir, S. S.; Rao, J. "Self-illuminating quantum dot conjugates for in vivo imaging." *Nat. Biotechnol.* **2006,** *22*, 339-343.

11. Hoffman, R. M. "The multiple uses of fluorescent proteins to visualize cancer *in vivo*." *Nat. Rev. Cancer* **2005,** *5*, 796-806.

12. Shaner, N.; Steinbach, P. A.; Tsien, Y. T. "A guide to choosing fluorescent proteins." *Nat. Methods* **2005,** *2*, 905-909.

13. Achilefu, S. "Lighting Up Tumors with Receptor-specific Optical Molecular Probes." *Technol. Cancer Res. Treat.* **2004,** *3*, 393-410.

14. Ye, Y.; Bloch, S.; Achilefu, S. "Polyvalent Carbocyanine Molecular Beacons for Molecular Recognitions." *J. Am. Chem. Soc.* **2004,** *126*, 7740-7741.

15. Cheng, Z.; Wu, Y.; Xiong, Z.; Gambhir, S. S.; Chen, X. "Near-infrared fluorescent RGD peptides for optical imaging of integrin $\alpha_v\beta_3$ expression in living mice." *Bioconjugate Chem.* **2005,** *16*, 1433-1441.

16. Pham, W.; Medarova, Z.; Moore, A. "Synthesis and application of a water-soluble near-infrared dye for cancer detection using optical imaging." *Bioconjugate Chem.* **2005,** *16*, 735-740.

17. Lee, H.; Mason, J. C.; Achilefu, S. "Heptamethine Cyanine Dyes with a Robust C─C Bond at the Central Position of the Chromophore." *J. Org. Chem.* **2006,** *71*, 7862-7865.

18. Masotti, A.; Vicennati, P.; Boschi, F.; Calderan, L.; Sbarbati, A.; Ortaggi, G. "A Novel Near-Infrared Indocyanine Dye─Polyethylenimine Conjugate Allows DNA Delivery Imaging *in Vivo*." *Bioconjugate Chem.* **2008,** *19*, 983-987.

19. Strekowski, L. *Heterocyclic Polymethine Dyes: Synthesis, Properties and Applications*. Springer: Berlin, 2008.

20. Zhang, Z.; Berezin, M. Y.; Kao, J. L. F.; d'Avignon, A.; Bai, M.; Achilefu, S. "Near-Infrared Dichromic Fluorescent Carbocyanine Molecules." *Angew. Chem., Int. Ed.* **2008,** *47*, 3584-3587.

21. Achilefu, S.; Dorshow, R. B.; Bugal, J. E.; Rajagopalan, R. "Novel Receptor-Targeted Fluorescent Contrast Agents for In Vivo Tumor Imaging." *Invest. Radiol.* **2000,** *35*, 479-485.

22. Achilefu, S.; Bloch, S.; Markiewicz, M. A.; Zhong, T.; Ye, Y.; Dorshow, R. B.; Chance, B.; Liang, K. "Synergistic effects of light-emitting probes and peptides for targeting and monitoring integrin expression." *Proc. Natl. Acad. Sci. USA* **2005,** *102*, 7976-7981.

23. Ye, Y.; Bloch, S.; Xu, B.; Achilefu, S. "Design, synthesis, and evaluation of near indrared fluorescent multimeric RGD peptides for targeting tumors." *J. Med. Chem.* **2006,** *49*, 2268-2275.

24. West, W.; Pearce, S. "The Dimeric State of Cyanine Dyes." *J. Phys. Chem.* **1965,** *69*, 1894-1903.

25. Ott, P. "Hepatic elimination of indocyanine green with special reference to distribution kinetics and the influence of plasma protein binding." *Pharmacol. Toxicol.* **1998,** *83*, 1-48.

26. Saxena, V.; Sadoqi, M.; Shao, J. "Degradation kinetics of iodocyanine green in aqueous solution." *J. Pharm. Sci.* **2003,** *92*, 2090-2097.

27. Cardillo, J. A.; Jorge, R.; Costa, R. A.; Nunes, S. M.; Lavinsky, D.; Kuppermann, B. D.; Tedesco, A. C.; Farah, M. E. "Experimental selective choriocapillaris photothrombosis using a modified indocyanine green formulation." *Br. J. Ophthalmol.* **2008,** *92*, 276-280.

28. Saxena, V.; Sadoqi, M.; Shao, J. "Enhanced photo-stability, thermal-stability and aqueous-stability of indocyanine green in polymeric nanoparticulate systems." *J. Photochem. Photobiol. B: Biol.* **2004,** *74*, 29-38.

29. Wu, C.; Barnhill, H.; Liang, X.; Wang, Q.; Jiang, H. "A new probe using hybrid virus-dye nanoparticles for near-infrared fluorescence tomography." *Opt. Commun.* **2005,** *255*, 366-374.

30. Deng, T.; Li, J.-S.; Jiang, J.-H.; Shen, G.-L.; Yu, R.-Q. "Preparation of near-IR fluorescent nanoparticles for fluorescence-anisotropy-based immunoagglutination assay in whole blood." *Adv. Funct. Mater.* **2006,** *16*, 2147-2155.

31. Kim, K.; Lee, M.; Park, H.; Kim, J.-H.; Kim, S.; Chung, H.; Choi, K.; Kim, I.-S.; Seong, B. L.; Kwon, I. C. "Cell-Permeable and Biocompatible Polymeric Nanoparticles for Apoptosis Imaging." *J. Am. Chem. Soc.* **2006,** *128*, 3490-3491.

32. Sharma, P.; Brown, S.; Walter, G.; Santra, S.; Moudgil, B. "Nanoparticles for bioimaging." *Adv. Colloid Interface Sci.* **2006,** *123-126*, 471-485.

33. Soto, C. M.; Blum, A. S.; Vora, G. J.; Lebedev, N.; meador, C. E.; Won, A. P.; Chatterji, A.; Johnson, J. E.; Ratna, B. R. "Fluorescent Signal Amplification of Carbocyanine Dyes Using Engineered Viral Nanoparticles." *J. Am. Chem. Soc.* **2006,** *128*, 5184-5189.

34. He, X.; Chen, J.; Wang, K.; Qin, D.; Tan, W. "Preparation of luminescent Cy5 doped core-shell SFNPs and its application as a near-infrared fluorescent marker." *Talanta* **2007**, 1519-1526.

35. Yang, Z.; Zheng, S.; Harrison, W. J.; Harder, J.; Wen, X.; Gelovani, J. G.; Qiao, A.; Li, C. "Long-Circulating Near-Infrared Fluorescence Core-Cross-Linked Polymeric Micelles: Synthesis, Characterization, and Dual Nuclear/Optical Imaging." *Biomacromolecules* **2007,** *8*, 3422-3428.

36. Yu, J.; Yaseen, M. A.; Anvari, B.; Wong, M. S. "Synthesis of Near-Infrared-Absorbing Nanoparticle-Assembled Capsules." *Chem. Mater.* **2007,** *19*, 1277-1284.

37. Almutairi, A.; Akers, W. J.; Berezin, M. Y.; Achilefu, S.; Frechet, J. M. J. "Monitoring the Biodegradation of Dendritic Near-Infrared Nanoprobes by in Vivo Fluorescence Imaging." *Mol. Pharmaceutics* **2008,** *5*, 1103-1110.

38. Altinoglu, E. I.; Russin, T. J.; Kaiser, J. M.; Barth, B. M.; Eklund, P. C.; Kester, M.; Adair, J. H. "Near-Infrared Emitting Fluorophore-Doped Calcium Phosphate Nanoparticles for In Vivo Imaging of Human Breast Cancer." *ACS Nano* **2008,** *2*, 2075-2084.

39. Bringley, J. F.; Penner, T. L.; Wang, R.; Harder, J. F.; Harrison, W. J.; Buonemani, L. "Silica nanoparticles encapsulating near-infrared emissive cyanine dyes." *J. Colloid Interface Sci.* **2008,** *320*, 132-139.

40. Chen, W. "Nanoparticle fluorescence based technology for biological applications." *J. Nanosci. Nanotechnol.* **2008,** *8*, 1019-1051.

41. Lee, S.; Cha, E.-J.; Park, K.; Lee, S.-Y.; Hong, J.-K.; Sun, I.-C.; Kim, S. Y.; Choi, K.; Kwon, I. K.; Kim, K.; Ahn, C.-H. "A near-infrared-fluorescence-quenched gold-nanoparticle imaging probe for *in vivo* drug screening and protease activity determination." *Angew. Chem., Int. Ed.* **2008,** *47*, 2804-2807.

42. Lim, Y. T.; Noh, Y.-W.; Han, J. H.; Cai, Q.-Y.; Yoon, K.-H.; Chung, B. H. "Biocompatible polymer-nanoparticle-based bimodal imaging contrast agents for the labeling and tracking of dendritic cells." *Small* **2008,** *4*, 1640-1645.

43. Rodriguez, V. B.; Henry, S. M.; Hoffman, A. S.; Stayton, P. S.; Li, X.; Pun, S. H. "Encapsulation and stablization of indocyanine green within poly(styrene-alt-maleic anhydride)-block-poly(styrene) micelles for near-infrared imaging." *J. Biomed. Opt.* **2008,** *13*, 14-25.

44. Burns, A. A.; Vider, J.; Ow, H.; Herz, E.; Penate-Medina, O.; Baumgart, M.; Larson, S. M.; Wiesner, U.; Bradbury, M. "Fluorescent Silica Nanoparticles with Efficient Urinary Excretion for Nanomedicine." *Nano Lett.* **2009,** *9*, 442-448.

45. Kirchherr, A.-K.; Briel, A.; Maeder, K. "Stabilization of Indocyanine Green by Encapsulation within Micellar Systems." *Mol. Pharmaceutics* **2009,** *6*, 480-491.

46. Josephson, L.; Kircher, M. F.; Mahmood, U.; Tang, Y.; Weissleder, R. "Near-Infrared Fluorescent Nanoparticles as Combined MR/Optical Imaging Probes." *Bioconjugate Chem.* **2002,** *13*, 554-560.

47. Kircher, M. F.; Mahmood, U.; King, R. S.; Weissleder, R.; Josephson, L. "A Multimodal Nanoparticle for Preoperative Magnetic Resonance Imaging and Intraoperative Optical Brain Tumor Delineation." *Cancer Res.* **2003,** *63*, 8122-8125.

48. Veiseh, O.; Sun, C.; Gunn, J.; Kohler, N.; Gabikian, P.; Lee, D.; Bhattarai, N.; Ellenbogen, R.; Sze, R.; Hallahan, A.; Olson, J.; Zhang, M. "Optical and MRI Multifunctional Nanoprobe for Targeting Gliomas." *Nano Lett.* **2005,** *5*, 1003-1008.

49. Choi, J. H.; Nguyen, F. T.; Barone, P. W.; Heller, D. A.; Moll, A. E.; Patel, D.; Boppart, S. A.; Strano, M. S. "Multimodal Biomedical Imaging with Asymmetric Single-Walled Carbon Nanotube/Iron Oxide Nanoparticle Complexes." *Nano Lett.* **2007,** *7*, 861-867.

50. Edwards, W. B.; Akers, W. J.; Ye, Y.; Cheney, P. P.; Bloch, S.; Xu, B.; Laforest, R.; Achilefu, S. "Multimodal imaging of integrin receptor-positive tumors by bioluminescence, fluorescence, gamma scintigraphy, and single-photon emission computed tomography using a cyclic RGD peptide labeled with a near-infrared fluorescent dye and a radionuclide." *Mol. Imaging* **2009,** *8*, 101-110.

51. Wang, L.; Reipa, V.; Blasic, J. "Silicon nanoparticles as a luminescent label to DNA." *Bioconjugate Chem.* **2004,** *15*, 409-412.

52. Burns, A.; Ow, H.; Wiesner, U. "Fluorescent core-shell silica nanoparticles: towards "Lab on a Particle" architectures for nanobiotechnology." *Chem. Soc. Rev.* **2006,** *35*, 1028-1042.

53. Lai, J. T.; Filla, D.; Shea, R. "Functional Polymers from Novel Carboxyl-Terminated Trithiocarbonates as Highly Efficient RAFT Agents." *Macromolecules* **2002,** *35*, 6754-6756.

54. Moore, J. S.; Stupp, S. I. "Room temperature polyesterification." *Macromolecules* **1990,** *23*, 65-70.

55. Sun, G.; Cheng, C.; Wooley, K. L. "Reversible Addition Fragmentation Chain Transfer Polymerization of 4-Vinylbenzaldehyde." *Macromolecules* **2007,** *40*, 793-795.

56. Sun, G.; Fang, H.; Cheng, C.; Lu, P.; Zhang, K.; Walker, A. V.; Taylor, J.; Wooley, K. L. "Benzaldehyde-functionalized polymer vesicles." *ACS Nano* **2009,** *3*, 673-681.

57. Sun, G.; Lee, N. S.; Neumann, W. L.; Freskos, J. N.; Shieh, J. J.; Dorshow, R. B.; Wooley, K. L. "A fundamental investigation of cross-linking efficiencies within discrete nanostructures, using the cross-linker as a reporting molecule." *Soft Matter* **2009**, submitted.

58. Unexpected shoulder/bumps were noticed from the GPC profile of **II** (Figure 7.1C), at both high and low molecular weight ends. This observation indicated the relatively lower chain transfer efficiency of the mPEG5k macro-CTA, compared with the

mPEG2k macro-CTA used for the chain extension to block copolymer **I** (smaller low molecular weight bumps on Figure 7.2B GPC cursor). However, the relatively larger polydispersity of **II** did not affect its assembly behavior and uniform core-shell micelles with narrow size distributions was still obtained.

59. Lowe, A. B.; McCormick, C. L. "Reversible addition-fragmentation chain transfer (RAFT) radical polymerization and the synthesis of water-soluble (co)polymers under homogeneous conditions in organic and aqueous media." *Prog. Polym. Sci.* **2007,** *32*, 283-351.

60. Stenzel, M. H. "RAFT polymerization: an avenue to functional polymeric micelles for drug delivery." *Chem. Commun.* **2008**, 3486-3503.

61. York, A. W.; Kirkland, S. E.; McCormick, C. L., "Advances in the synthesis of amphiphilic block copolymers via RAFT polymerization: Stimuli-responsive drug and gene delivery." *Adv. Drug Delivery Rev.* **2008,** *60*, 1018-1036.

62. Harris, J. M., *Poly(ethylene Glycol) Chemistry: Biotechnical and Biomedical Applications*. Plenum Press: New York, 1992.

63. Sun, G.; Hagooly, A.; Xu, J.; Nyström, A. M.; Li, Z.; Rossin, R.; Moore, D. A.; Wooley, K. L.; Welch, M. J. "Facile, efficient approach to accomplish tunable chemistries and variable biodistributions for shell crosslinked nanoparticles (SCKs)." *Biomacromolecules* **2008,** *9*, 1997-2006.

64. The $\lambda_{max,\ abs}$ for **NP2** was shifted to 500 nm, *i.e.*, a 12 nm of red-shift relative to the fluorescein small molecule.

65. For the PEO_{45}-based PEO-*b*-PVBA system, an extending of the PVBA block segment length to 26 repeating units would cause a dramatically morphological switching from nanoparticles to vesicles. Therefore, the hydrophilic PEO block was replaced with longer PEO_{113} and the hydrophobic PVBA block was correspondingly lengthened to 46 repeating units to retain the block length ratio constant at *ca.* 2.5 (hydrophilic *vs.* hydrophobic).

66. Berezin, M. Y.; Lee, H.; Walter, A.; Achilefu, S., "Near Infrared Dyes as Lifetime Solvatochromic Probes for Micropolarity Measurements of Biological Systems." *Biophys. J.* **2007,** *93*, 2892-2899.

Chapter 8

Conclusions

Design and synthesis of discrete and robust polymeric nanostructures bearing the characteristic of serving as chemoselectively functionalizable platform for biomedical applications is an area of long-term interest in material science. This desire becomes emergent as the significantly positive impacts of nanotechnology to traditional healthcare has been heightened in nearly every medical district, including diagnostics, therapy, and clinical applications.

The efforts to achieve precise and facile manipulations over the functionalization of existed shell crosslinked (SCK) nanoparticle platform formed the first portion of this dissertation (chapter 2 and 3). The general strategy exerted in these works was to design synthetic pathway of functionalized SCKs from a "more *Bottom-up*" approach, *i.e.*, coupling functionalities to block polymer precursor before assembly into nanostructures. The efficiency of this approach was confirmed by the construction of DOTA-SCKs, with high loading capacity of radionuclide ^{64}Cu (chapter 2, *ca.* 400 copper per spherical nanoparticle). Extension of the "pre-grafting" strategy to build PEGylated SCKs (chapter 3) with tunable biodistributions and the following targeting SCKs under developing now demonstrated the supremacy and versatility of this synthetic methodology. Meanwhile, *in vivo* positron emission tomography (PET) imaging at low-dose administration was realized by the characteristic of enhanced labeling efficiency, provided by the SCKs prepared through this pathway.

Fundamental investigations in chapter 4 addressed the utilization of active ester (*N*-acryloxysuccinimide, NAS) and probing crosslinkers for better understanding the chemical and physical factors involved during the shell crosslinking process. In the meantime, interesting photo-physical properties of pyrazine-based chromophores were discovered including the blue shift of maximum absorption and dual-emission of fluorescence, which strictly relied upon the internal nanostructure environment. The pre-installation of NAS as amidation site across the micellar structures not only reduced the reaction complexity entailed in carbodiimide mediated amidation, but also enabled selectivity for conjugation of functionalities bearing "critical" activity-related carboxylic acids, for example, the aspartic acid in RGD peptide motif.

While amidation dominated half portion of this dissertation, the left-over part of this dissertation (chapter 5 to 7) was focus on one of the most reactive electrophiles, benzaldehyde, to exploit its controlled polymerization and applications of the form polymers as building component in supramolecular assembly and functionalization.

Reversible addition-fragmentation chain transfer (RAFT) polymerization of 4-vinyl benzaldehyde (VBA) was described in chapter 5. The PVBAs were confirmed with predictable molecular weight, narrow molecular weight distribution, and well-define architectures. Successful chain extension from PVBA based macro chain transfer agent (macro-CTA) afforded well-defined block copolymers with PVBA as reactive block segments allowing for post-polymerization modifications. These studies actually initialized the implements of controlled radical polymerization of carbonyl-bearing monomers.

PVBA-based amphiphilic block copolymer systems (poly(ethylene oxide)-*block*-poly(4-vinyl benzaldehyde), PEO-*b*-PVBA) were then established and their aqueous assemblies were studied (chapter 6 and 7). Dramatic self assembly behavior was noticed between two block copolymers (PEO_{45}-*b*-$PVBA_{18}$ and PEO_{45}-*b*-$PVBA_{26}$) having small structural difference. As characterized through a combination of transmission electron microscopy (TEM) and dynamic light scattering (DLS), uniform spherical micelles with narrow size distribution were formed from the PEO_{45}-*b*-$PVBA_{18}$ block copolymer precursor (chapter 7) while polymer vesicles (polymersomes, chapter 6) with tunable sizes were obtained from the PEO_{45}-*b*-$PVBA_{26}$ block copolymer, although the mechanism behind the difference was not clear at this stage.

The reactivity of the benzaldehyde functionalities was verified by crosslinking the polymersomes, and also by a one-pot crosslinking and functionalization approach to further render them fluorescent, each *via* reductive amination. The mechanic properties of croslinked vesicles have been significantly improved and the *in vitro* studies found these labelled vesicles to undergo cell association (chapter 6).

In chapter 7, the one-pot sequential crosslinking and functionalization protocol through reductive amination was utilized for installation of fluorescent probes (regular fluorescein and near-infrared cypate) onto micelles from PEO-*b*-PVBA block copolymers. The luminescence effiency of nanoparticles was evaluated and a clear relationship between quantum yield and the stoichiometry of loaded fluorophores was established.

As mentioned earlier in the Introduction section, nanomaterials prepared from the *Bottom-up* approach have grown dramatically during the past decades. The reason is

multifactorial but the ultimate goal is very clear, *i.e.*, continuous providing better nanoscale platforms for variety of applications.

Appendix

NMR Spectra of Compounds

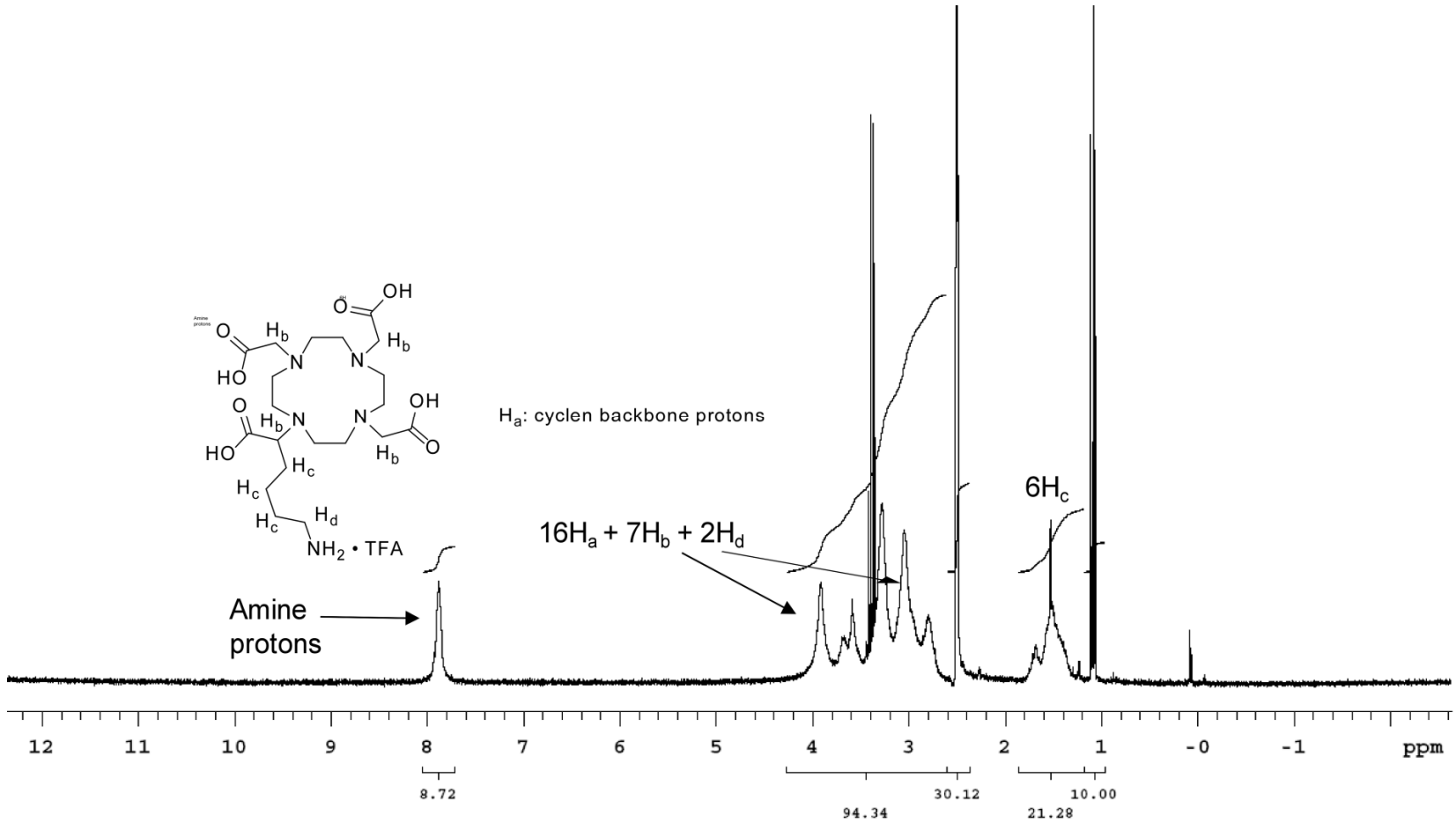
Amine protons
H_a: cyclen backbone protons
$16H_a + 7H_b + 2H_d$
$6H_c$
$NH_2 \cdot TFA$
12 11 10 9 8 7 6 5 4 3 2 1 -0 -1 ppm
8.72
94.34
30.12
21.28
10.00

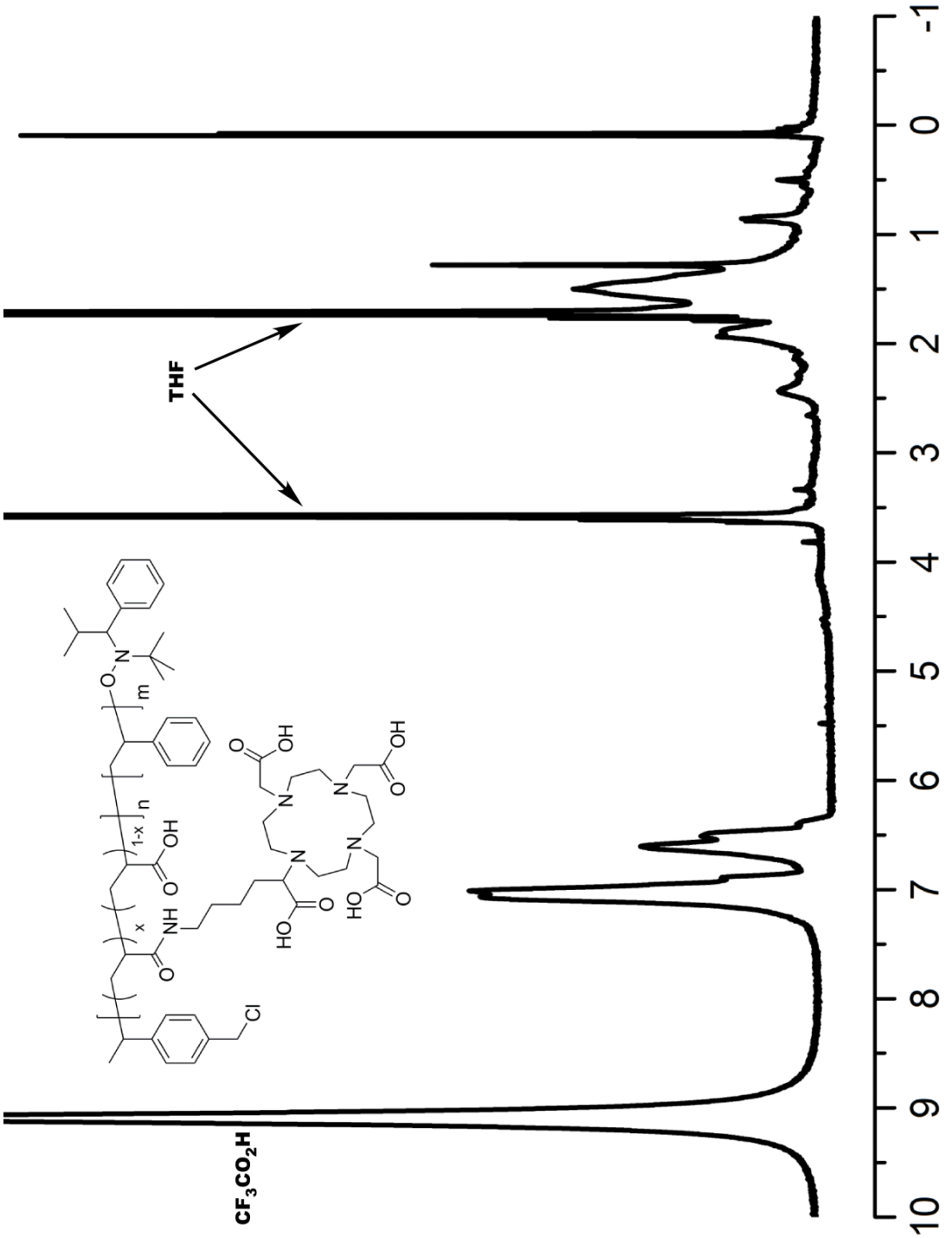
THF
CF3CO2H
10
9
8
7
6
5
4
3
2
1
0
-1

10
9
8
7
6
5
4
3
2
1
0
-1
Cl
O
NH
x
1-x
64
54
OH
O
N
O

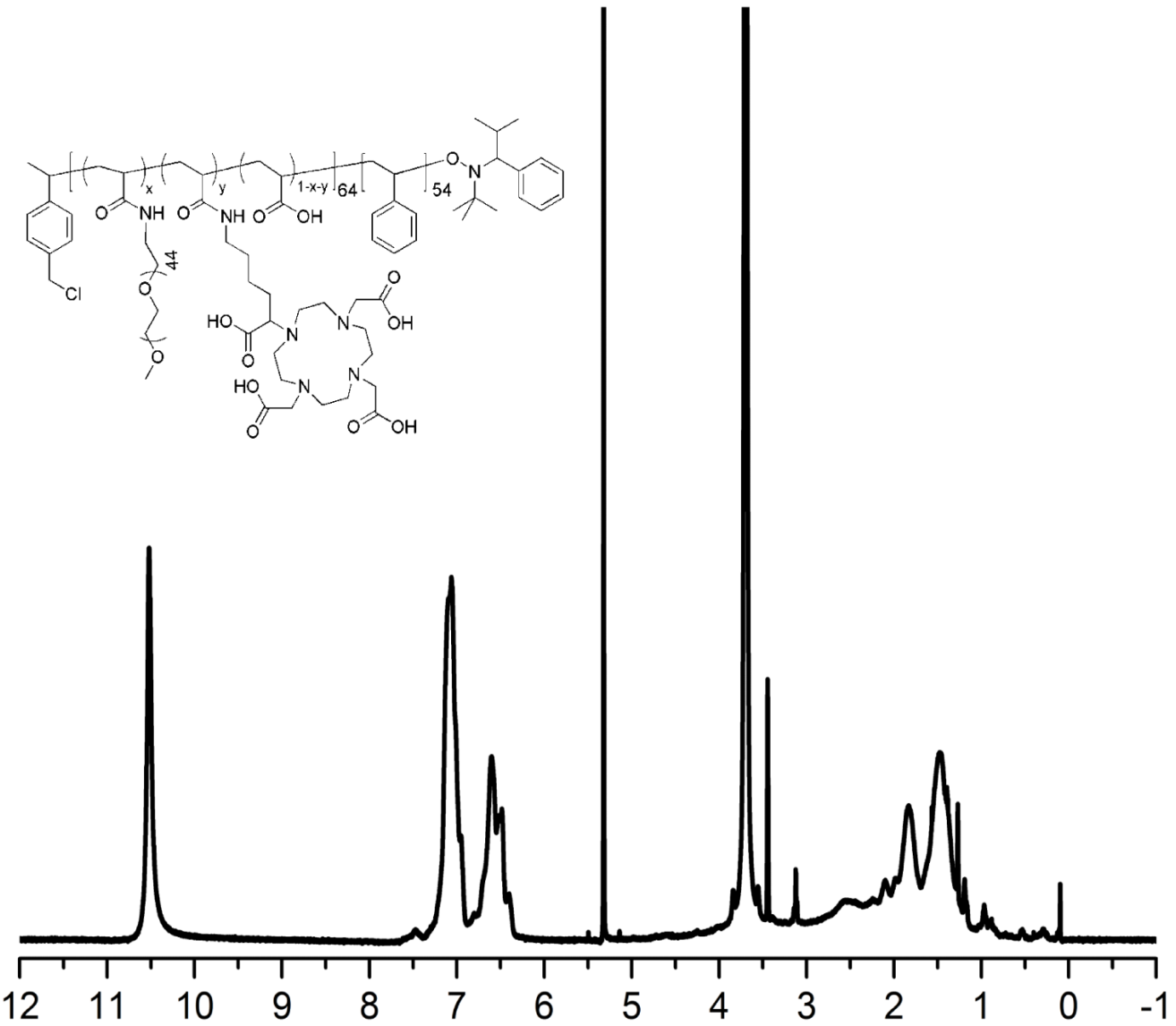
Cl
NH
NH
OH
HO
OH
HO
OH
x
y
1-x-y
64
54
44
12
11
10
9
8
7
6
5
4
3
2
1
0
-1

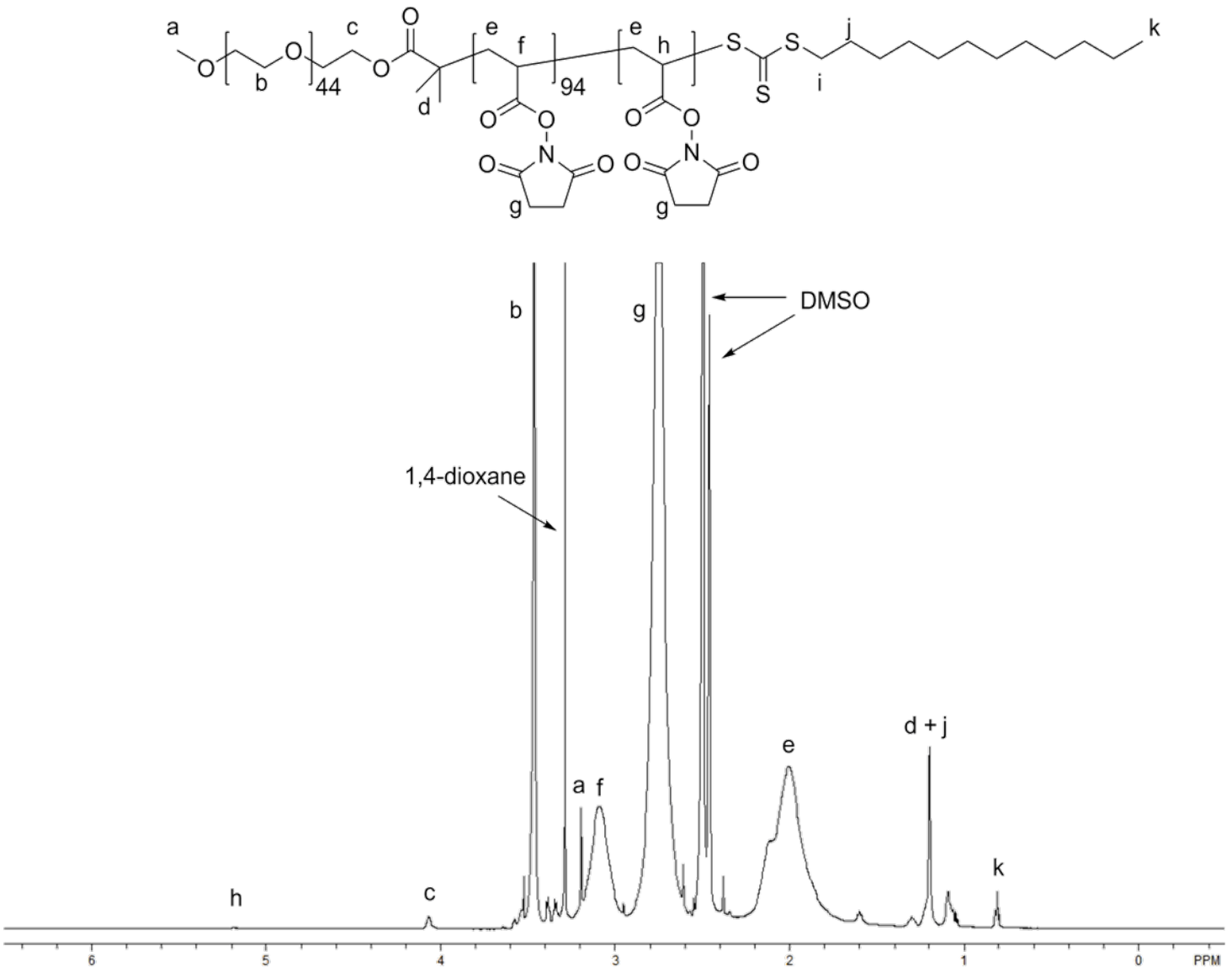
a
b
c
d
e
f
g
h
i
j
k
44
94
O
N
S
DMSO
1,4-dioxane
d + j
PPM
6
5
4
3
2
1
0

DMF
k + l + m
DMF
b
c
a
f
g
d + e + h + i + p
q
PPM
0
2
4
6
8
10

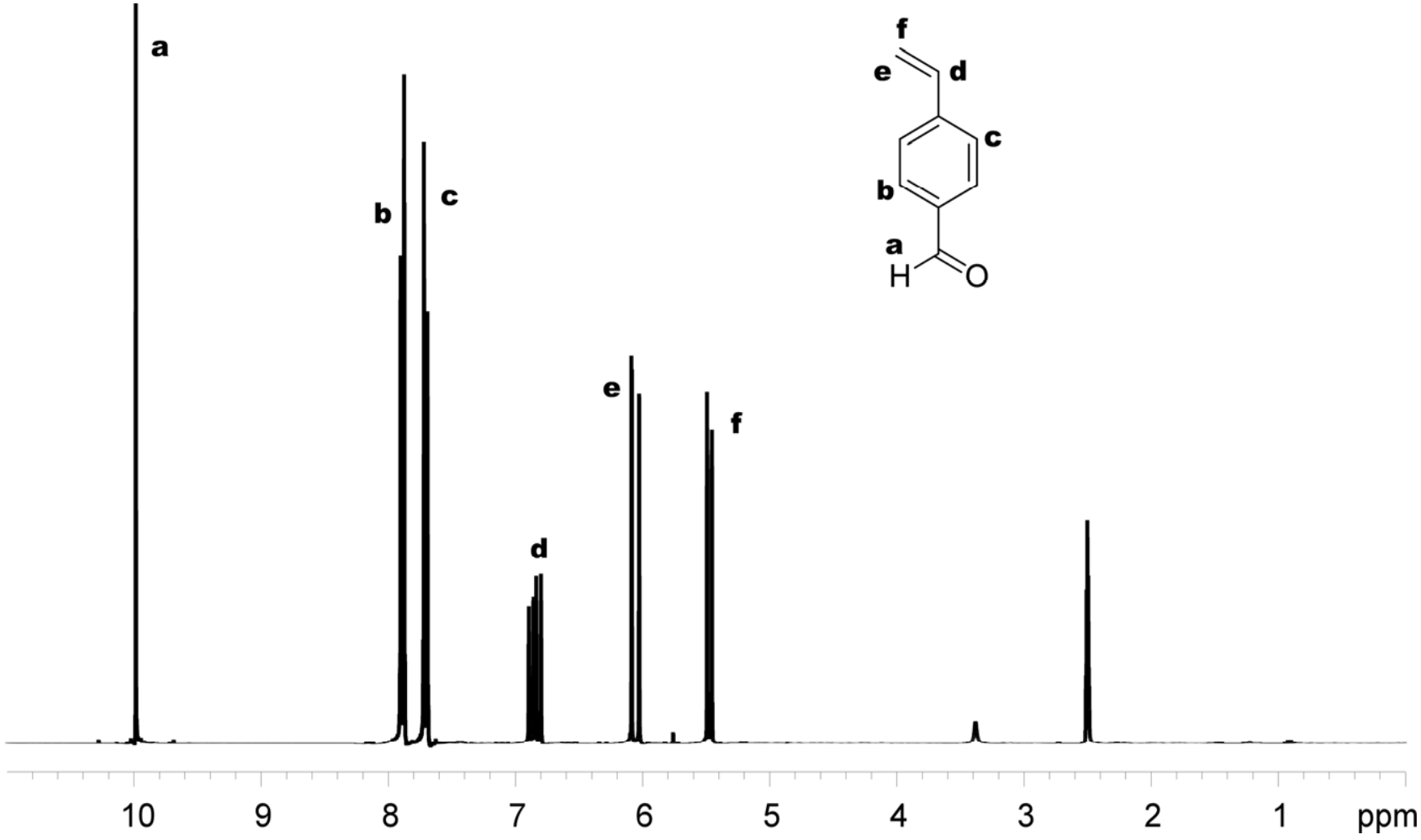
a
b
c
d
e
f
f
e
d
c
b
a
H
O
10
9
8
7
6
5
4
3
2
1
ppm

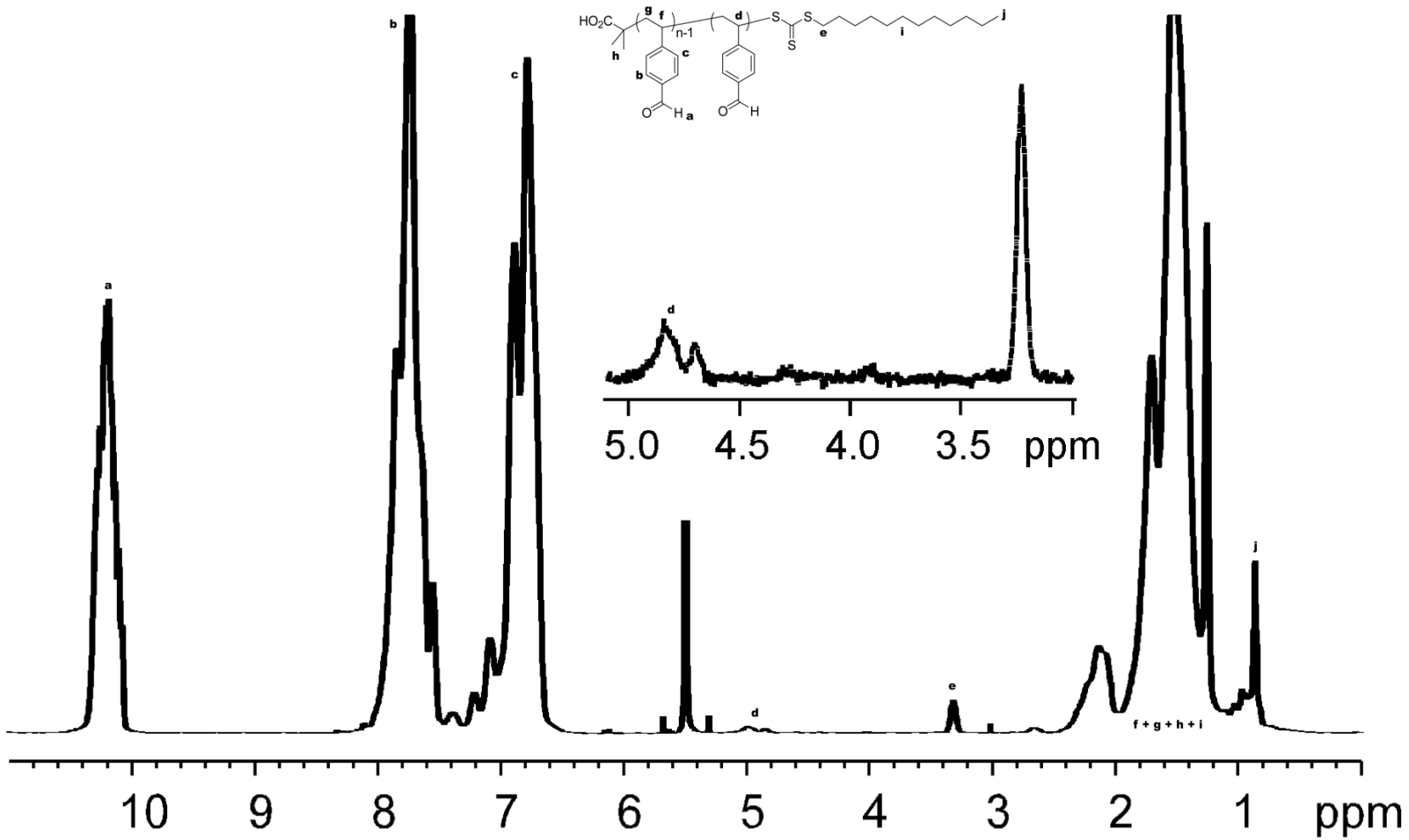
HO2C
g
f
n-1
d
S
S
S
e
i
j
h
c
b
O
H a
O
H
a
b
c
d
5.0
4.5
4.0
3.5
ppm
e
d
j
f+g+h+i
10
9
8
7
6
5
4
3
2
1
ppm

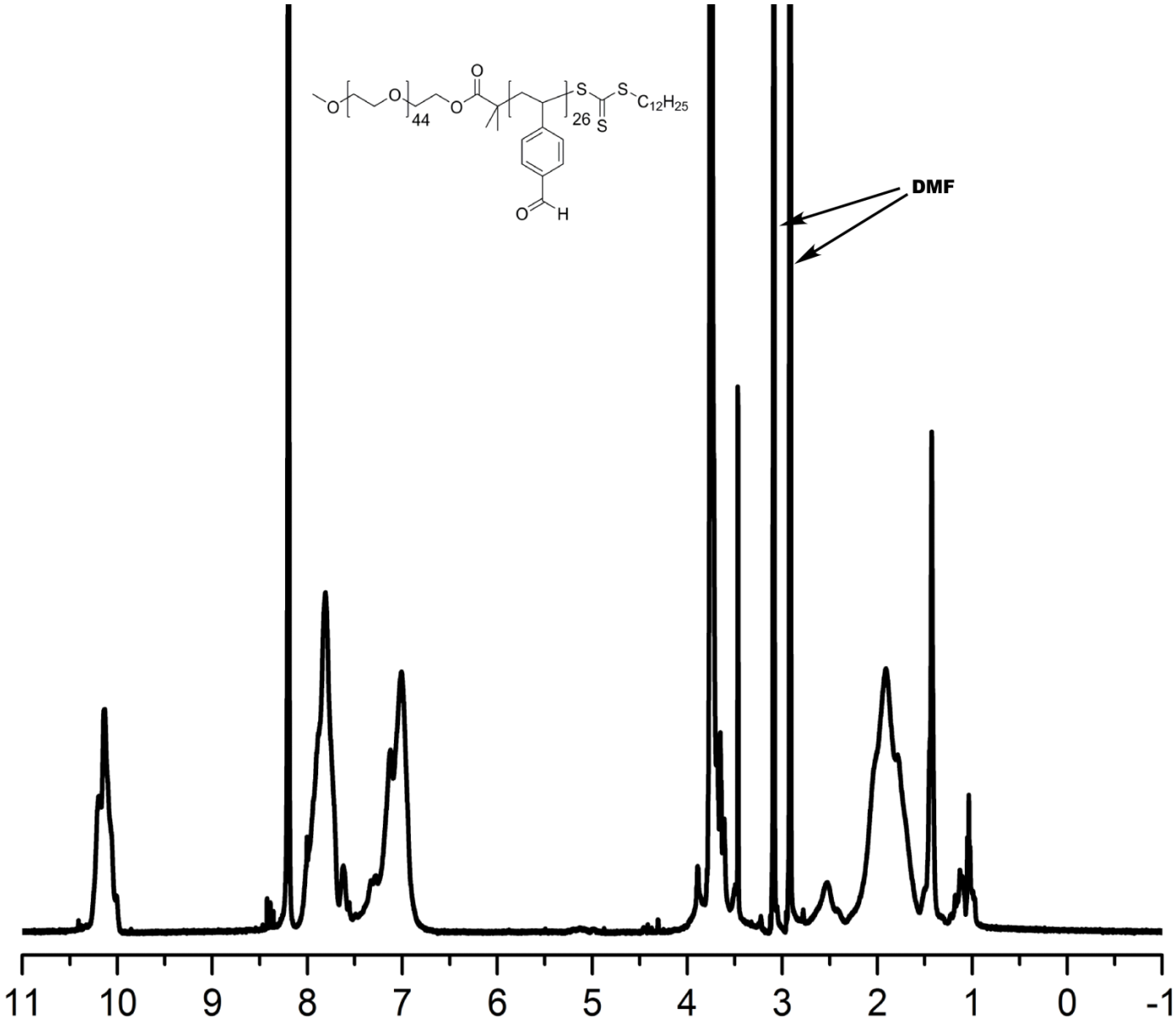
DMF
11
10
9
8
7
6
5
4
3
2
1
0
-1

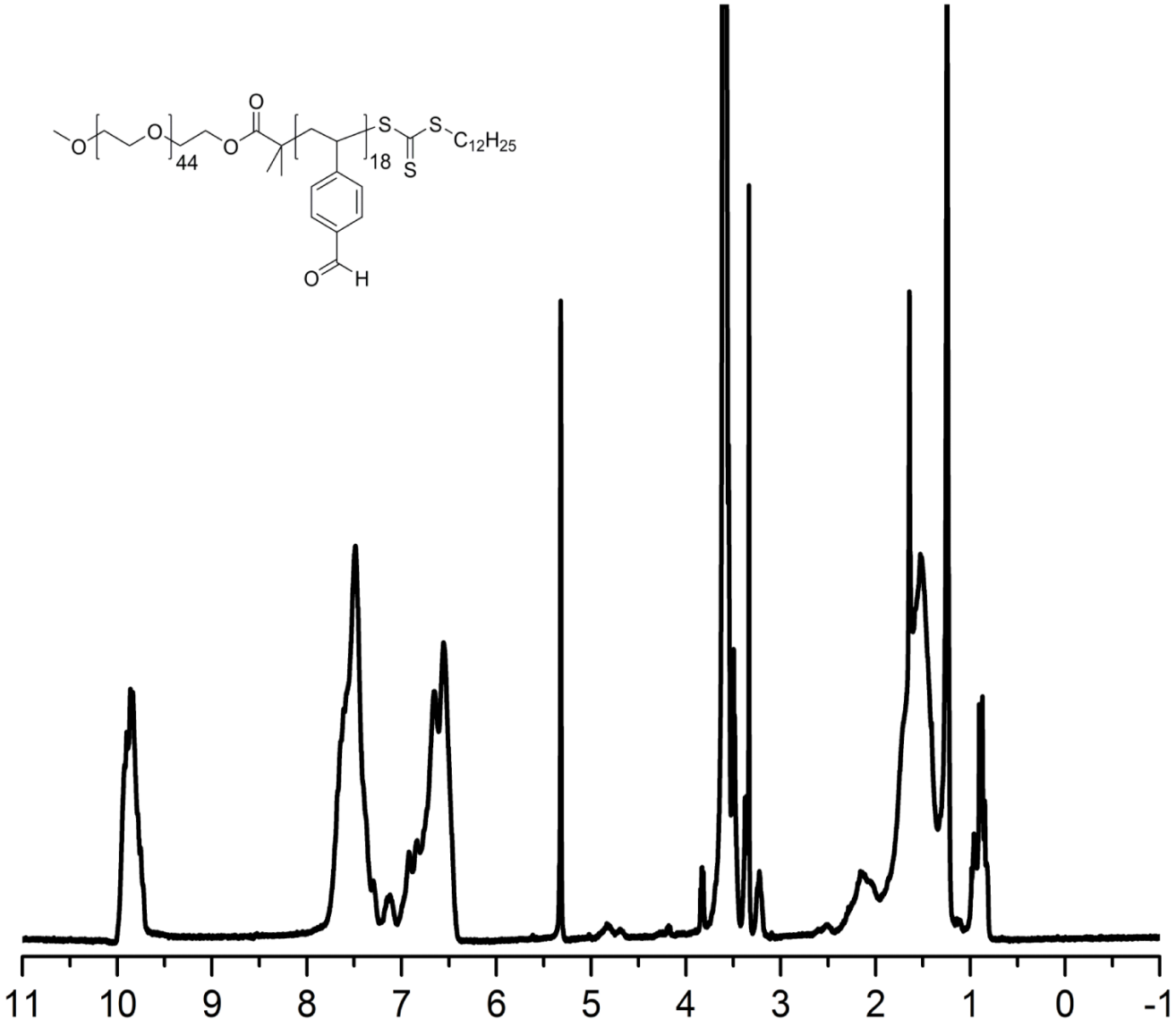
O
O
44
O
O
S
18
S
S
C12H25
O
H
11
10
9
8
7
6
5
4
3
2
1
0
-1

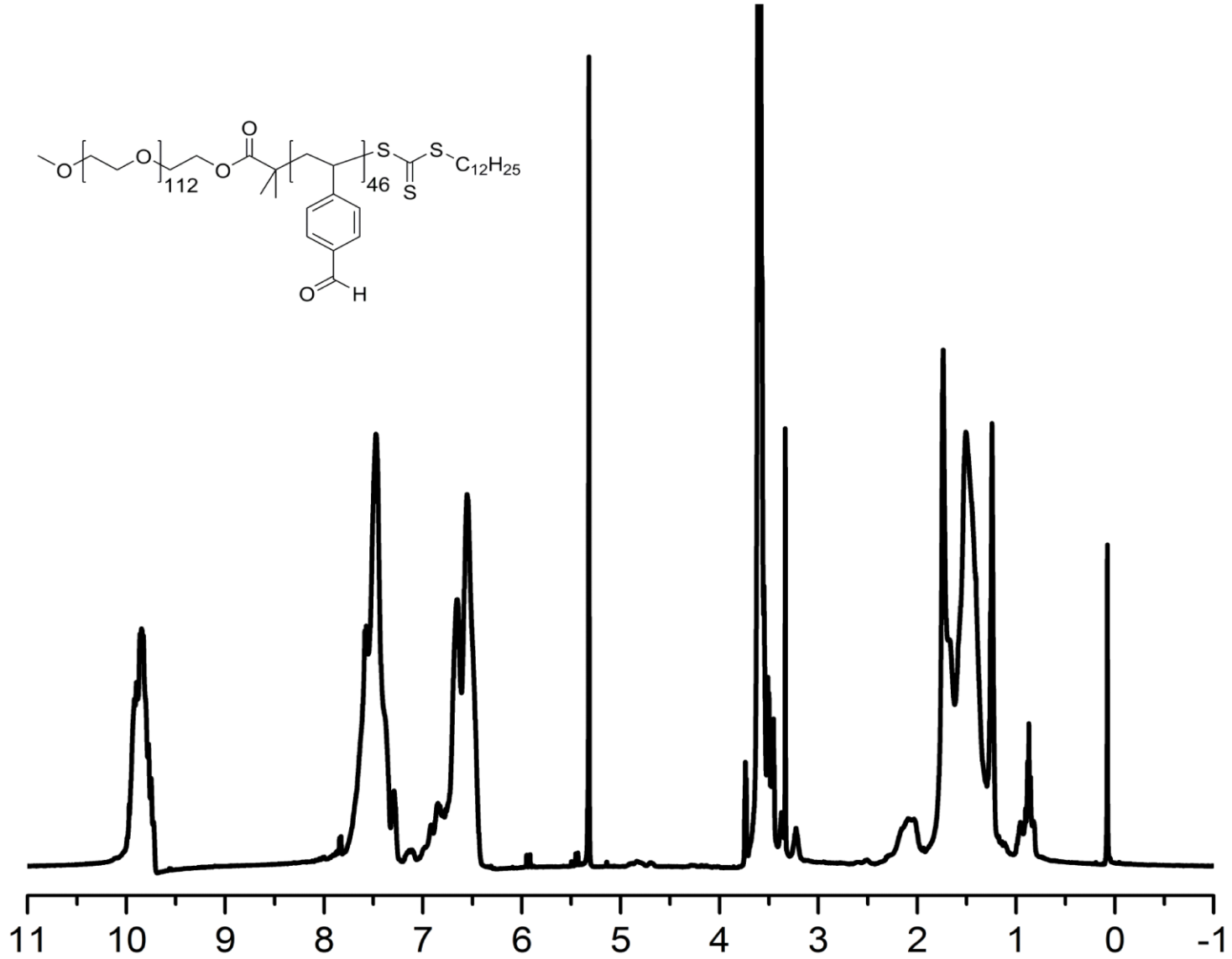
O
O
112
O
O
46
S
S
S
S
C12H25
O
H
11
10
9
8
7
6
5
4
3
2
1
0
-1